Novel Catalytic Materials for Selective Oxidation of Carbon Monoxide for Use in Fuel Cells

Thesis

Unrestricted.

Novel Catalytic Materials for Selective Oxidation of Carbon Monoxide for Use in Fuel Cells

Shailesh Kumar Jain

2004

A thesis submitted for the degree of
Doctor of Philosophy
To
The Open University

Department of Chemistry
The Open University
Walton Hall
Milton Keynes, MK7 6AA
United Kingdom

Submission date: 27 September 200
Award date: 22 December 2004

ProQuest LLC.
789 East Eisenhower Parkway
P.O. Box 1346
Ann Arbor, MI 48106 – 1346

To my father on his

60th birthday

"But in science the credit goes to the man who
convinces the world,
not to the man to whom the idea first occurs."

Francis Darwin
(1848-1925), British scientist

ABSTRACT

The present work includes the preparation, characterisation and testing of alumina supported Pt-based bimetallic catalysts for the selective removal of carbon monoxide in the presence of excess hydrogen, to be used as the feed stock for fuel cells. In this study, an attempt has been made to modify the Pt/Al_2O_3 (low– and high–dispersed) catalyst with Sn, Fe, Co, Cr, Mn, Ni and Cu as promoters using the surface organometallic chemistry (SOMC) route.

Various techniques have been employed to characterise the Pt/Al_2O_3 and the M-Pt/Al_2O_3 bimetallic catalysts. Inductively Coupled Plasma – Atomic Emission Spectroscopy (ICP-AES) technique has been used to determine the composition of the promoted catalysts. The presence of the expected amounts of the second metal in the bimetallic catalysts indicated success of the SOMC route for the preparation of the bimetallic catalysts.

The CO uptake by bimetallic catalysts has been found to be lower than that by Pt/Al_2O_3 catalyst. Decrease in the CO uptake during CO chemisorption experiments relative to the basic Pt/Al_2O_3 catalyst indicates the physical presence of the second metal on the Pt sites suggesting a selective reaction between the reduced surface Pt of the Pt/Al_2O_3 catalyst and the organometallic precursor of the second metal had occurred. The shift in the reduction peaks for the bimetallic catalysts in the Temperature Programmed Reduction (TPR) profile compared with that of unpromoted catalyst suggested physical proximity of the two metal species in the catalyst.

The presence of the two metals together with no observable change in the size of the particles in the bimetallic catalysts has been confirmed by using Transmission Electron Microscopy (TEM/STEM) together with Energy Dispersive X-Ray (EDX) analysis. This was yet another proof of successful deposition of second metal on Pt by the SOMC technique.

All the M-Pt/Al_2O_3 bimetallic catalysts (low–dispersed) prepared by the SOMC route were screened towards CO oxidation in the presence of excess H_2. Out of all the bimetallic catalysts screened, the best performing catalysts were chosen for the detailed study using two different gas mixtures, containing O_2:CO ratios of 2.5 and 1.

The most interesting feature of this study was the performance of Fe- and Co-promoted catalysts under different O_2:CO ratios. Both the systems, FePt and CoPt, brought the temperature for the complete CO oxidation down to the temperature range of 80 – 100 °C which is highly preferred for the commercial applications, while maintaining the high value of CO selectivity. The enhanced activity of the promoted Pt catalysts was suggested to be due to the presence of a metal oxide, MO_x (M = Fe and Co) which provides the site for O_2 adsorption and dissociation and therefore eliminates the normal inhibition observed in the oxidation of CO on Pt catalysts.

Contents

STATEMENT

I declare that the work included in this thesis was carried out by me, the author, during the period of October 2000 to September 2003 at the Department of Chemistry, The Open University (OU) under the supervision of Dr E. M. Crabb and Dr L. E. Smart.

The work in this thesis is the result of my own investigation apart from the elemental analysis carried out by Johnson Matthey Technology Centre (JMTC), Sonning Common, Berkshire, UK.

The Electron Microscopy and Temperature Programmed Reduction (TPR) studies were performed at JMTC which are fully acknowledged. TPR studies were made at OU.

The following presentations were made by me during my PhD work.

- Poster presentation – Science Engineering and Technology (SET) for Britain, March 2003, London, UK.
- *Catalytic Clean Up of Hydrogen Feed for Fuel Cells*, Poster presentation - EUROPACAT – VI, Innsbruck, Austria, September 2003.
- Oral presentation - 9th Annual Johnson Matthey Student Seminar, Bath, UK, January 2003.

Shailesh Kumar Jain

ACKNOWLEDGEMENTS

I wish to express my sincere gratitude and thanks to my research supervisors, Dr Eleanor M. Crabb and Dr Lesley E. Smart, for suggesting the research project, invaluable guidance, continued encouragement and moral support throughout the duration of my work in their laboratories at OU. Their patient interactions during the progress of this work have been instrumental in shaping me professionally as a researcher.

I also wish to acknowledge the very substantial help and guidance from Dr. Dave Thompsett (Johnson Matthey Technology Centre, UK) during the progress of the present work. I am indebted to Dr. Andrew Steele (Johnson Matthey Technology Centre, UK) for his valuable help and cooperation in carrying out the tests on the prepared catalysts under realistic conditions, to Dr. Valerie Self for her guidance during the early parts of the project and with temperature programmed reduction experiments, and to Mr. Gregory Goodlet (Johnson Matthey Technology Centre, UK) for all his help with the electron microscopy studies. Dr. Y. Qian is specially acknowledged and thanked for his efforts in preparing Sn-promoted catalysts.

Many thanks to the research and technical staff at the Department of Chemistry who have supported me at various stages of the work presented in this thesis. I am particularly thankful to Mr. Graham Jeffs, for all his technical expertise of Gas Chromatograph and many other laboratory related issues that enabled me to complete my experimental work without much hassle. Mr Brandon Cook for his help with TGA experiments and computer related issues.

I thankfully acknowledge, The Open University, UK for the award of studentship to me and Johnson Matthey Technology Centre for funding and the Case Award.

I feel very happy in acknowledging all the friends and colleagues who made my stay around the laboratories and office at OU and outside at Milton Keynes, pleasant and memorable.

And finally, the persons who have played the most important role in shaping my present, who are always behind the scenes, supporting, guiding and source of encouragement for me – my parents. I just want to say that you are my inspiration and I owe every bit my success to you.

1
Introduction

1.1 FUEL CELLS

Fuel cells are electrochemical devices that convert the chemical energy of a reaction directly into electrical energy. The easiest way to understand fuel cells is to think of them as an analogue of an ordinary battery. Both a fuel cell and a battery use electrochemical reactions to produce electricity. The major difference between the two is in the ability of a fuel cell to produce electricity continuously as long as a source of fuel, generally hydrogen, is available. On the other hand a battery needs to be recharged frequently. Since energy is not stored internally in a fuel cell, it will not "run down" like a battery. Fuel cells directly convert the fuel into electricity whereas a battery has to replenish its electrical energy from an external source.

Fuel cells convert hydrogen, or hydrogen-containing fuels, directly into electrical energy plus heat, through the electrochemical reaction of hydrogen and oxygen to form water (Fig. 1-1). The overall reaction in a hydrogen–oxygen fuel cell is

$$2H_2(g) + O_2(g) \rightarrow 2H_2O(l) + \text{Energy} \quad (1)$$

Unlike conventional power generation plants and internal combustion engines, the theoretical efficiency of a fuel cell is not limited by the Carnot inefficiency

problem for heat-to-work conversion, because a fuel cell transforms chemical energy directly into electrical energy [1]. As a result, based on the lower heating value of the fuel, a fuel cell system can exhibit about 40–60% fuel-to-electricity efficiency, significantly higher than almost all other energy conversion systems [2]. Fuel cell systems operating on pure hydrogen (H_2) produce only water as a by-product, thus eliminating all emissions locally [1].

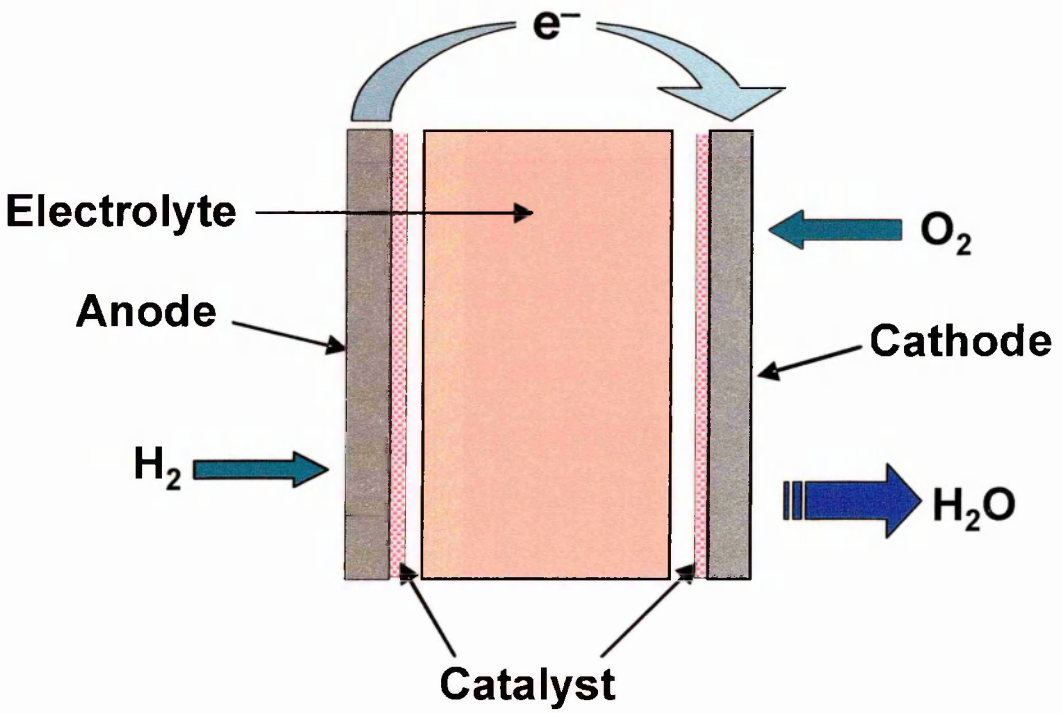

FIGURE 1-1: Schematic diagram for a hydrogen-oxygen fuel cell

1.2 WHY FUEL CELLS?

Fuel cells were mainly developed because of the requirements of space research in the late 1950s. Adaptation of the fuel cell technology from space applications to terrestrial use seemed logical. In response to the oil price shocks of the early 1970s, the initial terrestrial application of fuel cells was to increase power

generation efficiency and to improve the environment by lowering the exhaust emissions from power generators based on fossil fuels.

Fuel cells are expected to be able to power everything from homes and businesses, to cars and laptop computers in the future. Under pressure from environmentalists and regulatory authorities to improve fuel economy and reduce pollution, the auto industry has started to see an answer to their problems in fuel cells.

Ideally, a fuel cell runs on hydrogen which reacts with oxygen from the air electrochemically, resulting in the voltage generation between the two electrodes. The reactions occur in a chemical mediator known as an *electrolyte*. Fuel cells operate without combustion, making them virtually pollution-free. Since there are no moving parts, fuel cells are extremely quiet.

The most successful applications of fuel cell technology have been in the US space programme. The 1 kW polymer electrolyte fuel cell (PEFC) systems, also known as polymer-exchange membrane fuel cells (PEMFC), were used in the Gemini programme, the 1 kW alkaline fuel cell (AFC) systems were used in the Apollo programme and the 12 kW AFCs are being used in the space shuttle programme [1,2,3].

Small fuel cell systems in the 1–100 kW power range have become the focus of intense research and development activities. Among the potential applications for fuel cells systems in this power range are:

(a) primary propulsion for passenger and light-duty vehicles (50–100 kW);

(b) auxiliary power units (APUs) for operator quality-of-life, housekeeping needs for trucks and heavy-duty vehicles (2–10 kW) [4];

(c) portable power generation for residential and recreational needs (3–5 kW).

1.3 FUEL CELL TECHNOLOGIES

The key properties of a fuel cell, particularly the operating temperature, depend on the electrolyte used. For this reason, fuel cell technologies are named by their electrolyte. The following distinct types of fuel cells have been developed:

- Alkaline fuel cells
- Proton exchange membrane fuel cells
- Phosphoric acid fuel cells
- Molten carbonate fuel cells
- Solid oxide fuel cells
- Regenerative fuel cells
- Direct methanol fuel cells
- Metal-air fuel cells

These fuel cells operate at different temperatures and each is best suited for a particular kind of application.

Table 1-1 summarizes some of the potential applications of the various types of fuel cells mentioned above.

Table 1-1: VARIOUS TYPES OF FUEL CELLS AND THEIR PRESENT/POTENTIAL APPLICATIONS

Type of fuel cell	Operating Temperature / °C	Present / Potential Applications
Alkaline fuel cell (AFC)	~250	Used in space vehicles (Apollo, Shuttle), possible uses in land vehicles and submarines.
Proton Exchange Membrane fuel cell (PEMFC)	80 – 120	Best candidates for light-duty vehicles, for buildings and many other small applications.
Phosphoric acid fuel cell (PAFC)	150 – 220	Mid-to-large stationary power generation applications.

Molten carbonate fuel cell (MCFC)	600 – 700	Best suited for the provision of constant power in large utility applications.
Solid oxide fuel cell (SOFC)	800 – 1000	Promising option for high-powered applications, such as industrial uses or central electricity generating station.
Regenerative fuel cell	–	Self-fuelling UPS systems.
Metal-air fuel cell	−20 – 60	Electric mobile devices, electric vehicles and uninterruptible power supply for remote industrial, commercial, or residential uses.

In particular there has been a lot of interest in the PEMFCs mainly because these are now being considered to be one of the most promising options as a substitute to the internal combustion engine for a number of transport applications. It is the fuel for this type of fuel cell that is addressed in this thesis and further description will be limited to PEMFC.

1.4 PROTON EXCHANGE MEMBRANE FUEL CELLS

PEM technology was developed at the General Electric Co. (USA) in the early 1960s, through the work of Thomas Grubb and Leonard Niedrach. For transportation systems, the PEMFC is considered to be the leading fuel cell technology for primary propulsion [2,3,5,6]. The features of the PEMFC that make it attractive for transportation systems are its high power density and low operating temperature (about 80 °C). This low temperature of operation is an important requirement for a quick

startup. Since it is a solid system containing no free corrosive liquid, (unlike for example the AFC), it is easy to transport.

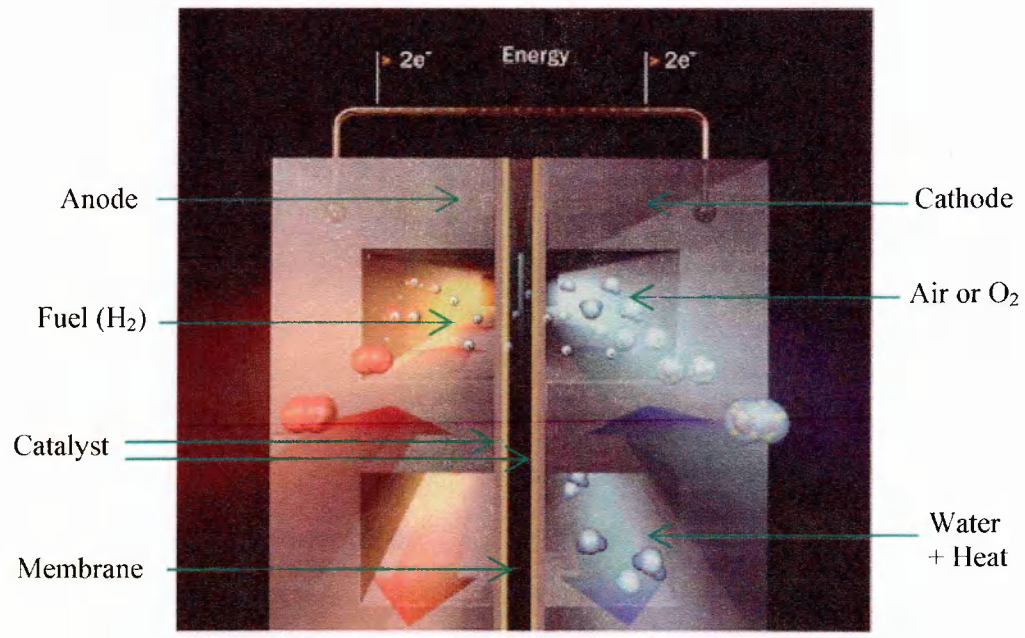

FIGURE 1-2: Basic design of the Proton Exchange Membrane Fuel Cell (PEMFC)

The PEM fuel cell consists of a proton-conducting membrane, such as a perfluorinated sulfonic acid polymer, which acts as the electrolyte, sandwiched between two porous carbon electrodes impregnated with the platinum catalyst (Fig. 1-2). The back of the electrodes is made hydrophobic by coating with an appropriate compound, such as Teflon®. This non-wetting coating provides a path for gas diffusion to the catalyst layer.

The use of organic cation-exchange membrane polymers in fuel cells was originally conceived by W. T. Grubb[7,8] in 1959. The function of the ion membrane is to provide an ion conductive gas barrier. Strong acids were used to provide a contact between the adjacent membrane and catalytic surfaces. Later, it was found that the cell

could function without adding any acid. As a result, present PEMFCs do not use any electrolyte other than the hydrated membrane [9].

In the PEMFC hydrogen at the anode provides a proton, releasing an electron in the process that passes through the external circuit to reach the cathode (Eq. (2)). The proton, which remains solvated by water molecules, diffuses through the membrane to the cathode to react with oxygen and the returning electron [10]. Water is subsequently produced at the cathode (Eq. (3)).

Reaction at the anode: $2H_2(g) \rightarrow 4H^+(aq) + 4e^-$ (2)

Reaction at the cathode: $O_2(g) + 4H^+(aq) + 4e^- \rightarrow 2H_2O(l)$ (3)

Overall reaction: $2H_2(g) + O_2(g) \rightarrow 2H_2O(l) + \text{Energy}$ (1)

Due to the intrinsic nature of the materials used, low-temperature operation at about 80 °C is possible. The cell is also able to sustain operation at very high current densities. These attributes lead to a fast start capability and the ability to make a compact and lightweight fuel cell [10].

Transportation applications mean that the fuel of choice will probably be methanol, although hydrogen storage on-board in the form of pressurized gas and the partial oxidation of petrol [11] are also being considered. The PEMFC based on natural gas or other hydrogen-rich gases is also being considered for stationary power applications.

The lack of an infrastructure for producing and distributing H_2 has led to a research effort to develop on-board fuel processing technology to generate hydrogen from hydrocarbon fuels using 'reforming' reactions (to be discussed in next section) [3,5]. For transportation applications, the primary focus has been on reforming petrol, the main reason being that the infrastructure for the production and distribution of

petrol already exists to supply internal combustion engines [12,13]. For Auxiliary Power Units (APUs) the focus is on reforming both petrol (for cars [14]) and diesel (for trucks and heavy-duty vehicles [15]).

The lower operating temperature of a PEMFC results in both advantages and disadvantages. Low temperature operation is advantageous because the cell can start from ambient conditions quickly, especially when pure hydrogen fuel is available. The disadvantage in the low temperature operation is the need of a platinum catalyst to promote the electrochemical reaction. At these temperatures the catalyst is also susceptible to poisoning by impurities in the gas stream.

1.5 HYDROGEN PRODUCTION PROCESSES

Hydrogen can be produced from a wide variety of sources, using a number of different technologies. Until the 1950s, water electrolysers were in large scale use for hydrogen (or oxygen) production. Currently, electrolysis provides only a small percentage of the world's hydrogen production.

Water electrolysis involves the catalytic decomposition of water into hydrogen and oxygen using electricity.

$$\text{Electrolysis:} \quad 2H_2O(l) \rightarrow 2H_2(g) + O_2(g) \tag{4}$$

The high energy input in this route, however acts as a barrier to commercial application.

More typically hydrogen is produced by the processing of hydrogen-containing fuels. A fuel processing system converts hydrocarbon or other organic fuels to hydrogen of purity suitable for fuel cell operation. In order to deliver hydrogen on-board, one of the key parts of the new technology is a ***fuel reformer***.

A fuel reformer can be described as a device that uses heat and a catalyst to change the chemical composition of a hydrocarbon fuel to liberate hydrogen. The fuels include petroleum-derived liquids, such as naphtha and petrol, petroleum-derived gases, such as methane and propane, and other fuels such as methanol and ethanol.

The main types of fuel processing technologies are:

1. Catalytic Steam Reforming
2. Partial Oxidation
3. Auto-thermal Reforming

The ***steam reforming process*** involves the reaction of the hydrocarbon fuel with steam in the presence of a catalyst and heat supplied from an external source. One of the biggest advantages of the steam reforming system is its high efficiency towards hydrogen generation. This process can be described by a general equation:

$$CH_x(g) + H_2O(g) \xrightarrow{\text{heat}} CO(g) + (1 + 0.5x)\, H_2(g) \quad (5)$$

Steam reforming of light hydrocarbons, especially methane, is used for many large scale manufacturing processes that require hydrogen. Steam reforming is an endothermic process. In large-scale manufacturing processes the reaction is conducted in tube furnaces fired at 800 °C and at pressures up to 30 atm [16]. Coke produced by thermal cracking (Eq. (6)) or the Bouduard reaction (Eq. (7)) leads to the deactivation of the catalyst.

$$CH_x(g) \rightarrow C(s) + 0.5x\, H_2(g) \quad (6)$$

$$2CO(g) \rightarrow C(s) + CO_2(g) \quad (7)$$

The deactivation processes are major problems especially when the steam to carbon ratio is close to the stoichiometric ratio. In order to minimize the coke

formation, excess steam has been used to ensure that any carbon formed is gasified, as follows:

$$C(s) + H_2O(g) \rightarrow CO(g) + H_2(g) \quad (8)$$

The ***partial oxidation process*** involves the reaction of the hydrocarbon fuel (CH_x) with limited oxygen supply to generate hydrogen. Limited oxygen supply means that the oxygen to fuel ratio is less than that required for complete combustion. This process can be described by a general equation:

$$2CH_x(g) + O_2(g) \leftrightarrow xH_2(g) + 2CO(g) \quad (9)$$

Partial oxidation can be carried out in two ways: with a catalyst (called *catalytic partial oxidation*) and without a catalyst (called *non-catalytic partial oxidation*). The reaction rate for partial oxidation is much higher than for the steam reforming, but the hydrogen yield per carbon in the hydrocarbon fuel is lower. For non-catalytic partial oxidation, temperatures above 1000 °C are required in order to achieve higher reaction rates. The catalytic partial oxidation process has attracted much attention because it does not require the extreme temperature conditions and as a result, a better control over the reaction could be achieved. In this process coke formation is also minimised and there is a wider choice of materials for the construction of the reactor.

Whereas steam reforming is an endothermic process, partial oxidation is an exothermic process. So, obviously the next logical step seems to be the combination of the two processes.

In the ***auto-thermal reforming process***, the hydrocarbon fuel is treated with steam and oxygen in presence of a catalyst to produce hydrogen. The heat generated during the oxidation process can be utilised for the steam reforming process and as a

result no external heating is needed. Another feature of this process is that many different types of hydrocarbon fuels can be used to generate hydrogen quite efficiently.

Carbon monoxide produced in the reforming process is converted to carbon dioxide and more hydrogen in a high-temperature water gas shift (WGS) stage followed by a low-temperature shift stage. In both stages, the *water-gas shift* reaction (Eq. (10)) takes place.

$$CO(g) + H_2O(g) \xrightarrow{catalyst} CO_2(g) + H_2(g) \qquad (10)$$

Catalytic steam reforming of methanol or partial oxidation of petrol followed by water gas shift reaction will produce a gas stream with 30–75% H_2, 15–20% CO_2, ~10% H_2O, 0–25% N_2 and 0.5–1% (up to 10^4 ppm) CO.

The CO produced in the reforming process, even after WGS reaction, is one of the major difficulties to overcome before the commercial application of PEMFCs becomes a reality. A number of studies have shown that the presence of even very small quantities of CO (ca.10 ppm) in the reformed gas stream can seriously reduce the efficiency of the fuel cell [17]. At the operating temperature of PEMFCs (below 150 °C) CO is preferentially adsorbed onto the surface of the Pt anode catalyst preventing access of H_2 to the sites and hence inhibiting the H_2 oxidation reaction. Research efforts to counteract this problem are concentrating in two areas:

1. to improve the tolerance of the Pt catalyst to CO and,
2. to the reduce the levels of CO impurity present in the gas stream.

In order to avoid unnecessary loss of energy conversion efficiency of the fuel cell, the CO concentration in the reformer fuel stream needs to be reduced further to less than 10 ppm [18,19,20]. The work described in this thesis addresses this second problem.

1.6 CO "CLEAN-UP" OF THE REFORMED GAS

There are several well tried methods known for removing CO from a mixed gas stream. These include:

- Reduction of CO to CH_4
- Selective oxidation of CO to CO_2
- Adsorption by hydrogen permeable membranes

Each of the methods, however, faces some limitations in their use in fuel cells.

■ ***Reduction of carbon monoxide to methane*** – This method of removing CO from the reformate mixture is to convert CO to methane. This method is known as methanation. Methanation requires three molecules of hydrogen (Eq. (11)) for each CO molecule to be reduced to CH_4. In other words, the hydrogen loss is equivalent to at least three times the concentration of CO removed.

$$CO(g) + 3H_2(g) \rightarrow CH_4(g) + H_2O(g) \quad (11)$$

Also, selective methanation of CO is very difficult to achieve and control in the presence of a large excess of CO_2 [21].

■ ***Selective oxidation of carbon monoxide to carbon dioxide*** – CO can be oxidised to CO_2 selectively in the presence of a catalyst. There are several catalysts known for the selective oxidation of CO in the presence of hydrogen. A suitable catalyst should ideally oxidise CO with as little oxidation of H_2 as possible. Some catalysts require low temperatures [22] or such a narrow temperature window23 that the clean-up reactor would require very careful cooling and temperature control.

$$CO(g) + 0.5O_2(g) \rightarrow CO_2(g) \quad (12)$$

■ ***Adsorption of carbon monoxide by Pd based membranes*** – Pd-based membranes have been used to remove CO from hydrogen streams. These Pd-membranes suffer from hydrogen embrittlement yielding unacceptably short membrane lifetimes. Consequently Pd-alloys are preferred, ideally as supported foils or coated ceramics to avoid large quantities of expensive Pd [24]. However, this method requires a high pressure differential between both sides of the membrane at high temperatures. Such membranes still tend to develop fine cracks which lead to undesirable leakage of CO. Suitable membrane materials such as Pd/Ag alloys have been developed for successful adsorption of CO. Modern and low-cost membranes work with a very thin noble metal layer.

Out of all the methods mentioned above for the cleaning up of the reformed gas mixture, catalytic selective oxidation appears to be the most promising and cost-effective approach.

The work described in this thesis will look at developing catalysts for the selective removal of CO in hydrogen rich streams using selective (or preferential) oxidation of CO (PrOx). This is the final step in the chain of the processes constituting a fuel processing technology for the on-board generation of hydrogen for applications in cars etc. shown in Fig. 1-3. The aim is to produce a hydrogen gas feed stream for PEMFC containing less than the 10 ppm CO.

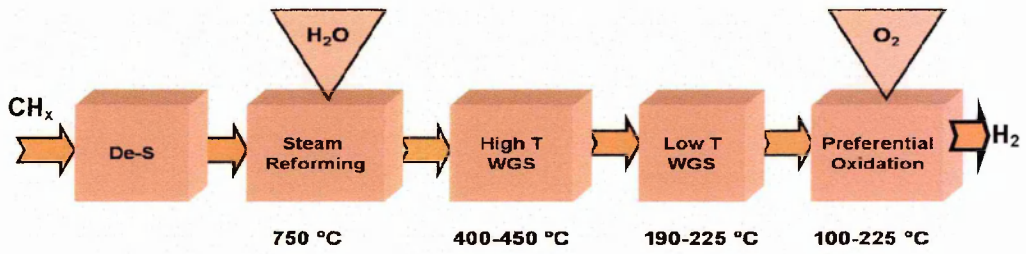

FIGURE 1-3: Schematic diagram of a typical fuel processor for on-board H_2 generation.

De-S = De-sulphurisation
WGS = Water Gas Shift

From Fig. 1-3, it is clear that as the Preferential Oxidation (PrOx) reactor is placed between the low-temperature shift reactor (~200 °C) and the PEMFC (~80 °C) it should operate over the temperature range 80–200 °C. Many researchers have reported low temperature oxidation of carbon monoxide [25] and hydrocarbons over various transition metal oxides [26,27,28] but very few of these materials seem to work under real conditions, i.e., in the presence of H_2O, SO_2, etc.

One of the major requirements for the commercial catalyst is that it should retain its activity even in the presence of hydrogen (H_2), moisture (H_2O), carbon dioxide (CO_2) etc., and over the lifetime of the car. Exposure to high temperatures can damage catalysts by sintering the noble metal particles, resulting in a decrease in catalytic activity. Sintering of the noble metal catalysts impairs the low temperature activity. In order to achieve concentrations of less than 10 ppm CO in the H_2 from the fuel processor, the conversion of the CO has to be 99.9%.

1.7 SELECTIVE CO OXIDATION

The first patent for selectively oxidizing CO in the presence of hydrogen by a Pt/Al_2O_3 catalyst was awarded to Engelhard in 1963 [29]. Platinum catalysts supported on alumina (Pt/Al_2O_3) have been used to oxidize CO [30]. Oh and Sinkevitch studied the selectivity and activity of alumina-supported Pt, Pd, Ru and Rh with a gas stream containing 900 ppm CO, 800 ppm O_2 and 0.85% H_2, and found Ru and Rh to be very selective compared to Pt/alumina [31]. Kahlich *et. al.*[32] studied the kinetics of the selective CO oxidation in H_2-rich gas on Pt/Al_2O_3 in detail, and observed that over 0.5% Pt/Al_2O_3 it is not possible to have more than 80% conversion of 1% CO with 1% O_2 in the presence of hydrogen even at temperatures as high as 250 °C. They also observed that the presence of hydrogen increases the rate of CO oxidation by as much

as a factor of five. Based on their model they estimated that the best temperature for preferential oxidation of CO over a Pt/Al_2O_3 catalyst is ~200 °C and that 2.5 times the stoichiometric amount of oxygen would be needed to completely oxidize 1% CO. The selectivity and activity of Pt supported on zeolites (A-type, mordenite and X-type) and on Al_2O_3 was investigated by Igarashi *et. al.* [33]. Their results showed that Pt/Al_2O_3 had the highest activity but the selectivities of Pt/A and Pt/mordenite catalysts were somewhat better.

The properties of bimetallic catalysts are often found to be superior to those of monometallic catalysts [34]. Current research efforts are concentrating on improving the performance of Pt supported on alumina, using other metals as promoters in particular some of the first row transition metals such as Fe and Co. Initial results have shown Fe and Co to be very effective promoters. Korotkikh and Farrauto [35] investigated selective oxidation of 1% CO by a proprietary 5% Pt/Al_2O_3 catalyst promoted by iron oxide in a stream of mostly hydrogen with oxygen. They were able to observe high selectivity and activity at low temperatures. Also, Schubert *et. al.* [36] reported the superior performance of a carbon-supported PtSn bimetallic catalyst over the commercial Pt/Al_2O_3 catalyst towards the PrOx reaction. They showed their supported PtSn bimetallic catalyst to be more active and selective than the commercial Pt/Al_2O_3 even at lower temperatures (0–80 °C). Lane and co-workers [37] showed a mixed metal catalyst (Co/Pt supported on TiO_2) to be very active at low temperatures and not significantly inhibited by the reformate gases.

In order to maximise the promotional effect of the second metals it is imperative that the metals are in intimate contact. The surface of such a catalyst can therefore be thought of comprising particles consisting of both metals together, so-called "bimetallic" particles. (In this thesis we take 'bimetallic' to indicate that the two

metals are associated together but do not necessarily exist as an intimate mixture or alloy of the two.) A preparation method which ensures the two metals are in intimate contact is thus sought.

1.8 PREPARATION METHODS FOR BIMETALLIC CATALYSTS

The traditional methods for the preparation of bimetallic catalysts are:

- Impregnation method — this method involves addition of a solution of the second metal ions to a previously prepared mono-metallic catalyst. The catalyst is then dried, calcined and followed by reduction if a metallic catalyst is desired.
- Precipitation method — this method involves the mixing of the two or more solutions or suspensions of material in the presence a finely divided support, causing precipitation. This is generally followed by filtration, washing, drying and heating.
- Ion-exchange method — this method involves the exchange between metal-complex ions and ionic species present on the support. For example, $[Pt(NH_3)_4]^{2+}$ in aqueous solution may exchange protons on the metal oxide support.

The traditional methods for preparing bimetallic catalysts are not always successful in creating bimetallic particles. Instead, analytical microscopy shows that these methods quite often lead to the formation of multi-component systems including mono- and bimetallic particles of both metals on the surface of the support. The lack of

homogeneity in particles of bimetallic catalysts can be related to the difference of interaction strength between the support and the two precursors.

The design of catalysts with well-defined properties is thus important and this necessitates the preparation of catalysts under controlled conditions. New techniques have been developed in order to optimise the interactions between the two metals in bimetallic catalysts. The most successful method is the one which leads to a high dispersion on the support surface [38]. The main difficulty in the preparation of bimetallic catalysts is to create an intimate contact between the two metals, important for an effective bimetallic catalyst. The techniques such as impregnation and precipitation often prove to be unsatisfactory, since the high temperature decomposition of the precursor salts in reductive or oxidative atmospheres leads to a mixture of particle types [39].

The formation of nickel particles on alumina surface by thermal decomposition of $Ni(CO)_4$ by Parkyns [40], attracted attention towards the use of zero-valent metal compounds for the preparation of supported metal catalysts, and recently, for supported bimetallic catalysts. Also, the observed deviation, during the preparation of Pd-Ni catalysts by Faudon *et. al.* [41], with respect to the mean composition was greatly reduced in the case where an organometallic compound of nickel was grafted on the pre-reduced Pd particles. The process involved in the production of small supported metal particles using organometallics, thereby linking organometallic chemistry to surface chemistry has led to a new field of chemistry called ***Surface Organometallic Chemistry*** **(SOMC).** This branch of chemistry deals with the interaction between organometallic compounds and surfaces [42].

1.9 SURFACE ORGANOMETALLIC CHEMISTRY (SOMC)

Surface organometallic chemistry (SOMC) is a relatively new field of chemistry [43]. It deals with the reactions of organometallic compounds with the surface of a monometallic catalyst [44,45,46,47] and offers new possibilities for preparing heterogeneous catalysts. In recent years, there has been increasing interest in the application of SOMC to the preparation of bimetallic catalysts [48,49,50].

Unlike conventional catalyst preparation techniques, SOMC techniques can control the relative location of the two components by utilizing a very selective surface reaction between the reduced surface of a first metal, generally a noble metal, and an organometallic compound of the second metal. This phenomenon has been widely used to modify the surface of supported metallic particles, which leads to a new class of bimetallic catalysts. The organometallic compounds considered for this purpose have been the complexes of the main group elements, such as the mononuclear complexes. The support surfaces may be those of metal oxides, the internal or external surfaces of zeolites, or the surfaces of supported metal particles in zero or higher oxidation states.

In order to study the effects of the promoter on the noble metal, these bimetallic catalysts should be as homogeneous and precise in composition on the atomic scale as possible. Since the SOMC route does not involve any high temperature treatment, it can be one of the best ways to achieve such homogeneity. The basic strategy of the SOMC route is to utilize a "controlled" surface reaction, in which transformation of the monometallic materials into homogeneous bimetallic catalysts can be understood in terms of molecular processes. Due to the above advantages, the SOMC route has been used to prepare the bimetallic catalysts for fuel cells [48,51].

The reactions between the organometallic compounds $M'R_n$ (M′ is the second metal, R may be C_2H_5, C_4H_9, C_5H_5 or any other alkyl-related group) and the surface of the reduced supported metal M (M is the first metal, generally a noble metal such as Pt) may occur in one of two ways:

(a) The organometallic complex may react with the surface of the metal on which hydrogen has been pre-adsorbed under an inert atmosphere [52].

(b) The organometallic complex may react with the metallic surface in the presence of a partial pressure of hydrogen under dynamic conditions.

The latter approach has been followed during the present work. An attempt has been made to promote Pt supported on alumina by SOMC technique using various promoters such as Cr, Mn, Fe, Co, Cu, Ni and Sn.

A general mechanism has been proposed based on the reaction between tetraethyl-tin and Pt supported on Al_2O_3 [52]. It is believed that reducing the mono-metallic catalyst (Pt/Al_2O_3) produces hydrogen sites adsorbed on the parent metal (Pt–H) [53]. The reaction between the organometallic precursor of the second metal ($M'R_n$) and the pre-adsorbed hydrogen on the reduced surface of a monometallic catalyst (M–H) has been proposed to proceed via the formation of a surface physisorbed organometallic species (M_x–$M'R_{(n-x)}$). (Eq. (13))

$$x\ M\text{–}H + M'R_n \rightarrow M_x\text{–}M'R_{(n-x)} + x\ RH \qquad (13)$$

Further reaction under hydrogen results in the stepwise hydrogenolysis of the remaining alkyl groups of the second metal, yielding a metallic particle with the two metals (M_x–M′) in intimate contact (Eq. (14)) and the alkane (if alkyl precursor is used).

$$M_x\text{–}M'R_{(n\text{-}x)} + 0.5(n\text{-}x)\,H_2 \rightarrow M_x\text{–}M' + (n\text{-}x)\,RH \qquad (14)$$

The M_x–M′ species is thought to exist as naked M′ 'ad-atoms' localised on specific crystal faces on the metallic particle [54,55].

We expect a similar mechanism can be used for the reaction between cyclopentadienyl complexes used in the preparation of some of our catalysts, and the Pt monometallic surface [48,49]. For example, iron is believed to be deposited on to Pt by the decomposition of ferrocene in the presence of hydrogen according to reaction (15):

$$Fe(C_5H_5)_2 + 2H_{ads} \rightarrow Fe + 2C_5H_6 \qquad (15)$$

1.10 OUTLINE OF THE THESIS

The main aim of the work presented in this thesis was to develop suitable alumina-supported Pt- based bimetallic catalysts for selective CO oxidation. Chapter 2 mainly focuses on the experimental techniques used. This includes the preparation of the bimetallic (M-Pt) catalysts using the SOMC method and the techniques used to characterise these catalysts. Chapter 3 is concerned with the characterisation of the prepared catalysts by the following techniques:

a. UV-Visible spectroscopy
b. Inductively Coupled Plasma – Atomic Emission Spectroscopy
c. CO Chemisorption
d. Transmission Electron Microscopy
e. Thermal Analysis

Chapter 4 deals with the standardisation of the CO testing conditions for the catalysts prepared and screening of the various bimetallic catalysts prepared using Cr, Mn, Fe, Co, Ni, Cu and Sn as the promoters. Chapter 5 mainly deals with the testing of the best performing bimetallic catalysts after different treatments and under different gas mixtures. All the catalysts were tested using two different gas mixtures containing 0.50% CO, 1.25% O_2, 24.5% H_2 and balance N_2, and 0.50% CO, 0.50% O_2, 24.5% H_2 and balance N_2.

1.11 REFERENCES

1 A. J. Appleby, Edited by J. J. McKetta and W. A. Cunningham , *Encyclopaedia of Chemical Processing and Design*, Marcel Dekker, New York, **24,** 1, (1986)

2 K. Kinoshita and E. J. Cairns, (Eds.) J. Kroschwitz, M. Howe-Grant, *Kirk-Othmer Encyclopaedia of Chemical Technology*, 4th ed., Wiley, New York, **11**, 1098, (1994)

3 L. Carrette, K. A. Friedrich and U. Stimming, *Fuel Cells*, **1**, 5, (2001)

4 *www.netl.doe.gov/newsroom/backgrounder/mb-0007.html (accessed on 02/01/2004)*, Title: "Fuel Cell Auxiliary Power Unit (APU) to Reduce Heavy Duty Truck Engine Idling", National Energy Technology Laboratory, U.S. Department of Energy (2004)

5 J. H. Hirschenhofer, D. B. Staufer, R. R. Engleman and M. G. Klett, *Fuel Cell Handbook, 4th ed.*, US Department of Energy, **DOE/FETC-99/0176**, (1999)

6 T. R. Ralph and G. A. Hards, *Chem. Ind.*, **Issue No. 9**, 337, (1998)

7 W. T. Grubb, *Proceed. 11th Ann. Batt. Res. Develop. Conference*, PSC Publications Committee, Red Bank, NJ, 5, (1957)

8 W. T. Grubb Jr., *U.S. Patent No.* **2,913,511**, Nov. 17, (1959)

9 H. Grune, *1992 Fuel Cell Seminar Program and Abstracts*, The Fuel Cell Seminar Organizing Committee, Nov. 29 – Dec. 2, (1992), Tucson, Arizona, 161, (1992)

10 J. C. Amphlett, M. Farahani, R. F. Mann, B. A. Peppley and P. R. Roberge, *Proceedings of the 26th Intersociety Energy Conversion Engineering Conference*, August 4-9, (1991), Conversion Technologies/Electrochemical Conversion, American Nuclear Society, La Grange, Illinois, **3**, 624, (1991)

11 A. J. Appleby and E. B. Yeager, *Energy*, **137**, 11, (1986)

12 A. D. Little Inc., *Multi-fuel Reformers for Fuel Cells Used in Transportation—Assessment of Hydrogen Storage Technologies*, US Department of Energy, **DOE/CE/50343-1**, (1994)

13 R. L. Espino and J. L. Robbins, *Fuel and fuel reforming options for fuel cell vehicles*, in: *Proceedings of the 30th International Symposium on Automotive Technology and Automation*, Florence, Italy, (1997)

14 *http://www.delphiauto.com/news/pressReleases/pr439-02162001(accessed on 04/11/2003)*, Title: "BMW & Delphi Present The First Development Vehicle Equipped With A Solid-Oxide Fuel Cell", Press Release, Delphi (Feb 16, 2001)

15 H. H. Dobbs Jr., T. Krause, R. Kumar and M. Krumpelt, in: A.J. McEvoy (Ed.), *Proceed. 4th European Solid Oxide Fuel Cell Forum*, Lucerne, Switzerland, 85, (2000)

16 L. D. Pesce and W. R. Jenks, (Ed.) J. A. Kent, *Riegel's Handbook of Industrial Chemistry, 9th ed.*, Van Nostrand Reinhold, New York, 1068, (1992)

17 M. Gotz and H. Wendt, *Electrochemica Acta*, **43**(24), 3637, (1998)

18 H. F. Oetjen, V. M. Schmidt, U. Stimming, and F. Trila, *J. Electrochem. Soc.*, **143**, 3838, (1996)

19 A. J. Appleby and F. R. Foulkes, *Fuel Cell Handbook*, Van Nostrand Reinhold, NY, (1989)

20 K. Kordesch and G. Simander, *Fuel Cells and Their Application,* VCH Publishers, NY, 1996

21 M. G. Poirier, *et. al., 1st Int. Symp. On New Materials Fuel Cells System,* Montreal, July, 258, (1995)

22 M. Haruta, S. Tsubota and T. Kobayashi, *J. Catal.*, **144**(1), 175, (1993)

23 R. M. Torres Sanchez, A. Ueda, K. Tanaka and M. Haruta, *J. Catal.*, **168**, 125, (1996)

24 A. Siddle, *et. al.*, *Fuel Processing for Fuel Cells – A Status Review and Assessment of Prospects*, **ETSU F/03/00252/REP** (2003)

25 D. A. H. Cunningham, T. Kobayashi, N. Kamijo, and M. Haruta, *Catal. Lett.*, **25**, 257, (1994)

26 Y. Yao, *J. Catal.*, **33**, 108, (1974)

27 J. J. Spivey, *Ind. Eng. Chem. Res.*, **26**, 2165, (1987)

28 R. S. Drago, K. Jurczyk, D. J. Singh, and V. Young, *Appl. Catal. B*, **6**, 155, (1995)

29 M. L. Brown and A. W. Green, *U.S. Patent No.* **3,088,919**, May 7 (1963)

30 J. G. E. Cuhn, *U.S. Patent No.* **3,216,783**, Nov. 9 (1965)

31 S. H. Oh and R. M. Sinkevitch, *J. Catal.*, **142**(1), 254, (1993)

32 M. J. Kahlich, H. A. Gasteiger and R. J. Behm, *J. Catal.*, **171**, 93 (1997)

33 H. Igarashi, H. Uchida, M. Suzuki, Y. Sasaki and M. Watanabe, *Appl. Catal. A: Gen.*, **159**, 159 (1997)

34 J. H. Sinfelt, *Bimetallic Catalysts: Discoveries, Concepts and Applications*, Wiley, New York, (1983)

35 O. Korotkikh and R. J. Farrauto, *Catal. Today*, **62**, 249, (2000)

36 M. M. Schubert, M. J. Kahlich, G. Feldmeyer, M. Hüttner, S. Hackenberg, H. A. Gasteiger and R. J. Behm, *Phys. Chem. Chem. Phys.*, **3**, 1123, (2001)

37 W. S. Epling, P. K. Cheekatamarla and A. M. Lane, *Chem. Eng. Journ.*, **93**, 61 (2003)

38 R. Psaro and S. Recchia, *Catal. Today*, **41**, 139, (1998)

39 G. Lafaye, C. Micheaud-Especel, C. Montassier and P. Marecot, *Appl. Catal. A: General*, **230**, 19, (2002)

40 N. D. Parkyns, in: W. M. H. Sachtler, G. A. Schuit, P. Zwietering (Eds.), *Proceed. 3rd Internat. Cong. Catal.*, Amsterdam, **vol. 2**, (1964); North-Holland, Amsterdam, 914, (1965)

41 J. F. Faudon, F. Senocq, G. Bergeret, B. Moraweck, G. Clugnet, C. Nicot and A. Renouprez, *J. Catal.*, **144**, 460, (1993)

42 J. M. Basset and A. Choplin, *J. Mol. Catal.*, **21**, 95, (1983)

43 J. Margitfalvi and S. Szabo, *Catalytic Dehydrogenation*, Elsevier, Amsterdam, **27**, 373, (1986)

44 B. Didillon, C. Houtman and T. Shay, *J. Am. Chem. Soc.*, **115**, 9380, (1993)

45 F. Humblot, J.P.Candy, F. Le Peltier and B. Didillon, *J. Catal.*, **179**, 459, (1998)

46 J. P. Candy, B.Didillon and E.L. Smith, *J. Mol. Catal.*, **86**, 179, (1994)

47 B. Coq, A. Bittar and R. Dutartre, *J. Catal.*, **128**, 275, (1991)

48 E. M. Crabb and R. Marshall, *Appl. Catal. A: General*, **217**, 41, (2001)

49 E. M. Crabb, M. K. Ravikumar, Y. Qian, A. E. Russell, S. Maniguet, J. Yao, D. Thompsett, M. Hurford and S. C. Ball, *Electrochem. Solid-State Lett.*, **5**, 5, (2002)

50 Y.A. Ryndin and Y. I. Yermakov, *Surface Organometallic Chemistry: Molecular Approaches to Surface Catalysis*, 127, (1988)

51 E. M. Crabb and M. K. Ravikumar, *Electrochim. Acta*, **46**, 1033, (2000)

52 J. Margitfalvi, M. Hegedüs, S. Göbölös, E. Karn-Tálas, P. Szedlacsek, S. Szabó and F. Nagy, *8th International Congress on Catalysts*, **vol. IV** , Berlin, 903, (1984)

53 J. Margitfalvi, H. P. Jalett, E. Talas, A. Baiker and H. U. Blaser, *Catal. Lett.*, **10**, 325, (1991)

54 F. Lefebvre, J. -P. Candy, C. C. Santini and J. -M. Basset, *Topics in Catalysis*, **4**, 211, (1997)

55 B. Coq, A. Goursot, T. Tazi, F. Figuéras and D. R. Salahub, *J. Am. Chem. Soc.*, **13**, 1485, (1991)

2

Experimental Techniques

This chapter includes information regarding the materials and reagents used and the methods employed for the preparation, characterisation and evaluation of catalysts in this study.

2.1 MATERIALS AND REAGENTS USED

The materials and the reagents used in the present study and their sources are listed below. These were used as received and no pre-treatment was given to these materials.

Table 2-1: DETAILS OF THE MATERIALS USED IN THE PRESENT STUDY

Material/Reagent	Grade	Source
5% Pt/Al_2O_3	—	Johnson Matthey, UK
Tetra-n-butyl tin	LR*	Acros Organics
Bis (cyclopentadienyl) iron	LR	Aldrich Chem. Co.
Bis (cyclopentadienyl) nickel	LR	Aldrich Chem. Co.
Bis (cyclopentadienyl) chromium	LR	Aldrich Chem. Co.

Bis (cyclopentadienyl) cobalt	LR	Aldrich Chem. Co.
Bis (cyclopentadienyl) manganese	LR	Aldrich Chem. Co.
Manganese (II) acetylacetonate	LR	Strem Chemicals
Copper (II) acetylacetonate	LR	Strem Chemicals
Hydrogen	High Purity	Air Products
Nitrogen	High Purity	Air Products
Carbon monoxide (pure)	High Purity	Aldrich Chem. Co.
2% CO in H_2	High Purity	Air Products
5% O_2 in N_2	High Purity	Air Products
0.5% CO, 1.25% O_2, 24.5% H_2 in N_2	Special Gas	Air Products
0.5% CO, 0.5% O_2, 24.5% H_2 in N_2	Special Gas	Air Products
Heptane	HPLC	Aldrich Chem. Co.
Toluene	LR	Aldrich Chem. Co.

* LR: Laboratory reagent

2.2 PREPARATION OF THE BIMETALLIC CATALYSTS

The common methods used for the preparation of the bimetallic catalysts are based on the principle of co-impregnation, successive impregnation or co-exchange with the salts of two metals [1,2]. However, these traditional methods of preparation often lead to the formation of multicomponent systems including some bi- and monometallic particles.

Surface Organometallic Chemistry [3,4] (SOMC) provides a novel method of preparing supported bimetallic catalysts. In the preparation of a supported metal catalyst, generally, a suitable precursor is decomposed on the surface of the support by heating in an oxidising atmosphere. This treatment leads to formation of the corresponding metal oxide. The metal oxide so formed is then reduced by hydrogen. The SOMC route involves the addition of a second metal as an organometallic compound to a solution containing the reduced, supported metal catalyst; in this work, Pt/Al_2O_3. The organometallic precursor of the second metal reacts with the pre-adsorbed hydrogen on the surface of the platinum, thus creating an intimate contact between the two metals. In principle, SOMC provides a greater control in the location of the metals in a bimetallic catalyst than any other method.

2.2.1 SOMC APPARATUS

A specially designed reactor constructed in our laboratory for the preparation of the bimetallic catalysts is shown in Fig. 2-1.

A heating mantle was used to heat the reactor. A small length of PTFE tubing was extended from the exit of the reactor, and with the help of a metallic T-piece, one side of it was fitted with a puncture seal. A sample of the effluent gas was taken through the puncture seal and injected into the gas chromatograph (GC) using a gas syringe.

A Perkin-Elmer 8410 gas chromatograph fitted with a flame ionization detector (FID) was employed in the present study. A Porapak-T on Chrompac 80/100 mesh column (OD $\frac{1}{8}$", 8 m long) operated at 100 °C was used for the analysis of the exit gas.

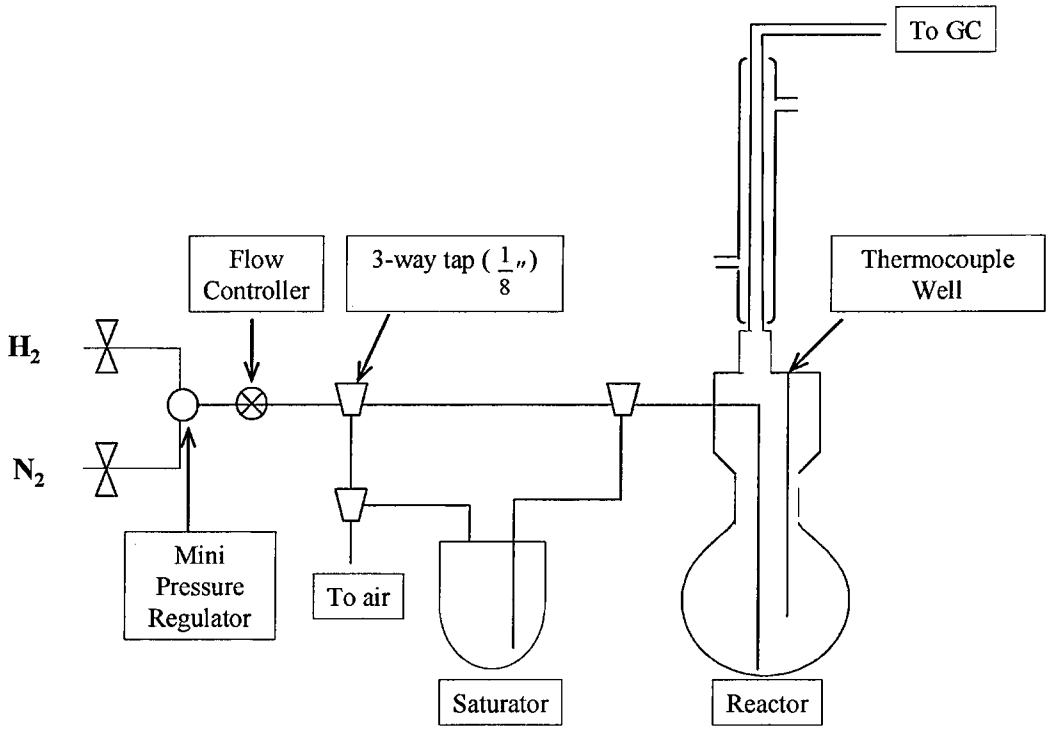

FIGURE 2-1: The SOMC apparatus for the preparation of the bimetallic catalyst

2.2.2 EXPERIMENTAL PROCEDURE

Two different catalysts (in two different batches) of proprietary 5% Pt supported on alumina was provided by Johnson Matthey, Sonning Common, UK. The respective Pt dispersion values (determined by CO pulsed technique at Johnson Matthey Technology Centre, UK) are listed in Table 2-2.

Table 2-2: DEFINITIONS FOR LOW AND HIGH DISPERSED Pt/Al_2O_3 SYSTEMS

System	Batch I	Batch II
Low	4.60%Pt, 29% dispersion	5.18% Pt, 26% dispersion
High	4.94% Pt, 51% dispersion	5.20% Pt, 54% dispersion

A known mass of the 5% Pt/Al_2O_3 catalyst, Table 2-3, was loaded into the pyrex glass reactor. The reactor was attached to the apparatus (as shown in Fig. 2-1) and mounted in the heating mantle. The catalyst was then purged with nitrogen for about half an hour to remove any air from the system. The Pt/Al_2O_3 catalyst was then reduced in the reactor under flowing hydrogen (flow rate: 60 – 100 $cm^3\ min^{-1}$) at 200 °C. The temperature was maintained at 200 °C for 3 hours and then the catalyst was allowed to cool down to room temperature under a hydrogen atmosphere.

The amount of each organometallic precursor (shown in column 4 of Table 2-3) required for the preparation of the bimetallic catalysts was calculated using the platinum metal dispersion obtained by the chemisorption studies of CO on Pt/Al_2O_3 (Table 2-2). Metal dispersion is defined as the fraction of the metal atoms on the surface of the catalyst compared to the number of metal atoms in the catalyst. The kind and the amount of the precursor used for the preparation are included in columns 3 and 4 of Table 2-3, respectively. The amount of precursor used was calculated using the following equation.

$$\text{Mass} = \frac{\text{Pt} - \text{loading} \times \text{dispersion} \times W_{catalyst} \times FW_{precursor} \times x}{195} \qquad (3)$$

where,

$FW_{precursor}$: Formula mass of the precursor used

195: Relative atomic mass of platinum

$W_{catalyst}$: Mass of the Pt/Al_2O_3 taken

x: Theoretical surface coverage of surface Pt atoms by M expressed in monolayer equivalents

Table 2-3: LIST OF THE BIMETALLIC CATALYSTS PREPARED IN THIS STUDY

System	$W_{catalyst}$ / g	Precursor used	$W_{precursor}$ / g
(1:2)SnPt(low) (I)	8.000	$Sn(n\text{-}C_4H_9)_4$	0.1072
(1:1)SnPt(low) (I)	8.000	$Sn(n\text{-}C_4H_9)_4$	0.2152
(1:2)FePt(low) (I)	8.000	$Fe(C_5H_5)_2$	0.0589
(1:1)FePt(low) (I)	10.00	$Fe(C_5H_5)_2$	0.1328
(1:2)CoPt(low) (II)	8.000	$Co(C_5H_5)_2$	0.0515
(1:1)CoPt(low) (II)	8.000	$Co(C_5H_5)_2$	0.1180
1:2 CrPt(low) (II)	2.500	$Cr(C_5H_5)_2$	0.0193
1:2 NiPt(low) (II)	4.000	$Ni(C_5H_5)_2$	0.0383
1:2 CuPt(low) (II)	3.000	Cu(II)- acetylacetonate	0.0293
1:2 CuPt(low) (II)[#]	2.000	Cu(II)- acetylacetonate	0.0184
1:2 MnPt(low) (II)[#]	2.500	Mn(II)-acetylacetonate	0.0219
(1:2)SnPt(high) (I)	8.000	$Sn(n\text{-}C_4H_9)_4$	0.1885
(1:1)SnPt(high) (I)	8.000	$Sn(n\text{-}C_4H_9)_4$	0.3769
(1:2)FePt(high) (I)	8.000	$Fe(C_5H_5)_2$	0.0963
(1:1)FePt(high) (I)	6.000	$Fe(C_5H_5)_2$	0.1412
(1:2)CoPt(high) (II)	8.000	$Co(C_5H_5)_2$	0.1128
(1:1)CoPt(high) (II)	8.000	$Co(C_5H_5)_2$	0.2068

$W_{precursor}$: weighed amount of the precursor taken for the preparation of the catalysts

(I), (II) refer to the fact that the catalysts were prepared using Batch-I or II of the monometallic catalyst, respectively.

[#] Catalyst preparation carried out in toluene.

Note: This is to acknowledge Dr. Y. Qian for his efforts in preparing SnPt catalysts used in the present study.

In general, the required amount of the organometallic precursor was dissolved in heptane or toluene (see Table 2-3) in air, except when $Co(C_5H_5)_2$, $Mn(C_5H_5)_2$ and $Ni(C_5H_5)_2$ were used. Mn, Co and Ni precursors are air sensitive so these preparations were carried out inside a glove-box under an argon atmosphere. The Mn and Ni precursors, also being moisture sensitive, were dissolved in dry heptane and added to the saturator under nitrogen. After purging the saturator with nitrogen gas for 15-20 minutes to remove air from the system, the contents of the saturator were transferred into the reactor containing the reduced Pt/Al_2O_3 catalyst under nitrogen by changing the direction of the gas flow. Hydrogen gas was then passed through the reactor. The reaction was allowed to continue at room temperature for about 12 hours and then at approximately 95 °C for a further 8–12 hours. Sometimes, when the solvent level in the reactor seemed to be low, more heptane was added to the reactor vessel through the saturator, after purging with nitrogen for about 20 minutes. The reactor was monitored by analysing the exit gas using gas chromatography.

After the reaction, the contents of the reactor were discharged, filtered, and washed repeatedly with heptane (or toluene) to remove any unreacted organometallics. The filtrates were transferred into a small volumetric flask, and any unreacted organometallic compound was determined by UV-Visible spectroscopy. The catalyst was allowed to dry out in the fume cupboard in the air.

The dried catalyst was transferred into the reactor and purged with nitrogen gas for about 30 minutes to remove any air from the system. The contents of the reactor were then reduced under flowing hydrogen at 200 °C for 3 hours, and finally flushed with nitrogen for about 20 minutes to prevent combustion.

2.3 TECHNIQUES FOR THE CHARACTERISATION OF THE CATALYSTS

The following techniques were used for the characterisation of the catalysts prepared by the SOMC route in the present study:

- Ultraviolet–Visible (UV–Vis) Spectroscopy
- Transmission Electron Microscopy (TEM) and Scanning Transmission Electron (STEM) Microscopy
- CO Chemisorption
- Temperature Programmed Reduction (TPR)
- Thermal Analysis: Thermogravimetric Analysis / Differential Scanning Calorimetry (TGA-DSC)

2.3.1 ULTRAVIOLET-VISIBLE (UV–Vis) SPECTROSCOPY

INTRODUCTION

Ultraviolet–Visible (UV–Vis) spectra measure absorbance due to electronic transitions. The transitions which occur are in the energy domain of the ultraviolet (200 – 400 nm) and visible (400 – 800 nm) ranges of the electromagnetic spectrum. A UV–Vis spectrum is obtained by measuring light absorption as a function of wavelength [5]. The electronic absorption spectrum is a function of the molecule as a whole and is therefore not a good detector of functional groups. While electronic absorption spectra are lacking in qualitative information about a molecule, these spectra can be used as an excellent tool for telling us how much of a particular molecule is present in a given sample.

THEORY

Different molecules absorb radiation of different wavelengths. The electronic transitions observed in the structures we are concerned with arise from conjugated

π–bond systems. In these systems light promotes one electron from the highest-energy occupied (bonding) molecular orbital (HOMO) into the lowest-energy unoccupied (antibonding) molecular orbital (LUMO). The excited electron falls back after a certain amount of time. For organic molecules the most common transitions are π to π* or n to π*. Various electronic transitions possible in a molecule are shown in Fig. 2-2.

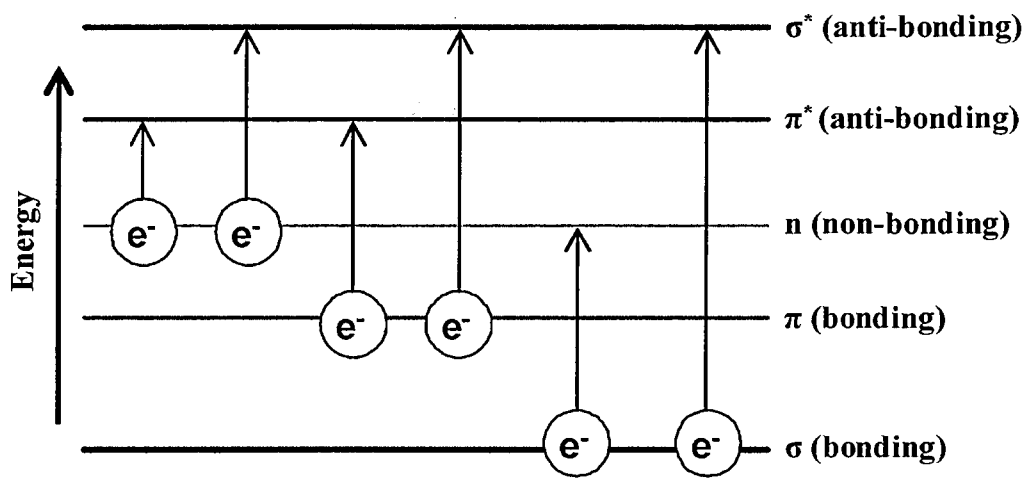

FIGURE 2-2: Various electronic transitions of σ, π and n electrons

The spectrum is measured by comparing the intensity of light at a fixed wavelength passing through a cell containing solvent only (I_0), with the intensity passing through a cell containing the sample dissolved in the same solvent (I_t), and repeating this for all wavelengths. Generally data is presented in terms of absorbance (A) where

$$A = \log(I_0/I_t) \tag{4}$$

The main reason for this is the linear dependence of the absorbance on the concentration of the absorbing species in the solution (c). Lambert–Beer's law states

that the absorbance in a UV–Vis spectrum depends upon the path length of the sample cell (l) and the molar concentration of the sample in the solution.

$$A = \varepsilon l c \tag{5}$$

where the constant of proportionality, ε is known as *absorptivity*.

APPARATUS

UV–Vis spectra were collected using a UVIKON XL (Biotek Instruments) spectrophotometer. A schematic diagram of the working of a UV–Vis spectrophotometer is shown in Fig. 2-3. A beam of light from a visible and/or UV light source is separated into its component wavelengths by a monochromator, either a prism or a grating. A half-mirrored device is used to split each monochromatic beam into two equal intensity beams. One beam, the sample beam, passes through a quartz cuvette (Fisher brand FB 55147) containing a solution of the compound being studied in a transparent solvent, here heptane or toluene. The other beam, referred to as the reference beam, passes through an identical cuvette containing only the solvent. The intensities of these light beams are then measured by electronic detectors and compared.

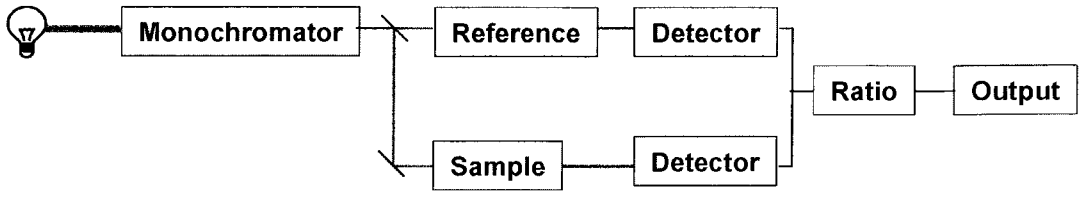

FIGURE 2-3: A schematic diagram of a typical UV–Visible spectrophotometer.

EXPERIMENTAL PROCEDURE

For the present studies, a standard solution of the metal precursors was prepared and UV–Vis spectra were measured. Spectra of the filtrates were also obtained after the preparation of the bimetallic catalysts. Knowing the absorbance of the two solutions of same precursor, the amount of precursor left in the filtrate (c_2) was calculated as follows:

$$\frac{A_1}{A_2} = \frac{c_1}{c_2} \Rightarrow c_2 = \frac{A_2}{A_1} c_1 \tag{6}$$

where A_1, A_2 and c_1, c_2 are the absorbances and concentrations of the standard solution and filtrate, respectively. Knowing the volume of the filtrate collected, enabled the calculation of unreacted precursor.

UV-Vis spectroscopy was used to study any precursor remaining in the filtrate for the Fe and Co samples after the SOMC preparation. The standard solution of ferrocene was prepared with 0.0430 g $Fe(C_5H_5)_2$ in 20 cm^3 of heptane and that of cobaltocene contained 0.1100 g $Co(C_5H_5)_2$ in 20 cm^3 heptane.

Transition metal ions have such excited state levels that it is known that their absorption bands lay in the range 400 – 700 nm. Hence, in the UV–Vis spectra the absorption peak in the 200 – 400 nm range is a result of the presence of $-C_5H_5$ group in the solution. The position of peak maxima shifts with various metals.

2.3.2 TRANSMISSION ELECTRON MICROSCOPY (TEM), SCANNING TRANSMISSION ELECTRON MICROSCOPY (STEM) AND ENERGY DISPERSIVE X-RAY ANALYSIS (EDX)

INTRODUCTION

The electron microscopes constitute a family of very powerful experimental tools to characterise catalysts. All electron microscopes are based on a common principle of physical phenomena such as reflection and scattering, occurring when an accelerated electron beam interacts with matter. By using appropriate detection devices together with the electron microscope, these physical phenomena may be analyzed and very useful information about the texture, structure and the chemical constituents of the catalysts can be obtained.

The major attraction of Transmission Electron Microscopy (TEM) for a catalytic chemist comes from its inherent ability to provide details of the local microstructure of the catalyst, rather than the information averaged over the entire sample. The image in TEM effectively represents a projection of the sample in the direction of the beam. The apparent particle size depends on the defocus and on the relative height within the sample, so the shape of only that particular particle can be deduced from a single image in TEM.

Scanning Transmission Electron Microscopy (STEM) differs significantly from conventional Transmission Electron Microscopy (TEM) since in order to form an image of a specimen, it is not necessary to refocus the scattered electrons. The image is formed simply by detecting the electrons scattered in some direction as a function of the probe position. Therefore, it is easier in STEM to include the scattered electrons at much larger angles than in the conventional TEM.

THEORY AND INSTRUMENTATION

A standard TEM can be compared to an overhead slide projector. A projector shines a beam of light through the slide. As the light passes through the slide it will be affected by the structures and objects on the slide. This transmitted beam of light will then be projected onto the viewing screen, forming an enlarged image of the slide.

TEM shines a beam of electrons through the specimen and whatever part transmits through the specimen is projected onto a phosphor screen for the user to see. The basic construction of a modern transmission electron microscope [6] is shown schematically in Fig. 2-4.

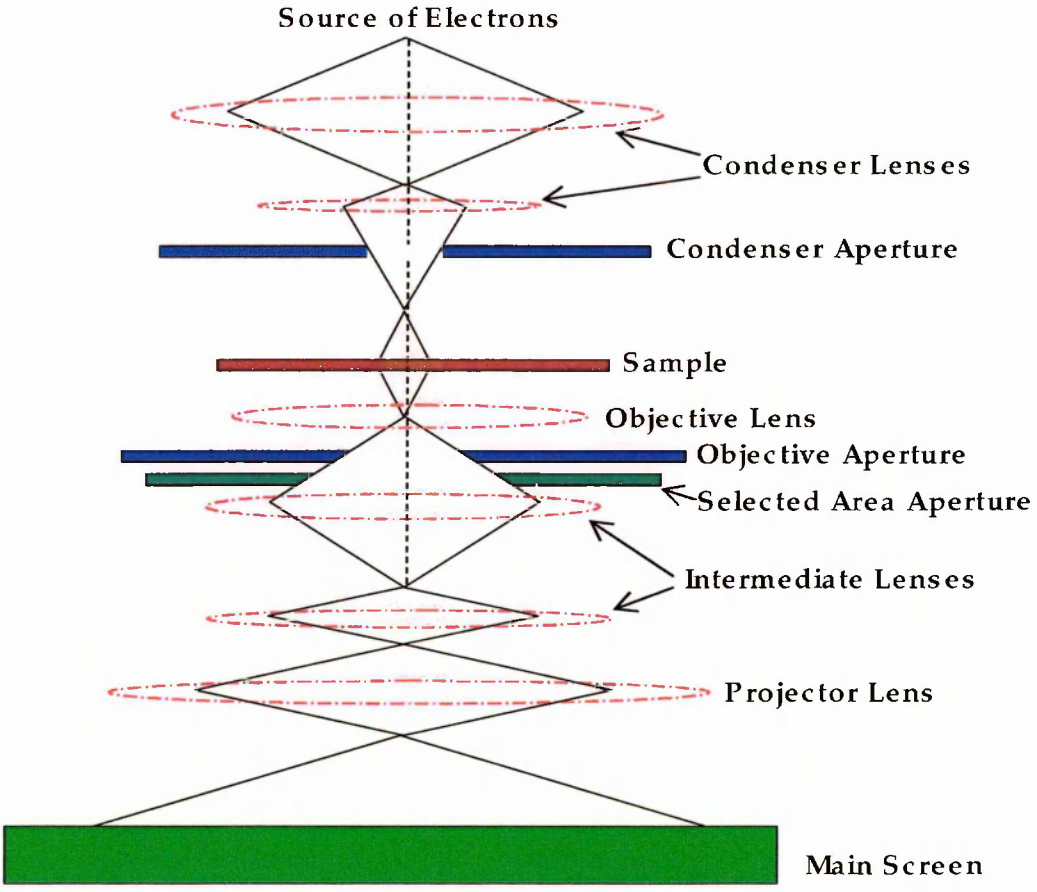

FIGURE 2-4: The schematic representation for the Transmission Electron Microscope.

Referring to the Fig. 2-4, the working of a TEM can be explained as follows:

- The 'Source' at the top represents an electron gun that generates a monochromatic stream of electrons.
- The condenser lenses help in focussing this stream of electrons into a small, thin and coherent beam. With the help of the first condenser lens, the general size range of the final spot that strikes the sample can be controlled, while the second lens can be used to change the size of the spot on the sample from a wide dispersed spot to a pin-pointed beam.
- A user can restrict the beam by selecting or knocking out high angle electrons with the help of a condenser aperture. High angle electrons are those far from the optic axis, the dotted line down the centre.
- The specimen is placed in the direction of the beam. When the beam strikes the sample, a part of it gets transmitted. With the help of the objective lens, this transmitted portion of the incident beam can be focussed into an image. By employing the objective and the selected area metal aperture, the beam can be restricted.
- The image, passed down the column through the intermediate and projector lenses, is enlarged all the way.
- The image strikes the phosphor image screen and light is generated, allowing the user to see the image. The intensity of the areas represents the thickness or density of the specimen which in turn reflect the amount of electrons transmitted.

The use of an annular dark field (ADF) detector in the scanning transmission electron microscope (STEM) was originally proposed by Crewe and colleagues [7,8] as a detector for large angle elastically scattered electrons. The idea for the *high angle*

annular detector (HAADF) arose out of the attempts to extend the Crewe's technique for imaging the small catalyst particles [9]. It has been pointed out that the use of a high angle (50–200 mrad) annular dark field detector should provide a signal that is proportional to the atomic number of the local specimen region because it involves a collection of high angle scattered electrons. Howie [10] suggested a modification that by increasing the inner angle of the inner detector, the Bragg's reflections could be prevented from reaching the detector. Despite the reduced efficiency of collecting only a fraction of total elastic scattering, the high angle detector has proved extremely successful for catalyst studies [11].

The high angle elastic scattering of electrons in STEM depends strongly on the atomic number ($\propto Z^{1.7}$) of the sample atoms (close to the Z^2 dependence of the Rutherford scattering cross-section [12,13]). This sensitivity with respect to atomic number is commonly known as *Z-contrast*. A Z-contrast image is formed in STEM by focussing an electron probe on the specimen and collecting electrons, point by point, that scatter out to high angles using a high angle annular dark field detector.

STEM has been found highly useful for catalytic studies, such as improving the image contrast especially for the detection of clusters of heavy atoms on low atomic number substrates. The novel use of HAADF-STEM for determining the three-dimensional structure of the supported metal nano-catalysts at very high spatial resolution of ~1 nm has been elegantly demonstrated for Pd-Ru nano-catalysts supported on silica [14].

The principle of operation and some applications of STEM have been nicely summarised by Oatley and co-workers [15]. A tiny, convergent electron beam is scanned over a defined area of the sample. Electrons transmitted through the specimen are collected on a detector further down the microscope column. At each spot, the

generated signal is simultaneously recorded by selected detectors, building up an image. The signal is usually obtained by detecting either the secondary electrons [16,17] or the characteristic X-rays [18,19,20].

The characteristic spectrum of X-rays emitted by the specimen after excitation by high-energy electrons is used to obtain information about its elemental composition. This is known as Energy Dispersive X-ray (EDX) analysis.

APPARATUS AND EXPERIMENTAL PROCEDURE

The transmission electron micrographs were taken on TEM model - FEI Tecani F20 (S-Twin) at Johnson Matthey Technology Centre (JMTC), UK, operating at an accelerating voltage of 200 kV. The instrument was fitted with an ultra-high resolution STEM HAADF detector with magnification range up to 10000 kx and the point resolution of 0.24 nm. EDX analysis was carried out using EDAX Si(Li) detector.

A small amount of the Fe-promoted catalyst was taken in a small sample bottle half-filled with deionised water. The system was sonicated in an ultrasonic bath for a few minutes to disperse the catalyst in water. A TEM Cu-grid (Holey carbon film on 300 mesh) was dipped in the dispersed medium for few seconds and then allowed to dry in air. In order to make sure that all the solvent evaporated, the grids were placed under an infrared lamp for 3–4 hours. The samples were prepared at least a day before the experiments were carried out.

The samples on the Cu-grid with Co-promoted catalysts were prepared using a dry-sample technique due to the time constraint. In this technique, a very small amount of catalyst was taken between two clean glass plates, pressed and rubbed to produce a very fine powdered layer of the catalyst on the plate. A Cu-grid was placed on the well powdered sample, and pressed between the two plates again for a few seconds. A good

amount of sample was taken up by the grid. With this dry sample preparation technique, there was no need to dry the grid before placing it inside the electron microscope under vacuum and so the microscopy experiments could be started right away.

2.3.3 DETERMINATION OF THE METAL DISPERSION BY CHEMISORPTION

Gas reactions catalysed by solid materials occur on the surfaces of porous catalysts. The rate of product formation is a function of the available surface area. In other words, the greater the surface area accessible to the reactants, the larger is the throughput. So, in the case of supported metal catalysts, the information on the metal surface area or dispersion is very important. Dispersion is defined as the ratio of metal atoms on the surface of the catalyst to the total metal atoms in the catalyst. The metal dispersion is important in predicting the performance of a catalyst, because only the metal particles on the surface acting as active sites are involved in adsorption, and hence in the reaction.

For typical supported metal catalysts, the total surface area (metal particle + support) can be determined using physisorption and the free-metal surface area or metal dispersion can be determined through the selective chemisorption of a suitable adsorbate [21]. Chemisorption plays an important role both in the laboratory research for the development of new catalysts, and in industrial production.

ADSORPTION

Accumulation of the molecular, atomic or ionic species of one substance over the surface of another is called adsorption. The surface on which adsorption takes place is called the *adsorbent* and the substance adsorbed is called the *adsorbate*.

Depending on the strength of interactions between adsorbate and adsorbent, there are two types of adsorption – *physical adsorption (physisorption)* and *chemical adsorption (chemisorption)*. Physisorption occurs with a low enthalpy of adsorption, ΔH_{ads}, generally <20 kJ mol^{-1} whereas the chemisorption process is associated with higher values of ΔH_{ads}, generally >80 kJ mol^{-1}.

In many cases, adsorption and absorption occur simultaneously and it is not possible always to distinguish these two experimentally, the generic term *sorption* is commonly used to describe the general phenomenon of gas uptake by solids.

ADSORPTION ISOTHERMS

The relationship, at a given temperature, between the equilibrium quantity of gas adsorbed by a solid surface and the equilibrium pressure is known as the *adsorption isotherm*. The extent of adsorption may be followed gravimetrically, volumetrically or by the measurement of changes in the physical properties of the adsorbent [22]. The measurement of adsorbate–adsorbent equilibrium is often very difficult, particularly in the case of strong adsorption because the equilibrium pressures are extremely low [23]. The first classification of physical adsorption isotherms was presented by Brunauer *et. al.* [24]. Many theories and models have been reported in the literature to explain these different types of isotherms [25].

CHEMISORPTION

Chemisorption is based on the formation of a strong chemical bond between the adsorbate molecules with the exposed metal surface of the adsorbent. The selected gas molecule is chemisorbed under the conditions which allow the formation of a monolayer of the adsorbate gas on the metal surface without significant uptake by the

non-metallic part (the support) through physical adsorption. This requires both a careful selection of a suitable gas, of the suitable experimental conditions and procedures, and knowledge of the stoichiometry of adsorption. Many useful reviews on the estimation of metal dispersion and describing various aspects of gas chemisorption are available in the literature [26,27,28].

The choice of the adsorbate gas depends upon the metal to be studied. Many workers have used the selective chemisorption of gases such as hydrogen, oxygen and carbon monoxide (CO) to estimate the surface area of the supported metal particles. Platinum, in particular, has been studied extensively [29,30,31]. By assuming a stoichiometry for the reaction between a surface metal atom and the chemisorbing gas, it is possible to calculate the ratio of surface to total metal atoms. The average size of the metal particle can be calculated by assuming certain geometry of the particles. Many workers have discussed various assumptions involved in such calculations [32,33]. Chemisorption permits the detection of the particles having an average size below that measurable by X-ray diffraction. The literature is in general agreement that platinum on supports such as alumina, silica-alumina [34,35] and silica gel is extremely well dispersed in freshly prepared catalysts which have not been reduced at temperatures above 500 °C. This conclusion has been derived from the observed H, O and CO to total Pt atomic ratios close to unity. In all cases, it was assumed that one surface metal atom chemisorbs only one atom of hydrogen or one molecule of carbon monoxide. This assumption was shown to be very much the case in real systems by Wilson and Hall [36].

Hydrogen chemisorption has proved to be a useful tool for the determination of the surface area of the supported platinum [37] and nickel [38]. But it has not been possible to apply this technique to supported palladium catalysts, because palladium

tends to absorb hydrogen [39]. From the study of a series of isotherms for the hydrogen-palladium system [40,41,42], it was suggested that in order to exclude interference of absorption during chemisorption measurements, the experiments should be carried out at higher temperatures and low hydrogen pressures [43].

The use of CO chemisorption for metal surface area measurements can be traced back to Emmett and Brunauer [44], who used it during their investigation of unsupported iron catalysts for ammonia synthesis. It was they who first distinguished between chemisorbed and physisorbed CO and used a double isotherm scan in order to establish the amount of strongly held (chemisorbed) CO. This procedure, used extensively by Yates *et. al.* [45], has now become standard practice in the determination of CO chemisorption isotherms on metals [46, 47, 48].

Scholten *et. al.* [39] proposed the use of carbon monoxide as an adsorbate for palladium. These investigators found reasonable agreement between the sizes of Pd crystallites on various supports as derived from CO chemisorption and determined by electron microscopy and X-ray line broadening. It has been suggested that the stoichiometry of CO chemisorption is also reasonably constant on small platinum crystallites and could conceivably correspond to $CO/Pt_{surface}$ equal to one [49].

LANGMUIR ADSORPTION ISOTHERM

The Langmuir adsorption isotherm model [50] is based on the assumption of monolayer adsorption on a homogeneous surface. The Langmuir isotherm equation remains the most commonly used for chemisorption because of its ability to fit a wide variety of adsorption data quite well. The simplicity of the isotherm equation and the ease with which its adjustable parameters can be estimated also contribute to its wide usage.

Let x be the amount of gas adsorbed at any given pressure, P and x_{max} be the maximum amount that the surface can take up, then the fractional surface coverage (θ) is given by:

$$\theta = \frac{x}{x_{max}} \tag{7}$$

Each unit area of surface is assumed to contain n unit of active sites, with each active site adsorbing only one atom or molecule of the gas. All sites are assumed to be energetically equivalent. A dynamic adsorption–desorption equilibrium gets established and the amount of gas adsorbed at a given pressure can be derived by equating the derived rates of the adsorption and desorption processes.

The equilibrium can be represented by the equation

$$A + M \rightarrow A—M$$

where A is the adsorbing molecule or atom and M is an adsorption site and A—M is the adsorbate–active site complex. The equilibrium constant (b) is defined by the relationship

$$b = \left(\frac{[A—M]}{[A][M]} \right)_{eq} \tag{8}$$

At equilibrium, [A] can be replaced by P, the pressure of A, and [M] which is concentration of vacant sites, by $n(1-\theta)$ and [A—M] is given by $n\theta$. Then

$$b = \frac{n\theta}{n(1-\theta)P} \tag{9}$$

On rearranging, one can write

$$\theta = \frac{bP}{1+bP} \tag{10}$$

where b is called the *adsorption coefficient* of A on the solid and P is the pressure of adsorbing molecule at equilibrium. This is known as the ***Langmuir adsorption isotherm*** (Fig. 2-5).

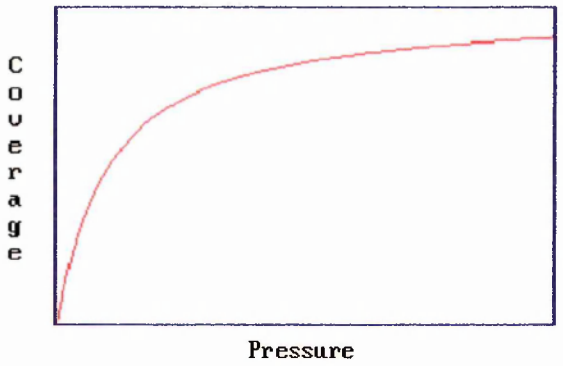

FIGURE 2-5: A typical Langmuir adsorption isotherm for the adsorption of a gas on a solid.

Not all adsorptions obey the Langmuir adsorption isotherm. Most importantly, the assumption of energetic equivalence of all sites is practically impossible. Also, since surfaces are not atomically smooth, the enthalpy of adsorption falls with the increasing surface coverage.

Other isotherms have been devised to eliminate the assumption of equivalence. By using more realistic assumptions, many modifications have been made to the Langmuir isotherm, which are well summarised in the monographs of Yang [51], Adamson [52], Ruthven [53], and Rudzinski and Everett [54].

DISPERSION MEASUREMENTS

The dispersion of a catalyst can be calculated from the Langmuir isotherm. This can be done by successively doping the sample with a known volume of gas (CO for Pt catalysts was used) at different pressures and plotting the quantity of gas adsorbed after each doping against the equilibrium pressure. The quantity of gas in the dosing volume to be doped onto the sample (Q_I^n) is:

$$Q_1^n = \frac{V_d}{RT_d}\left(P_d^n - P_e^{n-1}\right) \tag{11}$$

where

V_d : dosing volume

R : Universal gas constant

T_d : Dosing temperature

P_d^n : Pressure in dosing volume for doping n

P_e^{n-1} : Equilibrium pressure for doping (n-1)

Amount of gas in the gas phase after adsorption (Q_2^n):

$$Q_2^n = \frac{P_e^n}{R}\left(\frac{V_d}{T_d} + \frac{V_s}{T_s}\right) \tag{12}$$

where

V_s : Sample volume

T_s : Temperature of sample holder

P_e^n : Equilibrium pressure for doping n

Therefore the quantity of gas adsorbed onto the catalyst after each doping (Q_3^n) is:

$$Q_3^n = \left(\sum_1^n Q_1^n\right) - Q_2^n \tag{13}$$

The amount of CO adsorbed on the metal surface can be obtained from the volume of CO adsorbed at zero pressure (Q_0). Traditionally, the value of Q_0, more commonly known as Point A (shown in Fig. 2-6), is obtained by plotting Q_3^n against P_e^n (shown in Figs. 3-17 – 3-23) and extrapolating the horizontal portion of the isotherm back to the region of zero pressure. However, in our case not all the isotherms seemed to achieve a horizontal section in the pressure range studied and so the given values are calculated by extrapolation to zero pressure (Point A) and also Point B (value at start of the linear portion). Brunauer and Emmett initially suggested [55] that monolayer capacity might be represented by the Point A (shown in Fig. 2-6) but after a

detailed study [56] Point B was selected instead of Point A. Their selection was later supported by a good agreement between the amount of gas adsorbed at Point B and the monolayer capacity calculated by the BET equation for a variety of systems [57]. However the frequent divergence between the two quantities has been reported by the others [25]. If the isotherm was horizontal then both the values would give the same result.

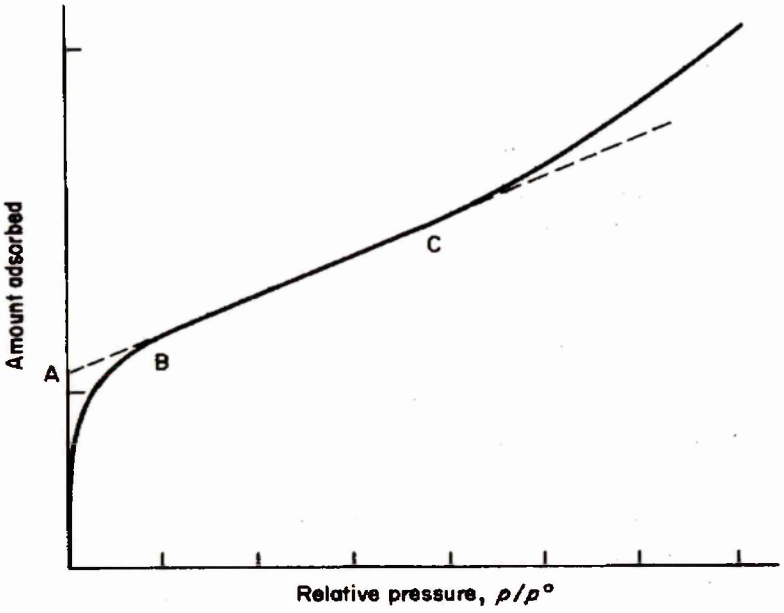

FIGURE 2-6: A typical isotherm showing 'Point A' and 'Point B'

For Pt catalysts, the amount of chemisorbed CO can be obtained from the relationship,

$$\frac{CO}{M} = \frac{Q_0}{\left(\text{Mass} \times \left(\frac{\%\,\text{Metal}}{RM}\right)\right)} \qquad (14)$$

where:

Q_0: Amount of CO adsorbed on the metal surface extrapolated to zero pressure.

CO/M: CO molecules adsorbed on to total number of metal atoms.

Mass: Mass of sample (g)

%Metal: Percentage metal in sample (expressed as % of weight of the support)

RM: Relative atomic mass of the metal component

Assuming that one CO molecule is chemisorbed per metal atom on the surface, the percentage of the surface atom i.e. the metal dispersion is given by the following relationship:

$$\text{Dispersion} = \frac{\text{CO}}{\text{M}} \times 100\ \% \qquad (15)$$

EXPERIMENTAL SET-UP

A volumetric system of a special design (shown in Fig. 2-7) was used for the adsorption measurements.

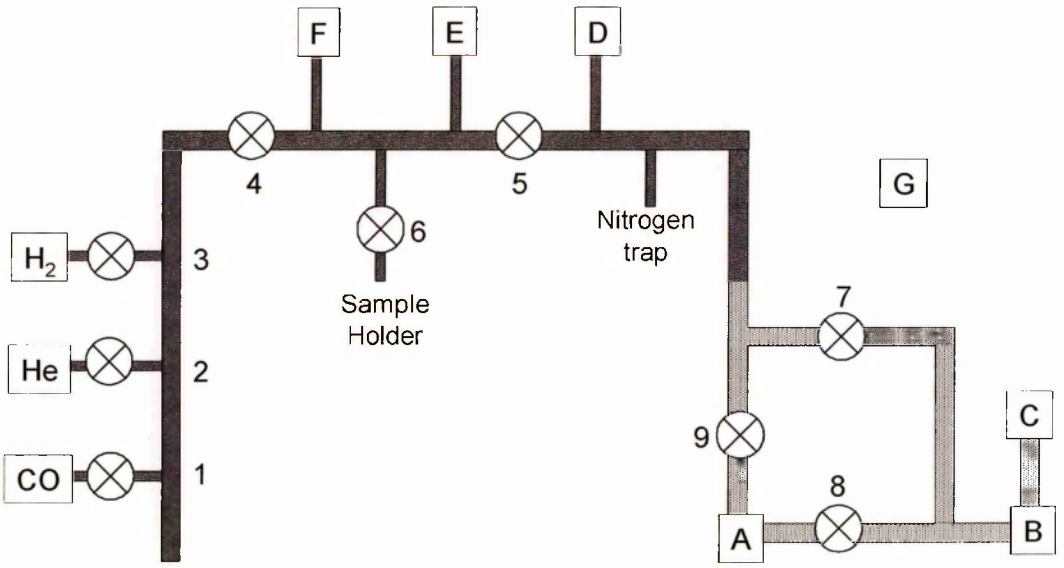

FIGURE 2-7: A schematic representation of the experimental set up used for chemisorption studies.

Key: Glass tubing

Metal tubing

The apparatus included an Edwards Active Pirani Gauge [C], an Edwards Active Inverted Magnetron [D], two Edwards Barocel Capacitance Barometers [E and F], and Edwards Active Gauge Controller [G]. The vacuum was maintained by an Edwards two way Rotary Pump [B] and Edwards Air Cooled Diffusion pump [A].

EXPERIMENTAL PROCEDURE FOR STUDYING CHEMISORPTION

The chemical adsorption of CO was carried out in a conventional volumetric apparatus, shown schematically in Fig. 2-7, at room temperature in the pressure range of 5–50 mbar. About 0.1 g sample of the catalyst was loaded into a calibrated sample holder (Fig. 2-8) and attached to the vacuum line.

The sample was out-gassed at 250 °C for about half an hour (10^{-3}-10^{-5} mbar pressure) and then allowed to cool to room temperature. The sample was reduced under 750 mbar pressure of hydrogen at 350 °C for half an hour and then out-gassed at the same temperature for a further half an hour. The furnace was removed and out-gassing was continued until the sample cooled down to room temperature.

Once cooled, a certain volume of carbon monoxide was allowed into the dosing volume (V_d) through tap 4 while tap 5 and 6 were still closed (Fig. 2-7), and the pressure was noted as P_d and the temperature as T_d. Pressure measurements were carried out using the capacitance barometer [E] and read on the gauge controller [G]. The temperature was measured using a thermocouple attached to the dosing volume, and read on a digital thermometer. After allowing the gas to be adsorbed on to the sample by opening tap 6, the equilibrium pressure (P_e) was noted. This procedure was repeated for a series of measurements between 5–50 mbar for the prepared Pt catalysts, taking pressure readings every 5 mbar (approx.).

CALIBRATION OF THE VOLUMES

The dosing volume (V_d) can be calculated, using two bulbs of known volumes, V_1 and V_2. The volumes V_1 and V_2 were determined by weighing the bulbs empty, and then after filling with distilled water. This experiment was repeated twice and the average value taken. Both the glass bulbs were attached to the vacuum line in turn and out-gassed to a final pressure of about 10^{-5} mbar. The dosing volume was wrapped with quartz wool to maintain isothermal conditions. A certain volume of nitrogen was admitted into the dosing volume and with taps 4, 5 and 6 closed, the pressure was noted as P_{d1} .Then the gas was allowed into each bulb by opening tap 6 and once the equilibrium was attained the pressure was noted as P_{e1}. The system was out-gassed and the same procedure was repeated with different pressures of nitrogen. This procedure was repeated using the second bulb to give P_{d2} and P_{e2}. The dosing volume was then calculated using the following equation:

$$V_1 - V_2 = V_d \left(\frac{P_{d1}}{P_{e1}} - \frac{P_{d2}}{P_{e2}} \right) \tag{16}$$

assuming the dosing temperature (T_d) is equal to the temperature of the sample (T_s).

Once V_d has been calculated, V_s, V_x and V_n were also calibrated, where V_s is the volume of the section below the tap 6, V_n is the volume below the pre-etched mark on the sample holder, and V_x is the volume between tap 6 and the pre-etched mark on sample holder (shown in Fig. 2-8).

With the empty sample holder and sinter attached to the line and out-gassed to $\sim 10^{-5}$ mbar, a small amount of nitrogen was admitted to the dosing volume and the pressure was noted as P_d. Tap 6 was then opened and the gas was allowed to equilibrate before closing tap 6 and noting the new pressure as P_e.

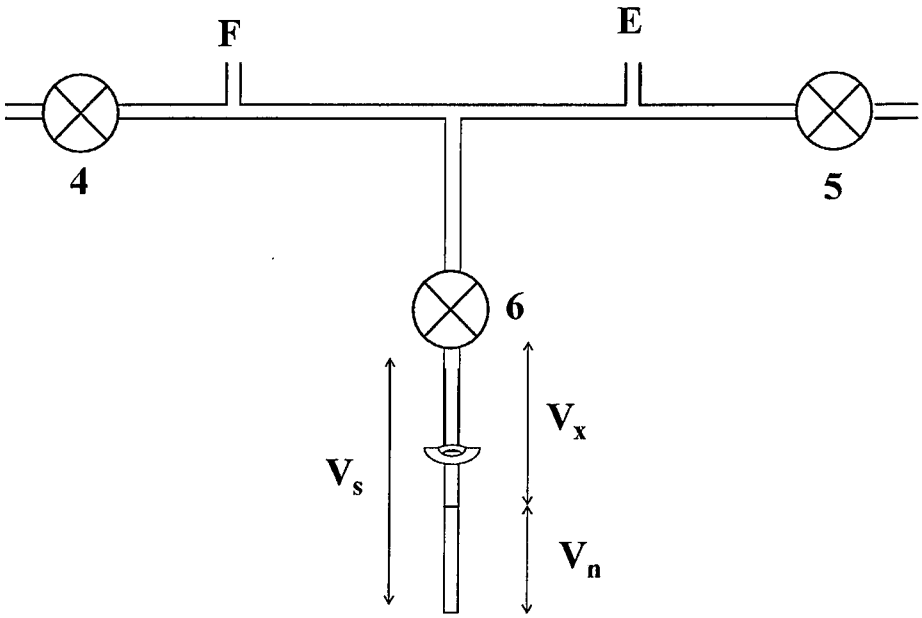

FIGURE 2-8: Diagram showing the position of V_x, V_s, and V_n on the vacuum line.

Using the gas laws, V_s can be given as:

$$V_s = V_d\left(\frac{P_d}{P_e} - 1\right) \tag{17}$$

Again assuming $T_s = T_d$

When the sample holder was immersed in liquid nitrogen up to the pre-etched mark and tap 6 reopened, the P_e decreased further until a new equilibrium was reached. If the new pressure is denoted as P_n then

$$V_n = (V_d + V_s)\left(\frac{P_e}{P_n} - 1\right)\left(\frac{T_n}{T_d - T_n}\right) \tag{18}$$

where T_n = temperature of liquid nitrogen

Each experiment to determine V_s, V_x and V_n was repeated 3–4 times and the individual values obtained were averaged to give the final values.

It must be noted that correction was made with consideration of the volume taken by the sample after each adsorption isotherm using helium.

2.3.4 TEMPERATURE PROGRAMMED REDUCTION (TPR)

Temperature programmed reduction (TPR) with hydrogen is a widely used technique for the characterisation of reducible solids and catalysts. The TPR technique [58] can provide information about the dispersion states of the metallic components as well as on the extent of metal-support and metal-metal interactions in the metallic catalysts. Details of this thermoanalytical technique and the physical principles underlying this technique have been presented in many research articles [59,60].

In TPR, a reducible catalyst or catalyst precursor is exposed to the flow of a reducing gas mixture while the temperature of the catalyst is raised linearly. This reducing mixture generally contains a few volume% of hydrogen in an inert gas. The reduction rate is generally followed by measuring the composition of the reducing mixture, in terms of hydrogen content, at the outlet of the reactor. The position of a peak in the TPR profile is determined by the chemical nature and environment of the chemical component. The experiment allows the determination of total amount of hydrogen consumed from which the degree of reduction can be calculated.

When there is more than one reducible metal present in the catalytic system, then the reduction profile for each component is looked at. This gives an indication about the location of the two metals [61,62].

THEORY

The reduction of metal oxides (MO_x) involves the adsorption of hydrogen on the metal oxide surface. Chemically it can be shown as:

$$MO_x\,(s) + xH_2\,(g) \rightarrow M\,(s) + xH_2O\,(g) \qquad (19)$$

A typical TPR profile is generally presented as the amount of hydrogen consumed by the reducible component, as a function of the temperature of the catalyst.

EXPERIMENTAL PROCEDURE

A schematic diagram for the TPR set-up is shown in Fig. 2-9. TPR experiments were performed both at the Open University (OU) and at Johnson Matthey Technology Centre (JMTC). The only significant difference between the two set-ups was that the JMTC facility allowed sub-ambient experiments to be performed from −100 °C upwards. The OU set-up performed experiments from room temperature upwards. It was made up using a gas chromatograph (Varian Model 3700 GAS) operating at ~60 °C and a Carbolite furnace controlled by a Eurotherm model 818 temperature programmer. The Pico Data Logger software (Pico Technology Ltd.) was used to collect and process the data. Based on similar principles, the self-designed TPR set-up was used for data collection at JMTC.

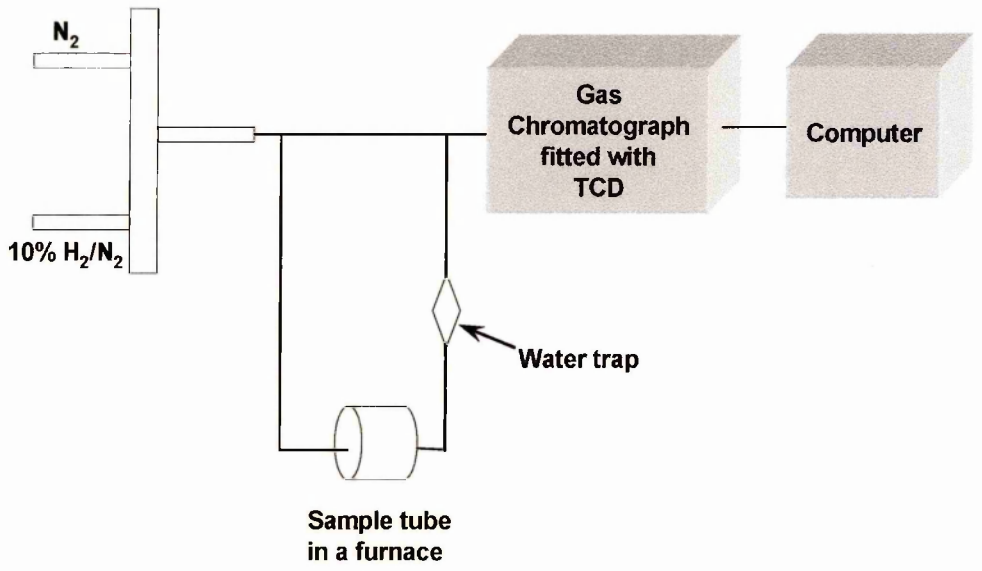

FIGURE 2-9: A schematic diagram for TPR set-up.

For the experiments conducted at JM, about 0.3 g of the catalyst was taken in a pyrex tube with a small bulb for the sample cell at the centre. (Approximately 0.1 g of the catalyst was used for the experiments performed at OU.) Both ends of the tube

were blocked using quartz wool. A thermocouple was inserted from one end into the catalyst bed in order to monitor the catalyst temperature. The tube was placed in the specially designed furnace which could go down to temperatures of about −100 °C. The program was set for the run between −100–600 °C. The catalyst was purged with nitrogen for about 20 minutes in order to remove any air in the system and then the reduction mixture (10% H_2 in N_2) was passed through the reference arm of the thermal conductivity detector (TCD) of the gas chromatograph (GC), then through the catalytic cell to the sampling arm of the TCD. The resistance of the filament in a TCD is highly sensitive to the surrounding gases. Since hydrogen has a high thermal conductivity, any change in its concentration in the gas mixture due to reduction of the sample, causes a decrease in conductivity in the sampling arm of the GC. This imbalance can usually be displayed by means of various computer programmes which relate the change in hydrogen concentration as a function of temperature and/or time.

Once the gas has passed over the solid catalyst, any water formed as a result of the reduction process was removed by the use of a trap-like molecular sieve, or a small column of dry silica beads. The system was monitored until the TCD display gave a stabilised reading. Once the stable reading was observed the computer controlled data collection program was started. Heating rate was maintained at 10 °C min^{-1}. After the experiment, the furnace was allowed to cool down to room temperature, and the catalyst was flushed with N_2 for about 10 minutes before it was removed from the cell.

2.3.5 THERMO-GRAVIMETRIC ANALYSIS (TGA) AND DIFFERENTIAL SCANNING CALORIMETRY (DSC)

Studying the changes in the physical and/or chemical properties of a substance(s) as a function of temperature is known as thermal analysis [63]. Thermal

analysis is quite useful in the investigation of decomposition, phase changes, loss of water or adsorbed gases etc. Generally the substance intended to be studied by thermal analysis is subject to a controlled temperature programme which may include heating, cooling, holding the temperature constant, or any combination of all of them.

Two of the most commonly used thermal analytical techniques are:

- Thermo-Gravimetric Analysis (TGA)
- Differential Scanning Calorimetry (DSC)

THEORY

Thermo-Gravimetric Analysis (TGA) records the changes in the mass of the sample being studied under a controlled atmosphere as a function of temperature. This mass-change may occur as a result of adsorption-desorption, dehydration, decomposition, etc. All these processes leading to a change in mass of the substance may involve one or more physical/chemical phenomena such as bond breaking or bond formation etc., at higher temperatures. The ability to change the atmosphere during the TGA experimentation, particularly from an inert to a reactive atmosphere, can provide additional information about the material composition and its thermal stability.

Differential Scanning Calorimetry (DSC) examines the heat flow associated with physical changes, such as phase transformation, within the system as a function of temperature. The technique provides qualitative and quantitative information about physical and chemical changes that involve endothermic or exothermic processes or changes in heat capacity, and so permits the determination of transition temperatures due to changes of state or phase such as melting and crystallization, and heat capacity. DSC has been extensively used in determining many thermodynamic parameters such as specific heat, reaction kinetics, thermal stability and glass transition temperatures.

INSTRUMENTATION

The TGA/DSC data was collected on a Rheometric Scientific Simultaneous Thermal Analyzer (STA) which combines a sensitive balance for use in Thermo-gravimetric Analysis, with a heat-flux DSC hang down (Fig. 2-10) for simultaneous DSC and TGA experiments. Fig. 2-11 shows the schematic diagram of the TGA/DSC set-up.

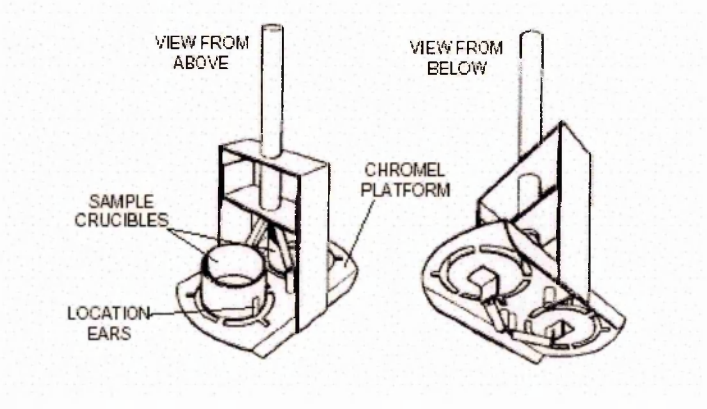

FIGURE 2-10: The heat-flux TG-DSC hangdown (Taken from reference 64)

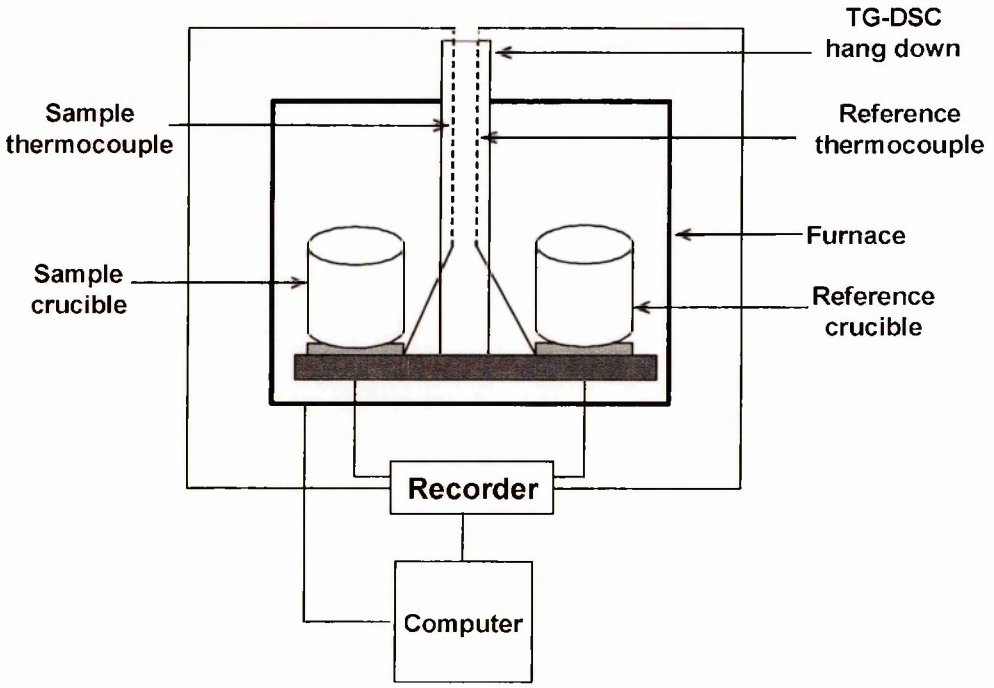

FIGURE 2-11: Schematic block diagram of TGA/DSC set up

The system used was a heat-flux instrument where the sample and the reference were heated by the same source and the temperature difference between the sample and the reference was measured. Water was circulated at 1 psi during the experiments for cooling purposes.

In order to carry out differential scanning calorimetry measurements, the hang-down, which was equipped with a heat-flux plate, was heated. This heating of the flux plate created a temperature differential between the sample and the reference. This temperature difference caused the thermocouples to generate a voltage that was proportional to the heat flow. By measuring the heat absorbed or evolved by a sample as it was heated (or cooled) under a controlled temperature and atmosphere, DSC was able to record changes in specific heat capacity and latent heat associated with the sample that indicate changes in amorphous and crystalline structures.

This instrument is capable of performing TGA measurements concurrent with the differential thermal analysis on the same sample. The advantages for simultaneous TGA and DSC are obvious. Both analyses are carried out at the same time, assuring identical conditions. This completely eliminates any correlation problems between TGA and DSC that exist when experiments are carried out on separate test instruments.

EXPERIMENTAL PROCEDURE

The sample and the reference (empty) crucibles (both made of alumina) were calibrated under the experimental conditions such as air flowing at a fixed flow rate of ca 50 cm^3 min^{-1}, and the baseline was set. About 5–10 mg of the sample was placed into a tared TGA sample crucible which was attached to a sensitive microbalance assembly. The sensitivity of the balance was one tenth of a milligram (0.1 mg). The

sample holder portion of the TGA balance assembly was subsequently placed inside a high temperature furnace. The 10% H_2 in N_2 gas mixture was flowed over the sample at 50 cm^3 min^{-1} when experiments were performed under a reducing atmosphere. The heating rate was maintained at 5 °C min^{-1} up to the desired temperature (800 °C). Air (zero grade) was used to perform experiments under air.

The balance assembly measured the initial sample mass at room temperature and then continuously monitored changes in sample mass (losses or gains) as heat was applied to the sample. Typical mass loss profiles have been analyzed for the amount or percent of mass loss at any given temperature, the amount (or percent) of non-combusted residue at some final temperature, and the temperatures of various sample degradation processes.

2.3.6 TESTING THE CATALYTS FOR SELECTIVE OXIDATION OF CARBON MONOXIDE

DRY TESTS

From the stoichiometry of the reaction, $CO(g) + 0.5O_2(g) \rightarrow CO_2(g)$, we have $[CO] = 2[O_2]$. The excess oxygen with respect to the minimum amount of oxygen required for CO oxidation to CO_2 in the absence of side-reactions is characterised by the process parameter λ, defined by the following relationship [65],

$$\lambda = \frac{2[O_2]}{[CO]} \qquad (20)$$

In the present study all the catalysts prepared by the SOMC technique were tested for the oxidation of carbon monoxide in the presence of excess hydrogen in a fixed-bed laboratory reactor, under different values of λ i.e. under different O_2:CO ratios.

Various researchers have used gas mixtures with different O_2:CO ratios (i.e. different λ values). However for present study, a mixture with $\lambda = 5$ i.e. $[O_2]$:[CO] = 2.5 was chosen in order to oxidise the entire CO in the mixture. From the relationship (20), the λ value in the Preferential Oxidation (PrOx) reactor process should be closer to unity (i.e., stoichiometric value) not to oxidize excessive amounts of hydrogen. With this objective and from the point of view of improving the selectivity of the catalysts, all the catalysts were also tested/screened at $\lambda = 2$ i.e. $[O_2] = [CO]$ in the present study.

The reactor (shown in Fig. 2-12) consists of a programmable Lenton tube furnace. The reactor was a 6 mm (outer diameter) pyrex tube housed in an electric furnace. The gases were fed downstream from three cylinders containing 5% O_2 in N_2, 2% CO in H_2 and pure N_2. A flow controller was used to control the flow rate of the gases from each cylinder. With the help of these flow controllers, the flow of the respective gas mixture was set so as to give a final feed mixture of 1.25% O_2, 0.5% CO, ~ 25% H_2 and the balance N_2. Since there was no water present in these samples of the gaseous feedstock, the experiments carried out with these mixtures are referred to as *dry CO tests* in this thesis. About 70 mg of the catalyst was taken in a pyrex tube and sandwiched between quartz wool plugs. An Inconel Sheath (Ni-Cr / Ni-Al) thermocouple (temperature range: −200 °C – 1100 °C) was inserted into the catalyst bed to measure the temperature of the catalyst. A stable linear rise in the reactor temperature was maintained by an external controller. However, it must be noted that the temperature values quoted in the present studies are those actually measured by a chromel-alumel thermocouple positioned downstream of the catalyst bed.

Many studies have shown that the oxidation of Pt reduces its ability to catalyse an oxidation reaction. Ostermaier *et. al.* [*66*] found that the rate of ammonia oxidation on alumina-supported Pt decreased rapidly as Pt crystallites were oxidised during the

reaction. Similarly in the case of CO oxidation, Herz and Marin [67] suggested that a supported catalyst, in which a large fraction of Pt is present in the reduced state, will have a higher initial activity towards CO oxidation than a supported catalyst given an oxidising treatment. In the light of these observations, each catalyst under examination in this study was reduced under the 2% CO/H_2 mixture at 40 °C for 40 minutes, prior to studying the selective oxidation of CO.

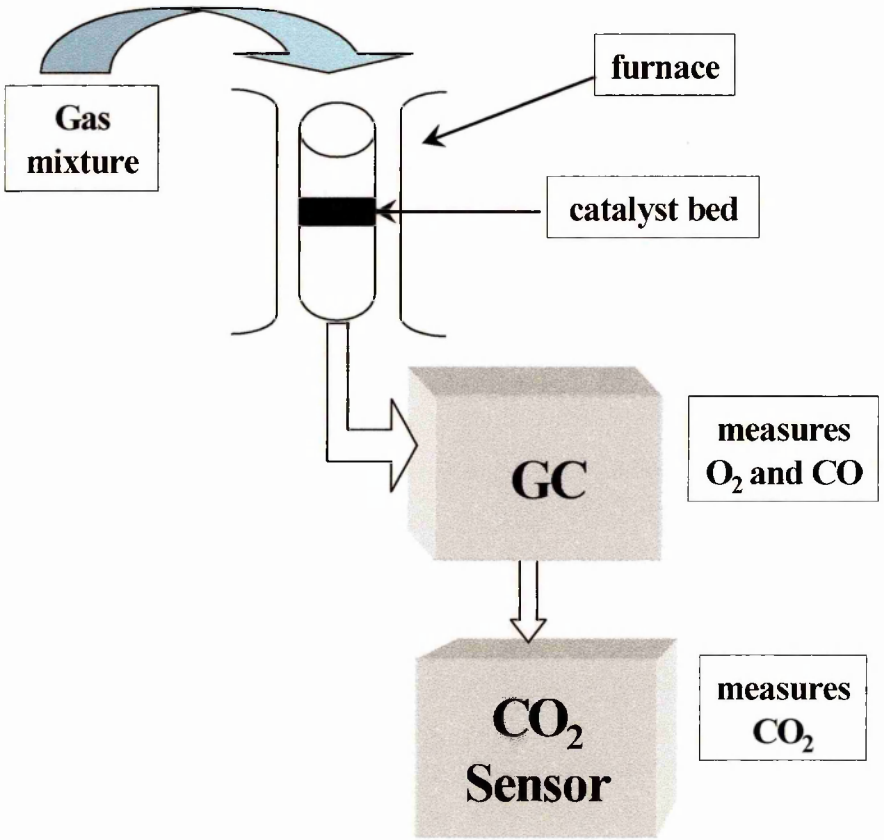

FIGURE 2-12: A schematic diagram for the testing of the catalysts at the OU

The reaction products were analysed using a gas chromatograph (Ai Cambridge GC 94) fitted with a TCD with Molecular Sieve 5A 100–120 mesh (3 feet long and $\frac{1}{8}$" external diameter). A CO_2 sensor (Servomex Analyser Series 1400) was also used to

analyse the amount of CO_2 in the output. This provided us with an effective way to crosscheck the CO consumption monitored on the GC and the CO_2 formed during the tests on the CO_2 sensor. Calibration of the CO_2 sensor with respect to the GC, using a calibration gas mixture and also the gas mixture used for the CO tests, gave very consistent results (within ± 0.01%). The amount of CO consumed as analysed by GC was in good agreement with that shown on the CO_2 sensor.

The term, '*Consumption of CO, O_2 (vol %)*' is defined as the amount of CO and O_2 (in vol %) present in the gas mixture consumed during the reaction (analytically).

The main objective of the present study was to remove CO from the reformate gas mixture with the minimum consumption of hydrogen. Thus the selectivity of a catalyst towards the oxidation of CO becomes an important factor to be considered in developing a preferential oxidation catalyst. The selectivity of a catalyst may be defined as the partitioning of the limited supply of oxygen between CO and H_2 present in the reformed gaseous mixture. In other words, the CO selectivity is the ratio of the amount of oxygen used in oxidising CO (g) to CO_2 (g) to the total amount of oxygen consumed in the reaction. The term selectivity of a catalyst towards CO oxidation (S(CO)) is defined as follows:

$$S(CO) = \frac{\text{Amount of oxygen used in CO oxidation}}{\text{Total amount of oxygen consumed in the reaction}} \times 100\%$$

As neither H_2 and H_2O concentrations were measured in the experiment the hydrogen selectivity ($S(H_2)$) was calculated on the assumption that any difference between O_2 and CO consumption can be accounted for by H_2 oxidation.

It should be noted that the CO conversion referred to in the text as consumption of CO (%) is the fraction of the total CO present in the gas mixture (containing 0.50%

CO) that has been oxidised e.g. 50% CO conversion on the figure represents 0.25% CO that has been converted to CO_2.

WET TESTS

As a part of the present study all the catalysts prepared by the SOMC route, were also screened under a simulated reformate gas mixture at the Johnson Matthey Technology Centre, Sonning Common, UK. A schematic diagram of the set-up for testing the catalysts is shown in Fig. 2-13.

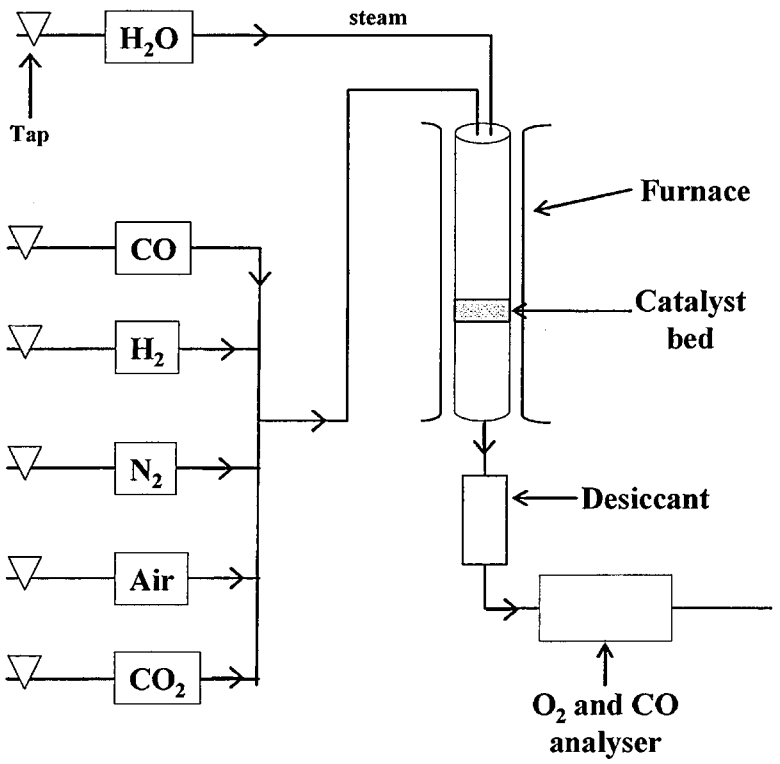

FIGURE 2-13: A schematic diagram for the testing of the catalysts at JMTC

Prior to the tests, the catalyst was pelletized, crushed and sieved through mesh in order to obtain particles in the 250-355 μm size range. Approximately 50 mg of the

catalyst was mixed with approximately 150 mg of cordierite and loaded into the reactor. For these studies, the gas composition was set to 60% H_2, 0.1% CO, 20% CO_2, 0.15% O_2 and balance nitrogen. The temperature of the reactor was maintained at 150 °C throughout the experiment. Once the temperature of the reactor reached 150 °C, 10% H_2O was added to the feed and the catalyst was left for 1 hour to stabilise. The total flow rate during this stabilisation period was maintained at 3×10^4 cm^3 min^{-1}. During this period, both CO and O_2 were monitored in order to note any deactivation of the catalyst. After about 1 hour, the amounts of CO and O_2 consumed were followed as a function of space velocity. Space velocity is defined as the amount of gas flowing (in cm^3) per unit time (in min) per unit mass (in g) of the catalyst loaded into the reactor. The space velocity was varied by changing the flow rate of the gas mixture. The tests were started at a space velocity of 2×10^3 cm^3 min^{-1} g^{-1} over the catalyst, gradually increasing stepwise up to about 2×10^4 cm^3 min^{-1} g^{-1}.

The results obtained from the CO oxidation studies are described and discussed in Chapter 4 and 5 of this thesis.

2.4 REFERENCES

1 A. D. O'Cinneide and F. Gault, J. Catal., 37, 311, (1975)

2 R. L. Garten and J. M. Sinfelt, J. Catal., 62, 127, (1980)

3 E. M. Crabb and R. Marshall, Appl. Catal. A: General, 217, 41, (2001)

4 E. M. Crabb, M. K. Ravikumar, Y. Qian, A. E. Russell, S. Maniguet, J. Yao, D. Thompsett, M. Hurford and S. C. Ball, Electrochem. Solid-State Lett., 5, 5, (2002)

5 B. J. Clark, T. Frost and M. A. Russell, UV Spectroscopy Technique, instrumentation,data handling, Chapman & Hall, UK, (1993)

6 *http://www.unl.edu/CMRAcfem/temoptic.htm* (accessed on 17/04/2003), Title: "Transmission Electron Microscope (TEM)", University of Nebraska-Lincoln.

7 A. V. Crewe, J. Wall and L. M. Welter, J. Appl. Phys., 39, 5861,(1968)

8 A. V. Crewe and J. Wall, J. Mol. Biol., 48, 375, (1970)

9 S. J. Pennycook and D. E. Jesson, Ultramicroscopy, 37, 14, (1991)

10 A. Howie, J. Microscopy, 117, 11, (1979)

11 S. B. Rice, J. Y. Yoo, M. M. Disko and M. M. J. Treacy, Ultramicroscopy, 34, 108, (1990)

12 S. J. Pennycook and S. J. Boatner, Nature, 336, 565, (1988)

13 E. J. Kirkland, R. F. Loane and J. Silcox, Ultramicroscopy, 23, 77, (1987)

14 M. Weyland, Topics in Catalysis, 21(4), 175, (2002)

15 C. W. Oatley, W. C. Nixon and R. F. W. Pease, Advan. Electron. Electron Phys., 21, 181, (1965)

16 K. C. A. Smith and C. W. Oatley, Brit. J. Appl. Phys., 6, 391, (1955)

17 T. E. Everhart, O. C. Wells and C. W. Oatley, J. Electron. Control, 7, 97, (1959)

18 H. H. Pattee Jr., J. Opt. Soc. Am., 43, 61, (1953)

19 P. Duncumb, Brit. J. Appl. Phys., 10, 420, (1959)

20 V. E. Cosslett and W. C. Nixon, X-Ray Microscopy, Cambridge University Press, Cambridge, England, 202, (1960)

21 F. Pinna, Catal. Today, 41, 129, (1998)

22 C. Wedler (translated by D. Klemperer), Chemisorption: An Experimental Approach, Butterworths, London.

23 D. J. Shaw, Introduction to Colloid and Surface Chemistry, 3rd Ed., Butterworths, US, (1980)

24 S. Brunauer, L. S. Deming, W. E. Deming, E. Teller, J. Amer. Chem. Soc., 62, 1723, (1940)

25 S. J. Gregg and K. S. W. Sing, Adsorption, Surface Area and Porosity 2nd Ed., Academic Press, New York, (1982)

26 R. Anderson, Structure of Metallic Catalysts, Academic Press, New York, 295, (1975)

27 J. J. F. Scholten, in: B. Delmon, P. Grange, P. A. Jacobs, G. Poncelet (Eds.), Preparation of Catalysts II, Elsevier, Amsterdam, 232, (1979)

28 C. H. Bartholomew, Catalysis (Specialist Periodical Report), 11, 93, (1994)

29 A. F. Benton, J. Amer. Chem. Soc., 48, 1850, (1926)

30 T. A. Dorling and R. L. Moss, J. Catal., 5, 111, (1966)

31 T. A. Dorling and R. L. Moss, J. Catal., 7, 378, (1967)

32 T. R. Hughes, R. J. Houston and R. P. Sieg, Ind. Eng. Chem. Process Des. Develop., 1, 96, (1962)

33 L. Spenadel and M. Boudart, J. Phys. Chem., 64, 204, (1960)

34 S. F. Adler and J. J. Keavney, J. Phys. Chem., 68, 208, (1960)

35 G. A. Mills, S. Weller and E. B. Cornelius, Actes Congr. Intl. Catal., 2nd (1960), Editions Technip, 2, 2221, (1961)

36 G. R. Wilson and W.K. Hall, J. Catal., 17, 190, (1970)

37 C. R. Adams, H. A. Benesi, R. M. Curtis and R.G. Meisenheimer, J. Catal., 1, 336, (1962)

38 J. H. Sinfelt, J. Phys. Chem., 68 (10), 2962, (1964)

39 J. J. F. Scholten and J. A. Konvalinka, J. Catal., 5, 1, (1966)

40 T. R. P. Gibb, 'Primary Solid Hydrides' in Progress in Inorganic Chemistry, (ed. F. A. Cotton), Vol. III, Interscience New York, 315, (1962)

41 D. P. Smith, Hydrogen in Metals, Univ. of Chicago Press, Chicago Illinois, (1948)

42 F. A. Lewis, 'The Palladium Hydrogen System', Acad. Press, London and New York, (1967)

43 P. C. Aben, J. Catal., 10, 224-229, (1968)

44 P. H. Emmett and S. J. Brunauer, J. Amer. Chem. Soc., 59, 310, (1937)

45 D. J. C. Yates and J. H. Sinfelt, J. Catal., 8, 348, (1967)

46 M. A. Vannice, J. Catal., 37, 449, (1975)

47 M. A. Vannice, J. Catal., 44, 152, (1976)

48 M. A. Vannice, J. Catal., 50, 228, (1977)

49 J. Freel, J. Catal., 25, 149, (1972)

50 L. Fan, C. Zhu, Principles of Gas-Solid Flows, Cambridge University Press, UK, (1998)

51 R. T. Yang, Gas Separation by Adsorption Processes, Butterworth, Boston, (1987)

52 A. W. Adamson, Physical Chemistry of Surfaces, Wiley Interscience, NY, (1990)

53 D. M. Ruthven, Principles of Adsorption and Adsorption Processes, Wiley Interscience, New York, (1984)

54 W. Rudzinski and D. H. Everett, Adsorption of gases on Heterogeneous Surfaces, Academic Press, London, (1992)

55 S. Brunauer and P. H. Emmett, J. Amer. Chem. Soc., 57, 1754, (1935)

56 P. H. Emmett and S. J. Brunauer, J. Amer. Chem. Soc., 59, 1553, (1937)

57 S. Brunauer, P. H. Emmett and E. Teller, J. Amer. Chem. Soc., 60, 309, (1938)

58 A. Jones and B. McNicol, Temperature-Programmed Reduction for Solid Materials in Chemical Industries, Vol. 25, Marcel Dekker, New York, (1986)

59 N. W. Hurst, S. J. Gentry, A. Jones and B. D. McNicol, Catal. Rev. Sci. Eng., 24, 233, (1982)

60 D. A. M. Monti and A. Baiker, J. Catal., 83, 323, (1983)

61 W. Juszczyk, J. Pielaszek, Z. Karpinski and F. Pinna, Appl. Cat. A: Gen., 144, 281, (1996)

62 F. Pinna, M. Selva, M. Signoretto, G. Strukul, F. Boccuzzi, A. Benedetti, P. Canton and G. Fagherazzi, J. Catal., 150, 356, (1994)

63 *http://www.imp.mtu.edu/matchar/ta.html* (accessed on 22/10/2003), Title: "Thermal Analysis", Institute of Materials Processing, Michigan Technological University.

64 Y. Qian, Ph.D. Thesis, The Open University, UK (2004)

65 M. J. Kahlich, H. A. Gasteiger and R. J. Behm, J. Catal., 171, 93, (1998)

66 J. J. Ostermaier, J. R. Katzer and W. H. Manogue, J. Catal., 41, 277, (1976)

67 R. K. Herz and S. P. Marin, J. Catal., 65, 281, (1980)

3

Characterisation of Catalysts – Results

The catalysts prepared in this study have been characterised by employing the following techniques:

1. UV-visible spectroscopy of filtrate
2. Elemental analysis
3. Transmission Electron / Scanning Transmission Electron Microscopy
4. CO Chemisorption
5. Temperature Programmed Reduction (TPR)
6. Thermal Analysis (TGA-DSC)

3.1 PREPARATION OF M-Pt/Al_2O_3 BIMETALLIC CATALYSTS (M = Cr, Mn, Fe, Co, Ni, Cu and Sn)

A number of different samples of 5%Pt supported on alumina were provided by Johnson Matthey, Sonning Common, UK. The respective Pt dispersion values for these samples (as determined by CO pulsed technique at Johnson Matthey Technology Centre, UK) are listed in Table 3-1, given overleaf:

Table 3-1: CHARACTERISTICS OF LOW AND HIGH-DISPERSED Pt/Al_2O_3 SYSTEMS

System	Batch I	Batch II
Low	4.60%Pt, 29% dispersion	5.18% Pt, 26% dispersion
High	4.94% Pt, 51% dispersion	5.20% Pt, 54% dispersion

A series of $M\text{-}Pt/Al_2O_3$ (M = Sn, Fe, Co, Cr, Mn, Ni and Cu) bimetallic catalysts was prepared from the monometallic Pt/Al_2O_3 samples by the SOMC method. A series of second metal precursors including tetrabutyl tin, metallocenes ($M(C_5H_5)_2$) where M = Fe, Co, Cr and Ni, and M-acetylacetonate (acac) where M = Mn and Cu, were used for the preparation of the catalysts used in the present study (Table 3-2). An attempt was made to cover the surface Pt sites with half a monolayer of Sn, Fe, Co, Cr, Mn, Ni and Cu on Pt/Al_2O_3(low) samples and full monolayer coverage was attempted using Sn, Fe and Co on both the Pt/Al_2O_3 samples. Table 3-2 shows all the bimetallic catalysts prepared by the SOMC technique and the different precursors used. Column 3 of Table 3-2 shows the colour of the solution of all precursors in heptane unless mentioned otherwise.

All the bimetallic catalysts prepared by SOMC route have been listed in Table 3-2. The details of the preparation procedure are given in Chapter 2 of this thesis and are summarised below:

For each catalyst the required amount of the organometallic precursor, shown in column 2 of Table 3-3, was dissolved in heptane (or toluene) and added under N_2 to the reactor containing the reduced Pt/Al_2O_3 catalyst.

Table 3-2: TABLE SHOWING THE CATALYSTS PREPARED AND THE PRECURSOR USED FOR EACH SYSTEM

System	Precursor used	Colour of solution
(1:2)SnPt(low) (I)	$Sn(n\text{-}C_4H_9)_4$	colourless
(1:1)SnPt(low) (I)	$Sn(n\text{-}C_4H_9)_4$	colourless
(1:2)FePt(low) (I)	$Fe(C_5H_5)_2$	orangish-yellow
(1:1)FePt(low) (I)	$Fe(C_5H_5)_2$	orangish-yellow
(1:2)CoPt(low) (II)	$Co(C_5H_5)_2$	deep blue
(1:1)CoPt(low) (II)	$Co(C_5H_5)_2$	deep blue
(1:2)CrPt(low) (II)	$Cr(C_5H_5)_2$	dark green
(1:2)NiPt(low) (II)	$Ni(C_5H_5)_2$	bluish-green
(1:2)CuPt(low) (II)	Cu(II)- acetylacetonate	blue (partially soluble)
(1:2)CuPt(low) (II)[#]	Cu(II)- acetylacetonate	light blue (in toluene)
(1:2)MnPt(low) (II)[#]	Mn(II)-acetylacetonate	colourless (in toluene)
(1:2)SnPt(high) (I)	$Sn(n\text{-}C_4H_9)_4$	colourless
(1:1)SnPt(high) (I)	$Sn(n\text{-}C_4H_9)_4$	colourless
(1:2)FePt(high) (I)	$Fe(C_5H_5)_2$	orangish-yellow
(1:1)FePt(high) (I)	$Fe(C_5H_5)_2$	orangish-yellow
(1:2)CoPt(high) (II)	$Co(C_5H_5)_2$	deep blue
(1:1)CoPt(high) (II)	$Co(C_5H_5)_2$	deep blue

I and II refers to the different batches of Pt/Al_2O_3 used for the preparation of the catalysts (Table 2-1)

[#] preparation carried out in toluene as solvent

Hydrogen gas was then passed through the reactor. The reaction was allowed to continue at room temperature for about 12 hours and then at 90 – 95 °C for a further 8 – 12 hours. The reaction was continuously monitored by analyzing the exit gas using gas chromatography. After the reaction, the contents of the reactor were discharged, filtered, and washed repeatedly with heptane (toluene) to remove unreacted organometallics.

For the M-Pt/Al_2O_3 (M = Cr, Fe and Co) bimetallic catalysts, cyclopentane evolution was observed after the precursor solution was mixed with the reduced monometallic catalyst at room temperature. The initial colour of the solution (dark green for chromocene, deep yellow for ferrocene and deep blue for cobaltocene) changed slightly to a lighter shade and after about 2–3 hours a maximum was observed in cyclopentane evolution at room temperature before decreasing until almost no cyclopentane was detected after about ten hours. Continuous monitoring of the exit gas showed two distinct peaks on the gas chromatograph, the first being assigned to cyclopentane and the second larger peak to heptane. On heating the reaction to 90–95 °C, further cyclopentane evolution was observed until after nearly 8 hours no cyclopentane could be detected. This may suggest that the precursors either reacted quite easily with Pt/Al_2O_3 or they decomposed at room temperature.

During the course of the reaction the colour intensity of the organometallic precursor solution changed considerably. The intensity of the colour of the organometallic precursor in heptane solution decreased to a light colour, or disappeared completely during the reaction at ~95 °C, depending on the metal present.

The filtrates (~100 cm^3) were transferred into a volumetric flask, and any unreacted organometallic compound was determined by UV-visible spectroscopy. Typical UV-visible spectra of the filtrate for the alumina-supported M-Pt (M = Fe and

Co) bimetallic catalysts are shown in Figs. 3-1 and 3-2 and the results have been given in column 3 of the Table 3-3.

Table 3-3: MASS OF PRECURSOR USED AND DATA FROM UV-VIS SPECTRAL ANALYSIS

System	$W_{precursor}$ taken (g)	$W_{precursor}$ detected in filtrate (g)	$W_{precursor}$ deposited (%)
(1:2)SnPt(low) (I)	0.1072	0	100
(1:1)SnPt(low) (I)	0.2152	0	100
(1:2)FePt(low) (I)	0.0589	0	100
(1:1)FePt(low) (I)	0.1328	0.0004	≈100
(1:2)CoPt(low) (II)	0.0515	0.0013	97
(1:1)CoPt(low) (II)	0.1180	0.0171	86
(1:2)CrPt(low) (II)	0.0193	0	100
(1:2)NiPt(low) (II)	0.0383	n.d.	n.d.
(1:2)CuPt(low) (II)	0.0293	n.d.	n.d.
(1:2)CuPt(low) (II)[#]	0.0184	n.d.	n.d.
(1:2)MnPt(low) (II)[#]	0.0219	n.d.	n.d.
(1:2)SnPt(high) (I)	0.1885	0	100
(1:1)SnPt(high) (I)	0.3769	0	100
(1:2)FePt(high) (I)	0.0963	0.0030	97
(1:1)FePt(high) (I)	0.1412	0.0181	87
(1:2)CoPt(high) (II)	0.1128	0.0102	91
(1:1)CoPt(high) (II)	0.2068	0.0350	83

n.d.: not determined
[#] preparation carried out in toluene as solvent

The results showed the successful deposition of the desired amount of Sn, Fe and Cr in the low-dispersed catalysts. Ferrocene was detected in the filtrate collected after the preparation of the Fe-promoted high-dispersed catalysts. Similarly analysis of the Co samples suggested that some unreacted cobaltocene was remaining. A small amount of precursors observed in the filtrate after the preparation of the promoted catalysts, suggest that there was a limitation of deposition of these metals on the surface Pt, or that the reaction had not gone to completion. When no precursor was observed in the filtrate this could mean either that it had all reacted with the metal surface, or that any unreacted precursor had decomposed and was not detectable.

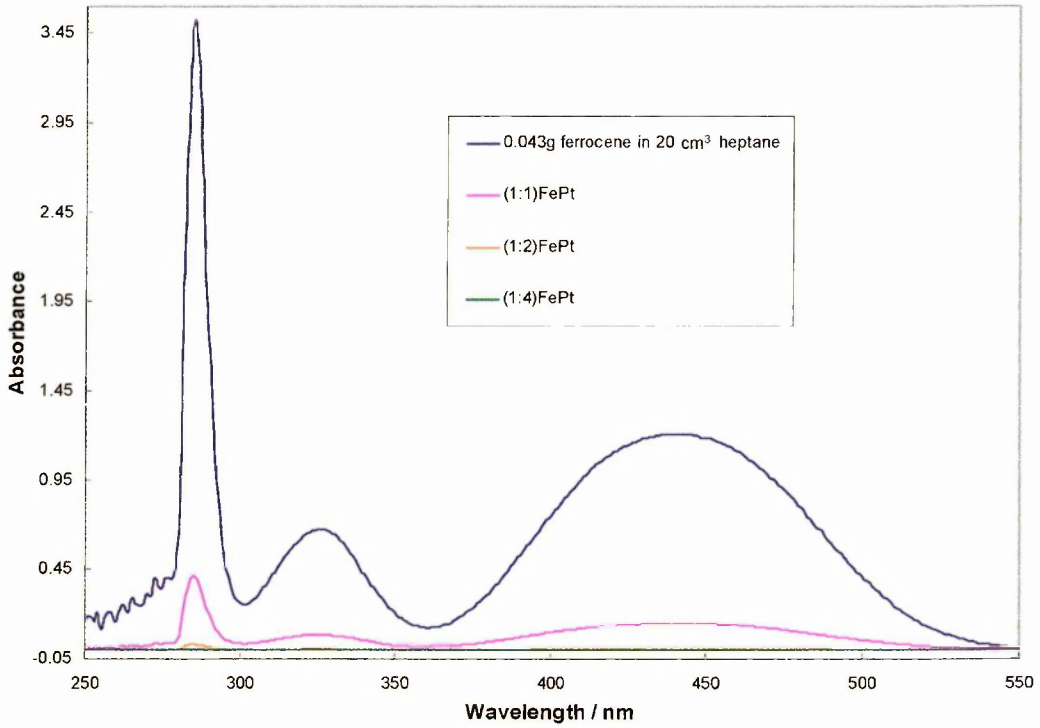

FIGURE 3-1: UV-visible spectra of the filtrates of $FePt/Al_2O_3$(high) catalysts

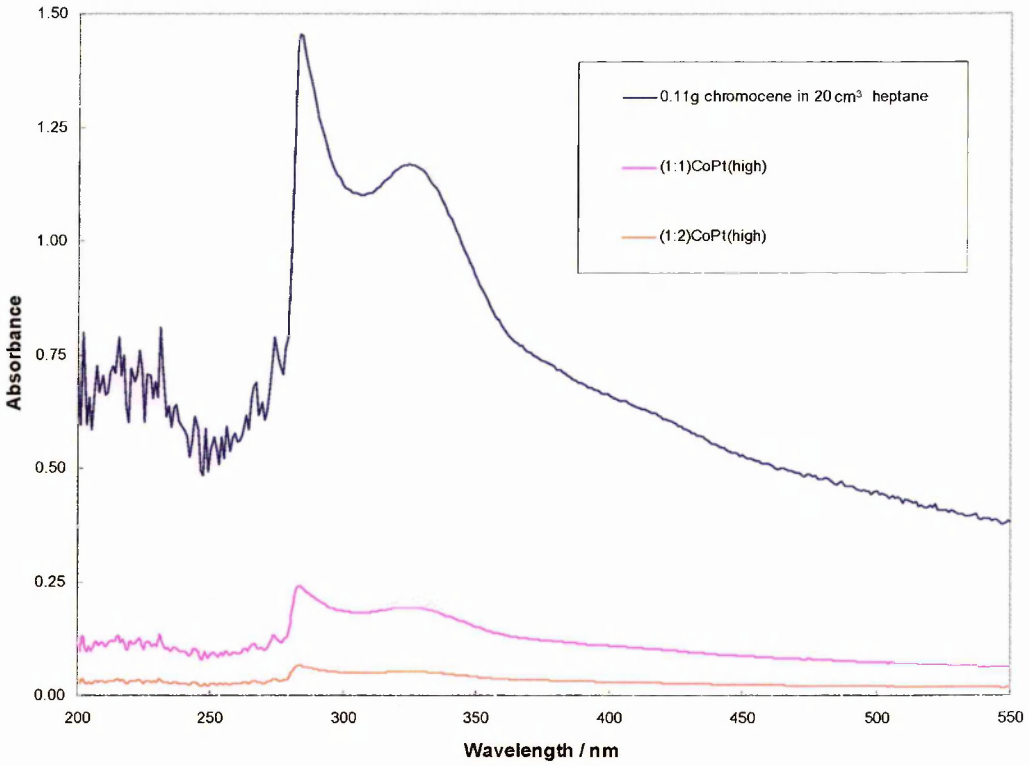

FIGURE 3-2: UV-visible spectra of the filtrates of $CoPt/Al_2O_3$ (high) catalysts

3.1.1 ELEMENTAL ANALYSIS OF THE PREPARED CATALYSTS

The assays of all the promoted Pt/Al_2O_3 catalysts were determined by Inductively Coupled Plasma Atomic Emission Spectroscopy (ICP-AES). These experiments were performed at the Johnson Matthey Technology Centre, Sonning Common, UK. The results obtained are given in Table 3-4.

The amount of Pt, as determined by ICP-AES analysis, in all the catalysts was found to be nearly the same within experimental error (of ± 10% of the determined value), indicating that almost no platinum was lost during the preparation. A comparison of the theoretical and experimental assays of the second metal indicates, considering experimental error, that almost all of the Sn and Fe were deposited on the Pt/Al_2O_3 catalyst for the $SnPt/Al_2O_3$ and $FePt/Al_2O_3$ catalysts in agreement with

UV-Vis results. However, the cobalt content was found to be lower than the nominal value for the $CoPt/Al_2O_3$ catalysts. This suggests that the reaction had not gone to completion again in agreement with UV-Vis results.

Table 3-4: ELEMENTAL ANALYSIS OF THE CATALYSTS PREPARED

Catalyst	Pt Assay (Mass%) (± 10 %)	Experimental %M (Mass%)(± 10 %)	Theoretical %M * (Mass%)
5%Pt/Al_2O_3(low) - I	4.60	—	—
5%Pt/Al_2O_3(low) – II	5.18	—	—
(1:2)SnPt(low) (I)	4.49	0.44	0.46
(1:1)SnPt(low) (I)	4.65	0.88	0.91
(1:2)FePt(low) (I)	4.62	0.20	0.22
(1:1)FePt(low) (I)	4.73	0.38	0.40
(1:2)CoPt(low) (II)	4.89	0.16	0.20
(1:1)CoPt(low) (II)	4.99	0.34	0.46
(1:2)CrPt(low) (II)	4.79	0.17	0.25
(1:2)NiPt(low) (II)	4.93	0.22	0.30
(1:2)CuPt(low) (II)	4.89	0.09	0.24
(1:2)CuPt(low) (II)#	4.91	0.23	0.22
(1:2)MnPt(low) (II)#	4.84	0.19	0.22
5%Pt/Al_2O_3(high) - I	4.94	—	—
5%Pt/Al_2O_3(high) – II	5.20	—	—
(1:4)SnPt/Al_2O_3	4.57	0.42	0.42

Catalyst	Pt Assay (Mass%) (± 10 %)	Experimental %M (Mass%)(± 10 %)	Theoretical %M * (Mass%)
(1:1)SnPt(high) (I)	4.57	1.58	1.58
(1:2)FePt(high) (I)	4.86	0.49	0.36
(1:1)FePt(high) (I)	4.65	0.73	0.70
(1:2)CoPt(high) (II)	4.53	0.33	0.44
(1:1)CoPt(high) (II)	4.65	0.67	0.80

Catalyst preparation carried out in toluene.

* Calculated by amounts of 5%Pt/Al_2O_3 and the Pt/Al_2O_3 dispersion as given in Table 3-1.

Note: All results reported for metal assays are within experimental error of ± 10%.

From the ICP-AES analysis, it was observed that the amounts of Cr and Ni deposited in attempted half monolayer coverage were significantly lower than the nominal values. This differs from the UV-vis results for CrPt catalyst where no unreacted chromocene was found in the filtrate after reaction. This suggests that chromocene precursor decomposes during the course of the reaction. In the case of the Cu catalyst, attempts were made to prepare a half monolayer of Cu on Pt using Cu-acetylacetonate as a precursor in different solvents. Solubility of the precursor in heptane being poor, this gave a low loading of Cu in the catalyst whereas much better solubility in toluene gave the desired results. Analysis of the MnPt catalyst, prepared from the acetylacetonate precursor in toluene, also gave results similar to the nominal value.

For simplicity, the catalysts are referred to throughout, by the nominal rather than the experimental coverage i.e. 1:2 or 1:1.

3.2 CHARACTERIZATION OF M-Pt/Al_2O_3 BIMETALLIC CATALYSTS

3.2.1 TRANSMISSION ELECTRON MICROSCOPY (TEM) AND ENERGY DISPERSIVE X-RAY ANALYSIS (EDX)

Fig. 3-3 shows a typical transmission electron micrograph for the 5%Pt/Al_2O_3(low) catalyst. The 5%Pt/Al_2O_3 catalyst seemed to be well dispersed and no indication of agglomeration of the Pt particles was observed. EDX analysis confirmed the dark spots to be Pt particles, and the lighter background was alumina.

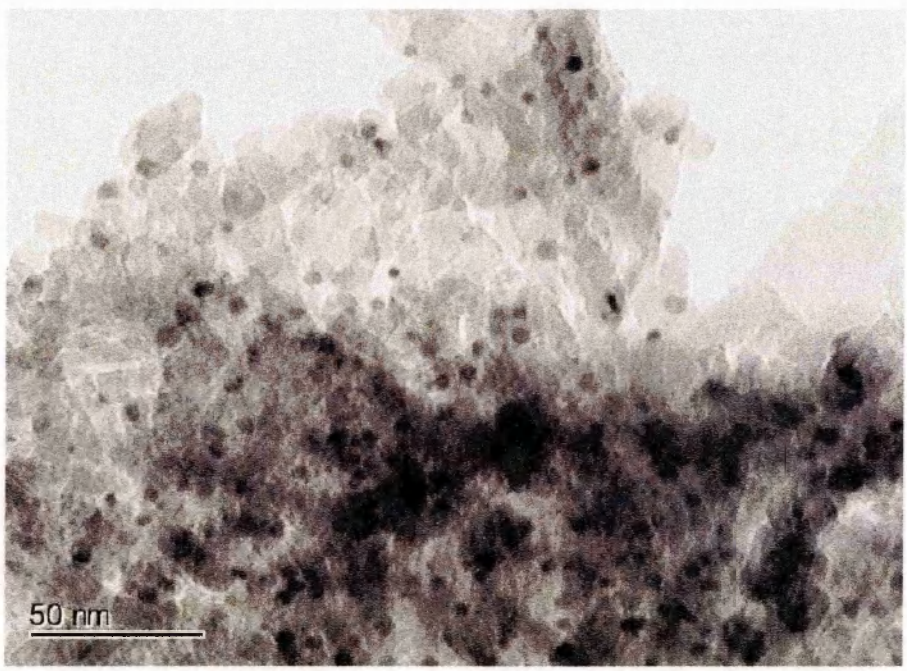

FIGURE 3-3: A typical transmission electron micrograph of 5%Pt/Al_2O_3(low) catalyst

The size of the Pt particles was measured directly from the micrographs. The size of the particles was found to be in the range of 2–7 nm with most of the particles found to be lying between 3–5 nm. The area with big dark spots was found to be

because of the extra thickness of the sample and not due to large particle size. This was determined by switching the same area containing the sample on the Cu-grid between bright and dark field mode.

A typical micrograph of the $SnPt/Al_2O_3$ catalyst, prepared by the SOMC route is shown in Fig. 3-4. The particle size does not change significantly although a slight increase is expected as a result of the method of preparation of bimetallic catalysts.

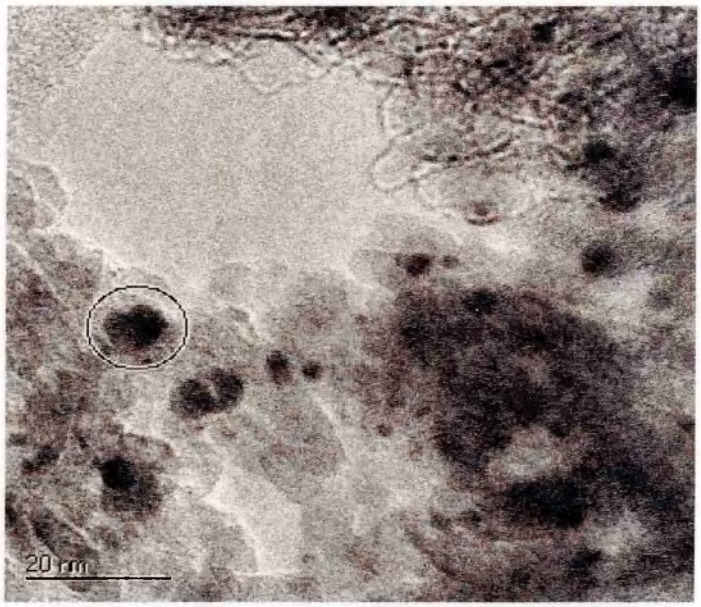

FIGURE 3-4: A typical transmission electron micrograph of (1:2) $SnPt/Al_2O_3$(low)

It has been reported that the supported SnPt catalysts when prepared by the SOMC route tends to give a SnPt species which was thought to exist as a Sn "ad-atom" on a Pt particle [1]. The localisation of these ad-atoms on the specific crystallographic sites on the metallic particles, particularly on the faces of bigger particles [2,3,4] and on the edge sites of the smaller ones has also been reported [5].

An increase in the average metal particle size with the addition of tin, using the SOMC technique, to Pd/SiO_2 has been reported by Coq *et. al.*[6]. Humblot *et. al.* [5] also reported an increase in the particle size (+0.5 Å) of Pt/SiO_2 after the addition of small amounts of tin. Similar findings have been reported by a number of groups [7,8]

for various supported noble metals. The addition of an atomic monolayer of the second metal over the platinum or palladium particles was thought to be the cause of such increase in the size of metal particles. Halttunen [9] also suggested that the deposition of second metal on the parent metal was the cause of such increase in the size of metal particle.

Fig. 3-5 shows a small section of Cu grid containing the (1:1)FePt(low) catalyst. It was found that with the addition of Fe to the Pt catalyst, there was no significant change in the particle size. EDX analysis of the area occupied by the particle confirmed the presence of the two metals in close proximity (Fig. 3-6).

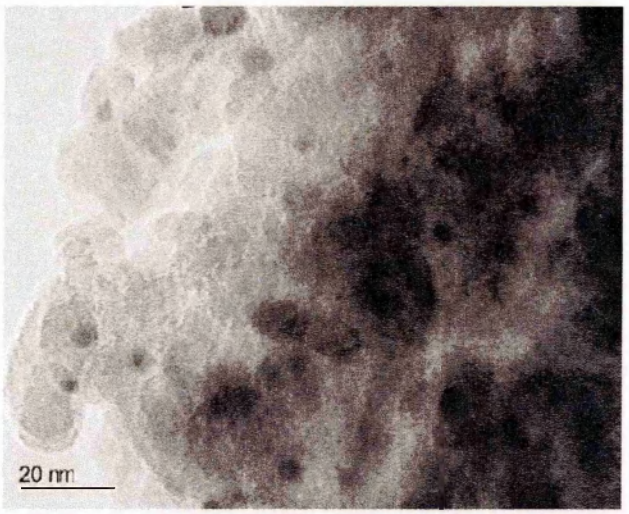

FIGURE 3-5: A typical transmission electron micrograph of (1:1)FePt/Al_2O_3(low)

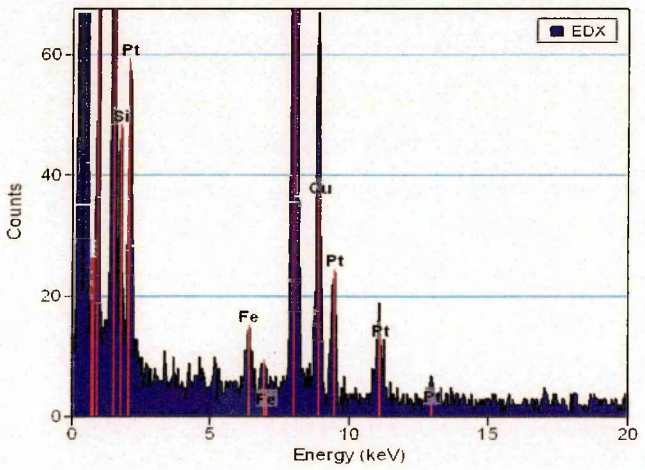

FIGURE 3-6: EDX analysis of area occupied by a FePt particle

A series of micrographs were taken for Co-promoted catalysts. The catalysts investigated were (1:2)CoPt(low), (1:2)CoPt(high) and (1:1)CoPt(low). The (1:2)CoPt low and high-dispersed catalysts were chosen to see if there were any difference between the catalysts with different dispersions, whereas the effect of the amount of Co was looked at using (1:2) and (1:1)CoPt(low) catalysts. (It was interesting to note that the (1:1)CoPt(low) catalyst had almost the same amount of Co as (1:2)CoPt(high) catalyst.)

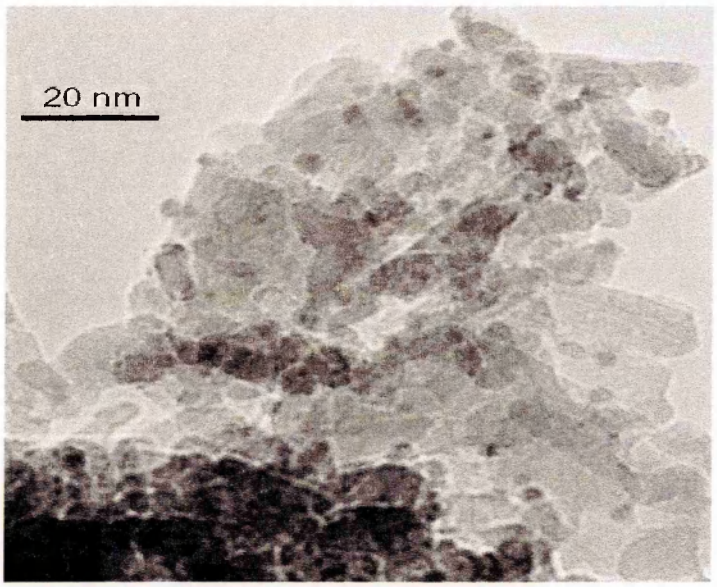

FIGURE 3-7: A typical transmission electron micrograph of (1:2)CoPt/Al_2O_3(low)

The micrograph of the (1:2)CoPt(low) catalyst shows well-dispersed metallic particles (Fig. 3-7). There was no apparent change in the size of the metal particles after promotion with Co. It was difficult to locate Co in this sample using EDX, probably because of the low loading (about 0.16%) of Co. However, its presence was confirmed by ICP-AES analysis and HAADF images.

A typical micrograph of the (1:2)CoPt(high) catalyst is shown in Fig. 3-8. It is found that the size of the metal particles varies over a wide range of less than 1 nm to about 11 nm.

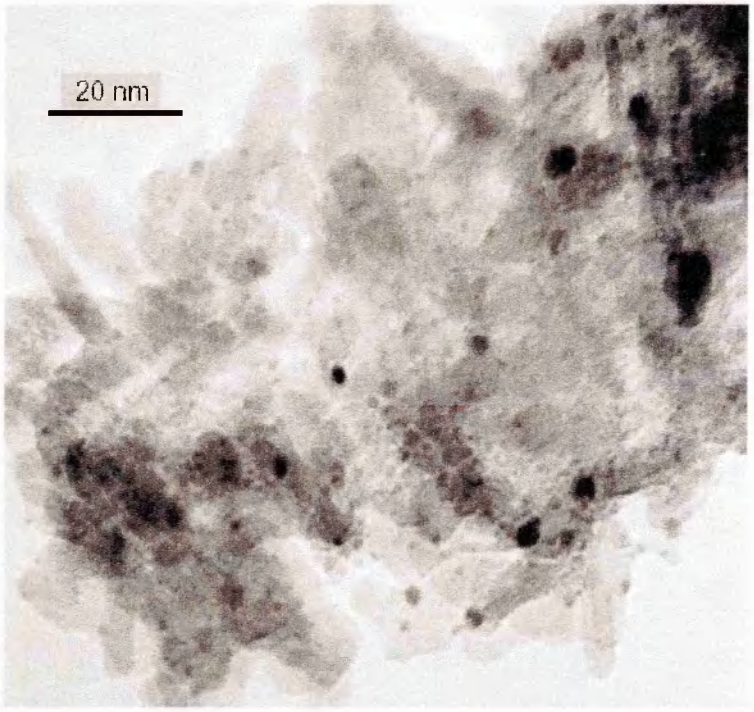

FIGURE 3-8: A typical transmission electron micrograph of (1:2)CoPt/Al_2O_3(high)

Fig. 3-9 shows the micrograph of a well-dispersed (1:1)CoPt(low) catalyst. The particle size was found to be similar to that in the unpromoted catalyst.

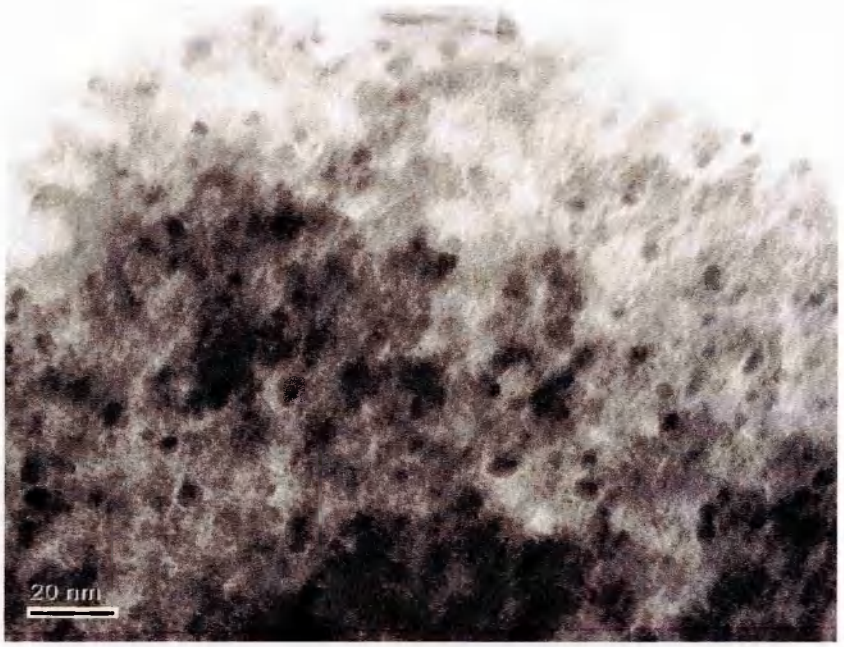

FIGURE 3-9: A typical transmission electron micrograph of (1:1)CoPt/Al_2O_3(low)

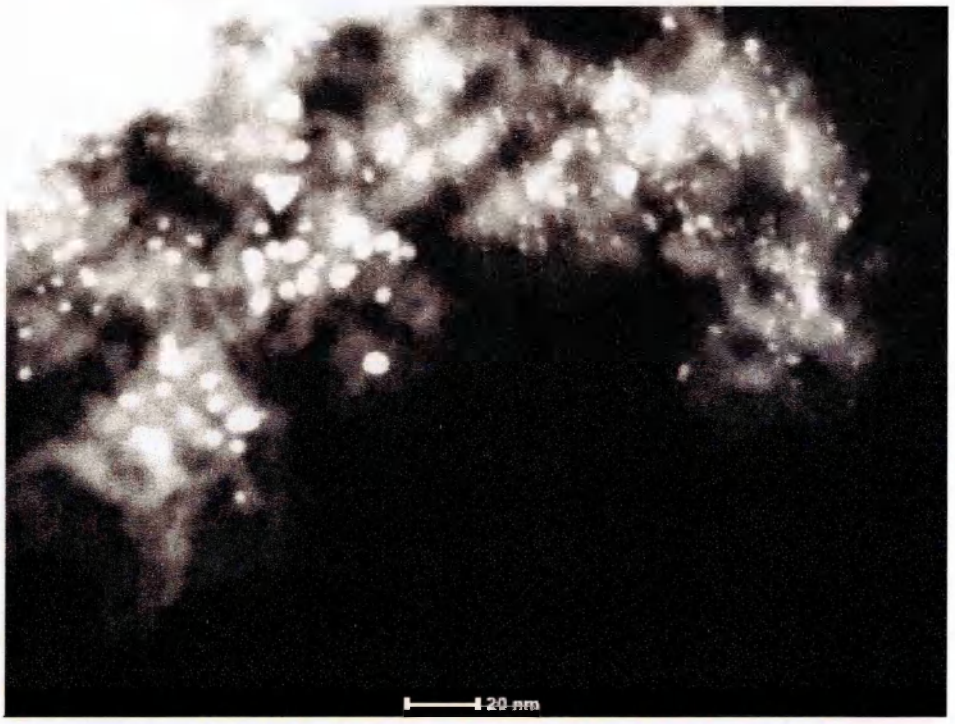

FIGURE 3-10: A typical HAADF image of (1:2)CoPt/Al_2O_3(low) catalyst

In order to confirm the location of the two metals relative to each other the HAADF imaging technique was used. Since the signal in this technique depends on

the atomic number of the specimen region, it is much easier to locate the heavier metal particles dispersed in the alumina background. A region of the grid with the (1:2)CoPt(low) catalyst was locked on the monitor and the dark field image was taken (Fig. 3-10). A big line scan of just over 50 nm was selected encompassing a few bright spots which were thought to be the metal particles, (Fig. 3-11a). EDX analysis was performed along the selected line (Fig. 3-11b). EDX confirmed the presence of the two metals along the line. When the results were quantified as a function of position of the two metals along each line (Figs. 3-11c and d), it was found that the position of the two metals is exactly the same with Pt and Co coinciding only at the positions where Pt was found.

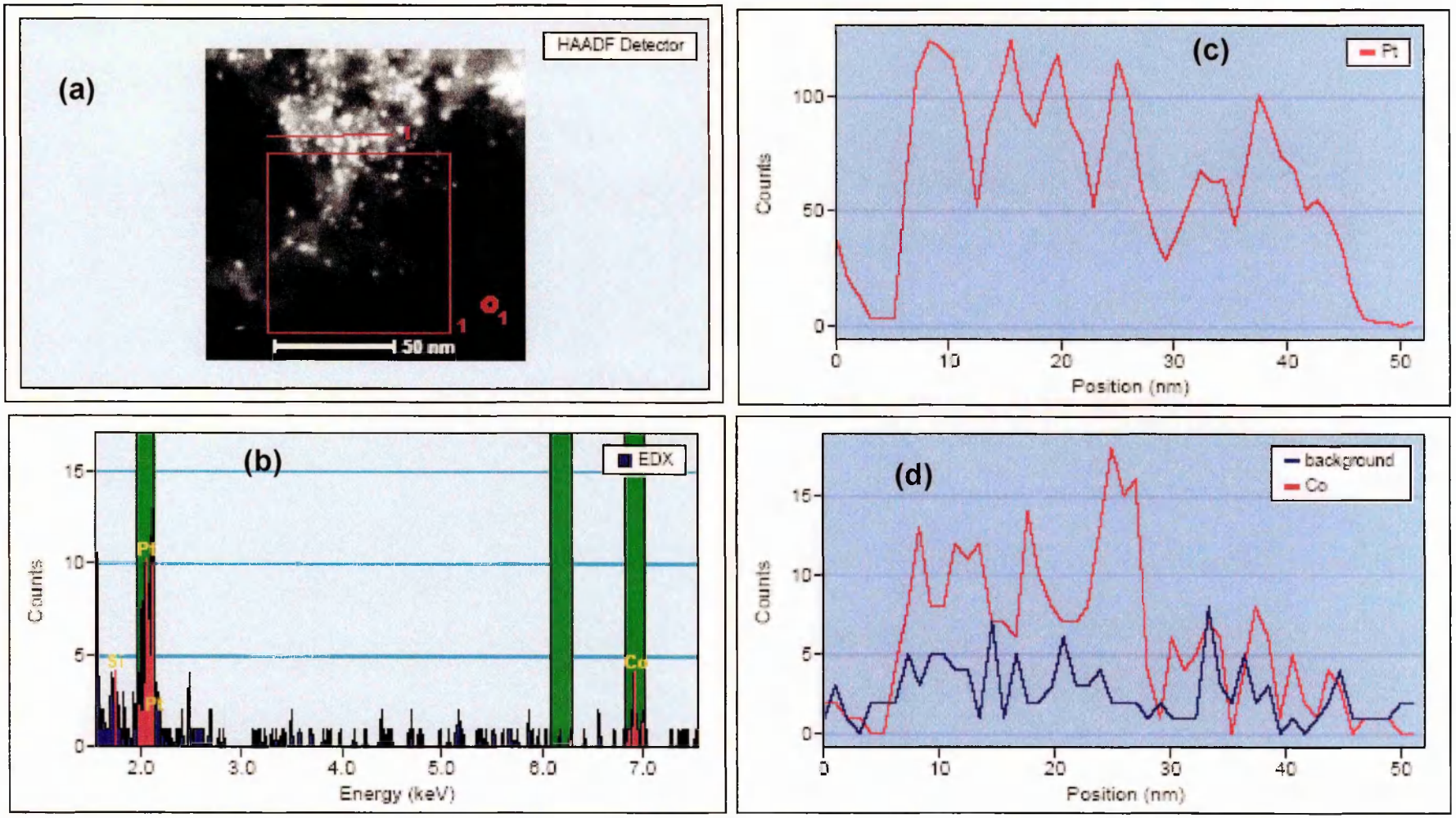

FIGURE 3-11: A typical HAADF image and EDX analysis of (1:2) $CoPt/Al_2O_3$(low) catalyst

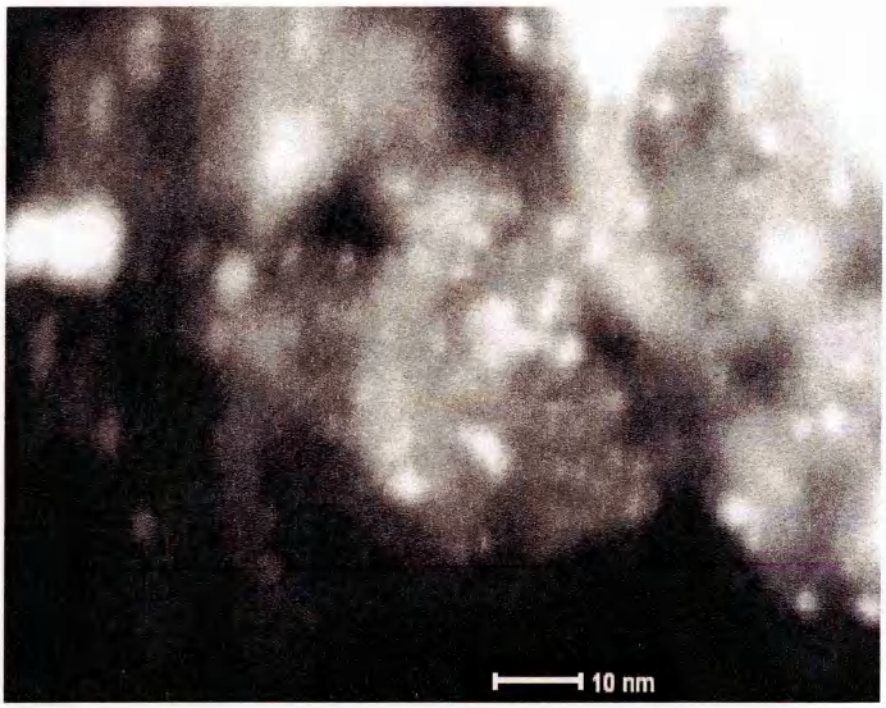

FIGURE 3-12: A typical HAADF image of (1:2)CoPt/Al_2O_3(high) catalyst

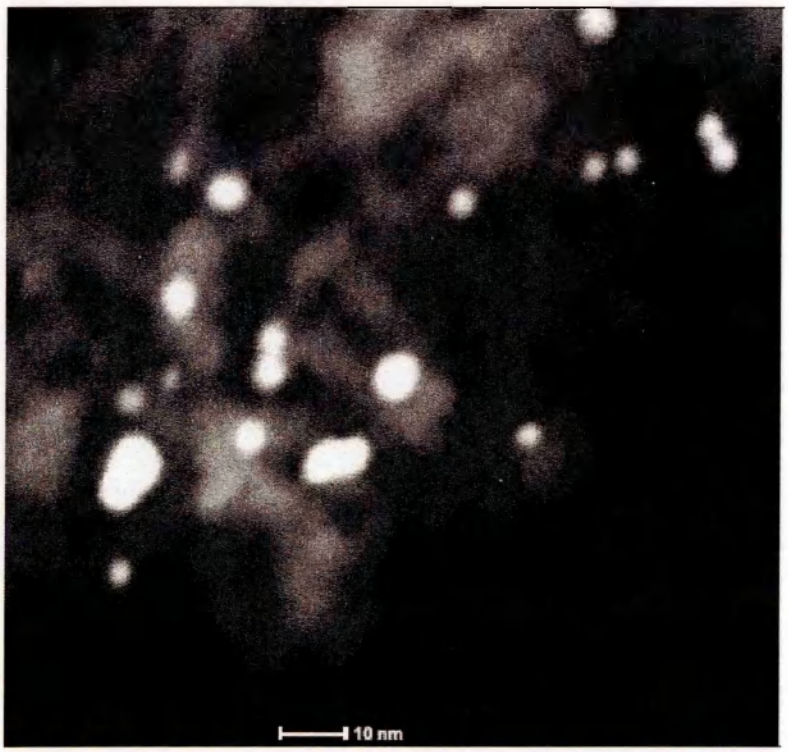

FIGURE 3-13: A TYPICAL HAADF image of (1:1)CoPt/Al_2O_3(low) catalyst

The HAADF images for (1:2)CoPt(high) and (1:1)CoPt(low) catalyst are presented in Figs. 3-12 and 3-13 respectively. The highly dispersed nature and wide range of particle size are clearly seen in the HAADF image for the (1:2)CoPt(high) catalyst (Fig. 3-12).

A line scan of just under 25 nm was performed on the (1:2)CoPt(high) catalyst (Fig. 3-14a). Again co-existence of the two metals at the same location is very clearly confirmed (Fig. 3-14b-d).

Similarly, a line scan performed on the (1:1)CoPt(low) catalyst of just under 20 nm, showed the presence of Pt and Co together, and the quantified results proved the two metals to coincide (Fig. 3-15a-d).

These TEM micrographs, HAADF images, EDX analysis and subsequent quantification of data, confirmed the physical location of the two metals to be the same, suggesting that the Co was deposited selectively with the Pt.

So from the electron micrographs it has been shown that two metals are in close contact. No monometallic tin, iron or cobalt particles were found on the support. These results agree with the selective deposition of the second metal by the reduction of the respective organometallic salts of tin, iron and cobalt by the means of hydrogen activated on the Pt surface.

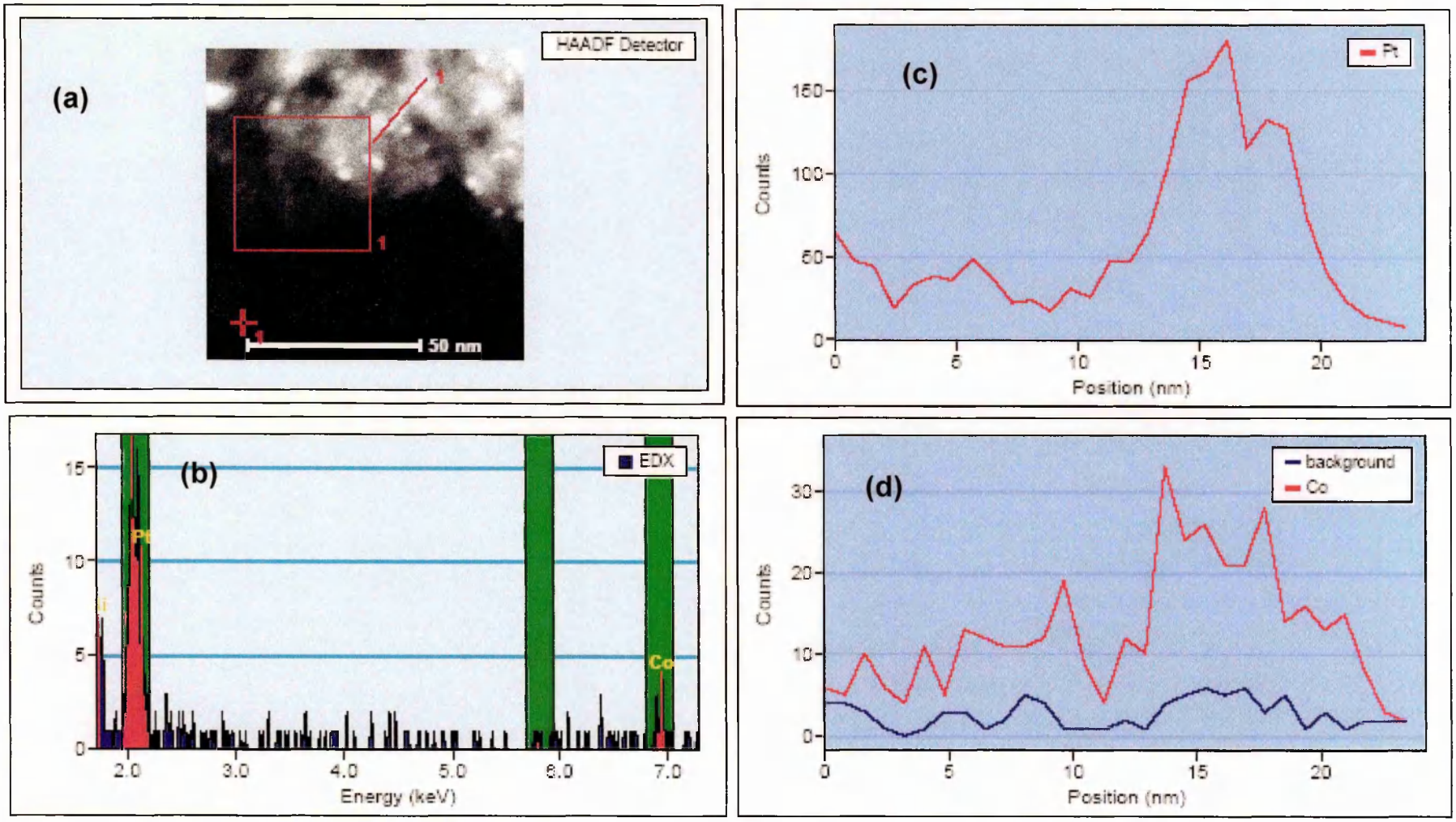

FIGURE 3-14: The HAADF image and EDX analysis of (1:2)CoPt/Al_2O_3(high) catalyst

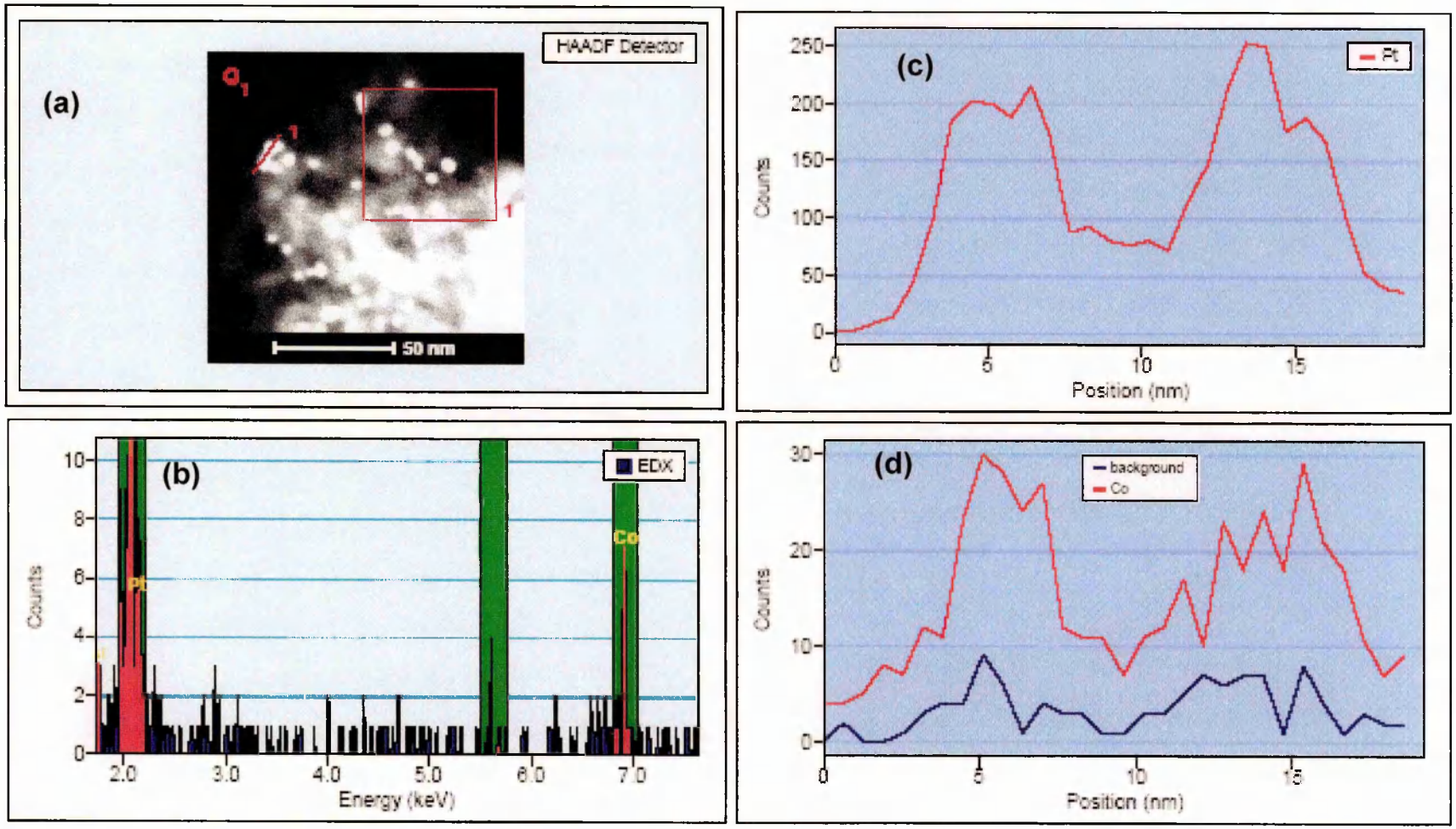

FIGURE 3-15: The HAADF image and EDX analysis of (1:1) $CoPt/Al_2O_3$(low) catalyst

3.2.2 CHEMISORPTION

Hydrogen chemisorption experiments were performed at the OU to determine the dispersion of unpromoted Pt particles in catalysts (Table 3-5). On highly dispersed Pt catalysts, dispersion values of over 100% (135 for high and 106 for low) were observed with hydrogen chemisorption, suggesting that the assumption of 1:1 stoichiometry (H:M) does not hold good for this adsorption on such highly dispersed samples. It was then decided to change the adsorbate gas to CO for the metal dispersion measurements in this work.

CO chemisorption (measured using the volumetric method, discussed in chapter 2) appeared to yield reproducible results which are in good agreement with the results (obtained by the pulsed technique) reported by the Johnson Matthey Technology Centre, Sonning Common, UK. As a result, CO was used as the adsorbate gas for further chemisorption experiments to determine the metal dispersion on the catalysts prepared in this study.

Table 3-5: TABLE OF COMPARISON FOR THE CHEMISORPTION RESULTS OBTAINED BY DIFFERENT METHODS

Sample	Dispersion (%)		
	H/Pt (OU)	CO/Pt (OU)	CO/Pt (JM)
5%Pt/Al_2O_3 (high dispersion)	(135)	48	51
5%Pt/Al_2O_3 (low dispersion)	(106)	36	29

OU: results obtained by chemisorption experiments performed at Open University

JM: results obtained by chemisorption experiments performed at JMTC

The results from chemisorption experiments conducted on the 5%Pt/Al_2O_3, reveal a high metal dispersion viz., CO/Pt = 36% and 48% for the low- and high-dispersed systems, respectively. Even though good consistency is observed in the

CO/Pt results for unpromoted Pt catalysts, the results for the promoted Pt catalysts are taken only in a qualitative sense, simply because the stoichiometry of the chemisorption between CO and the modified catalyst surface is not well known.

Fig. 3-16 shows a typical isotherm obtained by plotting Q_3^n against P_e^n and marked with Point A and Point B, used for the calculation of $\frac{CO}{M}$ (as described earlier).

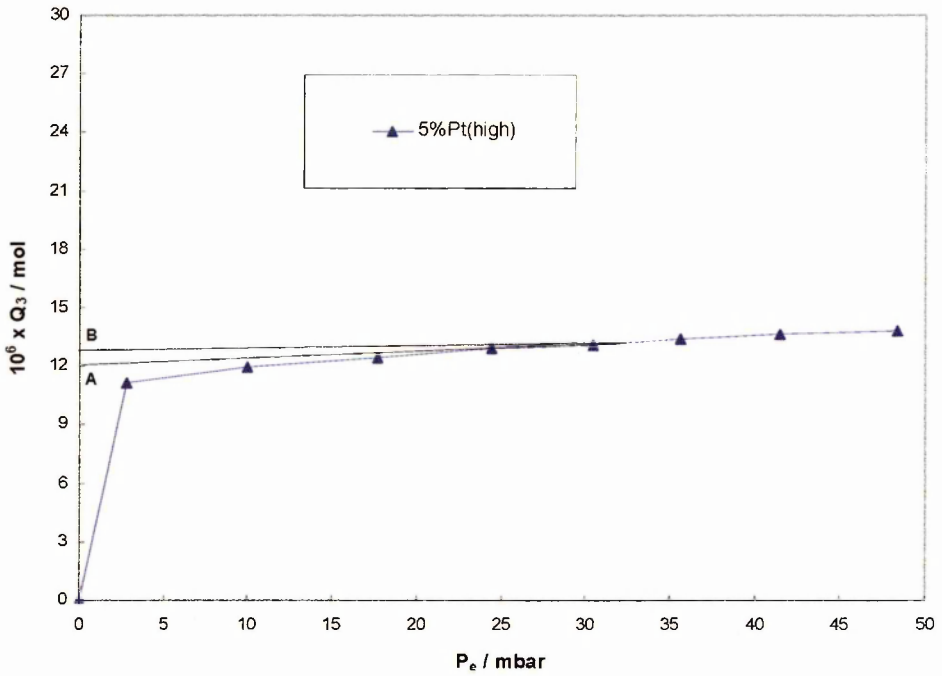

FIGURE 3-16: A typical isotherm marked with Point A and Point B, used in the calculations

Fig. 3-17 shows the data obtained from the CO chemisorption experiment over 5%Pt/Al_2O_3(high) catalyst and fitted to the modified Langmuir equation shown below:

$$\frac{P}{Q_3^n} = \frac{c}{Q_0} + \frac{P}{Q_0} \qquad (1)$$

where P is the pressure, c is an empirical constant and Q_0 is the monolayer capacity. A plot of $\frac{P}{Q_3^n}$ against P should yield a straight line with slope $\frac{1}{Q_0}$. The monolayer capacity can be calculated as reciprocal of the slope.

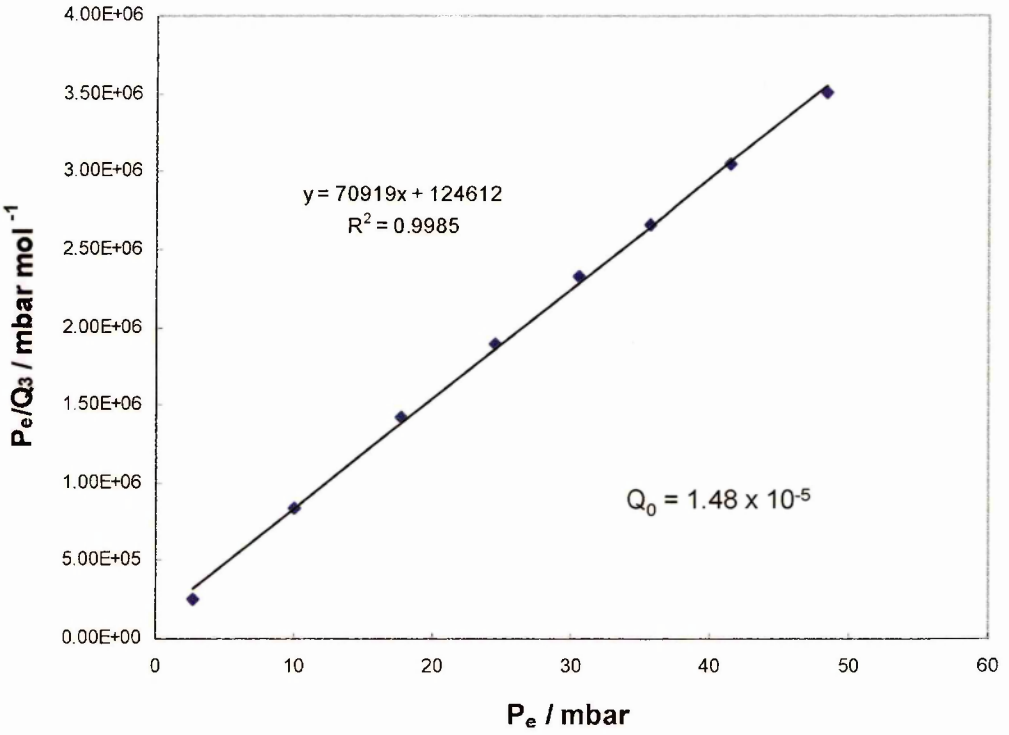

FIGURE 3-17: Langmuir fit to the CO chemisorption data collected over the 5%Pt/Al_2O_3(high)

$\frac{CO}{M}$ values calculated for the 5%Pt/Al_2O_3(high) catalyst using the above mentioned methods are shown in Table 3-6.

Table 3-6: DISPERSION VALUES CALCULATED FOR 5% Pt/Al_2O_3 (HIGH) CATALYST USING VARIOUS METHODS

Method	CO/M
Point A	0.48
Point B	0.53
Langmuir fit	0.59

The isotherms for the catalysts studied are shown in Figs. 3-18 – 3-24.

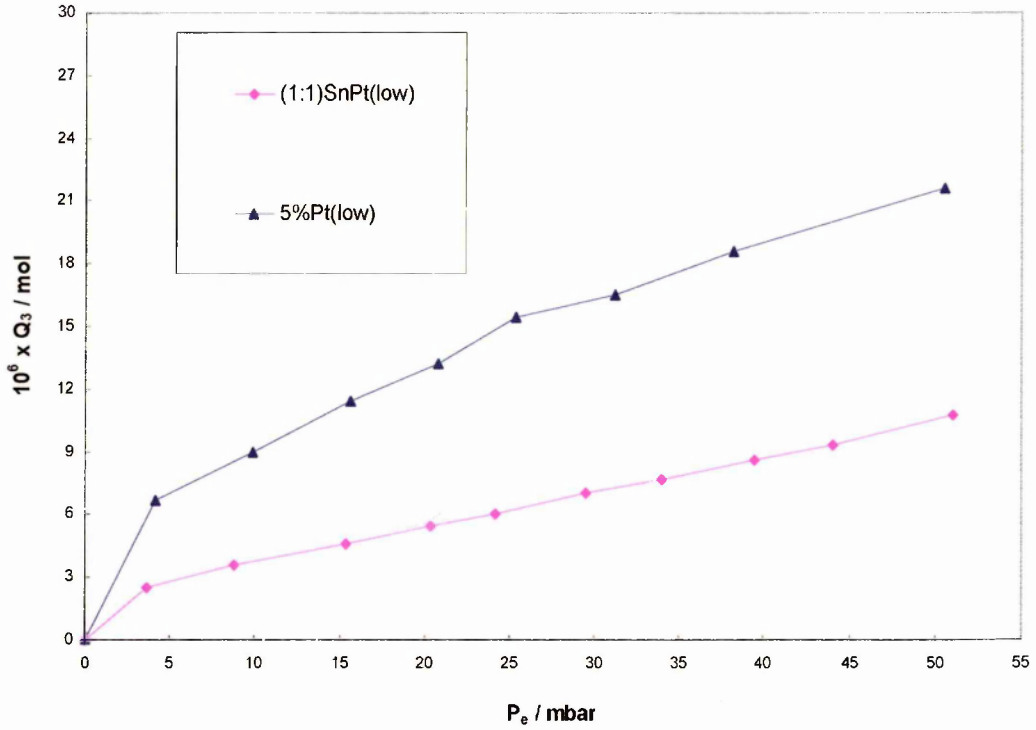

FIGURE 3-18: The CO chemisorption profiles for Pt/Al_2O_3 and $SnPt/Al_2O_3$(low) catalysts

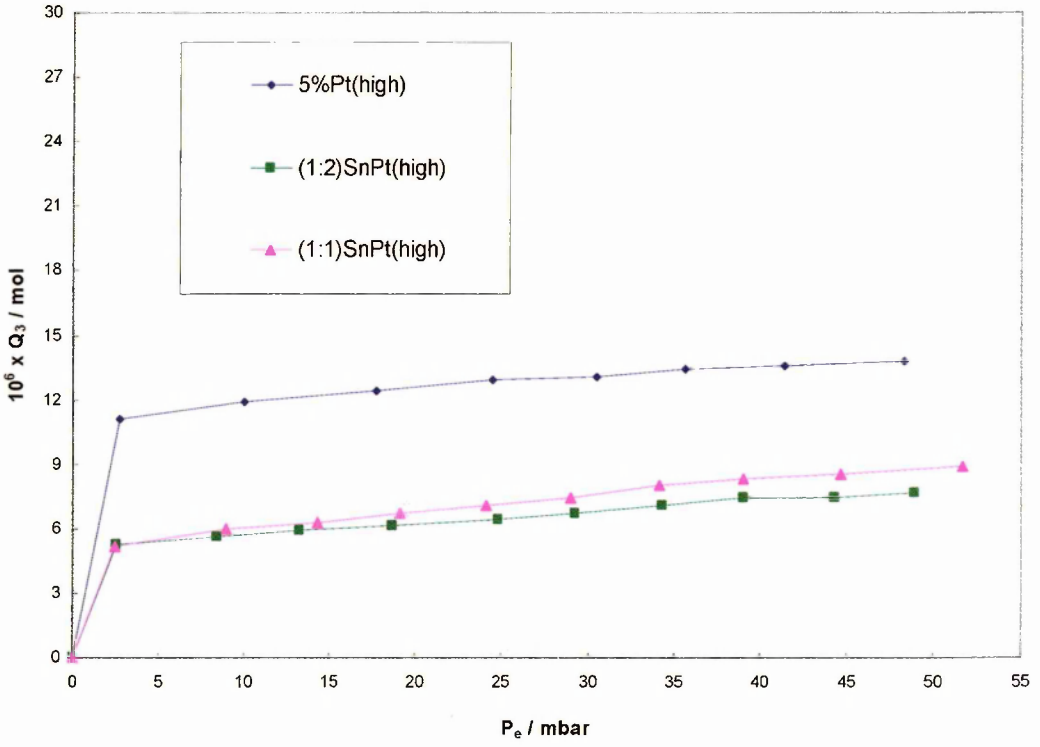

FIGURE 3-19: The CO chemisorption profiles for Pt/Al_2O_3 and $SnPt/Al_2O_3$(high) catalysts

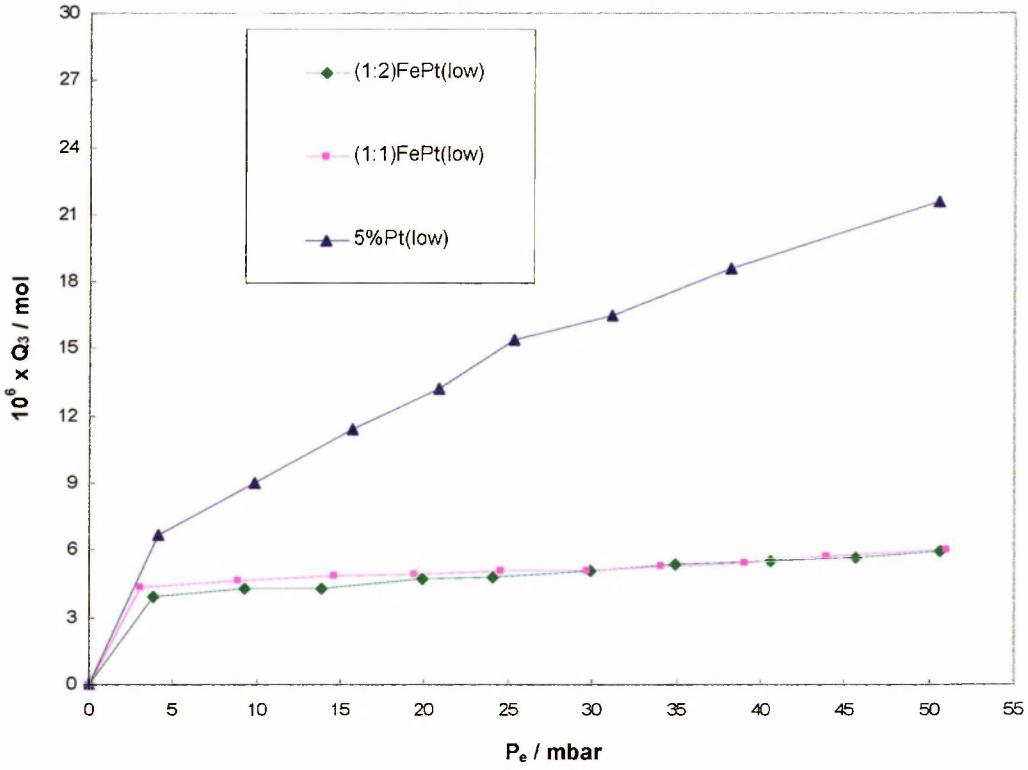

FIGURE 3-20: The CO chemisorption profiles for Pt/Al_2O_3 and $FePt/Al_2O_3$(low) catalysts

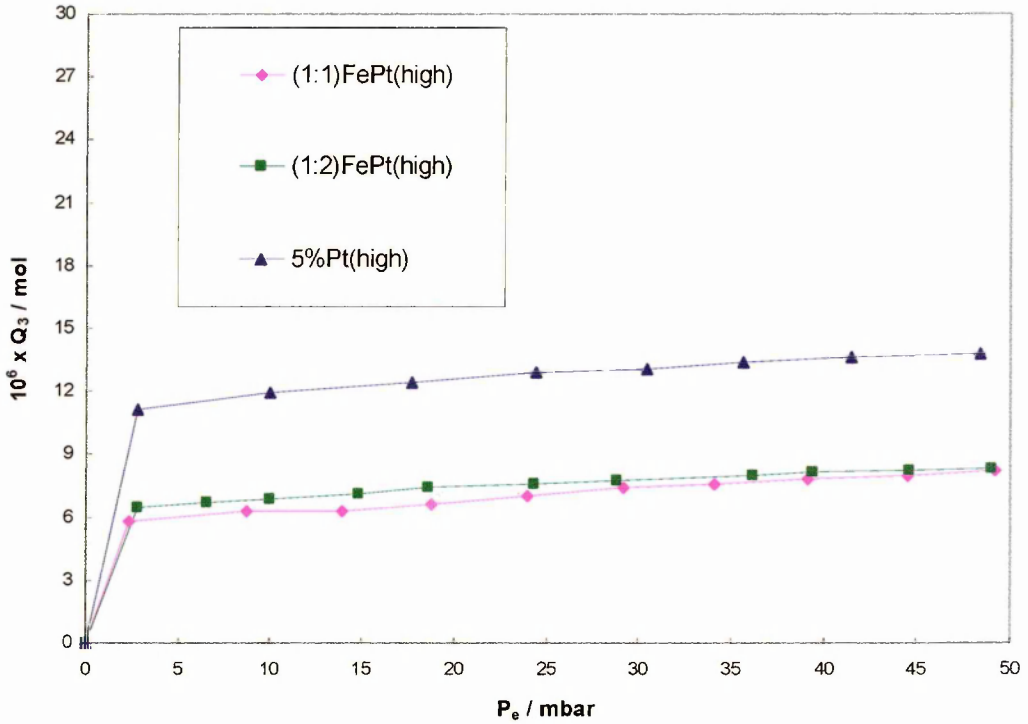

FIGURE 3-21: The CO chemisorption profiles for Pt/Al_2O_3 and $FePt/Al_2O_3$(high) catalysts

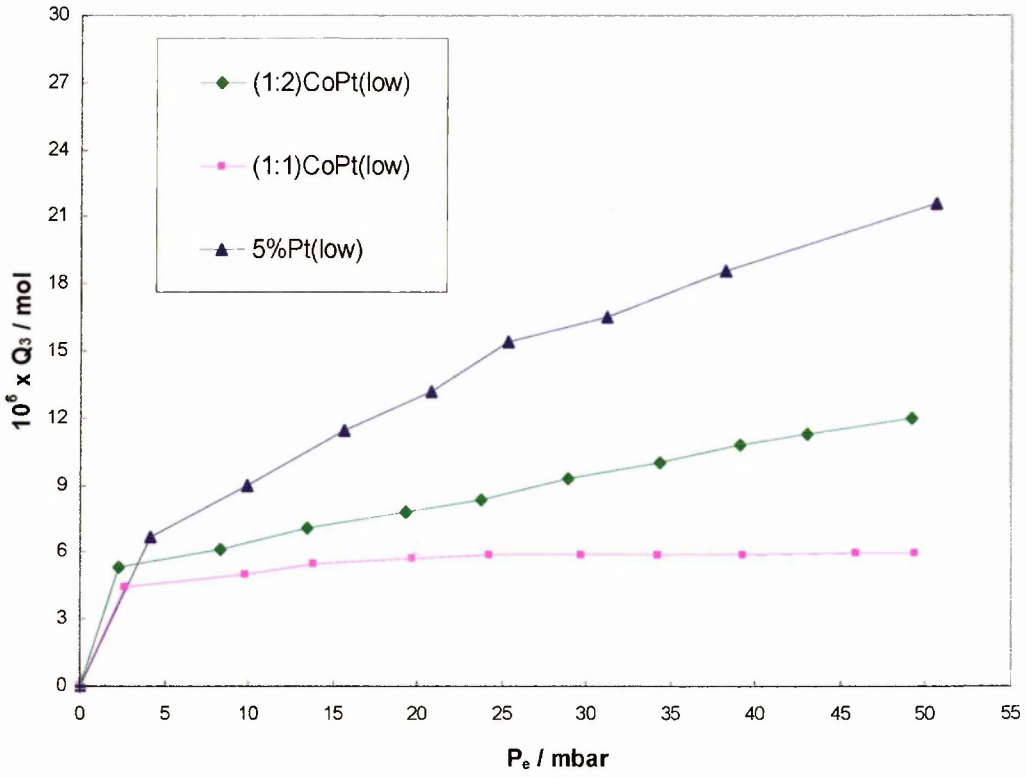

FIGURE 3-22: The CO chemisorption profiles for Pt/Al_2O_3 and $CoPt/Al_2O_3$ (low) catalysts

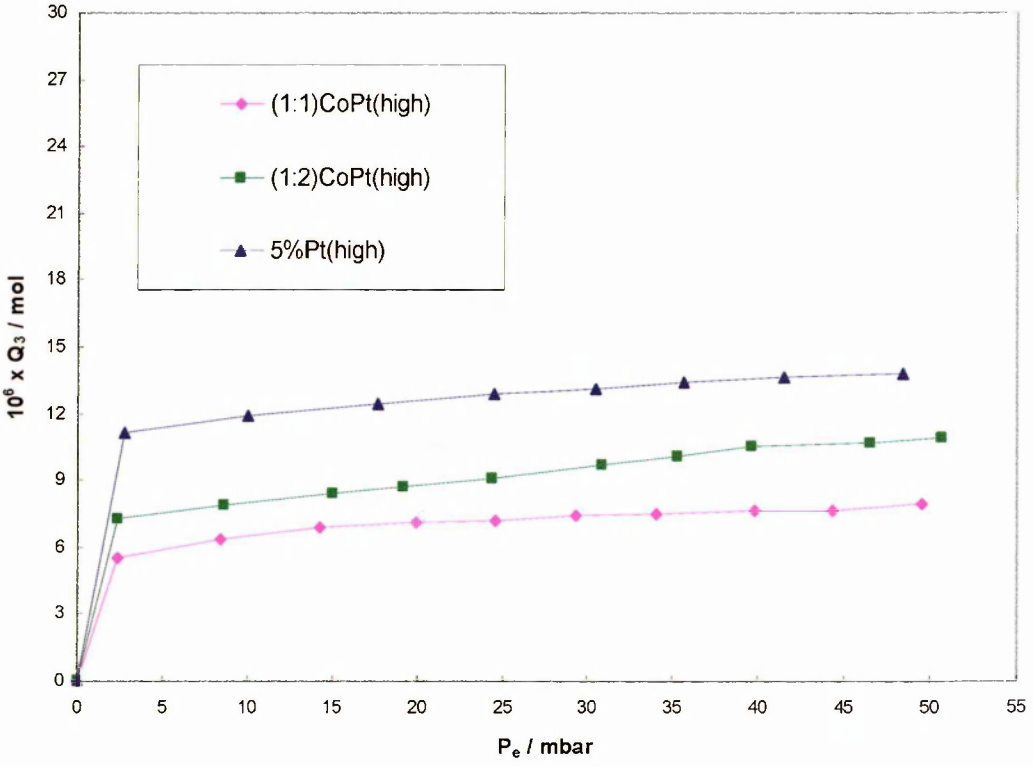

FIGURE 3-23: The CO chemisorption profiles for Pt/Al_2O_3 and $CoPt/Al_2O_3$ (high) catalysts

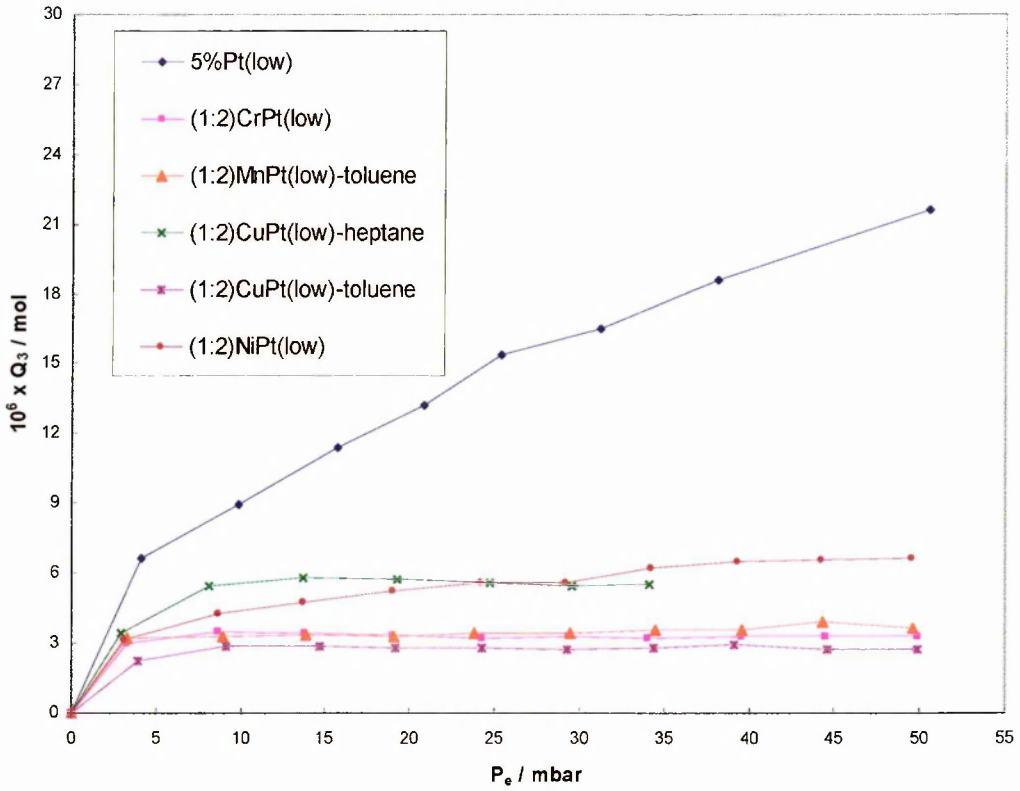

FIGURE 3-24: The CO chemisorption profiles for Pt/Al_2O_3 and (1:2) M-Pt/Al_2O_3(low) catalysts (where M= Cr, Mn, Ni, Cu)

In the discussion of our results, it is assumed that there was no significant change in the stoichiometry of CO adsorption on Pt surface with the addition of small amount of the promoter (corresponding to the composition range studied in the present work for the promoters studied). A similar assumption was also made by Pinna and co-workers during their studies on supported Pd-Fe catalysts [10].

Table 3-7 shows CO/M values calculated using monolayer capacity values from Point A, Point B and also by fitting the data to the Langmuir model. In our case not all isotherms (Figs. 3-18 – 3-24) seemed to achieve a horizontal section in the pressure range studied and so the given values are calculated by extrapolation to zero pressure (Point A, as the isotherm does not show horizontal region and Point B (value at start of the linear portion)). Within experimental limits the two data sets seem to agree nicely in

most cases. If the isotherm was horizontal then both the values would give the same result as is observed in some cases.

Table 3-7: CO CHEMISORPTION RESULTS FOR M-Pt/Al_2O_3 CATALYSTS

Catalyst	CO/M	CO/M $^+$	CO/M $^\infty$	Experimental %M (mass%)	Theoretical %M (mass%)
5%Pt/Al_2O_3(low)-I	0.36	0.65	0.95	—	—
5%Pt/Al_2O_3(low)-II	0.26*	—	—	—	—
(1:1)SnPt(low)	0.08	0.10	0.25	0.88	0.91
(1:2)FePt(low)	0.16	0.17	0.28	0.20	0.22
(1:1)FePt(low)	0.17	0.18	0.20	0.38	0.40
(1:2)CoPt(low)	0.19	0.20	0.23	0.16	0.20
(1:1)CoPt(low)	0.20	0.20	0.21	0.34	0.46
(1:2)CrPt(low)	0.13	0.13	0.12	0.17	0.25
(1:2)NiPt(low)	0.20	0.20	0.24	0.23	0.22
(1:2)CuPt(low)	0.09	0.09	0.10	0.09	0.24
(1:2)CuPt(low)#	0.20	0.20	0.20	0.22	0.30
(1:2)MnPt(low)#	0.11	0.11	0.12	0.19	0.22
5%Pt/Al_2O_3(high)-I	0.48	0.53	0.59	—	—
5%Pt/Al_2O_3(high)-II	0.54*	—	—	—	—
(1:4)SnPt(high)	0.30	0.32	0.51	0.42	0.42
(1:1)SnPt(high)	0.24	0.30	0.44	1.58	1.58

Catalyst	CO/M	CO/M $^{+}$	CO/M $^{\propto}$	Experimental %M (mass%)	Theoretical %M (mass%)
(1:1)FePt(high)	0.24	0.29	0.36	0.73	0.70
(1:2)CoPt(high)	0.36	0.40	0.48	0.33	0.44
(1:1)CoPt(high)	0.24	0.26	0.29	0.67	0.80

$^{\#}$ preparation carried out in toluene as solvent

$^{+}$ CO/M values calculated using Point B method

$^{\propto}$ CO/M values calculated using Langmuir model

* results reported by JM

Inspection of the results presented in Table 3-7 indicates a general decrease in the CO adsorbed on the promoted Pt catalysts compared to the unpromoted catalysts. The observed decrease in the amount of CO chemisorbed on the promoted Pt catalysts is attributed to the reduction in the number of the exposed Pt surface sites relative to the unpromoted Pt catalyst upon the addition of second metal. This again can be taken as evidence that the second metal is indeed deposited on the surface of the first metal and thus occupying some of the Pt sites otherwise available for the CO chemisorption.

For example, it can be seen that the addition of a half monolayer of tin to Pt/Al_2O_3(high) caused a decrease in the dispersion by a factor of two. TEM results show that the particle size in the promoted catalysts is not significantly different from that of the unpromoted catalysts. In addition, it has been shown that no change in dispersion occurs when a Pt/Al_2O_3 monometallic catalyst is treated to the same experimental procedure as in SOMC except that no organometallic precursor is present [11], thus a decrease in CO/M due to sintering of Pt particles can be discounted. This decrease observed seem consistent with the model expected given the nature of the preparation technique where the second metal is considered to be deposited on the surface of Pt

particles. Another interesting point emerging from the chemisorption results is that there is little difference in the CO adsorption with an increase in the amount of the second metal in most of the systems, highlighted for example with the SnPt(high) catalysts. It was found that the amount of CO adsorbed by the promoted catalysts with higher $M/Pt_{surface}$ ratios does not decrease as much would be expected as a result of covering more Pt sites. ICP-AES analysis on the SnPt(high) catalysts showed the amount of Sn deposited on the catalysts matched well with the predicted values. For low Sn content, such as in (1:4)SnPt(high) catalyst, there is a strong decrease in the amount of chemisorbed CO (from 0.5 to 0.3). Increasing the Sn content, as in (1:2) and (1:1)SnPt(high) catalysts only introduces a slight additional decrease in the chemisorbed CO values. Similar results have been observed by a number of authors for hydrogen and carbon monoxide adsorption on promoted catalysts [1,12]. Lieske and Volter [13] suggested the formation of a Pt-Sn alloy on alumina-supported Sn-promoted Pt catalysts to be the cause of the observed decrease in H_2 adsorption with increasing Sn content. Cortright and Dumesic [14] found that addition of Sn to Pt/SiO_2 reduces the number of active sites which strongly interact with carbon monoxide and hydrogen. Humblot *et. al.* [15] suggested that the first tin atoms on the metal surface affect the adsorptive properties of the Pt more than the subsequent ones, and that this is reflected in a large initial decrease in chemisorption. They also suggested that for low Sn content ($Sn/Pt_{surface} \leq 0.30$), the Sn atoms are located on particular sites of the surface of the metallic particle. For higher Sn content, a part of Sn atoms could migrate inside the particle or could even migrate on the support, in the close vicinity of the metallic particle. Similar results were seen for the other systems.

3.2.3 TEMPERATURE PROGRAMMED REDUCTION (TPR)

Most of the Temperature Programmed Reduction (TPR) experiments were carried out at Johnson Matthey Technology Centre, Sonning Common, on a sub-ambient TPR set up unless mentioned otherwise. About 0.3 g of each sample was analysed. TPR profiles for all these catalysts were collected in the range –100 - 600 °C.

In the TPR experiments conducted at the OU, alumina showed no peaks in the temperature range, 30 - 600 °C (Fig. 3-25). Voltage stabilization at the beginning of the experiment caused a large spike in the profile. These results indicated that the support material (γ-Al_2O_3) is not affected by hydrogen in the temperature range selected for the present study. Hence, all the peaks in the TPR profile can be attributed to the metallic part of the catalyst.

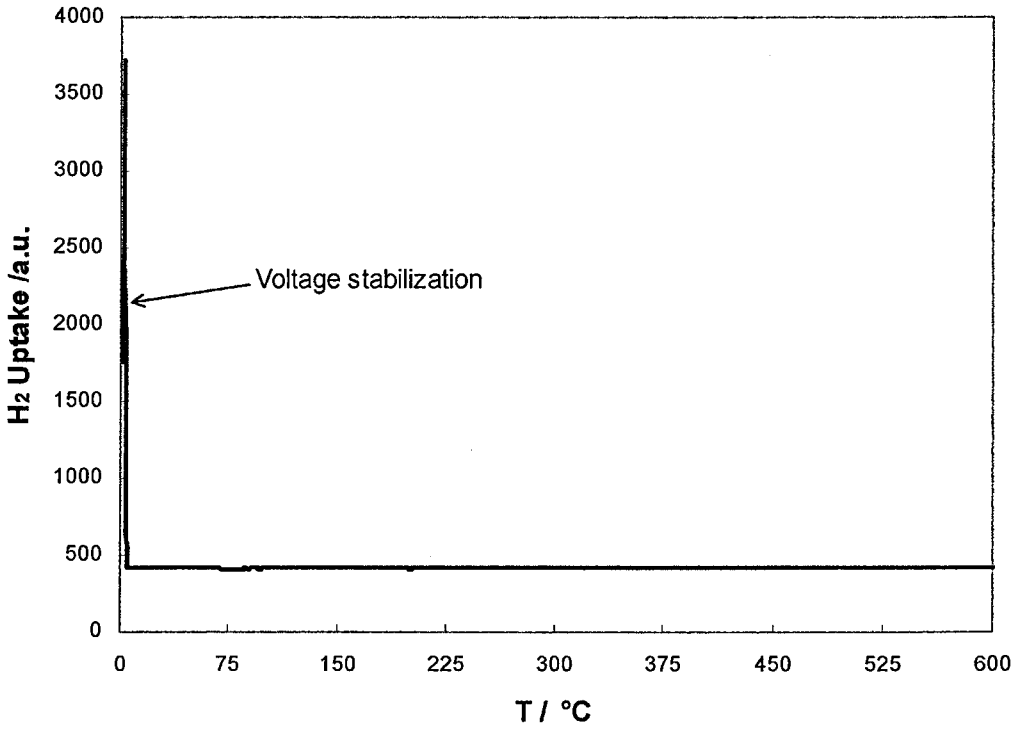

FIGURE 3-25: The TPR profile for γ-alumina (experiment performed at OU)

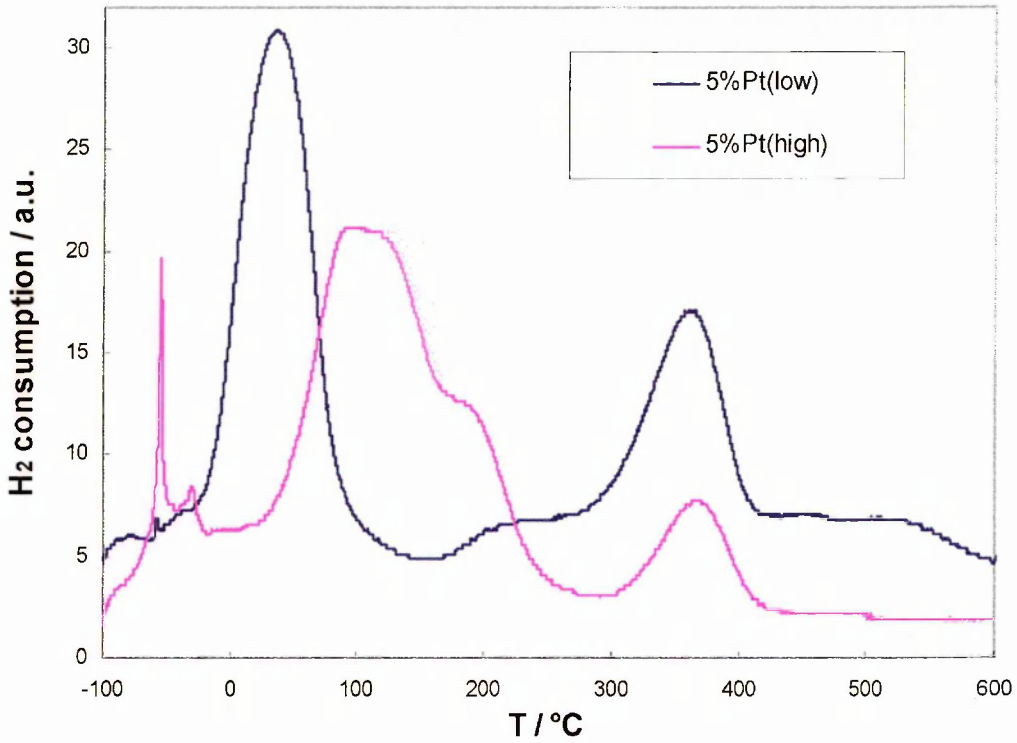

FIGURE 3-26: The TPR profile for 5%Pt/Al_2O_3(low) and (high) catalysts

The TPR profiles for both the Pt/Al_2O_3 (low and high) (Fig. 3-26) catalysts show a broad low temperature peak centred at 30 °C, starting sub-ambient at −100 °C and stretching to about 140 °C, for the low-dispersed catalyst. The low temperature region for the 5%Pt(high) catalyst showed H_2 uptake over a broader temperature range (−100 - 270 °C) compared to the corresponding low-dispersed catalyst, which could be attributed to a wider distribution of particle sizes. Similar 'sub-ambient' peaks were reported by Gland *et. al.* [16]. There was also a distinct peak at higher temperatures, centred at about 360 °C in both samples.

The TPR profile for 5%Pt/Al_2O_3(low) which had been reduced at 200 °C for 3 hours *ex-situ* then exposed to air, also showed the two distinct regions of hydrogen uptake (Fig. 3-27).

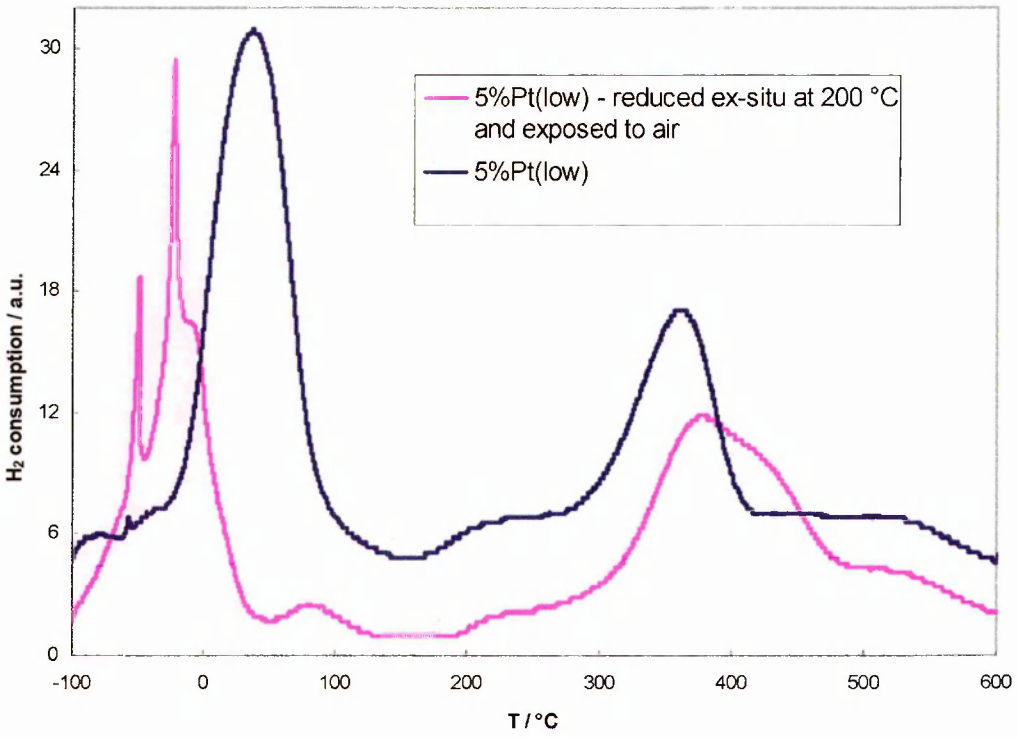

FIGURE 3-27: The TPR profile for 5%Pt/Al_2O_3(low) catalyst reduced at 200 °C for 3 hours and exposed to air

The sub-ambient peaks in the 'pre-reduced and then exposed' catalyst are very distinct. The large peak which lies at about 30 °C in the profile for the non-reduced catalyst was found to be shifted to −25 °C, indicating that the reducibility of the PtO_x species here is easier than in the non-reduced sample. Another very small peak was observed at about 80 °C. It has been reported that TPR studies of "reduced" catalysts [17] showed reduction peaks for Pt at temperatures substantially below that found for the bulk oxides.

The TPR profile for 5%Pt/Al_2O_3(high) catalyst reduced *ex-situ* at 200 °C for 3 hours (Fig. 3-28) was similar to that of the reduced ex-situ 5%Pt/Al_2O_3(low) catalyst. Two distinct regions of uptake were again observed. Pre-reduction of the 5%Pt(high) catalyst at 200 °C shifts the upper end of the low temperature broad peak to ~150 °C

from ~270 °C for the unreduced catalyst. The high temperature reduction peak is unshifted at about 360 °C.

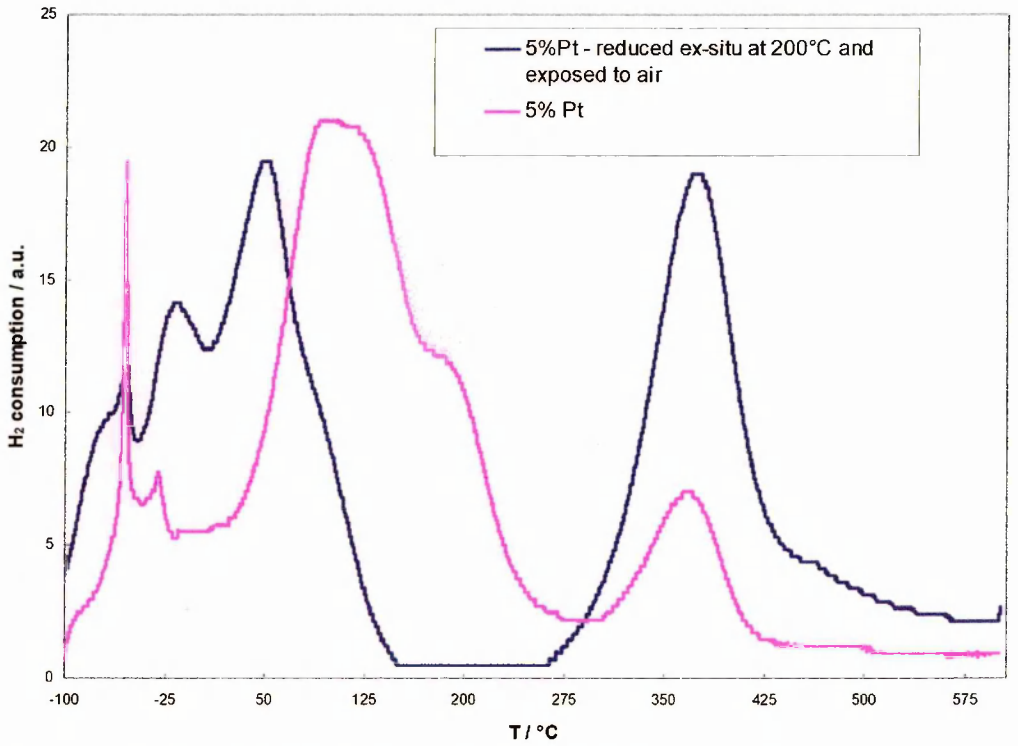

FIGURE 3-28: The TPR profile for 5%Pt/Al_2O_3(high) catalyst reduced at 200 °C for 3 hours and exposed to air

The 'two-stage' reduction has been reported by a number of different authors [17,18]. The low temperature peaks can be explained by the reduction of different forms of surface PtO_x, for example different forms of oxide or different sites. The high temperature peak can also be explained in a number of different ways. From our TPR results and previous literature studies concerning the reduction of Pt catalysts [19,20], it is thought that hydrogen adsorbed at high temperature could penetrate into the subsurface layers of Pt. H_2 adsorption in the temperature range of 300 – 500 °C was reported by Menon and Froment [21] during their studies on hydrogen adsorption and desorption from Pt supported on supports such as Al_2O_3, SiO_2, and TiO_2 at various

temperatures. They considered that hydrogen adsorbed at high temperature penetrated into the subsurface layers of Pt thus requiring high temperature for desorption.

However, the presence of an unusual high temperature peak in the reduced and non-reduced catalysts was of concern to us. Interestingly, the results from thermal studies (discussed later) also confirmed the H_2 uptake at temperatures between 300–500 °C (Figs. 3-38 and 3-39). One concern was that it might be due to undecomposed precursor on the surface deposited during the preparation procedure, however the preparation of the 5%Pt/Al_2O_3 catalyst involved heating the catalyst at 500 °C in air, as a result it is highly unlikely that any kind of Pt precursor is left un-decomposed.

An alternative explanation could be made in terms of the size of the Pt particles. We can attribute the peaks in the low temperature region to the reduction of PtO_x on relatively larger Pt particles, which are more easily reduced. The peak observed at higher temperature can be attributed to PtO_x on very small metal particles, which would not be reduced easily at low temperature. These small metal particles would be expected to interact very strongly with the support, resulting in the formation of Pt-O-Al type species on the surface which would be very difficult to reduce under normal conditions.

In order to probe these two regions of hydrogen uptake, another TPR experiment was conducted at the OU. The 5%Pt/Al_2O_3(high) catalyst was chosen for studies in the temperature range of 30-500 °C using 10% H_2/N_2 as the reducing mixture. A TPR experiment on the fresh sample showed the two regions of hydrogen uptake (as shown by the dark blue curve in Fig. 3-29) as expected. (As the OU set-up was not so sensitive these peaks are less well defined with little fine structure.) A new sample was then taken in the reactor and reduced at 150 °C *in situ* for three hours. The temperature 150 °C corresponds to the end temperature of the peak originating at low temperature.

After reduction, the catalyst was allowed to cool down to room temperature under the reducing mixture and a TPR experiment was performed. The TPR profile obtained on this sample showed only one broad peak at ~375 °C, as shown by the red curve in Fig. 3-29. Since the catalyst was reduced at 150 °C, there was no uptake of hydrogen observed at lower temperatures. This catalyst was then allowed to cool down to room temperature while still under the flowing H_2/N_2 mixture followed by another TPR run on the same catalyst. There was no hydrogen uptake by the catalyst this time (shown by the pink curve in Fig. 3-29). Having been previously reduced up to 500 °C the catalyst was expected to be totally reduced and hence no hydrogen uptake was observed.

The catalyst was then left in the reactor but was exposed to air. A TPR experiment performed after one day's exposure to the air (orange curve in Fig. 3-29) showed slight indication of hydrogen uptake at ~360 °C.

The sample was then exposed to air for 5 days. The TPR experiment on this sample clearly showed hydrogen uptake at higher temperatures, and a weak uptake at lower temperature (green curve in Fig. 3-29). These results indicate that both the peaks in TPR profile were very reproducible. Exposure to air re-oxidises the metal particles and as a result the peaks corresponding to hydrogen uptake were again observed in the TPR profile. This clearly discounts any thoughts that the high temperature peak is due to undecomposed precursor and lends support to the theory that the peaks in the TPR profile are due to the presence of small particles which are very reactive and more easily reoxidised.

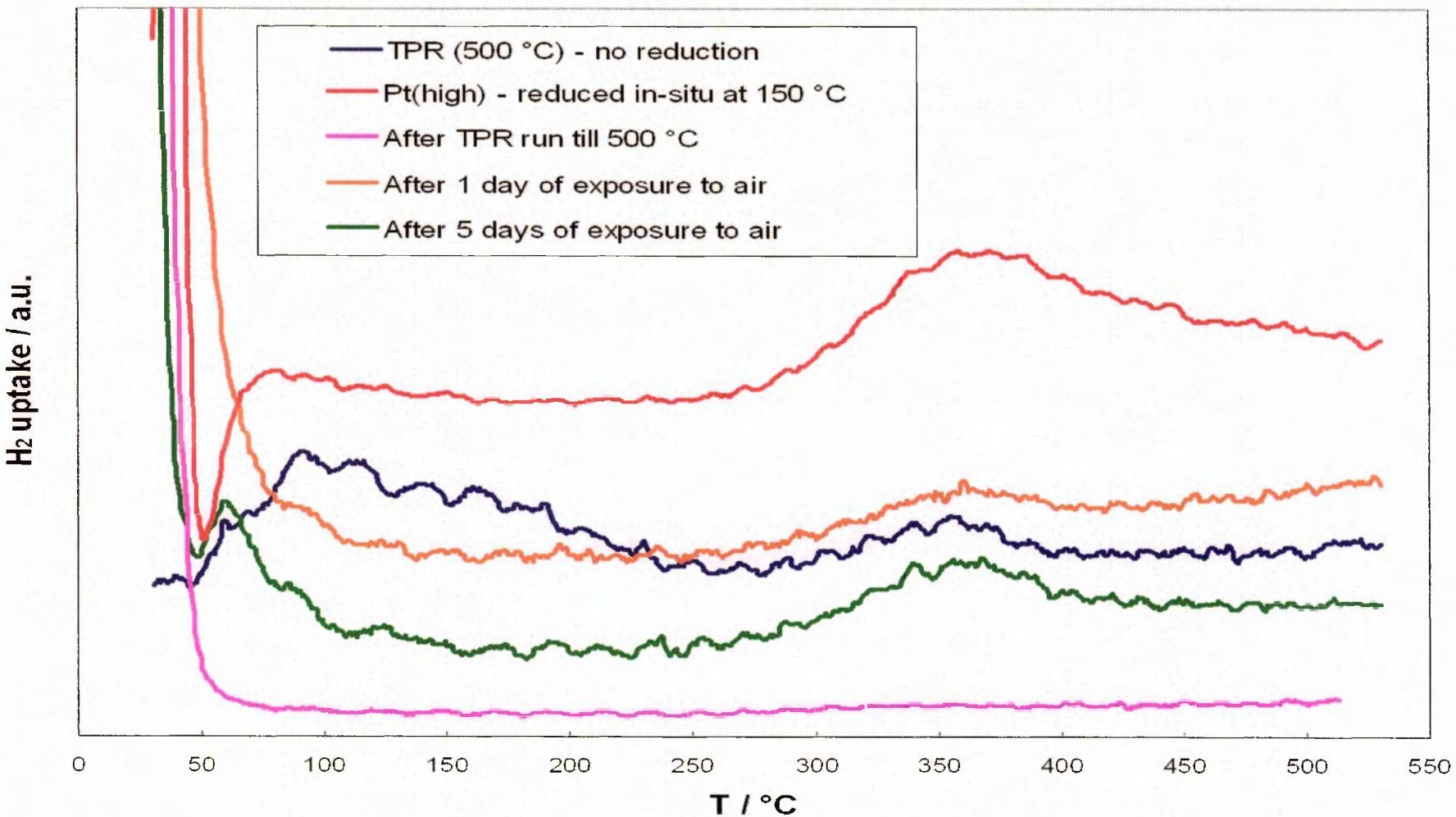

FIGURE 3-29: The TPR profile for 5%Pt/Al_2O_3(high) catalyst performed at OU

SnPt CATALYSTS

Compared to the Pt-only catalysts, very low uptake of hydrogen by SnPt catalysts was observed, and the scale for H_2 uptake had to be magnified about 60 times in order to observe any uptake by the (1:2)SnPt (Fig. 3-30) and (1:1)SnPt catalysts (Fig. 3-31). Again low and high temperature regions of hydrogen uptake were observed although the higher temperature peak was weaker, and for (1:1)SnPt no high temperature peak was observed. The low temperature peaks can again be attributed to the reduction of PtO_x species on the catalyst surface.

It has been reported by Babenkova and co-workers [22] that in their tin promoted Pt/Al_2O_3 (0.35% Pt) catalyst prepared by a metal-on-metal adsorption (underpotential deposition) method, Pt is present in a more highly reduced state than in their Pt/Al_2O_3. The presence of this highly reduced state of the metal species may provide an explanation for this low uptake of hydrogen by the tin promoted catalysts. Humblot and co-workers [15] also reported a sharp decrease in the volume of hydrogen adsorbed by a Sn-promoted Pt catalyst on a silica support, prepared by the SOMC route. They did, however, still see some H_2 adsorption.

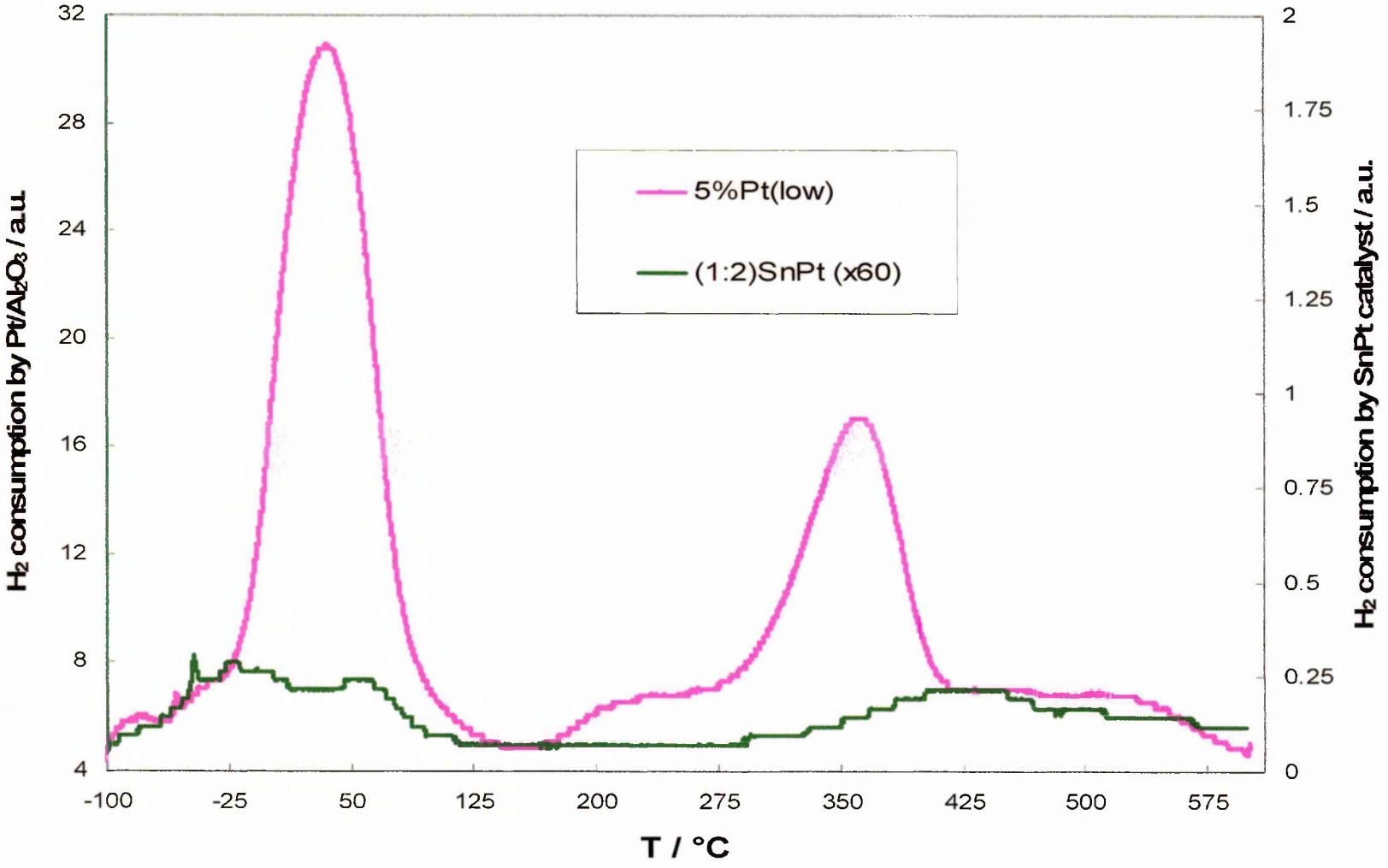

FIGURE 3-30: The TPR profile for (1:2)SnPt/Al_2O_3(low) catalyst

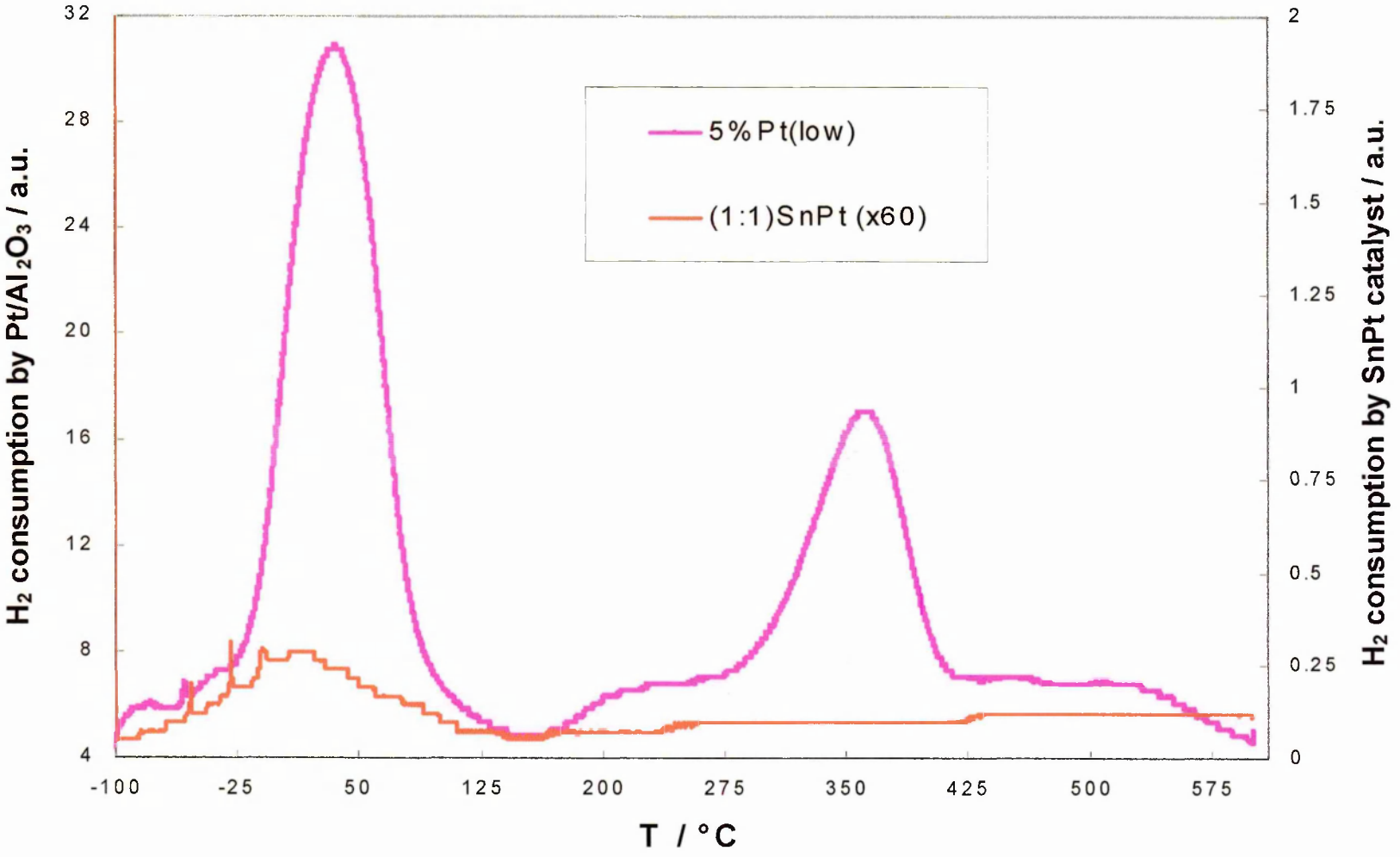

FIGURE 3-31: The TPR profile for (1:1)SnPt/Al_2O_3(low) catalyst

FePt CATALYSTS

The TPR profile for the (1:2)FePt catalyst (Fig. 3-32) has a sub-ambient peak and a large peak centred around 50 °C. It must be noted that unlike the SnPt bimetallic catalyst systems, the normalised scales have not been magnified to observe the hydrogen uptake by the Fe-promoted catalysts. Low temperature peaks have been attributed to the reduction of surface PtO_x species. The high temperature peak shows a shift towards slightly higher temperatures (~430 °C). This shift towards higher temperatures is likely to be due to interactions between Pt and FeO_x. For comparison, a TPR profile for Fe_2O_3 is shown in Fig. 3-34; Fe_2O_3 is only partially reduced below 500 °C with complete reduction at temperatures well over 600 °C. The "Fe-Pt" interaction in the catalyst also appears to increase the intensity of the high temperature peak in the TPR profile of the (1:2)FePt(low) catalyst.

With the addition of more iron in (1:1)FePt catalyst (Fig. 3-33), the intensity of the high temperature peak decreases as compared to that of the (1:2)FePt catalyst and the unpromoted catalyst. This is despite the fact that the CO/M dispersion values changes little. The excess amount of iron seems to affect the reduced state of Pt.

The increased uptake seen in the (1:2)FePt(low) catalyst could be attributed to additional adsorption because of the Fe-Pt species formed. We noted that previously that H_2 chemisorption could not be reliably used to estimate the monolayer coverage as the adsorption is not necessarily 1:1, especially for small particles. This may be a manifestation of the same effect, which is particularly apparent here in the case of the Fe-Pt interaction. As the quantity of the second metal increases to (1:1)FePt the effect appears to be diminished.

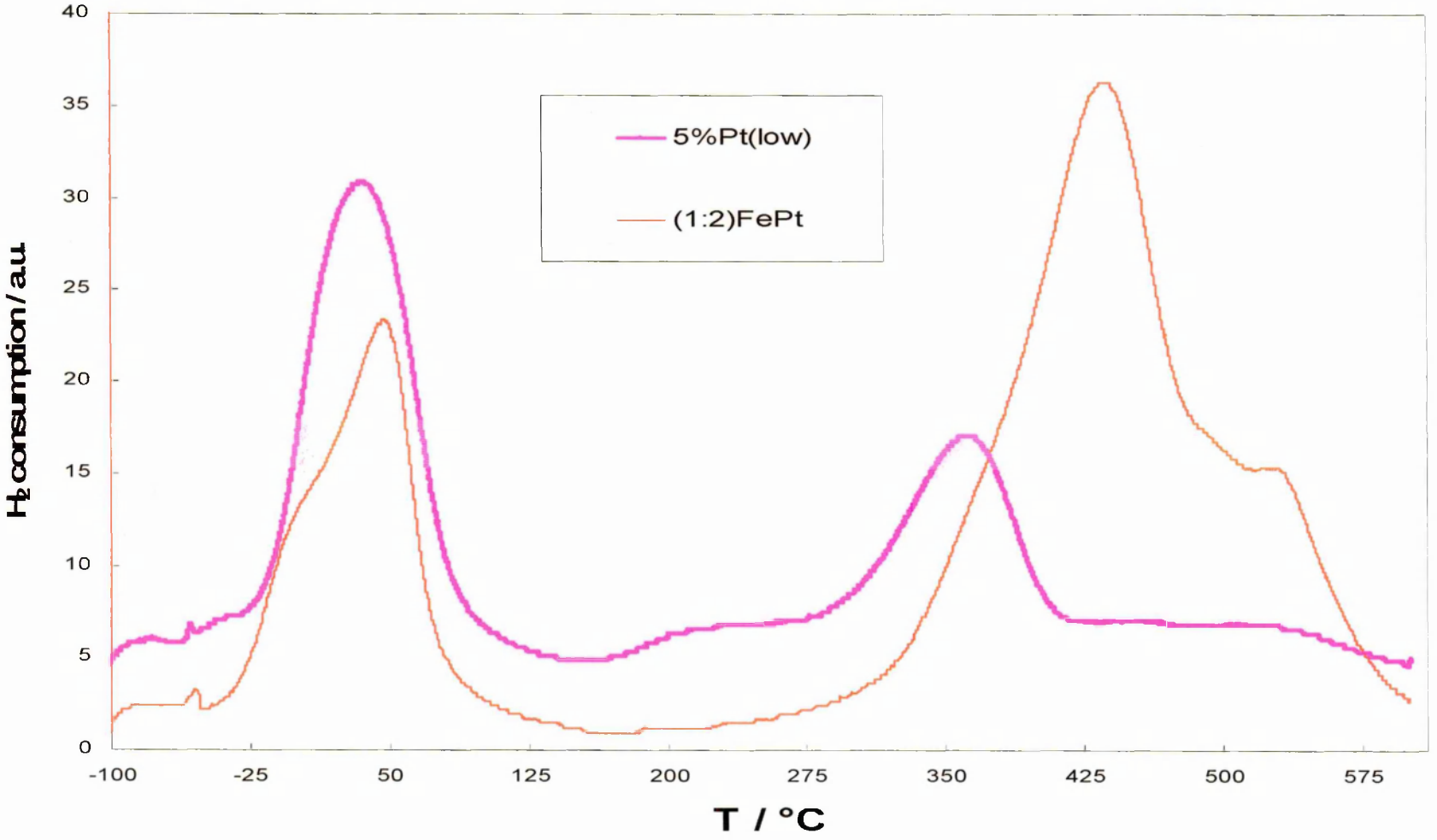

FIGURE 3-32: The TPR profile for (1:2)FePt/Al_2O_3(low) catalyst

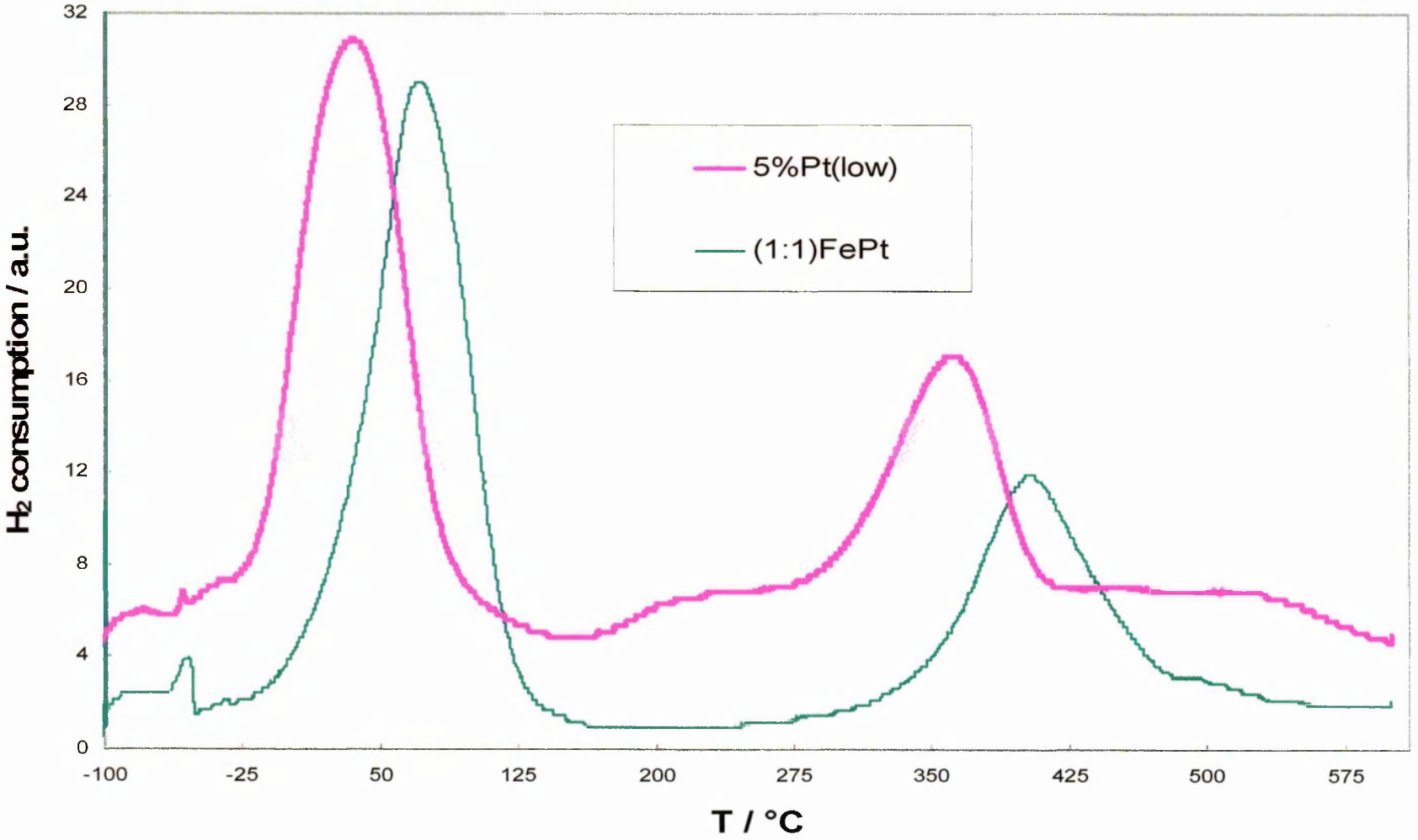

FIGURE 3-33: The TPR profile for (1:1)FePt/Al_2O_3(low) catalyst

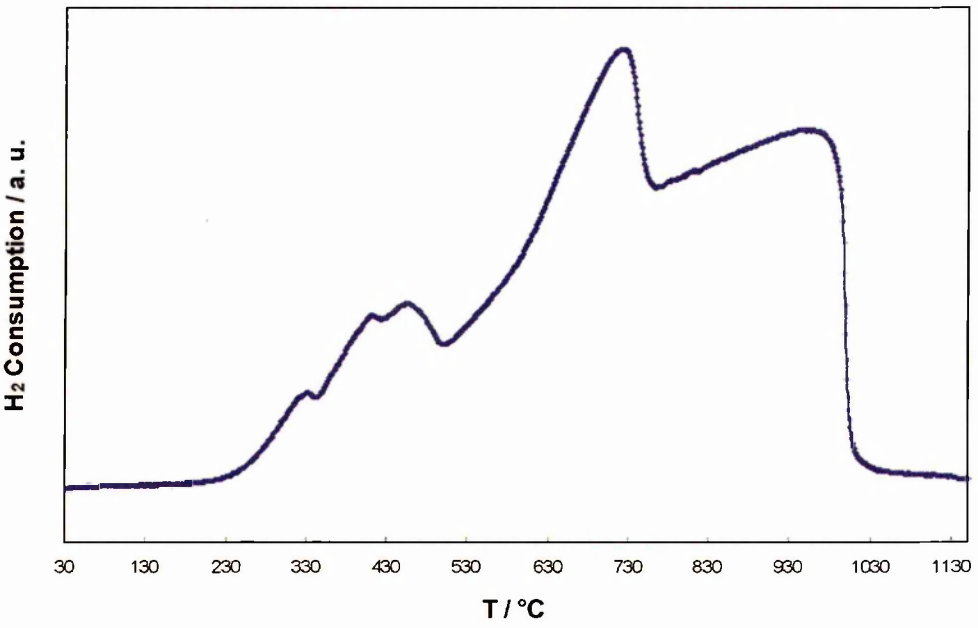

FIGURE 3-34: TPR profile for Fe(III) oxide

CoPt CATALYSTS

The TPR profiles for the (1:2)CoPt and (1:1)CoPt(low) catalyst (Figs. 3-35 and 3-36) have a sub-ambient peak and a large low temperature peak centred around 50 °C similar to Fe-promoted catalysts. The presence of promoting species near Pt affects the reducibility of Pt particles, which is clearly indicated by the shift in the peak maxima of the high temperature peak towards higher temperature (~420 °C). This effect of Co on the reducibility of Pt is expected to be a function of a Co-Pt interaction, as observed between Fe and Pt in the Fe-Pt system.

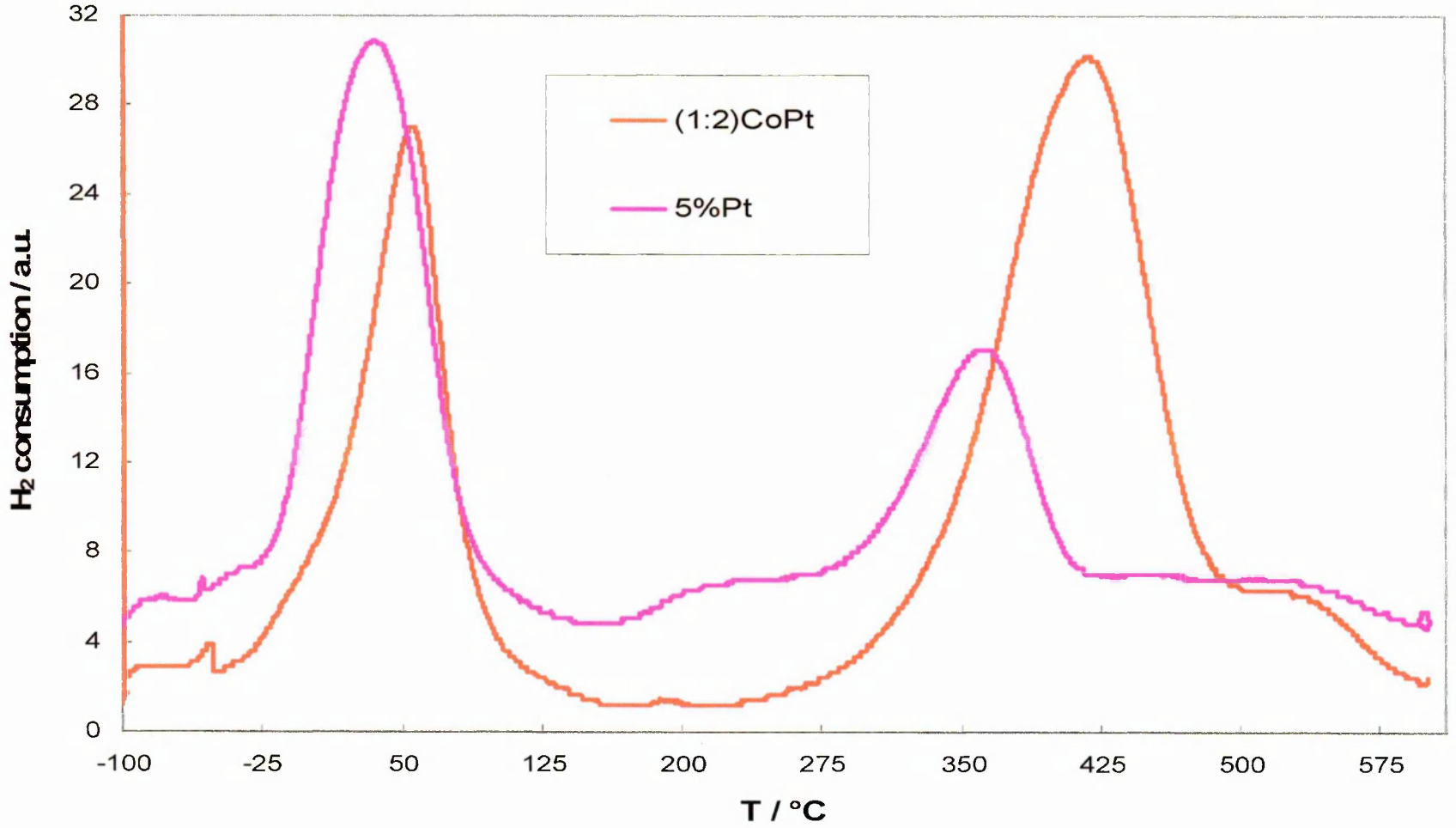

FIGURE 3-35: The TPR profile for (1:2)CoPt/Al_2O_3(low) catalyst

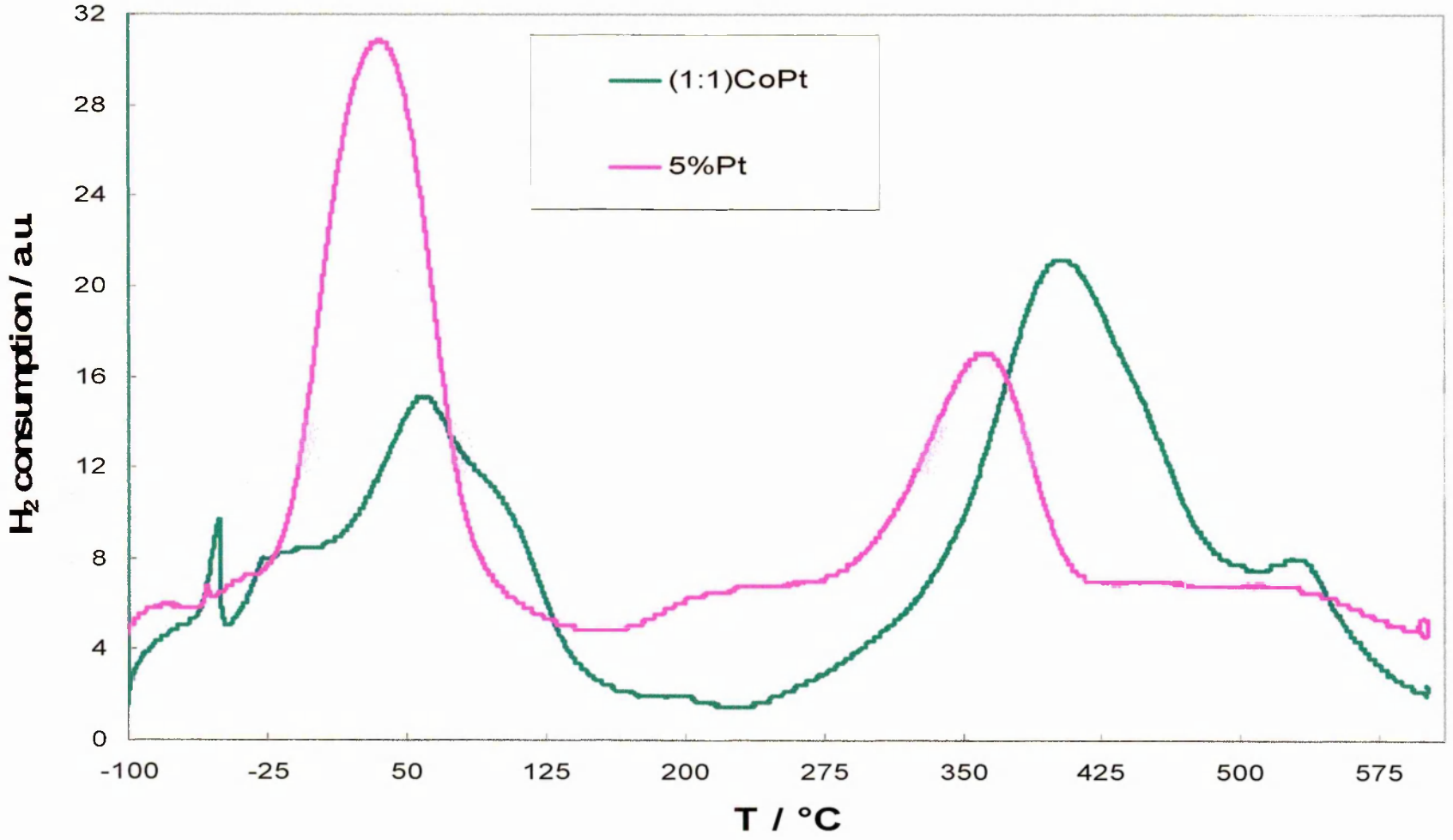

FIGURE 3-36: The TPR profile for (1:1)CoPt/Al_2O_3(low) catalyst

For comparison a TPR profile for CoO is shown in Fig. 3-37. Most of the CoO is reduced between 400 – 550 °C and only a small fraction, shown by a small peak, is reduced between 250 – 300 °C.

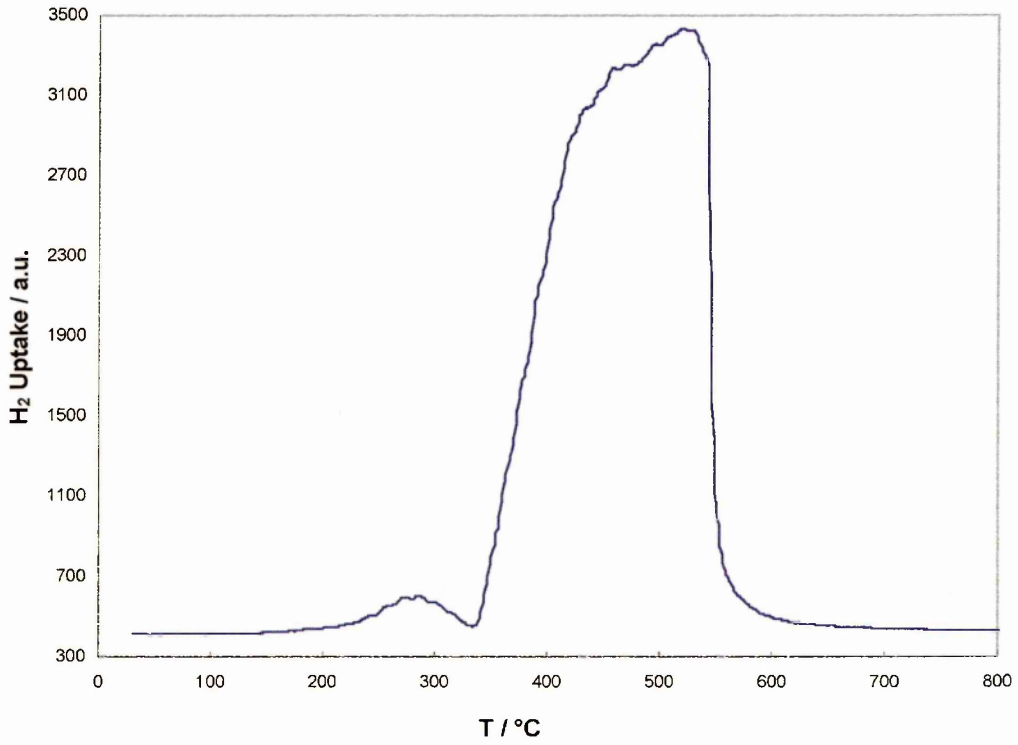

FIGURE 3-37: TPR profile for Co(II) oxide

The high temperature peak is found at similar temperatures to a TPR profile for Co/Al_2O_3 [23]. Here, CoO_x species were reported as being reduced at ~300 °C. This indicates that the increase in the intensity of the high temperature peak for the (1:2)CoPt catalyst may be due to the overlap of high temperature peaks of Pt and CoO_x/Al_2O_3 however, this is not likely to be a major reason given the small amount of cobalt present in the system. Due to the similarity with the TPR profile of the FePt(low) catalyst, it seems that the dispersed state of MO_x (where M = Fe and Co) might be interacting with

the surface Pt, leading to a formation of a mixed (M-Pt) species which takes up hydrogen at higher temperatures (~ 400 °C).

The intensity of the high temperature peak for the higher loaded (1:1)CoPt(low) catalyst again dropped (shifted to slightly higher temperature) similar to the Fe system and an additional small peak was also observed around 550 °C. This small peak could be ascribed to the presence of small amount of CoO_x on the surface [24] since the (1:1)CoPt catalyst system had twice the amount of cobalt compared with the (1:2)CoPt catalyst. The addition of more Co to the system (and Fe to FePt system) might be forming more MO_x (M = Fe and Co) on the surface which might block access to deeper PtO_x causing a decrease in hydrogen uptake.

3.2.4 THERMAL ANALYSIS

TGA studies were performed on Pt/Al_2O_3(low) and Fe and Co promoted Pt(low) catalysts in a 10% H_2/N_2 mixture. Fig. 3-38 shows TGA/DSC profiles for the parent $5\%Pt/Al_2O_3$(low) catalyst. Of the total mass loss of ~7.5% observed in the temperature range from room temperature to 800 °C, about 5% has been observed at ~150 °C. The loss of mass up to 120 °C is ascribed to the loss of moisture or gases adsorbed on the catalyst. The catalyst seemed to be very stable in the temperature range scanned. Similar observations were made when the parent $5\%Pt/Al_2O_3$(low) catalyst was heated in air (Fig. 3-39). About 5% loss in mass was observed below 200 °C and this was similarly ascribed to the loss of surface moisture or any pre-adsorbed gas. A small exotherm at 120 °C can be observed for Pt/Al_2O_3(low) in the reducing mixture which could be attributed to the reduction of PtO_x similar to the low temperature peak in the TPR. The second peak observed in the TPR at higher temperatures is not obvious.

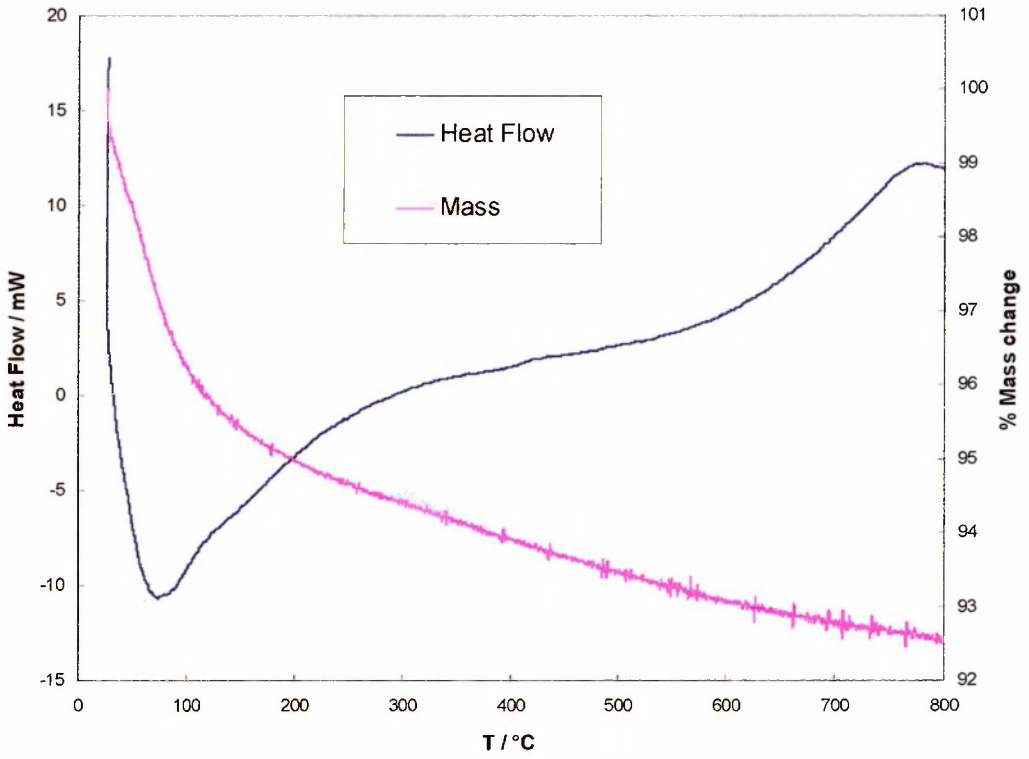

FIGURE 3-38: The TGA/DSC profiles for 5%Pt/Al_2O_3(low) catalyst in 10%H_2/N_2 mixture

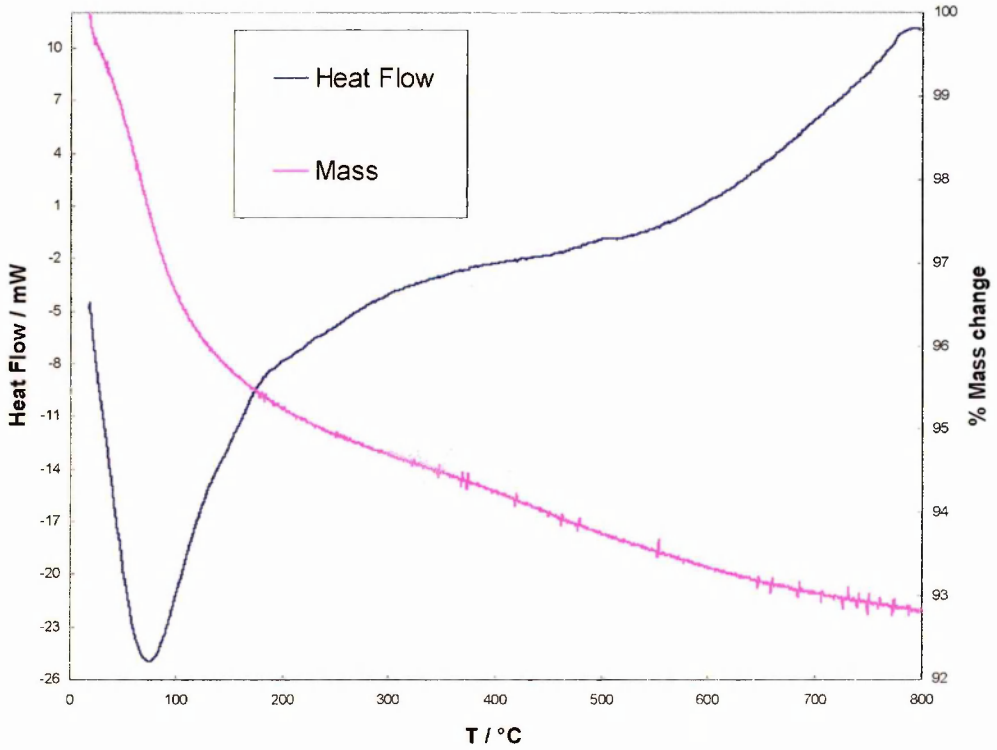

FIGURE 3-39: The TGA/DSC profiles for 5%Pt/Al_2O_3(low) catalyst in air

TGA/DSC results for the (1:2)FePt(low) catalyst treated in H_2/N_2 and air are shown in Fig. 3-40 and 3-41, respectively. Initial loss of moisture or any pre-adsorbed gas(es) from the surface of the catalyst is shown by the loss in mass and supported by the endotherms observed at temperatures below 100 °C. There is no appreciable change in the mass of the (1:2)FePt(low) catalyst between 300–600 °C. The overall change in the mass of the (1:2)FePt(low) catalyst is very similar to that for the unpromoted catalyst. The DSC thermograms under reducing conditions showed an exotherm at just over 100 °C (Fig. 3-40) which could be due to reduction of surface PtO_x species which are easily reduced. This exotherm was much more significant than that observed for the monometallic catalyst. This peak was absent in the thermogram run in air.

A second broad exothermic phenomenon is observed at temperatures above 300 °C which is similar to observations highlighted in the TPR profile for the (1:2)FePt(low) catalyst when there was an unusually high uptake of hydrogen at temperatures above 300 °C (Fig. 3-32). This was attributed to a Fe-Pt interaction and the reduction of Pt/FeO_x species. At temperatures above 400 °C, (1:2)FePt(low) catalyst under air gave an exotherm (Fig. 3-41) which can be attributed to the formation of oxidised metal species on the catalyst.

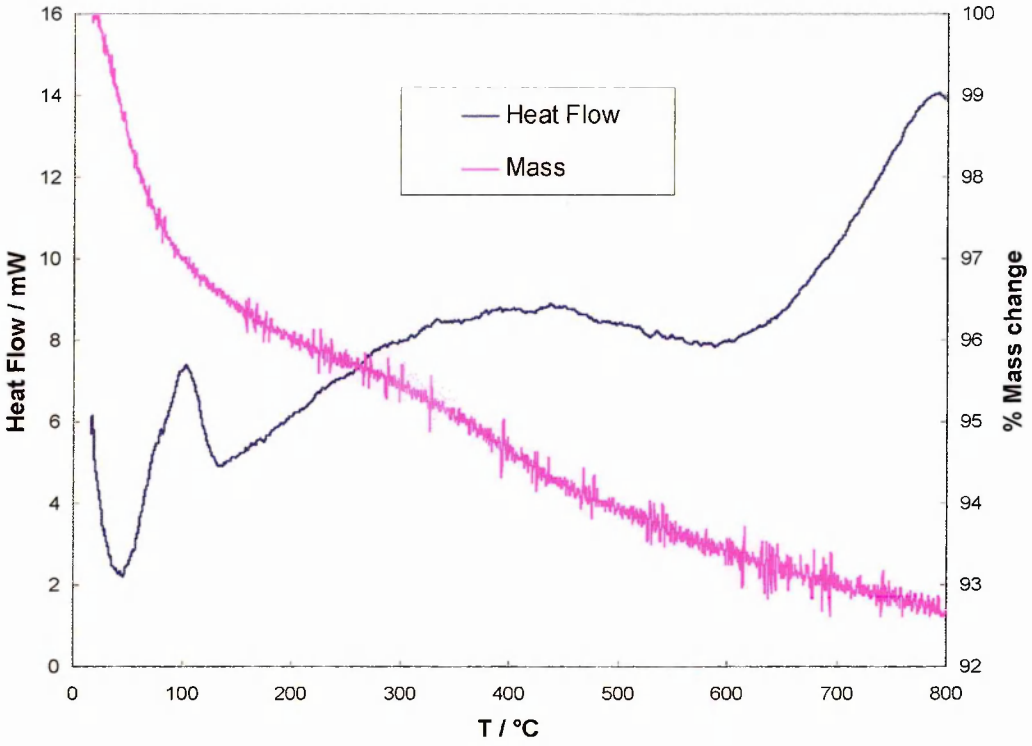

FIGURE 3-40: The TGA/DSC profiles (1:2)FePt/Al_2O_3(low) catalyst in 10% H_2/N_2 mixture

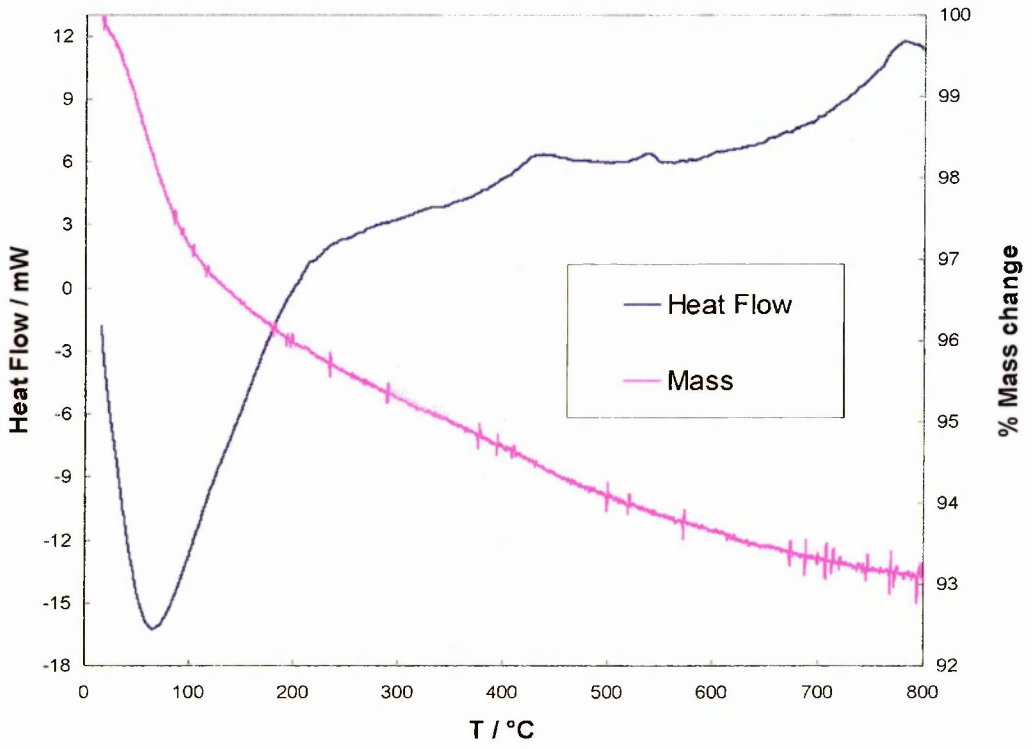

FIGURE 3-41: The TGA/DSC profiles (1:2)FePt/Al_2O_3(low) catalyst in air

The major part of the observed 6-7% loss in the mass of (1:1)FePt(low) catalyst occurs below 150 °C (Fig. 3-42 and 3-43), and is again attributed to the loss of moisture and other pre-adsorbed gases on the surface. The endotherm in the DSC thermogram supports this observation. The exotherm observed for (1:1)FePt(low) catalyst at ~150 °C again represents the reduction of surface PtO_x species as was observed during the TPR experiment on the same catalyst (Fig. 3-33). The large exothermic peak observed for (1:2)FePt(low) catalyst above 300 °C is absent and this again agrees with the observation made during the TPR experiment on the (1:1)FePt(low) catalyst where the intensity of the high temperature peak decreased compared to (1:2)FePt(low) catalyst.

Figs. 3-44–3-47 present TGA/DSC thermograms for (1:2)CoPt(low) and (1:1)CoPt(low) catalysts in 10%H_2/N_2 and in air, respectively. A total mass loss of ~8% was observed over the entire temperature range scanned during the experiment, and this is again ascribed to the loss of moisture and surface adsorbed gases. This was supported by the endotherm observed in the thermogram profile below 100 °C. The exotherm observed just over 100 °C in when the (1:2)CoPt(low) catalyst was heated under a reducing mixture is ascribed to the reduction of surface PtO_x species. Again there is some evidence of an exotherm around 300-450 °C for the (1:2)CoPt(low) catalyst however this is considerably less significant than for the analogous iron sample and was absent in the (1:1)CoPt(low) catalyst with the higher Co loading.

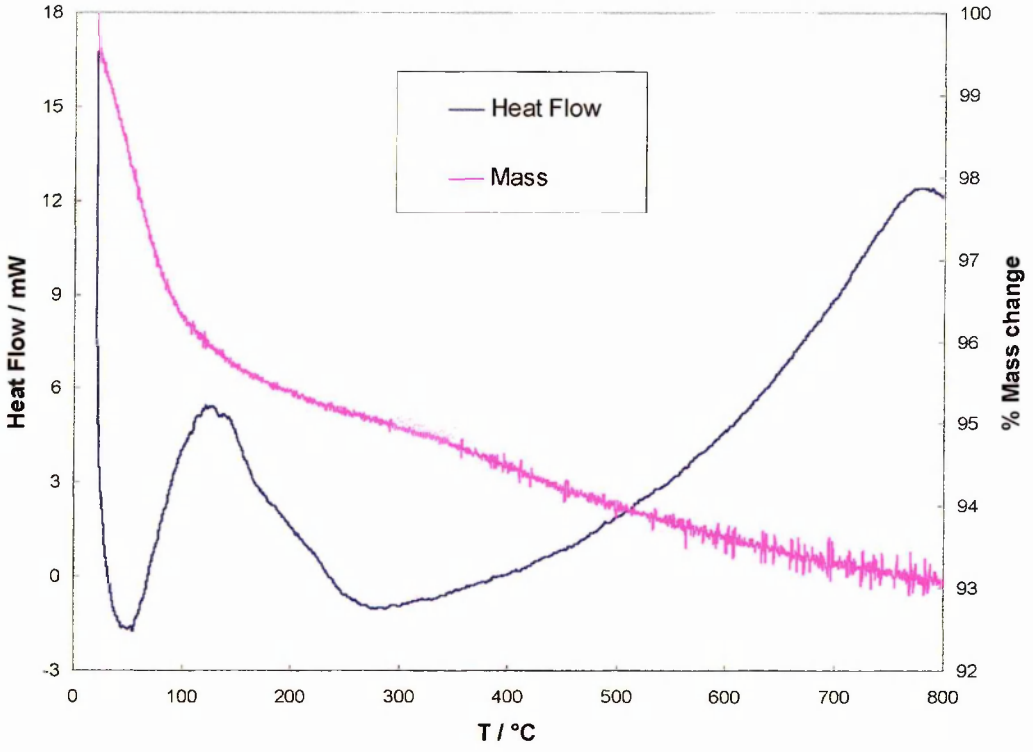

FIGURE 3-42: The TGA/DSC profiles (1:1)FePt/Al_2O_3(low) catalyst in 10%H_2/N_2 mixture

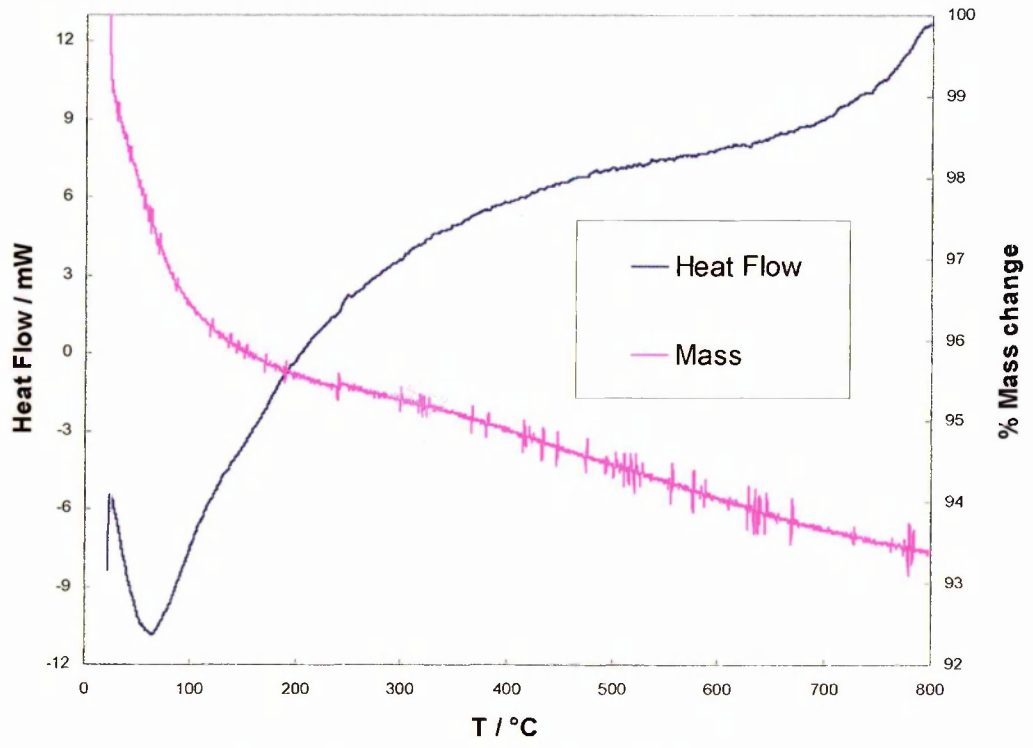

FIGURE 3-43: The TGA/DSC profiles (1:1)FePt/Al_2O_3(low) catalyst in air

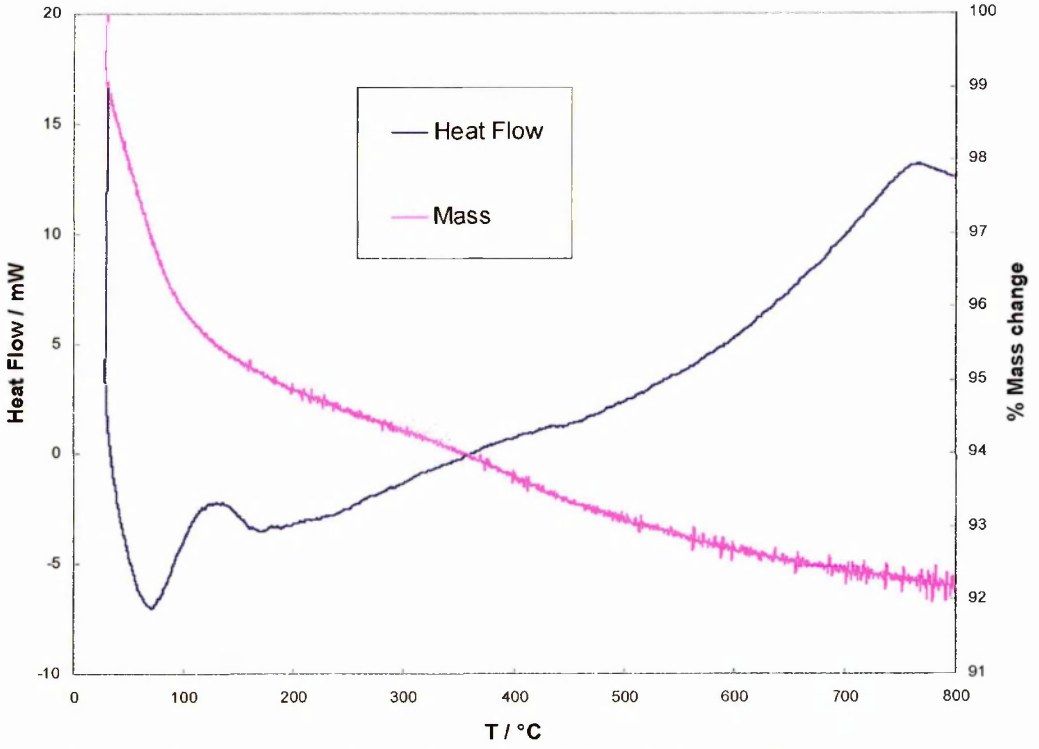

FIGURE 3-44: The TGA/DSC profiles (1:2)CoPt/Al_2O_3(low) catalyst in 10% H_2/N_2 mixture

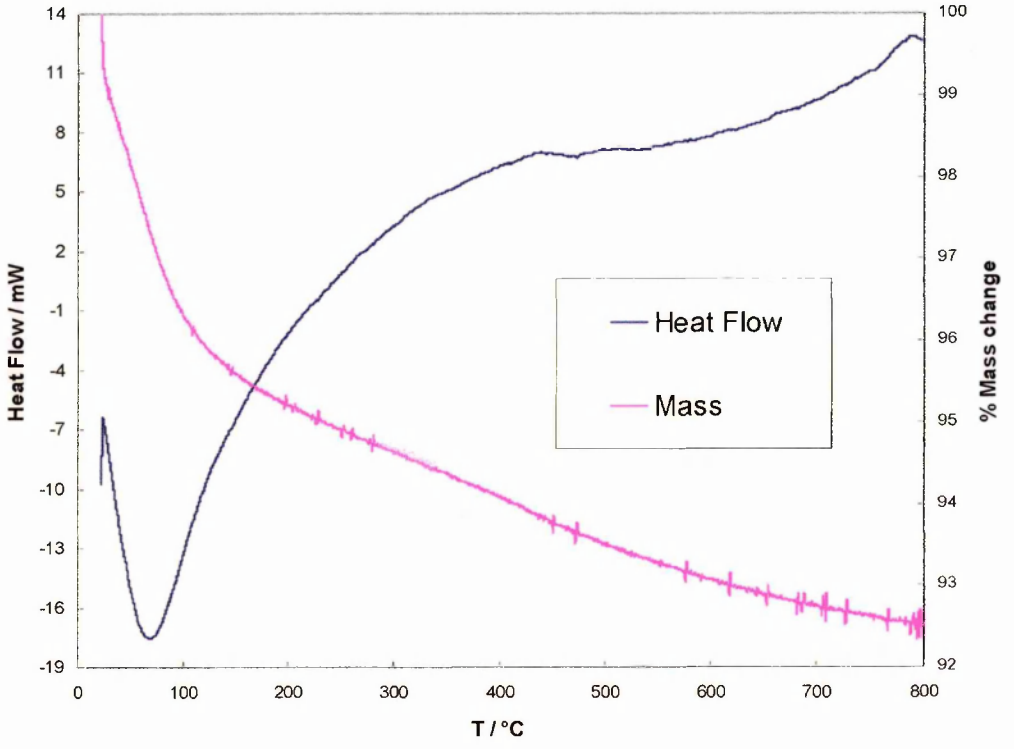

FIGURE 3-45: The TGA/DSC profiles (1:2)CoPt/Al_2O_3(low) catalyst in air

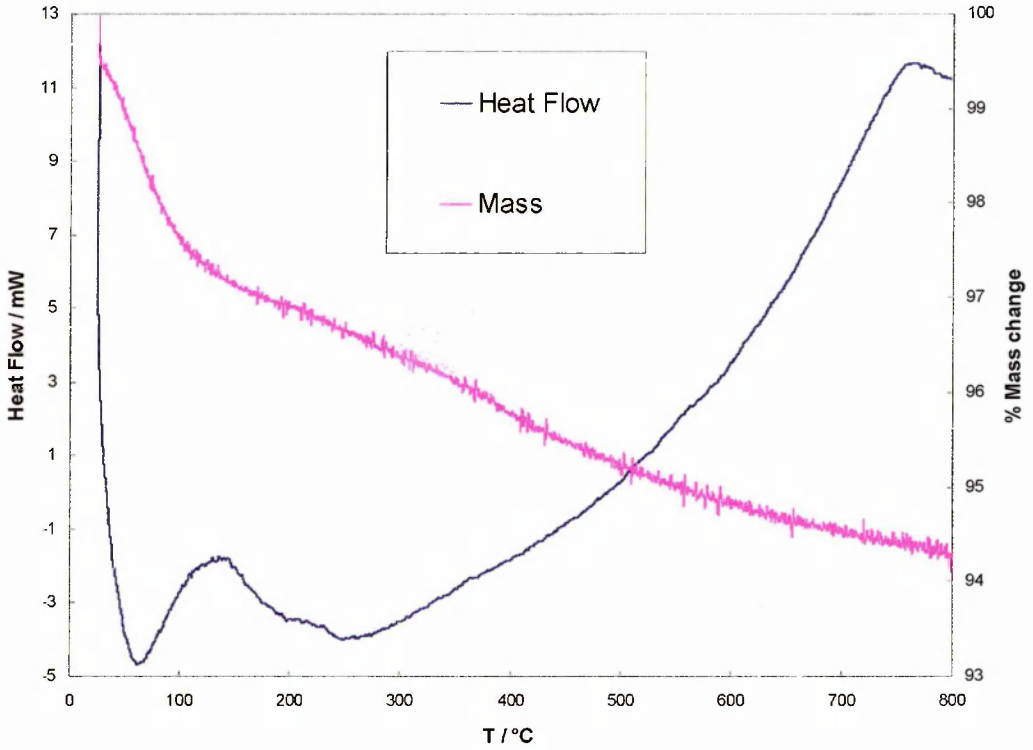

FIGURE 3-46: The TGA/DSC profiles (1:1)CoPt/Al_2O_3(low) catalyst in 10%H_2/N_2 mixture

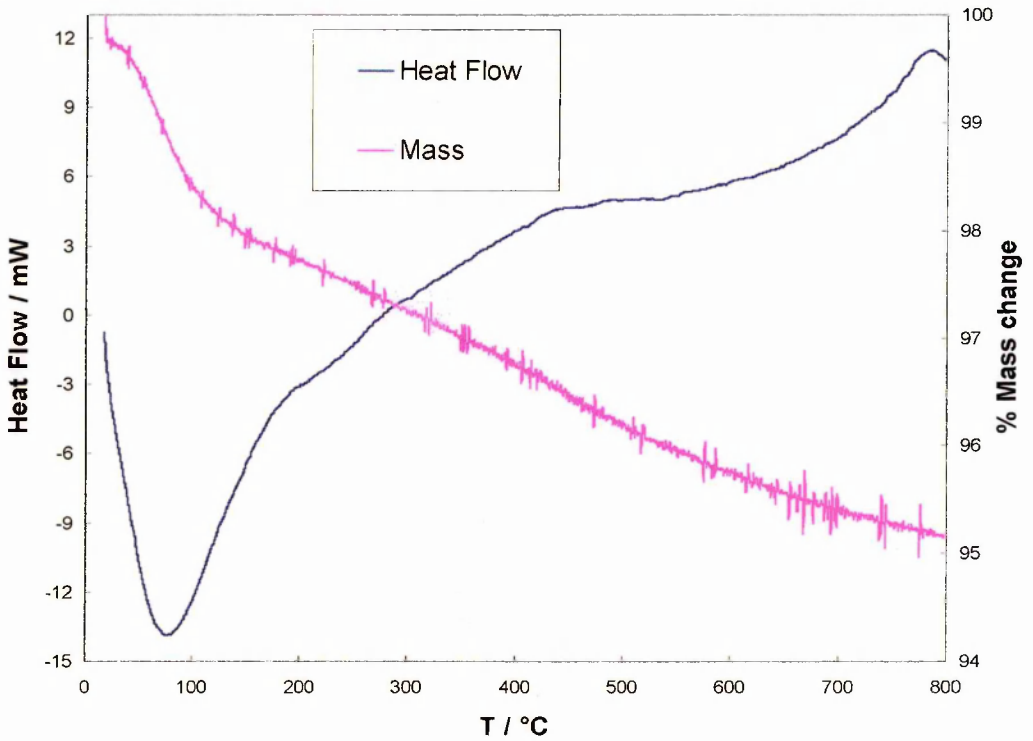

FIGURE 3-47: The TGA/DSC profiles (1:1)CoPt/Al_2O_3(low) catalyst in air

The DSC results agree well with the TPR results for both the Fe and Co catalysts and we attribute the high temperature peak in the TPR and the exotherm above 300 °C in the DSC to a "Fe-Pt" interaction with the reduction of a mixed iron/platinum/oxide species. It appears that this is more significant for (1:2)MPt catalysts (M = Fe and Co). It is possible that in the catalysts with higher loadings of the modifying metal that there is more bulk FeO_x or CoO_x on the surface which might block access to the surface. There is little evidence of the bulk oxide during characterisation of the catalysts, although low loading makes analysis difficult.

3.3 CONCLUSIONS

A range of Pt-based alumina supported bimetallic catalysts have been prepared by SOMC technique using various precursors such as; tetra-butyl tin, ferrocene, cobaltocene etc., and characterised using a range of techniques.

- Under the conditions employed during preparation of the catalysts by the SOMC route, the reaction of the second metal precursors with the reduced Pt surface is believed to result in the selective deposition of second metal on the Pt surface of the reduced Pt/Al_2O_3 catalyst.
- ICP-AES analysis confirmed the successful deposition of the second metal although the loading was somewhat less for the Cr- and Ni-promoted and higher loaded catalysts than the nominal values.
- A general trend is clear in that the amount of CO adsorbed by the catalysts decreases with the increasing amount of the second metal such as Sn, Fe and Co.
- From electron microscopy studies, it was confirmed that the size of the metal particles did not change significantly upon the addition of the second metal; hence the decrease in CO uptake could be attributed to the physical blockage of

the surface Pt by the second metal, covering some of CO adsorption sites. This could be taken as an evidence of successful method of preparation of bimetallic catalysts.

- From electron microscopy and EDX analysis, the physical location of the two metals was found to be the same within the limits of detection of the instrument. This was additional evidence of successful deposition of second metal on Pt by using the SOMC technique.
- The shift in the reduction peaks for the bimetallic catalysts in the TPR profile compared to that of unpromoted catalyst suggested strong interaction of the two metal species in the catalyst.
- Thermal analysis confirmed that there was no precursor left undecomposed on the catalyst surface during the preparation of the bimetallic catalyst, and also agreed well with the TPR results.

3.4 REFERENCES

1 E. M. Crabb, R. Marshall and D. Thompsett, *J. Electrochem. Soc.*, **147**, 4440, (2000)

2 F. Lefebvre, J. P. Candy, C. C. Santini and J. M. Basset, *Topics in Catal.*, **4**, 211, (1997)

3 J. P. Candy, B. Didillon, E. L. Smith, T. B. Shay and J. M. Basset, *J. Mol. Catal.*, **86**, 179, (1994)

4 B. Coq, A. Goursot, T. Tazi, F. Figuéras and D. R. Salahub, *J. Am. Chem. Soc.*, **113**, 1485, (1998)

5 F. Humblot, D. Didillon, F. Le Peltier, J. P. Candy, J. Corker, O. Clause, F. Bayard and J. M. Basset, *J. Am. Chem. Soc.*, **120**, 137, (1998)

6 H. R. Aduriz, P. Bodnariuk, B. Coq and F. Figuéras, *J. Catal.*, **119**, 97, (1989)

7 B. Coq, A. Bittar and R. Dutartre, *J. Catal.*, **128,** 275, (1991)

8 G. Neri, A. Donato, C. Milone, R. Pietropaolo and J. Schwank, *Mater. Chem. Phys.*, **44**, 145, (1996)

9 M. E. Halttunen, M. K. Niemela, A. O. I. Krause, T. Vaara and A. I. Vuori, *Appl.Catal. A: General*, **205**, 37, (2001)

10 F. Pinna, M. Selva, M. Signoretto, G. Strukul, F. Boccuzzi, A. Benedetti, P. Canton and G. Fagherazzi, *J. Catal.*, **150**, 356, (1994)

11 R. Marshall, PhD Thesis, The Open University, UK, (1998)

12 J. H. Sinfelt, *J. Catal.*, **29**, 308, (1973)

13 H. Lieske and J. Völter, *J. Catal.*, **90**, 96, (1984)

14 R. D. Cortright and J. A. Dumesic, *J. Catal.*, **148**, 771, (1994)

15 F. Humblot, J. P. Candy, F. Le Peltier, B. Didillon and J. M. Basset, *J. Catal.*, **179**, 459, (1998)

16 J. L. Gland, G. B. Fisher and E. B. Kollin, *J. Catal.*, **77**, 263, (1982)

17 B. D. McNicol and R. T. Short, *J. Electroanal. Chem.*, **92**, 115, (1978)

18 H. C. Yao, M. Sieg and H. K. Plummer Jr., *J. Catal.*, **59**, 365, (1979)

19 J. L. Falconer and J. A. Schwarz, *Catal. Rev. -Sci. Eng.*, **25**, 141, (1983)

20 A. Jones and B. McNicol, *Temperature-programmed reduction for solid materials characterization*, Marcel Dekker, (1986)

21 P. G. Menon and G. F. Froment, *Appl. Catal.*, **1**, 31, (1981)

22 L. V. Babenkova, S. Szabó, Yu G. Kulievskaya and V. G. Shalyukhin, *Models in Chemistry*, **129**, 831, (1992)

23 L. Gutierrez, E. A. Lombardo and J. O. Petunchi, *Appl. Catal. A: General*, **194-195**, 169, (2000)

24 M. Meng, P –Y. Lin and Y. –L. Fu, *Catal. Lett.*, **48**, 213, (1997)

4

Catalytic Oxidation of CO (I) - Preliminary Screening Studies

INTRODUCTION

The present plan of work was undertaken with the objective of developing suitable catalysts for the selective oxidation of the CO present in the feed-stream of a fuel cell, based on reforming of methanol. Our initial studies indicated the potential of bimetallic catalysts in such applications. In this study, a number of bimetallic catalysts of the type M-Pt-Al_2O_3 where M is a metal from the first row transition elements, were prepared through the Surface Organometallic Chemistry (SOMC) route, and examined for their performance towards selective oxidation of CO. The performance of these bimetallic catalysts has been compared with that of the corresponding parent monometallic catalyst in terms of their activity and selectivity towards CO oxidation, in the presence of excess hydrogen. Preliminary screening studies of a series of bimetallic catalysts (Pt/Al_2O_3(low) modified with half a monolayer of promoter) are presented in this chapter. The catalysts were screened initially in order to identify the most interesting systems. The studies presented in this chapter on the selected systems were

extended to high-dispersed catalysts and also to other loadings of the second metal, in the next chapter. For the present screening studies, a gas mixture containing 0.5% CO, 1.25% O_2, ~25% H_2 and the balance N_2 [referred to as the λ_5 system in this thesis] was used. Since there was no water present in the gaseous feedstock, the experiments carried out on these mixtures are referred to as *dry CO tests* in this thesis. The test gas did not contain CO_2 due to the interference with O_2 measurements. In addition, experiments with CO_2(g) and H_2O(g) in the feed gas mixture were carried out at the Johnson Matthey Technology Centre (UK). The results of these measurements are described later in this chapter under the heading *wet CO tests*. The feed for wet tests was made up of 60% H_2, 0.1% CO, 20% CO_2, 0.15% O_2 and the balance nitrogen.

4.1 PRELIMINARY STUDIES FOR THE STANDARDISATION OF EXPERIMENTAL CONDITIONS

Before any comparative screening of the catalysts was performed it was necessary to select the "standard" conditions for the experiments.

4.1.1 EFFECT OF FLOW RATE

The CO oxidation profile for 5%Pt/Al_2O_3(high) at the flow rate of 100 $cm^3 min^{-1}$ is shown in Fig. 4-1. As defined in Chapter 2, the term, '*Consumption of CO, O_2 (%)*' is defined as the amount of CO and O_2 present in the gas mixture consumed during the reaction (analytically). The term selectivity of a catalyst towards CO oxidation (S(CO)) is defined as follows:

$$S(CO) = \frac{\text{Amount of oxygen used in CO oxidation}}{\text{Total amount of oxygen consumed in the reaction}} \times 100\%$$

As neither H_2 and H_2O concentrations were measured in the experiment the hydrogen selectivity ($S(H_2)$) was calculated on the assumption that any difference between O_2 and CO consumption can be accounted for by H_2 oxidation.

It should be noted that the CO conversion as referred to in the text as 'consumption of CO (%)' is the fraction (as a percentage) of the total CO present in the gas mixture (containing 0.50% CO) that has been oxidised e.g. 50% CO conversion marked on a Figure, means that 0.25% CO has been converted to CO_2.

No significant activity was observed until about 60 °C after the gas mixture was allowed to flow over the catalyst, which was pre-reduced in a 2% CO/H_2 mixture at 40 °C for 40 minutes. Thereafter, an impressive profile for the oxidation of CO was observed with a rise in temperature until all the CO was oxidised at about 150 °C.

Another fresh sample of the same batch of $5\%Pt/Al_2O_3$(high) catalyst was examined at a total flow rate of 200 $cm^3\ min^{-1}$ of the test gas mixture. The CO oxidation profile for this catalyst is shown in Fig. 4-2. The catalyst was reduced at 40 °C under a 2% CO/H_2 mixture for 40 minutes before the test gas mixture was admitted to the system. As the catalyst temperature was gradually raised, the onset of CO oxidation was observed. Complete CO oxidation was achieved at 170 °C.

The CO oxidation profile for the unpromoted Pt catalyst remained essentially unchanged even when it was tested at different flow rates of 100 and 200 $cm^3\ min^{-1}$ (Figs. 4-1 and 4-2). The temperature for the maximum conversion at higher flow rate was observed to be 20 °C higher. Similarly in tests run with a promoted catalyst ((1:1)SnPt(high)) little difference was observed in the oxidation profiles at 100 $cm^3\ min^{-1}$and 200 $cm^3\ min^{-1}$ (Figs. 4-3 and 4-4). Consequently, it was decided to perform all the tests with 100 $cm^3\ min^{-1}$ flow rate of the test gas mixture unless stated otherwise.

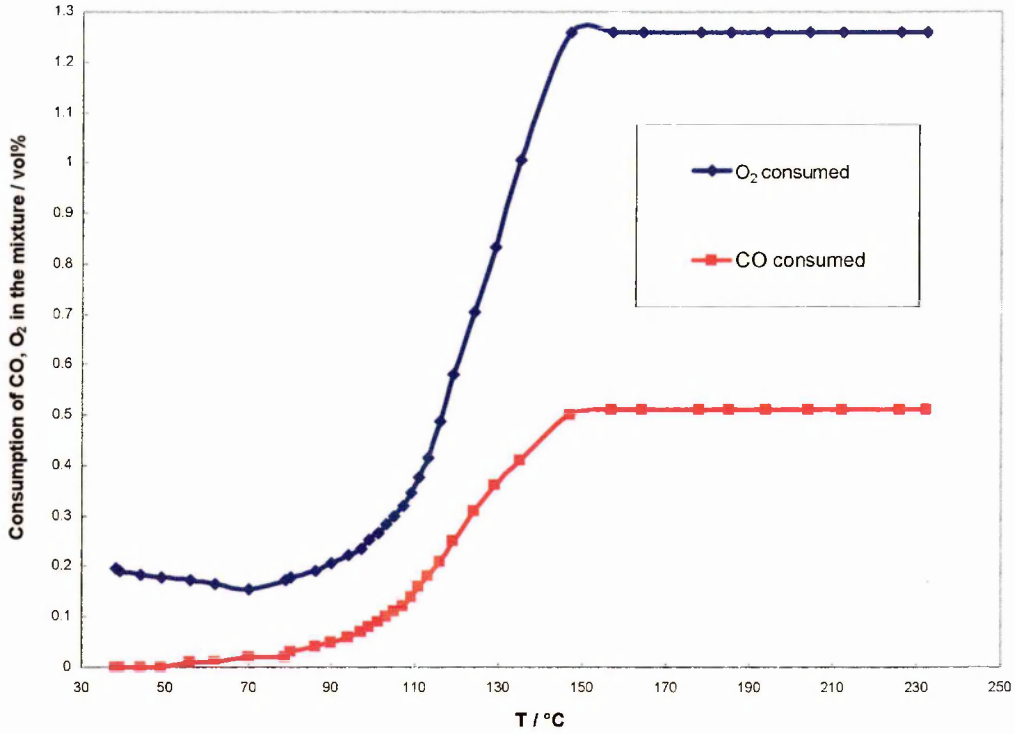

FIGURE 4-1: The CO oxidation profile for undiluted 5%Pt/Al_2O_3(high) tested at 100 cm^3 min^{-1} flow rate

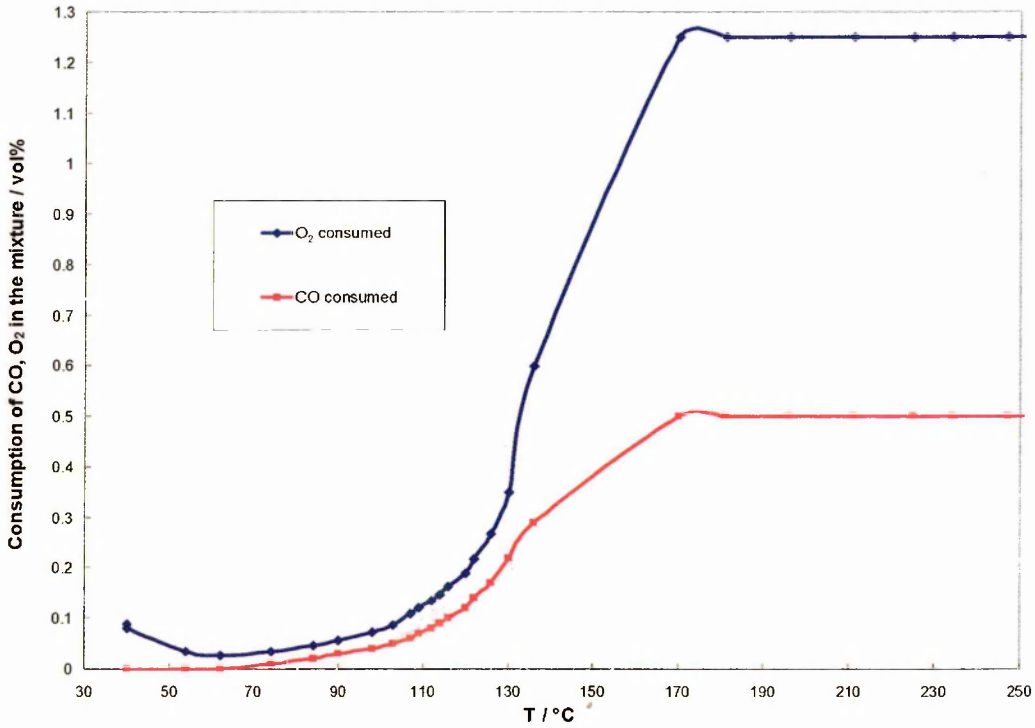

FIGURE 4-2: The CO oxidation profile for undiluted 5%Pt/Al_2O_3(high) tested at 200 cm^3 min^{-1} flow rate

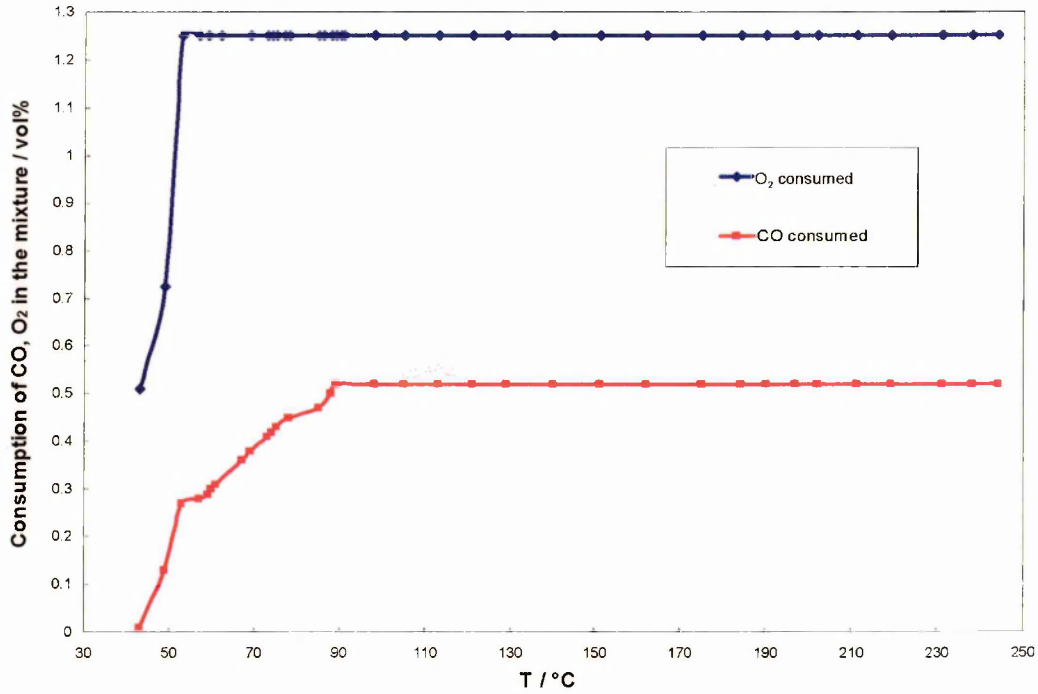

FIGURE 4-3: The CO oxidation profile for undiluted (1:1)SnPt/Al_2O_3(high) tested at 100 cm^3 min^{-1} flow rate

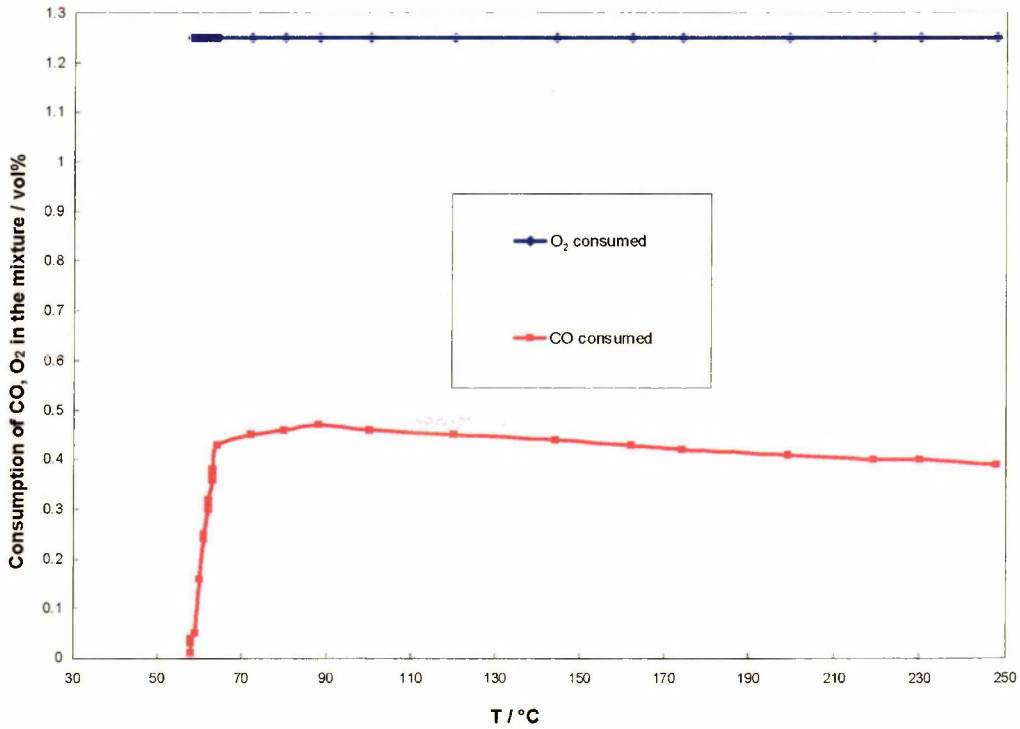

FIGURE 4-4: The CO oxidation profile for undiluted (1:1)SnPt/Al_2O_3(high) tested at 200 cm^3 min^{-1} flow rate

4.1.2 EFFECT OF DILUTION ON THE ACTIVITY OF THE BIMETALLIC CATALYST

When the experiment was performed under exactly the same conditions with the (1:2)FePt/Al_2O_3(high) catalyst (Fig. 4-5), the temperature of the catalyst continued rising sharply until about 85 °C, and all the CO in the mixture was oxidised by 88 °C. The CO conversion to CO_2 occurred in such a short period of time that analysis of the reaction mixture was difficult. No oxygen was observed in the analysed samples of the exit gas mixture indicating that the entire inlet O_2 was consumed by the reaction. Also, very small droplets of water were observed downstream from the reactor. A significant exotherm (40 – 50 °C) was observed throughout the experiment.

A very similar result was obtained when the (1:1)FePt/Al_2O_3(high) catalyst was tested under the same conditions (Fig. 4-6). In both the Fe-promoted Pt catalysts, a sharp exotherm (~ 40 – 50 °C) was observed, indicating the highly active nature of these bimetallic catalysts. Similar results were obtained for other bimetallic systems.

In order to be able to comment more meaningfully on the selectivity of the catalysts, however, it was necessary to slow the reaction down. As discussed previously, running the experiment at different flow rates (100 and 200 cm^3 min^{-1}) made little difference for (1:1)SnPt/Al_2O_3(high) catalyst, despite the change in residence time of the reactants over the catalyst surface. Thus it was necessary to examine other parameters such as diluting the catalyst with an inert solid, for example the alumina support, to try to control the reaction.

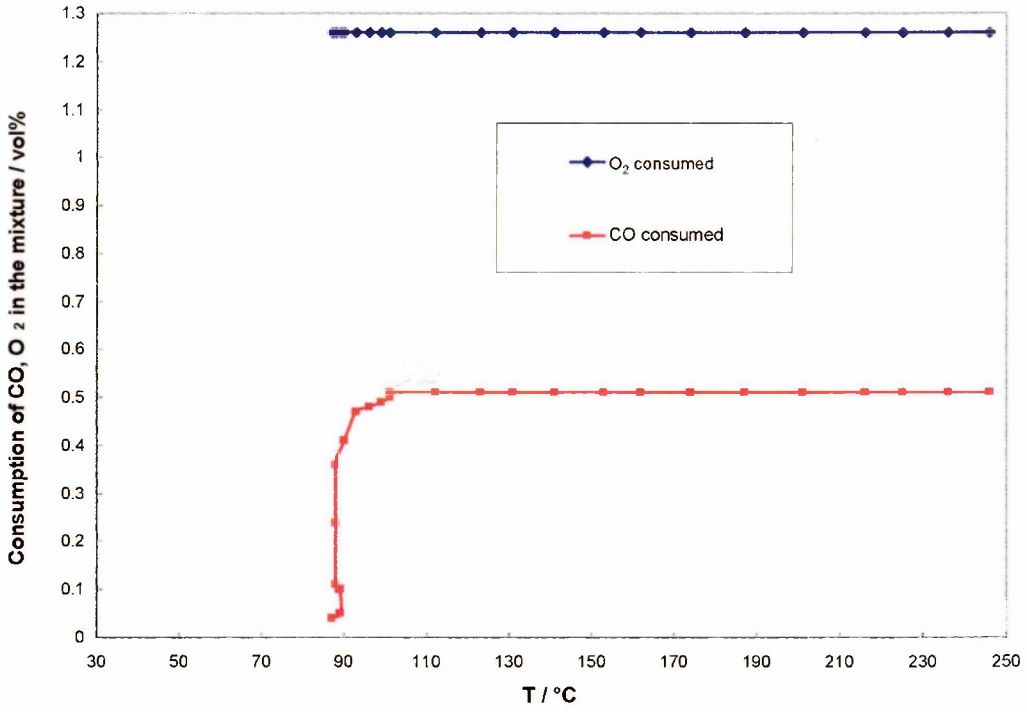

FIGURE 4-5: The CO oxidation profile of the undiluted (1:2) FePt/Al_2O_3(high) catalyst

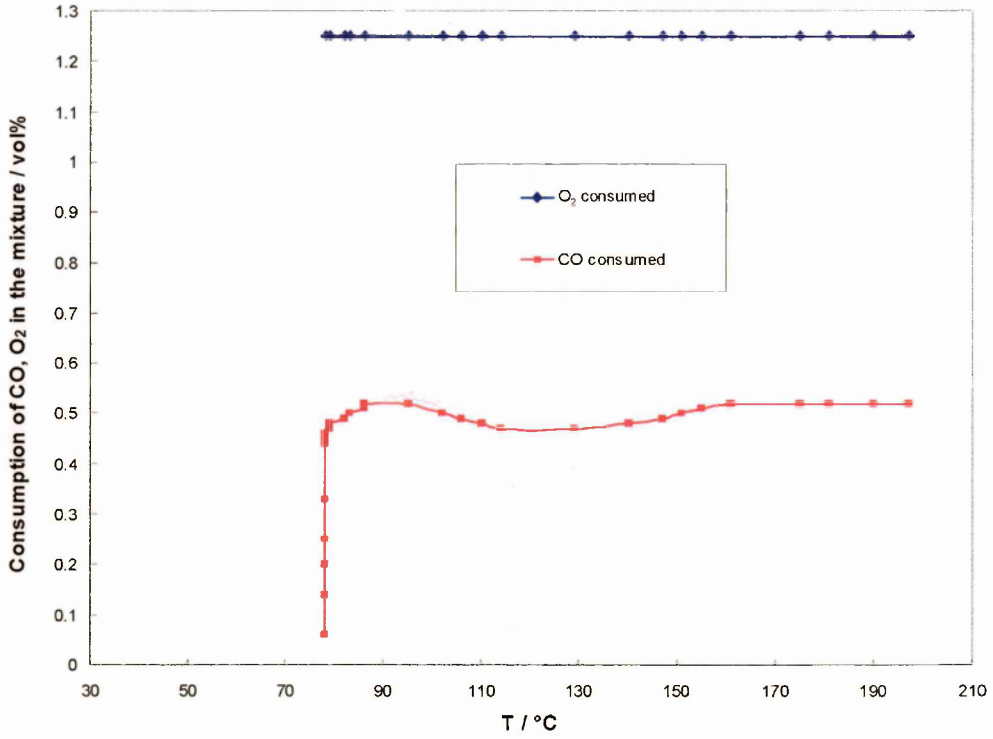

FIGURE 4-6: The CO oxidation profile of undiluted (1:1)FePt/Al_2O_3(high) catalyst

Initially a sample of (1:1)FePt/Al_2O_3(high) catalyst was diluted with equal amounts of the support, γ-Al_2O_3. The diluted catalyst was then examined for CO oxidation with the same gas mixture after pre-reduction at 40 °C. It was found that the reaction could be slowed down slightly with the catalyst dilution, but not significantly enough so as to distinguish between the performances of the diluted and undiluted catalysts. The high activity of the catalyst was observed even with the diluted catalyst as total oxidation of CO occurred by 89 °C (Fig. 4-7).

Another test was performed, this time with a one-fifth dilution of the (1:1)FePt(high) catalyst with the support material (Fig. 4-8). The one-fifth dilution refers to the mixing of a known amount of the catalyst with four times that amount of alumina. The catalyst was given the standard pre-reduction treatment (reducing at 40 °C for 40 minutes) prior to the test.

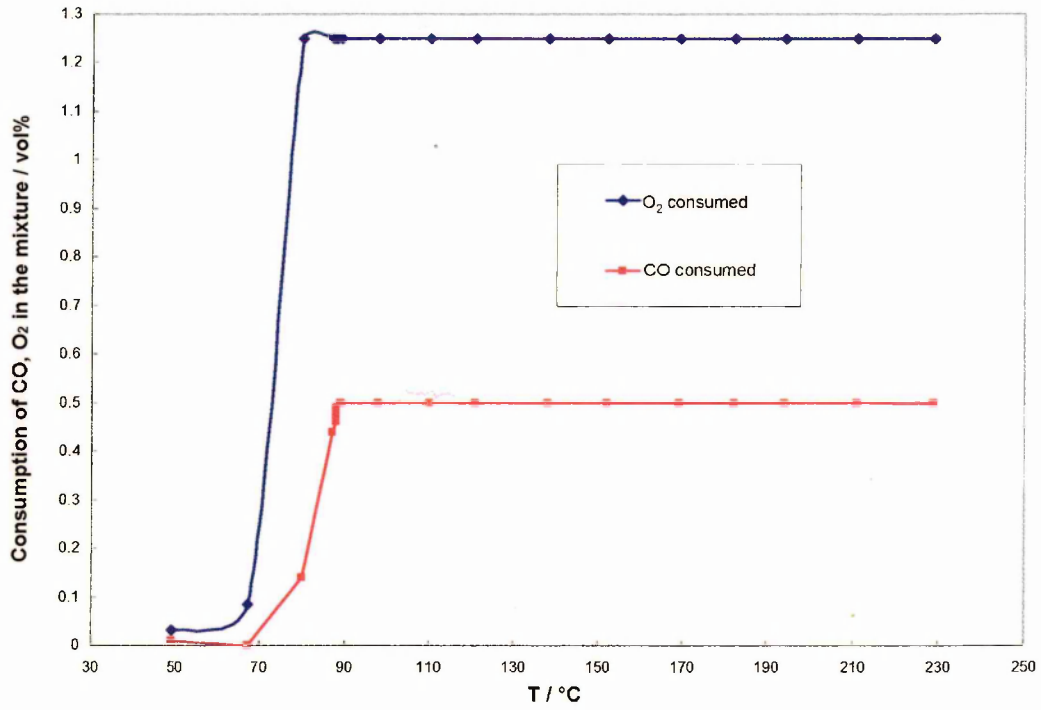

FIGURE 4-7: The CO oxidation profile for (1:1)FePt/Al_2O_3(high)– diluted with equal amounts of alumina

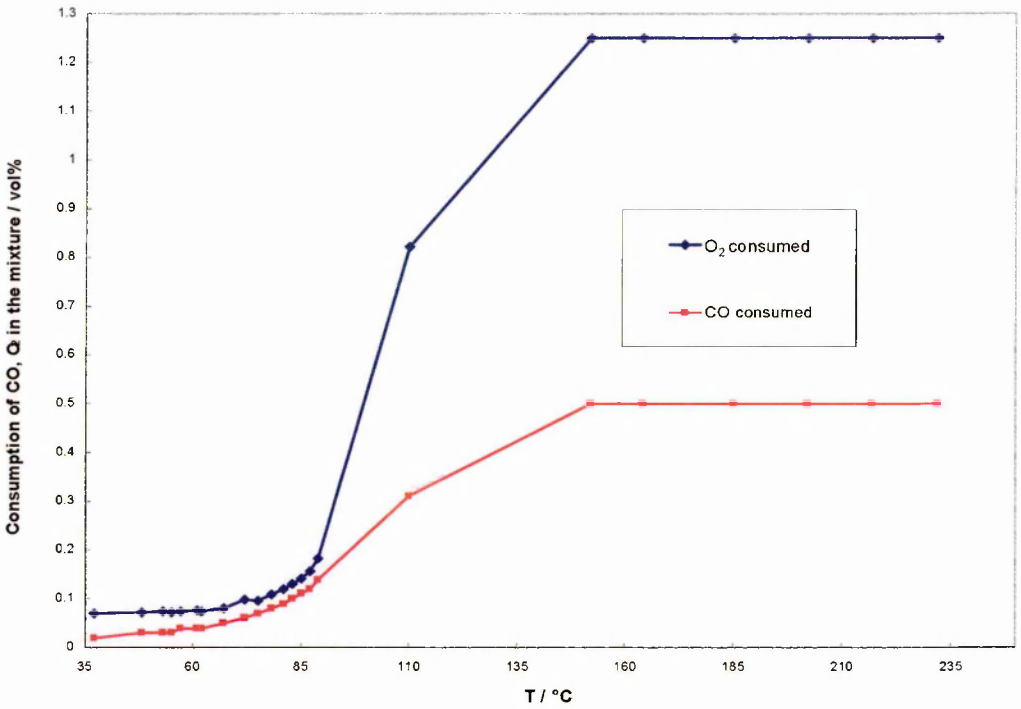

FIGURE 4-8: The CO oxidation profile for (1:1)FePt/Al_2O_3(high) – one-fifth dilution with alumina

It was observed that the CO conversion could be slowed down considerably with the one-fifth dilution of the catalyst. In this case, complete CO conversion was achieved at 148 °C. With the use of the one-fifth dilution catalyst, it was easier to monitor the consumption of oxygen during the test due to the lowering of the reaction rate.

On account of the higher activity of the bimetallic catalysts prepared through the SOMC route, even at 40 °C, the catalysts had to be diluted with the pure support material in order to maintain sufficiently low rates of CO conversion. It was decided to dilute all samples to 20% for routine examination.

From the observations made, it was decided that the suitable conditions for studying any catalyst showing high activity are

1. A flow rate of 100 $cm^3 min^{-1}$
2. Pre-reduction of catalyst at 40 °C for 40 minutes with 2% CO in H_2.
3. One-fifth dilution of the catalyst with the support.

4.2 INITIAL SCREENING TESTS (DRY) WITH EXCESS OXYGEN (λ_5)

The present *Dry CO Test* studies were carried out with a gas mixture containing 0.50% CO, 1.25% O_2, ~25% H_2 and the balance N_2. The test gas did not contain CO_2 due to the interference with O_2 measurements.

The bimetallic catalysts prepared by the SOMC route examined in these preliminary studies are listed in Table 4-1. The metal loadings determined from ICP-AES analysis and the dispersion values obtained from the carbon monoxide (CO) chemisorption experiments for these catalysts are also included in Table 4-1.

Table 4-1: LIST OF ALUMINA SUPPORTED M-Pt BIMETALLIC CATALYSTS (M= Fe, Co, Cr, Ni, Cu, Mn)

LOW-DISPERSED SYSTEMS

Catalyst	Pt (mass%)	M (mass%)	CO/Pt	Precursor used
(1:2)CuPt (in heptane)	4.89	0.09	0.09	$Cu(acac)_2$
(1:2)CuPt (in toluene)	4.91	0.23	0.20	$Cu(acac)_2$
(1:2)NiPt[#]	4.93	0.22	0.20	$Ni(C_5H_5)_2$
(1:2)CoPt	4.89	0.16	0.19	$Co(C_5H_5)_2$
(1:2)FePt	4.62	0.20	0.16	$Fe(C_5H_5)_2$
(1:2)MnPt (in toluene)	4.84	0.19	0.11	$Mn(acac)_2$
(1:2)CrPt	4.79	0.17	0.13	$Cr(C_5H_5)_2$

*CO/Pt refers to the fraction of Pt sites available on the surface of the catalyst as calculated from CO chemisorption studies.

[#] not tested as activity in wet tests (Section 4.4) was poor.

Pt CATALYST

There was no activity observed for the Pt/Al_2O_3(low) catalyst at 50 °C (Fig. 4-9). Less than 20% CO conversion (<0.10% CO consumption) was observed when the temperature of the catalyst was raised from 50 °C to about 150 °C. The O_2 consumption was also low, corresponding to selectivity to CO oxidation of about 40%. After this temperature, consumption of both CO and O_2 rise dramatically and 100% consumption of O_2 and CO (0.50% CO consumption) was achieved at just over 200 °C. Selectivity to CO at this point falls to about 20%, the maximum value at total O_2 consumption based on the stoichiometry of the mixture.

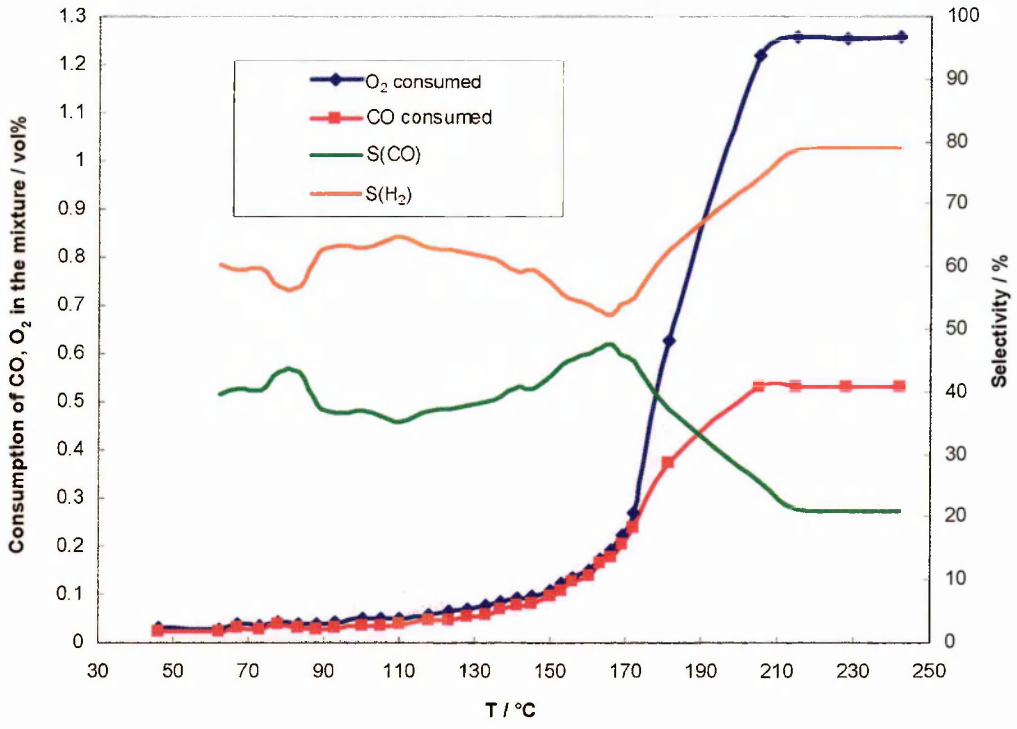

FIGURE 4-9: The CO oxidation profile and the selectivity towards CO oxidation for 5%Pt/Al_2O_3(low) catalyst

From the stoichiometry of the equation $CO + 0.5O_2 \rightarrow CO_2$, it is clear that each mole of CO requires only 0.5 mole of O_2 for complete oxidation. The initial $CO:O_2$ ratio

of 0.50 vol%:1.25 vol% (≡1:2.5) in the gas mixture meant that only 0.25 vol% of O_2 was required for complete oxidation leaving 1 vol% of O_2 to oxidise H_2. 1.25 vol% O_2 in the gas mixture meant five times the required amount of O_2 and hence a stoichiometric CO:O_2 ratio of 1:5.

Cu–PROMOTED Pt CATALYST

When the λ_5 gas mixture was passed over the pre-reduced (1:2)CuPt(low) catalyst prepared in either heptane or toluene, very low activity was observed at the beginning of the test at 40 °C over both the catalysts (Figs. 4-10 and 4-11, respectively). By 70 °C, only about 5% CO (~0.025 vol%) was oxidised over the catalyst prepared in heptane (Fig. 4-11). A gradual increase in CO conversion to ~20% (~0.10 vol%) was observed when the temperature of the catalyst was raised to 120 °C. 50% CO conversion (0.25 vol%) was observed at 146 °C, while oxygen consumption followed the CO consumption closely.

Complete CO oxidation was observed at 204 °C. The performance of the CuPt catalyst prepared in heptane has been observed to be very much like that of the Pt-only catalyst. From the ICP-AES results (Table 3-3) and also from the CO chemisorption data (Table 3-4), it is evident that the catalyst preparation was not fully successful using copper acetylacetonate as the precursor in heptane. This was probably due to low solubility of the precursor in heptane.

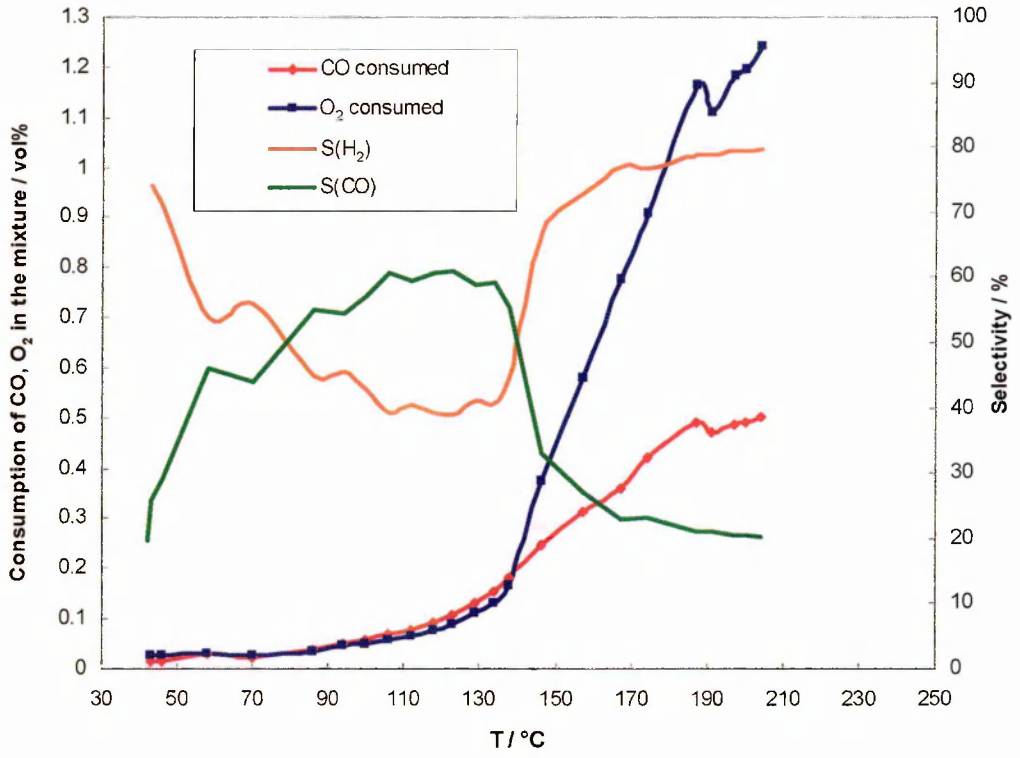

FIGURE 4-10: The CO oxidation profile and the selectivity towards CO oxidation for (1:2)CuPt/Al_2O_3(low) catalyst prepared in heptane

When the catalyst preparation was carried out in toluene, the ICP-AES and CO chemisorption results clearly indicated the successful deposition of Cu on Pt in the catalytic system. In the case of the CuPt catalyst prepared in toluene, about 5% CO conversion (~0.025 vol%) was observed around 50 °C, about 20% CO conversion (~0.10 vol%) was observed by 85 °C and 50% CO (0.25 vol%) was found to be oxidised by 115 °C. The complete oxidation of CO was achieved by 157 °C and the oxygen was also found to be totally consumed at the same temperature. The selectivity values for Cu-promoted catalysts at 50% CO conversion are presented in Table 4-2.

Table 4-2: THE ACTIVITY-SELECTIVITY AND RELATED PARAMETERS FOR THE CuPt CATALYSTS

Catalyst	CO/M	*T*(50) / °C	*S*(CO)/%	*T*(100) / °C
Pt/Al_2O_3(low)	0.29	172	45	205
(1:2)$CuPt/Al_2O_3$[#]	0.21	146	33	204
(1:2)$CuPt/Al_2O_3$[*]	0.10	115	41	157

T(100) is the temperature at which complete CO oxidation is observed, *T(50)* is the temperature at which 50% CO oxidation is observed, *S*(CO) is the selectivity towards CO oxidation at *T*(50), # Catalyst preparation carried out in heptane, * Catalyst preparation carried out in toluene

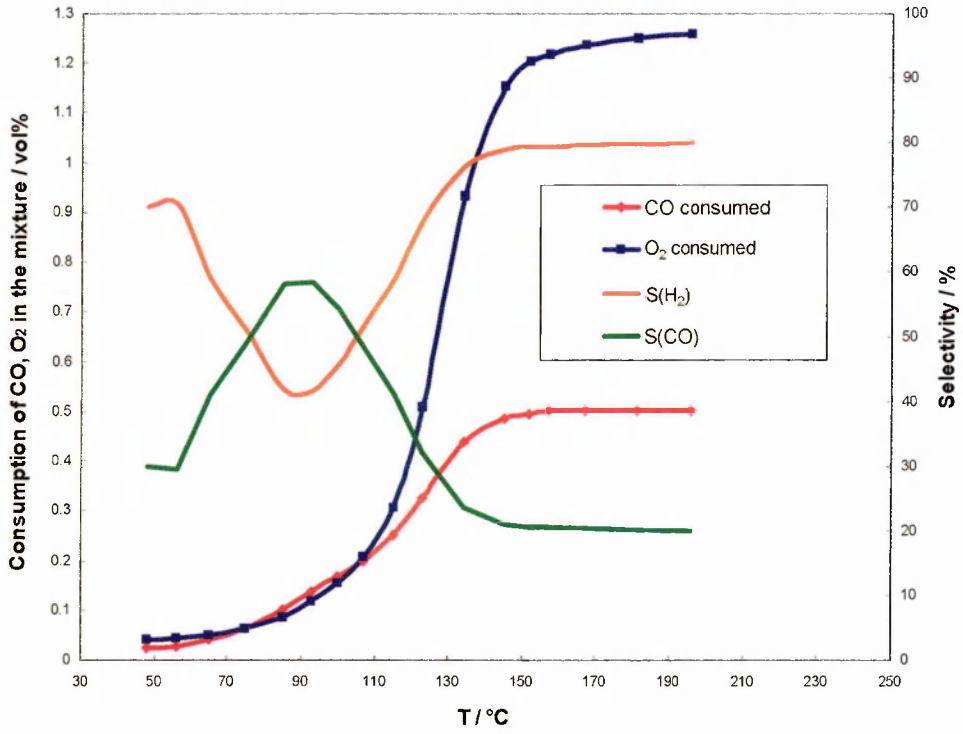

FIGURE 4-11: The CO oxidation profile and the selectivity towards CO oxidation for (1:2)$CuPt/Al_2O_3$(low) catalyst prepared in toluene.

It was interesting to observe that the catalysts prepared in different solvents using the same precursor could affect the catalytic performance quite significantly. It was decided for any other preparation using an acetylacetonate precursor to use toluene as the solvent rather than heptane.

Co–PROMOTED Pt CATALYST

Nearly 80% of CO (~0.40%) was already converted to CO_2 at the beginning of the test *i.e.* 30 °C when λ_5 gas mixture was passed over the (1:2)CoPt(low) catalyst, reduced at 40 °C (Fig. 4-12). With the rise in temperature the remaining CO was oxidised by 108 °C.

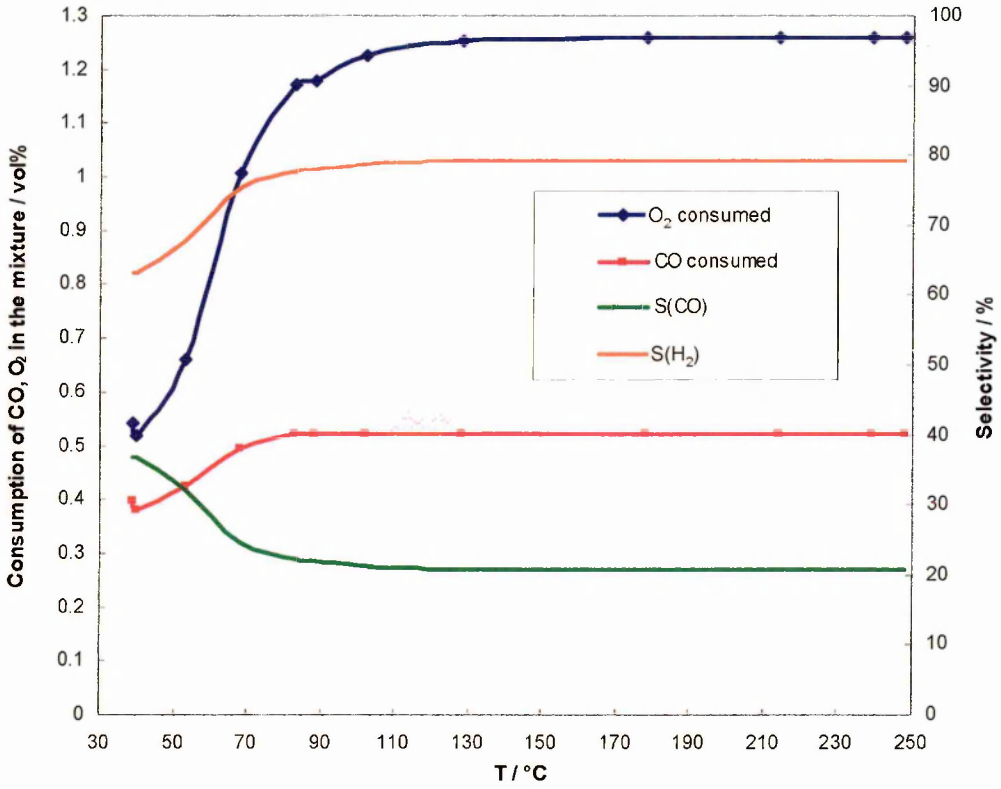

FIGURE 4-12: The CO oxidation profile and the selectivity towards CO oxidation for (1:2)CoPt/Al_2O_3(low) catalyst.

The selectivity values for Co promoted catalysts at 50% CO conversion and the other related parameters are presented in Table 4-3. From the Fig. 4-12, it is evident that the CoPt catalyst showed significantly better activity in the CO oxidation reaction than the Pt-only catalyst.

Table 4-3: THE ACTIVITY-SELECTIVITY AND RELATED PARAMETERS FOR THE CoPt CATALYSTS

Catalyst	CO/M	*T*(50) / °C	*S*(CO)/%	*T*(100) / °C
Pt/Al_2O_3(low)	0.29	172	45	205
(1:2)$CoPt/Al_2O_3$(low)	0.19	40*	47*	108

* Values reported for ~75% CO conversion

Fe–PROMOTED Pt CATALYST

When the gas mixture (λ_5) was introduced over the (1:2)FePt(low) catalyst after pre-reduction at 40 °C, 50% CO conversion (0.25 vol%) was observed initially at 40 °C (Fig. 4-13). The entire CO was oxidized by 100 °C, at which temperature complete consumption of oxygen in the mixture was also observed.

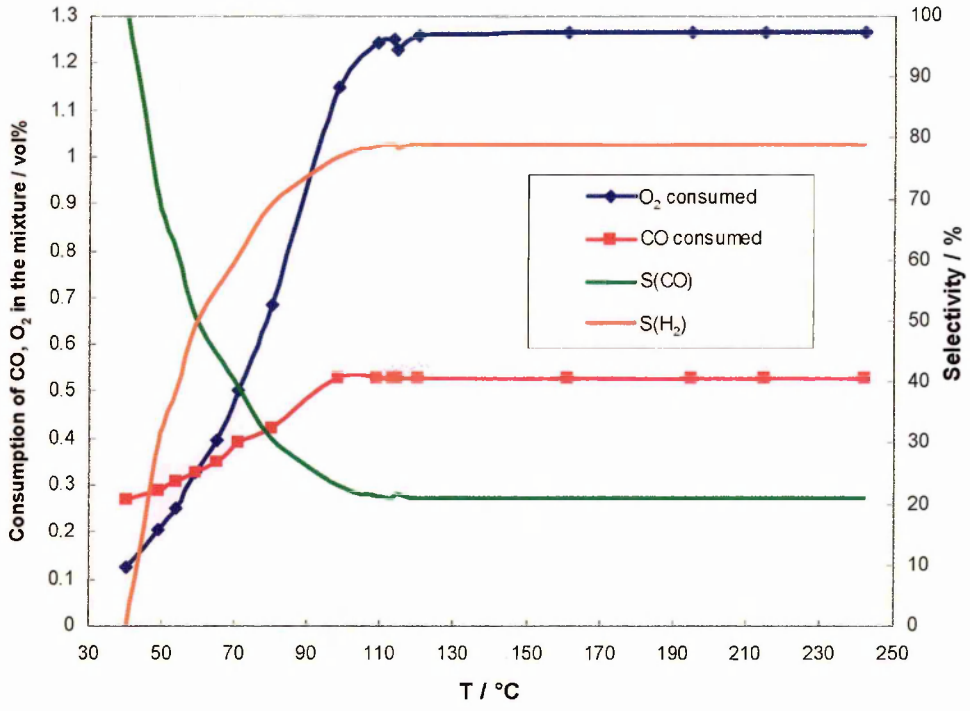

FIGURE 4-13: The CO oxidation profile and the selectivity towards CO oxidation for (1:2)$FePt/Al_2O_3$(low) catalyst.

The selectivity values for Fe-promoted catalysts at 50% CO conversion are presented in Table 4-4. From Fig. 4-13 it is evident that the FePt catalyst similarly showed significantly better performance towards CO oxidation than the Pt-only catalyst.

Table 4-4: THE ACTIVITY-SELECTIVITY AND RELATED PARAMETERS FOR THE FePt CATALYSTS

Catalyst	CO/M	*T*(50) / °C	*S*(CO)/%	*T*(100) / °C
Pt/Al_2O_3(low)	0.29	172	45	205
(1:2)$FePt/Al_2O_3$(low)	0.16	40	100	100

Mn–PROMOTED Pt CATALYST

The (1:2)MnPt(low) catalyst under λ_5 gas mixture at temperatures up to 110 °C showed low activity towards CO oxidation (Fig. 4-14). From Fig. 4-14 it is clear that the (1:2)MnPt(low) catalyst also showed poorer selectivity towards CO than the Pt-only catalysts in the lower temperature region. With the rise in temperature, an increase in the CO conversion was observed. 50% CO conversion (0.25 vol%) was achieved at 171 °C. The oxygen consumption curve was found to closely follow the CO consumption curve. Complete CO oxidation was observed at 223 °C, about 20 °C or so higher than the unpromoted Pt catalyst. The selectivity values for Mn-promoted catalysts at 50% CO conversion are presented in Table 4-5.

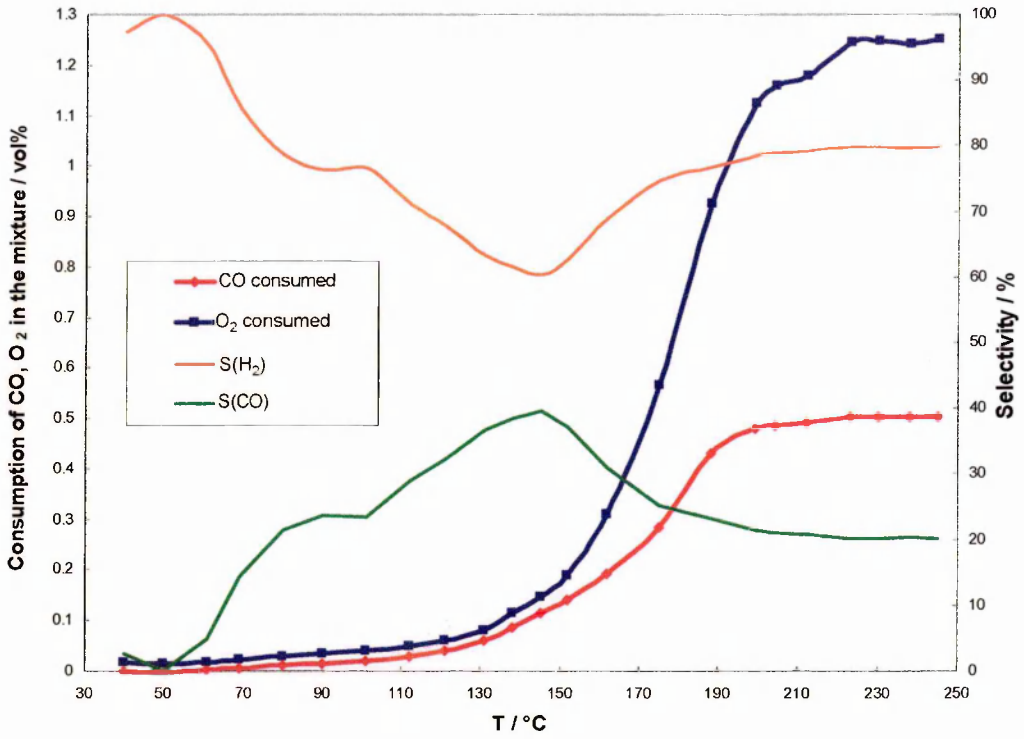

FIGURE 4-14: The CO oxidation profile and the selectivity towards CO oxidation for (1:2)MnPt/Al_2O_3(low) catalyst prepared in toluene.

Table 4-5: THE ACTIVITY-SELECTIVITY AND RELATED PARAMETERS FOR THE MnPt CATALYSTS

Catalyst	CO/M	*T*(50) / °C	*S*(CO)/%	*T*(100) / °C
Pt/Al_2O_3(low)	0.29	172	45	205
(1:2)MnPt/Al_2O_3(low)	0.11	171	28	223

Despite reports in the literature [1] that Mn is an effective promoter for the CO oxidation reaction, our results showed little difference in catalytic performance compared to the unpromoted catalyst. ICP-AES analysis indicated that the Mn was present at similar levels to that expected in this catalyst. No other characterization on this catalyst was performed, so it is possible that the Mn although present on the catalyst

was not closely associated with the Pt, or was not in the correct form to show high activity.

Cr–PROMOTED Pt CATALYST

The CO oxidation profile and the selectivity values for Cr-promoted catalysts at 50% CO conversion are given in Table 4-6. There was no observable activity until about 60 °C when (1:2)CrPt(low) catalyst was put on stream after reduction at 40 °C (Fig. 4-15). A very low activity (about 0.05 vol%) was observed with a rise in temperature until *ca* 140 °C. About 50% of the CO (0.25 vol%) was converted to CO_2 just below 180 °C, with a very similar profile to that of unpromoted Pt catalyst. Complete CO oxidation was observed at 225 °C, about 20 °C higher than observed for the Pt-only catalyst. All the oxygen was also consumed at the same temperature. From Fig. 4-15 it is quite clear that the CrPt catalyst showed poorer selectivity towards CO oxidation than the Pt-only catalysts in the lower temperature region.

Table 4-6: THE ACTIVITY-SELECTIVITY AND RELATED PARAMETERS FOR THE CrPt CATALYSTS

Catalyst	CO/M	*T*(50) / °C	*S*(CO)/%	*T*(100) / °C
Pt/Al_2O_3(low)	0.29	172	45	205
(1:2)$CrPt/Al_2O_3$(low)	0.13	180	35	224

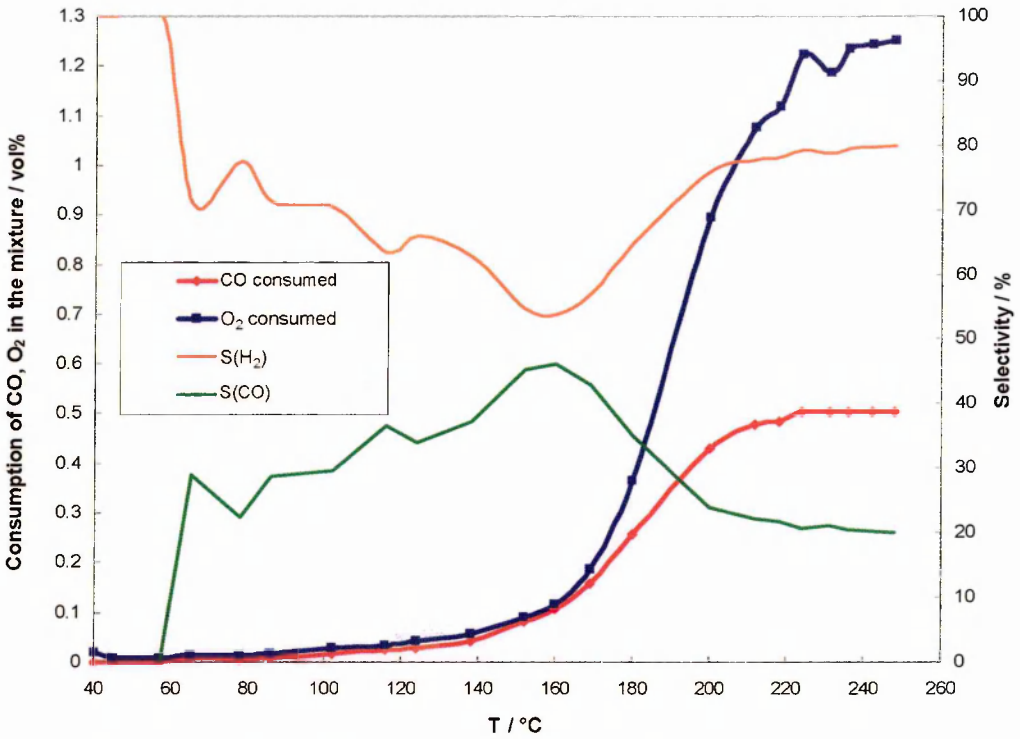

FIGURE 4-15: The CO oxidation profile and the selectivity towards CO oxidation for (1:2)CrPt/Al_2O_3(low) catalyst.

Sn–PROMOTED Pt CATALYST

For (1:2)SnPt(low) catalyst less than 20% CO conversion (0.10 vol%) was observed at 40 °C (Fig. 4-16). Increasing the temperature to just above ~100 °C resulted in 50% CO conversion (0.25 vol%). All the CO was converted (0.50 vol%) as the catalyst temperature reached ~140 °C. The selectivity values and the related parameters for Sn-promoted catalysts at 50% CO conversion are presented in Table 4-7. From Fig. 4-16 it is evident that the SnPt catalyst exhibits significantly better activity and selectivity in the CO oxidation reaction than the unpromoted catalyst.

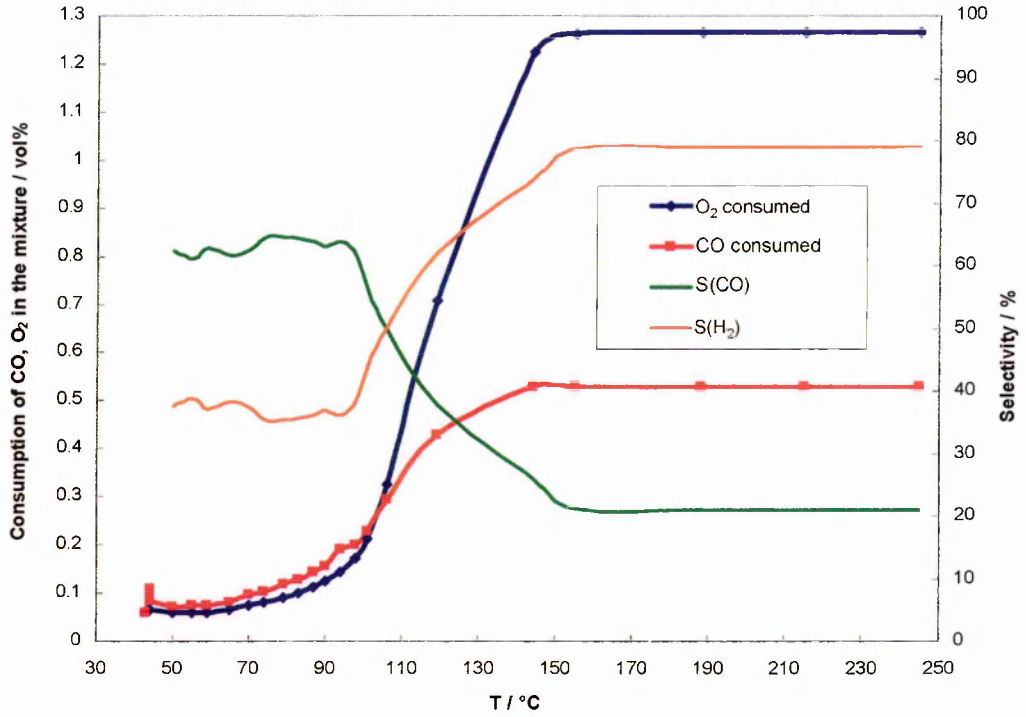

FIGURE 4-16: The CO oxidation profile and the selectivity towards CO oxidation for (1:2)SnPt/Al_2O_3(low) catalyst.

Table 4-7: THE ACTIVITY-SELECTIVITY AND RELATED PARAMETERS FOR THE SnPt CATALYSTS

Catalyst	CO/M	*T*(50) / °C	*S*(CO)/%	*T*(100) / °C
Pt/Al_2O_3(low)	0.29	172	45	205
(1:2)SnPt/Al_2O_3(low)	0.13	134	58	*T*(86)=211

From these initial screening of the (1:2)M-Pt(low) catalysts, where M=Cu, Co, Fe, Mn, Cr and Sn, using the λ_5 gas mixture it is clear that the Fe, Co and to a certain extent Sn have a significant effect on the activity and selectivity of the promoted catalysts.

All the above mentioned catalysts were also screened at Johnson Matthey Technology Centre, UK, under a simulated reformate gas mixture. Details of these tests are described under the section '*Wet Tests*'.

4.3 WET TESTS

All the catalysts, prepared by SOMC route, were screened under a simulated reformate gas mixture at the Johnson Matthey Technology Centre, Sonning Common, UK. For these studies

- About 50 mg of the catalyst was mixed with about 150 mg of cordierite and loaded into the reactor.
- The gas composition was set to 60% H_2, 0.1% CO, 20% CO_2, 0.15% O_2 and the balance nitrogen.
- The temperature of the reactor was maintained at 150 °C throughout the experiment.
- Once the temperature of the reactor reached 150 °C, 10% H_2O was added to the feed and the catalyst was left for 1 hour to stabilise.
- The total flow rate during ageing was maintained at 3×10^4 cm^3 min^{-1}.
- The tests were started at a space velocity of 2×10^3 cm^3 min^{-1} g_{cat}^{-1} over the catalyst, gradually increasing stepwise up to about 2×10^4 cm^3 min^{-1} g_{cat}^{-1}.

All the (1:2)M-Pt/Al_2O_3(low) catalysts were screened under the above mentioned conditions [where M= Cr, Mn, Fe, Co, Ni, Cu and Sn]. The results of these studies are shown in terms of the amount of CO left un-oxidised by the catalyst (in ppm) as a function of space velocity (in cm^3 min^{-1} g^{-1}), (Fig. 4-17). The catalysts were

compared to a good promoted catalyst prepared at Johnson Matthey Technology Centre, UK.

The M-Pt(low) catalysts, where M = Cr, Ni and Cu were found to be quite inactive towards the CO oxidation reaction under real conditions compared to the Johnson Matthey catalyst. The performance of the Ni–promoted Pt catalyst in the wet tests was found to be inferior to the other promoted catalysts and so, due to time constraints, the Ni–promoted Pt catalyst was not tested under dry conditions.

The inherent property of Mn to form a variety of oxides suggested initially that Mn–promoted catalysts might exhibit higher activity towards CO oxidation. However, it is interesting to see that the (1:2)MnPt(low) catalyst, prepared in toluene, which was apparently inactive in the previous study (Dry CO test), was quite active at low space velocities in the presence of H_2O vapour. Teng *et. al.* [1] found the MnOOH species to be more active than MnO_x towards CO oxidation in the presence of excess hydrogen, however the manganese oxy-hydroxide (MnOOH) tends to get dehydrated in the heated atmosphere. According to Teng *et. al.* [1] the high activity of the manganese catalyst may be due to a transition state from oxy-hydroxide to the oxide such as a mixed valence oxide or an amorphous phase having a high surface area. In the absence of H_2O in dry tests the MnO_x present on the surface of the catalyst seems to be stable enough not to participate in the CO oxidation actively.

From Fig. 4-17, it is clear that the Fe and Co promoted catalysts performed significantly better than the other catalysts over the range of space velocities considered. The Sn promoted catalyst show a very flat trend converting a similar amount of CO at the low and high values of space velocity. It was interesting to observe that Fe, Co and Sn promoted catalysts performed better than the other catalysts prepared by SOMC route in agreement with the dry tests.

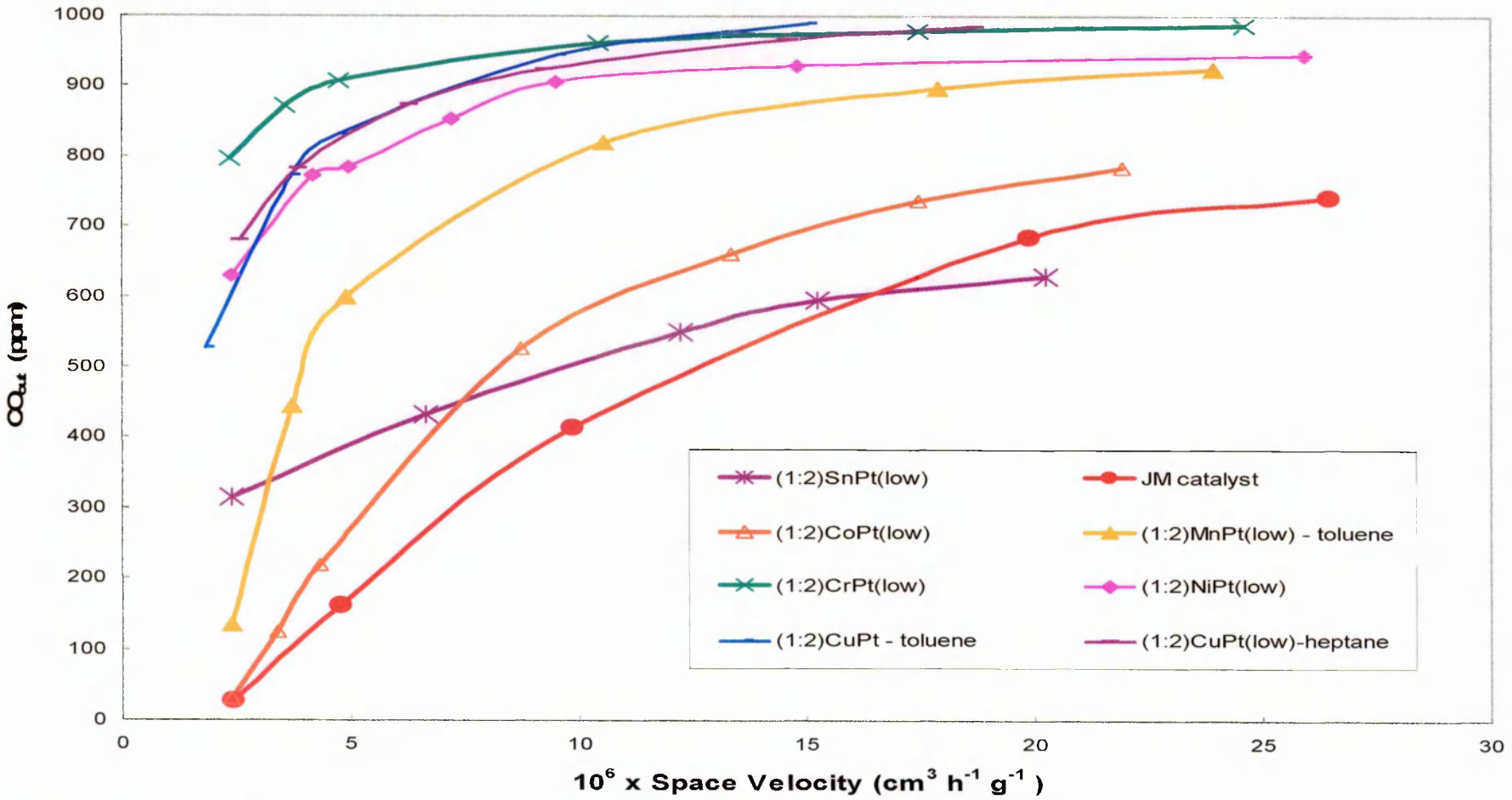

FIGURE 4-17: The plot of CO_{out} *vs.* Space Velocity at 150 °C, under a flowing gas mixture containing 60% H_2, 0.1% CO, 20% CO_2, 0.15% O

4.4 CONCLUSIONS

Preliminary studies were carried out in order to standardise the experimental conditions. From the results of the preliminary studies, it was decided that the conditions for testing any bimetallic catalyst are

- A flow rate of 100 cm^3 min^{-1}.
- Pre-reduction of the catalyst at 40 °C for 40 minutes with 2% CO in H_2.
- One-fifth dilution of the catalyst with the support material.

All the bimetallic catalysts were screened under a gas mixture containing 1.25% O_2, 0.50% CO, ~25% H_2 and the balance N_2. The Sn-, Co- and Fe-promoted Pt catalysts showed increased activity towards CO oxidation.

When these catalysts were tested at JMTC under a simulated reformate mixture containing 60% H_2, 0.1% CO, 20% CO_2, 0.15% O_2 and balance nitrogen, Fe- and Co-promoted catalysts did show comparable, if not better, activity than a commercial JM catalyst. Sn-promoted catalyst showed a performance very comparable to a good JM catalyst.

Based on the dry and wet test results, the Sn, Fe and Co catalytic systems were selected for further detailed studies. The results of the further studies on these catalytic systems are described and discussed in Chapter 5 of this thesis.

4.5 REFERENCES

1 Y. Teng, H. Sakurai, A. Ueda and T. Kobayashi, *Int. Jour. Hydrogen Energy*, **24**, 355, (1999)

5

Selective Catalytic Oxidation of CO (II)

Sn–, Co– and Fe–promoted Pt Catalysts

Based on the preliminary studies conducted on various bimetallic catalysts of the series M-Pt/Al_2O_3, three catalytic systems with M = Sn, Fe, and Co, showing high activity and selectivity towards CO oxidation, were chosen for the detailed examination. The results of these studies are presented and discussed in this chapter. The method of preparation and the characterisation of the M-Pt/Al_2O_3 catalysts (M = Sn, Fe, and Co) were described in detail in Chapters 2 and 3 respectively but are summarised briefly where appropriate.

The Sn–, Fe– and Co–promoted bimetallic catalysts prepared by the SOMC route, together with their metal loadings, and the dispersion values as obtained from the carbon monoxide (CO) chemisorption experiments, are listed in Table 5-1.

Table 5-1: LIST OF ALUMINA SUPPORTED M-Pt BIMETALLIC CATALYSTS

LOW–DISPERSED SYSTEMS

Catalyst	Pt (mass%) (± 10 %)	M (mass%) (± 10 %)	CO/Pt
5%Pt (batch I)	4.60	–	0.36
5%Pt (batch II)	5.18	–	0.26*
(1:2)SnPt(I)	4.60	0.44	-
(1:1)SnPt(I)	5.18	0.88	0.08
(1:2)FePt(I)	4.62	0.20	0.16
(1:1)FePt(I)	4.65	0.38	0.17
(1:2)CoPt (II)	4.89	0.16	0.19
(1:1)CoPt (II)	4.99	0.34	0.20

HIGH–DISPERSED SYSTEMS

5%Pt (batch I)	4.94	–	0.51
5%Pt (batch II)	5.20	–	0.54*
(1:2)SnPt(I)	4.43	0.82	0.24
(1:1)SnPt(I)	4.57	1.58	0.24
(1:2)FePt(I)	4.86	0.49	0.25
(1:1)FePt(I)	4.65	0.73	0.24
(1:2)CoPt (II)	4.53	0.33	0.36
(1:1)CoPt (II)	4.65	0.67	0.24

* Results reported by JM

Note: All results reported for metal assays are within experimental error of ± 10%.

The performance of the (1:2)MPt(low) catalysts (M = Sn, Fe and Co) were described briefly in Chapter 4 but are repeated again here for discussion.

The gas mixtures used in the present testing studies are described below:

- Gas mixture containing 0.50% CO, 1.25% O_2, ~25% H_2 and the balance N_2 [referred to as the λ_5 system].
- Gas mixture containing 0.50% CO, 0.50% O_2, ~25% H_2 and the balance N_2 [referred to as the λ_2 system].

Since there was no water present in these samples of the gaseous feedstock, the experiments carried out with these mixtures are referred to as *dry CO tests* in this thesis.

5.1 DRY CO TESTS IN EXCESS OXYGEN (λ_5)

The results of the detailed studies on the activity and selectivity of the catalysts belonging to the series M-Pt/Al_2O_3 where M = Sn, Fe, and Co are presented in this section, where the CO oxidation reaction was studied as a function of temperature using a dry gas composition λ_5, which contained excess oxygen in the gas mixture: 0.50% CO, 1.25% O_2, ~25% H_2 and the balance N_2.

The total flow rate of the reaction gas was maintained at 100 cm^3 min^{-1}. Before the test, each catalyst was reduced under a 2% CO/H_2 mixture for 40 minutes at 40 °C.

5.1.1 Pt CATALYST

The consumption profiles for CO and O_2 and the selectivity of the Pt/Al_2O_3(low) catalyst towards CO oxidation are shown in Fig. 5-1. The Pt/Al_2O_3(low)

catalyst showed low activity up to 50 °C (Fig. 5-1). On increasing the temperature of the catalyst gradually from 50 °C to about 150 °C, consumption of both CO and O_2 is observed with CO:H_2 selectivity of 40%:60%. With a further slow rise in temperature of the catalyst, CO conversion gradually reached about 40% (0.20 vol% CO) by ~170 °C, with CO selectivity values showing a maximum of ca 45%. 100% CO conversion (0.50% CO consumption) was achieved at just over 200 °C and oxygen was also found to be consumed completely at the same temperature.

The CO oxidation profile for the 5% Pt/Al_2O_3(high) catalyst shown in Fig. 5-2, is very similar to that for the low–dispersed catalyst, except that the complete CO conversion is observed at the marginally lower temperature of ~190 °C. This difference in the activity of the catalyst is attributed to the higher dispersion and hence higher surface area of the Pt particles in the catalyst.

Table 5-2 presents the values of $T(100)$, $T(50)$ and the corresponding selectivity values towards CO for Pt/Al_2O_3 catalysts.

TABLE 5-2: THE ACTIVITY-SELECTIVITY DATA FOR THE ALUMINA SUPPORTED Pt CATALYSTS

Catalyst	CO/M	$T(50)$ / °C	$S(CO)$/%	T_{max} / °C
5% Pt(low)	0.29	172	45	205
5% Pt(high)	0.51	166	41	197

$T(100)$ is the temperature at which complete (100%) CO gets converted to CO_2

$T(50)$ is the temperature at which 50% of CO gets converted to CO_2.

T_{max} is the temperature at which the maximum CO conversion was observed.

S(CO) is the selectivity at $T(50)$

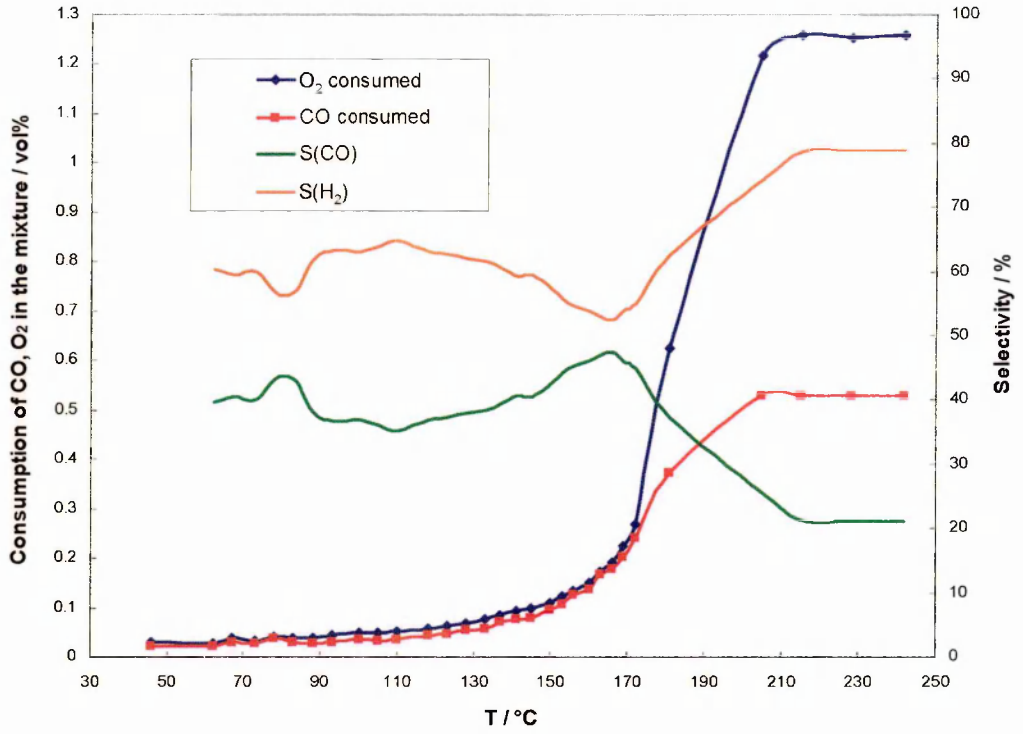

FIGURE 5-1: The consumption of CO and O_2 on 5% Pt/Al_2O_3(low) catalyst in λ_5 gas mixture

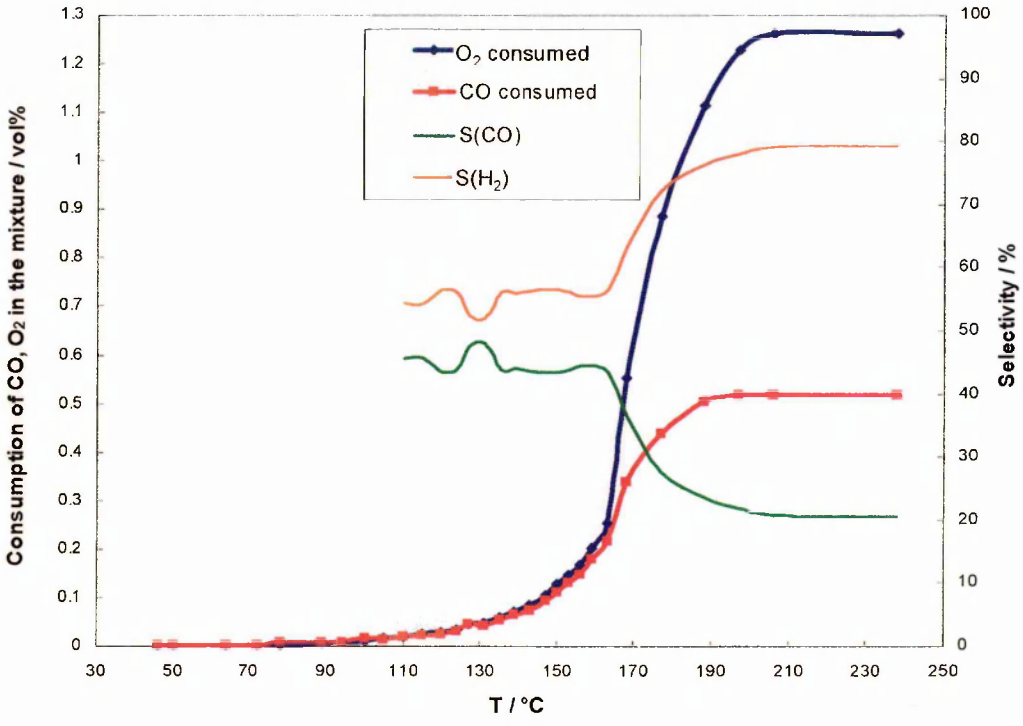

FIGURE 5-2: The consumption of CO and O_2 on 5% Pt/Al_2O_3(high) catalyst in λ_5 gas mixture

PROPOSED MECHANISM

According to the most widely accepted *Langmuir–Hinshelwood mechanism* [1], CO does not dissociate into atoms after chemisorption on the surface of platinum. Instead CO is bonded through the carbon atom to the platinum site.

Let S_{Pt} represent a site where chemisorption takes place, then the formation of site-CO complex, CO—S_{Pt}, can be described by the chemical equation:

$$CO(g) + S_{Pt} \rightleftharpoons CO—S_{Pt} \quad (1)$$

The double arrow indicates that the process occurs readily in both directions as the catalytic reaction proceeds. In other words, the CO chemisorption process is reversible in nature. Thus, the chemisorbed CO molecules can be released from the surface back into the vapour phase by a process called *desorption.*

According to the proposed mechanism, platinum activates oxygen and so increases the reactivity of carbon monoxide (CO) with oxygen (O_2). This activation of oxygen occurs via dissociation of the oxygen molecule on the surface of platinum to yield oxygen atoms bonded to the active sites (O—S_{Pt}) on the surface of the platinum. The activation of oxygen can be described by the chemical equation:

$$O_2(g) + 2S_{Pt} \rightleftharpoons 2\ O—S_{Pt} \quad (2)$$

The chemisorbed CO molecules can react easily with the neighbouring chemisorbed oxygen atoms to produce molecules of carbon dioxide that are readily released into the vapour phase as CO_2.

$$O—S_{Pt} + CO—S_{Pt} \rightleftharpoons CO_2(g) + 2\ S_{Pt} \quad (3)$$

Carbon monoxide (CO) competes with H_2 in its oxidation reaction. It is well known that in the absence of CO, oxidation of hydrogen over a Pt catalyst is instantaneous even at room temperature [2]. With CO present in the feed, the Pt

surface is covered by CO and hydrogen oxidation is inhibited at lower temperatures. Thermodynamically, CO adsorbs on the noble metal surfaces more strongly than H_2 or O_2 [3,4,5]. This can also be referred to as poisoning of the catalyst. Due to the strong adsorption tendency, CO would cover the catalyst surface almost completely at low temperatures, excluding other weakly adsorbed species [6], H_2 and O_2, from the active sites [7].

The catalytic oxidation of CO on Pt is usually described as a sudden self-acceleration of the surface reaction rate. According to the Langmuir-Hinshelwood mechanism, at atmospheric pressure [8,9,10,11], this generally occurs in a narrow temperature range. The temperature corresponding to the maximum gradient in the CO conversion vs temperature plot is known as the *light-off temperature*. This can be clearly seen in the profiles (Figs. 5-1 and 5-2) as the nearly vertical region of the CO and O_2 consumption curves at ~170 °C. For comparison purposes, the temperature at which 50% CO conversion (0.25 vol% CO CO) takes place, referred to as *T(50)*, seems to be a good approximation of light-off temperature. At the light-off temperature, heat is generated as a result of the exothermic reaction i.e. oxidation of CO. This heat generated exceeds the heat dissipation capacity of the system, and therefore the temperature of the catalyst increases rapidly. Due to this increase in temperature, the rate of CO oxidation also increases. An increase in the catalyst temperature leads to an increased CO desorption rate also. Once the reaction is initiated by the onset of CO desorption, the catalyst surface undergoes an abrupt decrease in the surface coverage of CO and as a result the number of active sites available for the oxygen adsorption increases. This in turn favours an increase in the reaction rate involving CO oxidation but also presumably allows hydrogen adsorption so this becomes a competing reaction. The high CO selectivity below 160 °C can be

explained in terms of the blocking action of the adsorbed CO which limits the extent to which oxidation of hydrogen can take place [12]. At temperatures above 165 °C, the active surface is expected to be only partially covered with CO [13]. The greater coverage of the catalyst surface by hydrogen now allows oxidation of hydrogen to proceed, and as a result selectivity towards CO decreases with an increase in temperature beyond 165 °C, as observed.

From the results obtained, both the Pt catalysts seemed to have a similar performance. The slightly better activity for the Pt(high) catalyst is due to the higher dispersion of Pt and hence the higher surface area of Pt in the Pt catalyst.

5.1.2 Sn-PROMOTED Pt CATALYSTS

Electron micrographs (Fig. 3-2) of Pt/Al_2O_3 showed that the Pt/Al_2O_3 catalyst has the Pt particles uniformly distributed on the support surface. The average size of the particles was found to be between 3–5 nm. Micrographs of $SnPt/Al_2O_3$ catalysts prepared in this study by the SOMC route showed that there was no significant change in the mean particle size in the catalyst compared to that of the unpromoted catalyst.

The CO oxidation profile for (1:2)SnPt(low) catalyst is shown in Fig. 5-3. At 46 °C about 20% of the CO (0.10 vol% CO) was observed to be converted to CO_2. 50% CO conversion (0.25 vol% CO) was observed at ~100 °C. The entire CO was oxidized, with simultaneous complete consumption of oxygen, by 140 °C. The CO oxidation profile for (1:1)SnPt(low) catalyst under excess oxygen was similar to that of the (1:2)SnPt(low) catalyst. About 10% CO conversion (0.05 vol% CO) was evident at the beginning of the test at 40 °C (Fig. 5-4) and 50% CO conversion (0.25 vol% CO) was observed at 93 °C. Complete CO oxidation was observed by 124 °C, and the oxygen was found to be completely consumed by the same temperature.

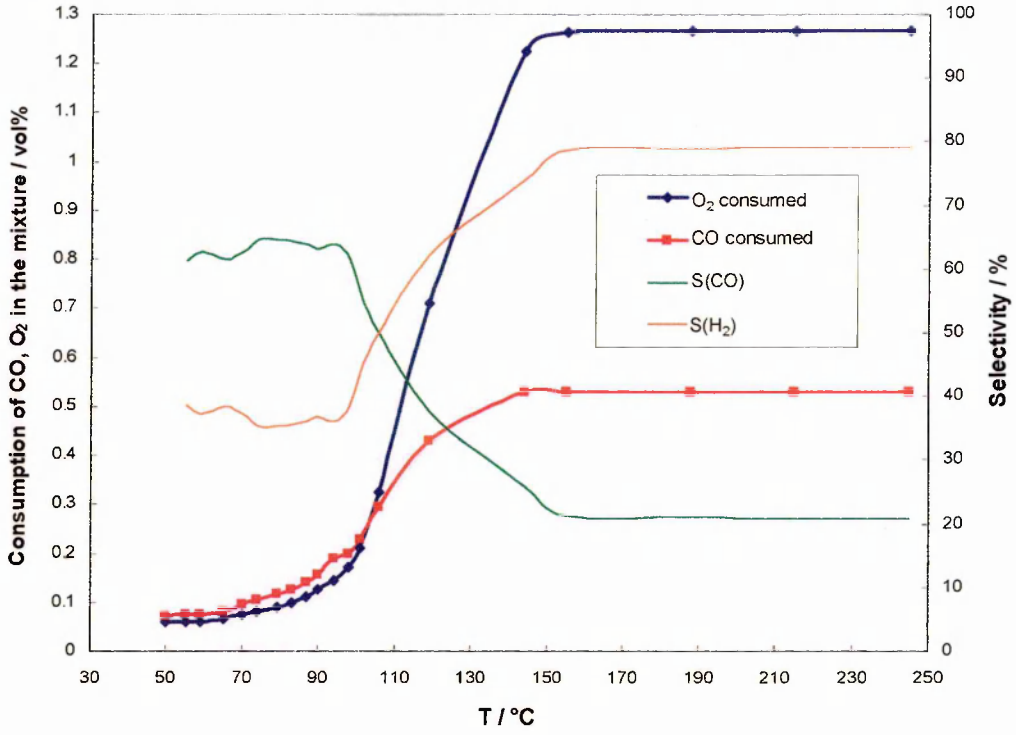

FIGURE 5-3: The consumption profiles of CO and O_2 on (1:2)SnPt/Al_2O_3(low) catalyst in λ_5 gas mixture

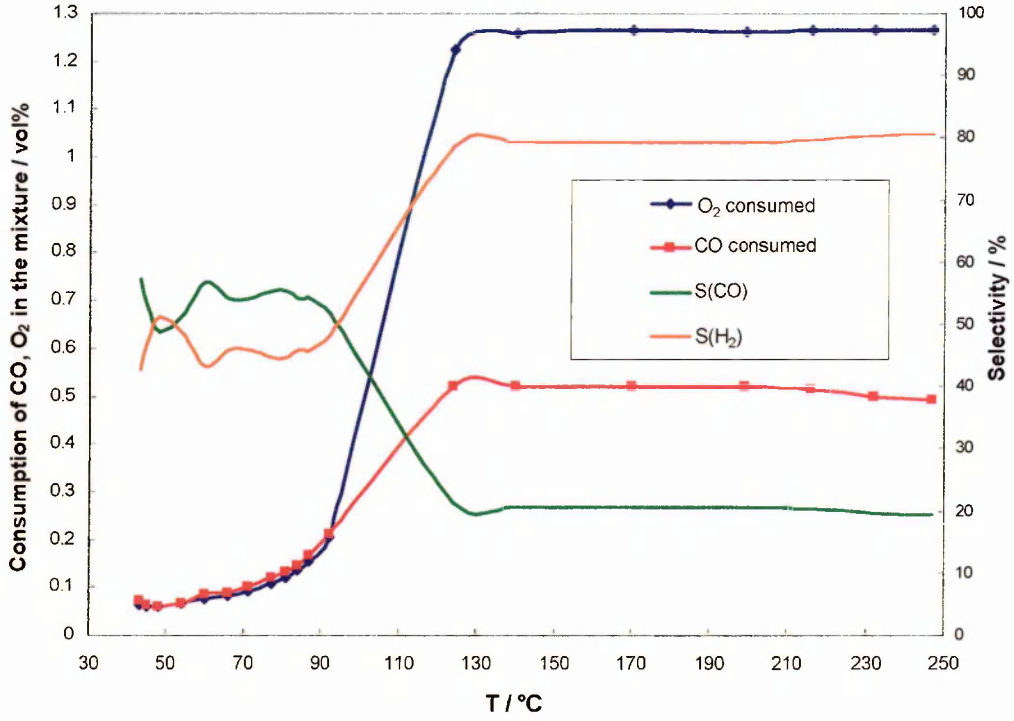

FIGURE 5-4: The consumption profiles of CO and O_2 on (1:1)SnPt/Al_2O_3(low) catalyst in λ_5 gas mixture

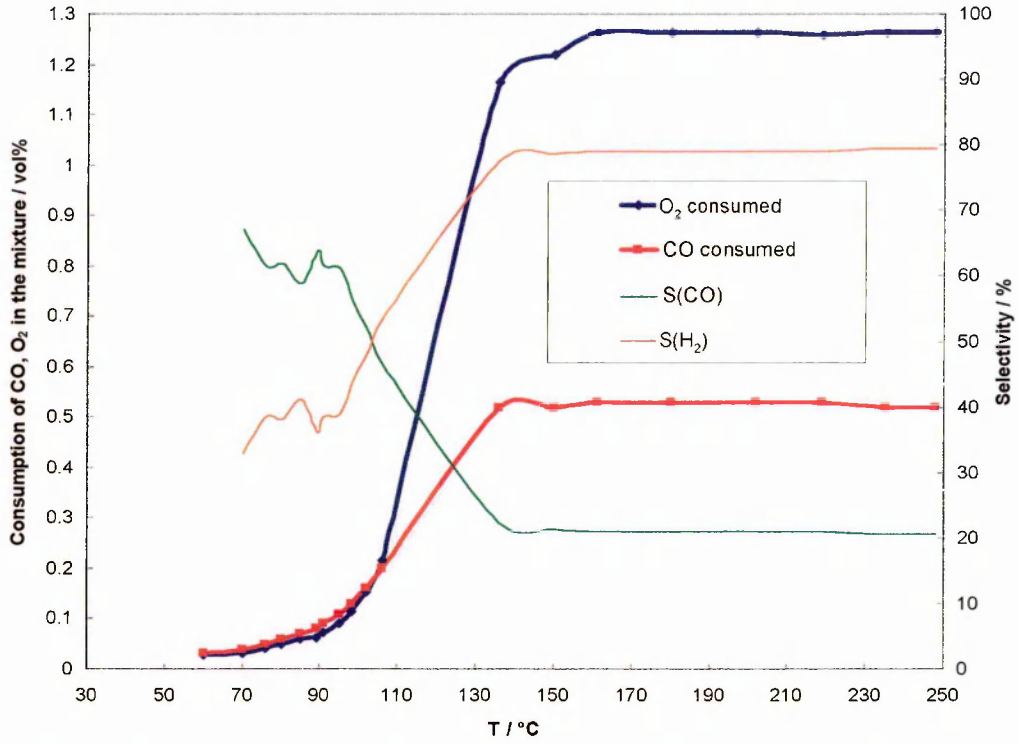

FIGURE 5-5: The consumption profiles of CO and O_2 on (1:2)SnPt/Al_2O_3(high) catalyst in λ_5 gas mixture

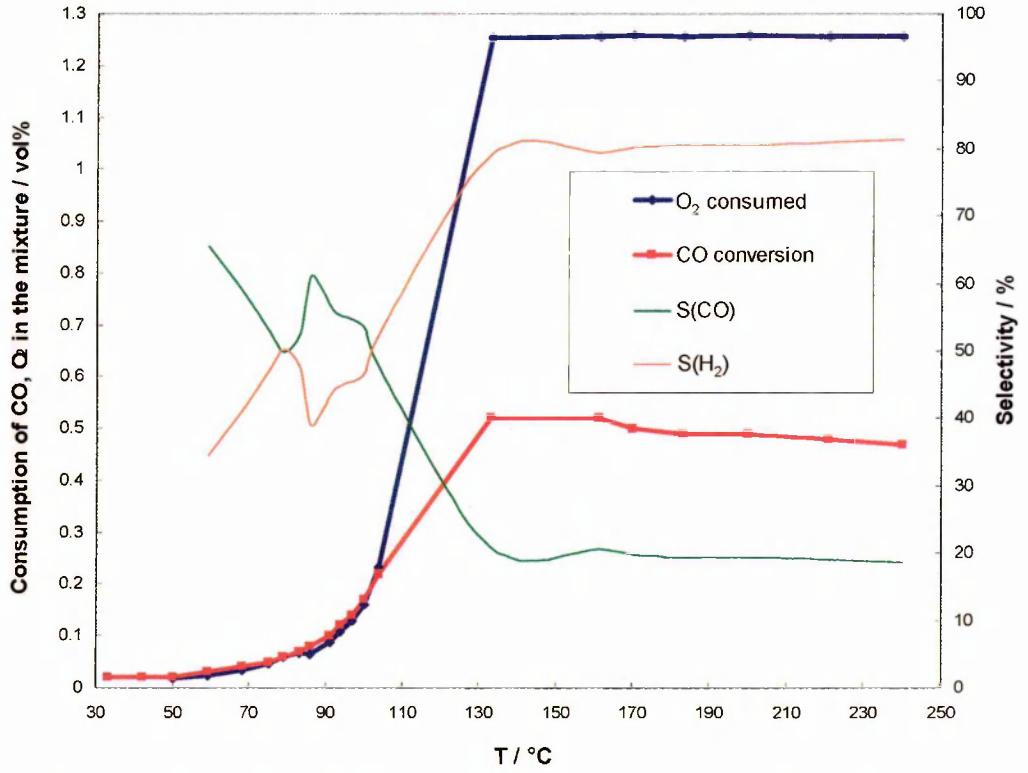

FIGURE 5-6: The consumption profiles of CO and O_2 on (1:1)SnPt/Al_2O_3(high) catalyst in λ_5 gas mixture

For the (1:2)SnPt(high) catalyst very low activity was observed at the beginning of the test (Fig. 5-5). With the rise in temperature, a slow increase in CO conversion reaching 50% (0.25 vol% CO) at 110 °C was observed. Once the complete oxidation of CO was achieved at 160 °C, all oxygen was also consumed. For (1:1)SnPt(high) catalyst, the CO conversion was observed to be very low in the beginning (Fig. 5-6), increasing gradually with temperature and reaching 50% conversion at 105 °C. Complete CO conversion was observed at 133 °C, but thereafter it decreased gradually with a rise in temperature. The low–dispersed catalysts showed better activity compared to the high–dispersed catalysts. However, the estimated selectivities were very similar in both systems.

The selectivity values for all the tin-promoted catalysts at 50% CO conversion and the related parameters are presented in Table 5-3. From the Figs. 5-3 to 5-6, it is seen that all the SnPt catalysts show better selectivity towards CO than that shown by the Pt-only catalysts in the low temperature region with < 40% CO conversion. At low temperatures, when CO coverage on the surface is high, hydrogen adsorption and its oxidation is practically inhibited because it is limited by the desorption of CO blocking the surface.

Table 5-3: THE ACTIVITY-SELECTIVITY AND RELATED PARAMETERS FOR THE SnPt CATALYSTS

Catalyst	CO/M	*T*(50) / °C	*S*(CO)/%	*T*(100) / °C
5% Pt(low)	0.29	172	45	205
(1:2)SnPt/Al_2O_3(low)	0.13	103	45	139
(1:1)SnPt/Al_2O_3(low)	0.08	93	45	124*
5% Pt(high)	0.51	166	41	197
(1:2)SnPt/Al_2O_3(high)	0.20	110	43	161
(1:1)SnPt/Al_2O_3(high)	0.20	107	50	130*

* CO conversion does not stay at 100%

From the results presented in Table 5-3, it is difficult to choose a best catalyst as all the Sn-promoted catalysts have similarly increased activity compared with Pt-only catalyst as T(100) is lower in all cases. There appears to be little difference between the performances of the low- and high–dispersed catalysts, similar to the case of the monometallic Pt catalyst.

PROPOSED MECHANISM

It is evident from the CO oxidation tests that the activity of the promoted catalyst is higher than that of the unpromoted Pt catalyst. In the case of the Pt catalyst, low activity is attributed to the poisoning of the catalyst by CO preventing the adsorption of O_2. Önsan and co-workers [14] showed that CO is not adsorbed on the SnO_x species in a SnO_x/Al_2O_3 catalyst. Therefore the difference in the activity of the catalysts may be attributed to the change in the nature of active sites involved in the CO oxidation over a bimetallic catalyst.

In addition to the Langmuir–Hinshelwood mechanism proposed for Pt catalyst, there is additional possibility that CO is adsorbed on the Pt sites (S_{Pt}) whereas O_2 is adsorbed dissociatively on the surface SnO_x sites (S_{MO_x} ; where M = Sn) [15]. A surface reaction can then take place between the adjacently adsorbed reactants to give CO_2 which then desorbs as the gaseous product. The sequence of elementary steps in the proposed mechanism is described below. S_{MO_x}

$$CO(g) + S_{Pt} \rightleftharpoons CO{-}S_{Pt} \quad (4)$$

$$O_2(g) + 2S_{MO_x} \rightleftharpoons 2\,O{-}S_{MO_x} \quad (5)$$

$$CO{-}S_{Pt} + O{-}S_{MO_x} \rightleftharpoons CO_2(g) + S_{MO_x} + S_{Pt} \quad (6)$$

where M = Sn and S_{Pt} are Pt sites

Boulahouache and co-workers [16] have explained the synergic effect between Pt and SnO_2 by the dissociative adsorption of oxygen on SnO_2 followed by the spill-over of oxygen onto the Pt sites, and subsequent reaction with the chemisorbed CO present on the Pt sites. Several hypotheses have been formulated in regard to the effect of the second metal, including the formation of a metal-Sn particle alloy, electronic interaction between the noble metal and Sn^{n-} ions etc [17,18,19].

5.1.3 Co-PROMOTED Pt CATALYSTS

Similarly to the tin oxide, the presence of cobalt oxide in the promoted catalyst also seems to have no effect on the size of the Pt particles and no separate phases of cobalt oxide are evident in the transmission electron micrographs (Figs. 3-4, 3-5 and 3-6). This suggests that CoO_x is highly dispersed in the catalyst. The EDX analysis performed on the area occupied by Pt particles shows the presence of Co also. This observation suggests that CoO_x is associated with only Pt particles as expected from the preparation conditions. A shift in the reduction temperature for Pt particles in the TPR profile in the case of Co-promoted Pt catalyst reflected strong Co–Pt interactions resulting from the close physical proximity of the two metals.

As the λ_5 gas mixture was passed over the reduced catalyst surface, CO conversion and the temperature of the (1:2)CoPt(low) catalyst was found to rise quite sharply. At the start of the test, it is observed that over 50% CO (0.25 vol% CO) has already been oxidized, whilst a slightly smaller amount of oxygen was found to have been consumed (Fig. 5-7). CO oxidation rises with the rise in temperature and complete CO conversion (0.50 vol% CO) was observed at ~80 °C.

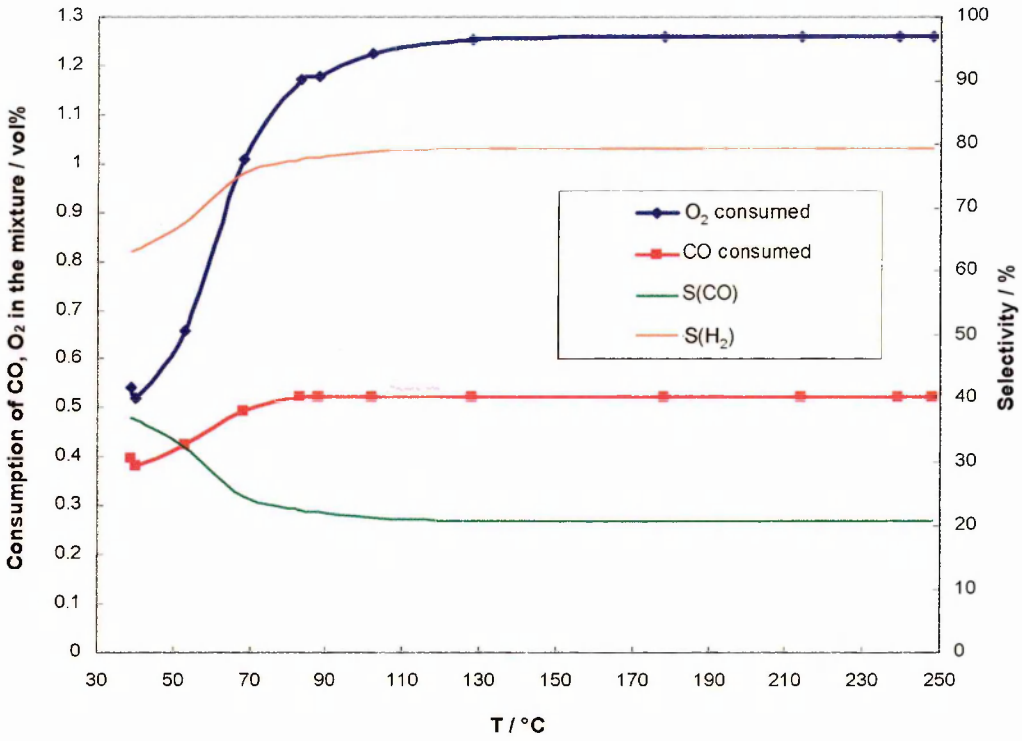

FIGURE 5-7: The consumption profiles of CO and O_2 on (1:2)CoPt/Al_2O_3(low) catalyst in λ_5 gas mixture

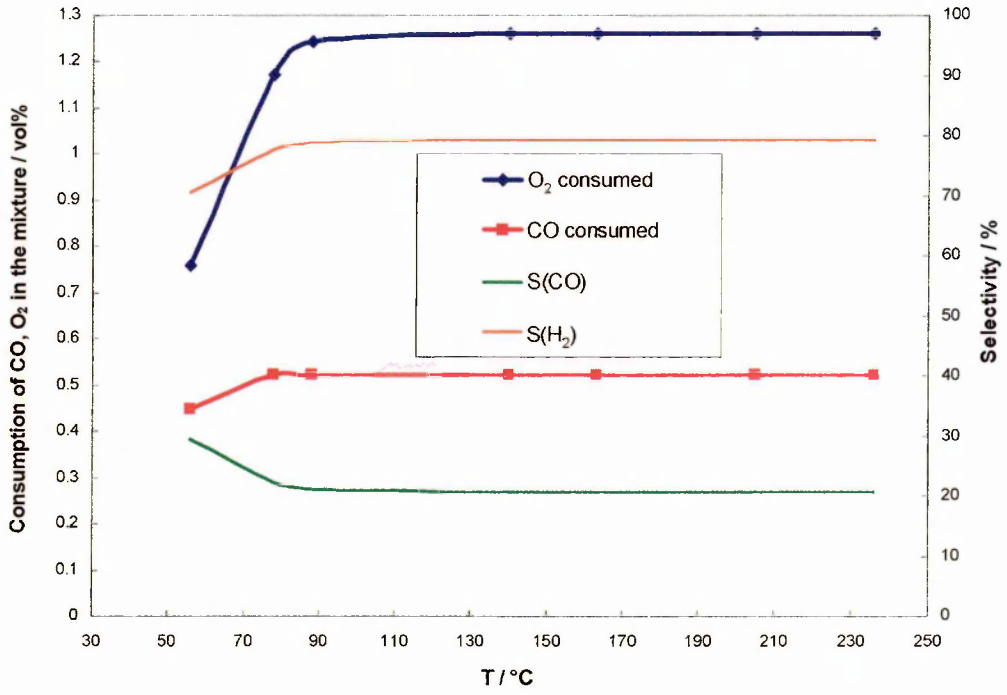

FIGURE 5-8: The consumption profiles of CO and O_2 on (1:1)CoPt/Al_2O_3(low) catalyst in λ_5 gas mixture

A very similar trend was observed with the (1:1)CoPt(low) catalyst (Fig. 5-8). Just over 80 % of CO (>0.40 vol% CO) was oxidized at the beginning of the test. The rise in temperature resulted in the increased CO conversion. Complete oxidation of CO was again observed at ~80 °C.

To examine the effect of time on the activity of the Co-promoted catalysts, it was decided to perform time-dependent studies on the CoPt(low) catalysts. Catalysts can be aged in an artificial way by high temperature treatments and/or exposures to strongly oxidising or reducing gas mixtures [20,21]. In the time-dependent studies conducted, the catalyst under examination was aged under the λ_5 gas mixture for a few hours until no more decrease in CO conversion was observed, before the temperature was raised. It was expected that the high initial activity of the Co-promoted catalysts could be affected as a result of being on-stream for a few hours under the flowing gas mixture after reduction at 40 °C for 40 minutes.

The typical consumption profiles of CO and O_2 for the (1:1)CoPt(low) catalyst, when monitored after pre-reduction and allowed to cool under the λ_5 gas mixture, as a function of time are shown in Fig. 5-9. The high CO conversion, observed at the beginning of the experiment, started to decrease when the catalyst was allowed to cool under the gas mixture. Over 95% CO conversion was observed immediately at the beginning of the test and again indicated the high activity of the (1:1)CoPt(low) catalyst. The CO conversion decreased with time and within the first two hours, the CO conversion dropped to 40% (0.20 vol% CO) and remained constant for the next few hours. During this time the temperature decreased from 54 °C recorded initially, to ~25-30 °C. After allowing the catalyst to cool down for 3.5 hours, the CO and O_2 consumption profile were monitored on heating the catalyst up to 250 °C (Fig. 5-10).

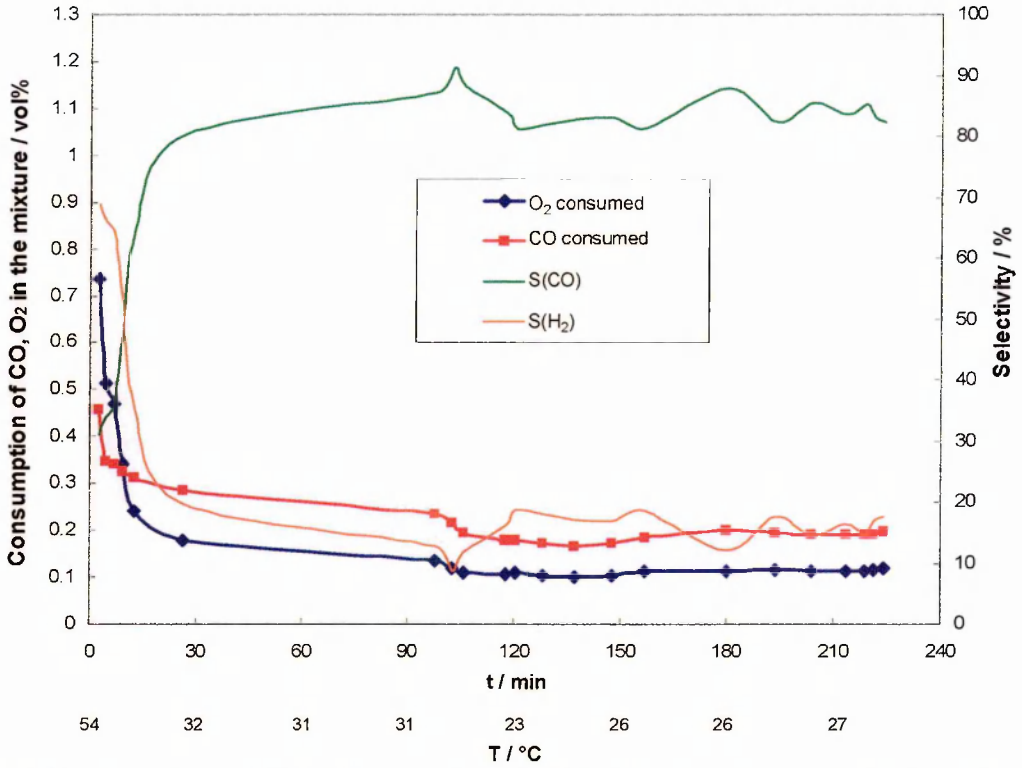

FIGURE 5-9: A typical plot for the time-dependent study performed on (1:1)CoPt/Al_2O_3(low) catalyst in λ_5 gas mixture

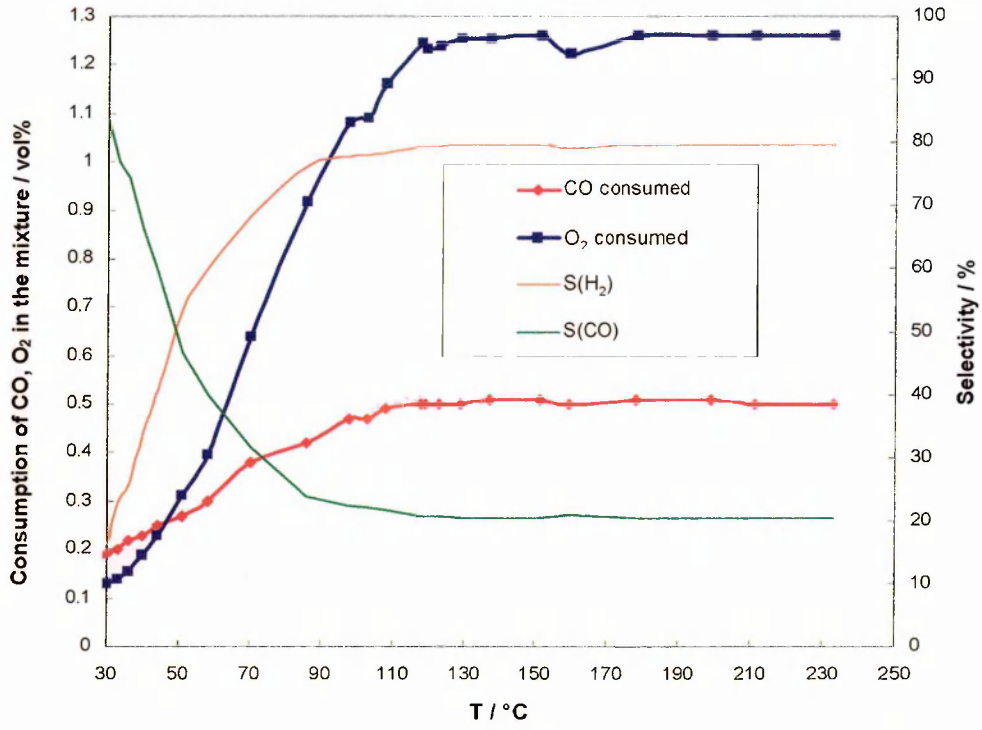

FIGURE 5-10: The consumption profiles of CO and O_2 for CO oxidation on (1:1)CoPt(low) catalyst, after being allowed to stand under a λ_5 gas mixture for 3.5 hours.

The profile showed lower activity at the same temperature (<80% CO conversion (<0.40 vol% CO) at 70 °C) compared to the fresh (1:1)CoPt(low) catalyst (>90% CO conversion (>0.45 vol% CO)) seen in Fig. 5-8. Complete oxidation of CO was achieved at 118 °C compared to ~80 °C for the fresh sample.

Again, similar observations were made for the (1:2)CoPt(low) catalyst. High CO conversion at the beginning of the test, after reduction treatment at 40 °C, was observed. Slight deactivation of the catalyst was observed when it was allowed to cool under the λ_5 gas mixture at 30 °C. The CO conversion fell to ~30% (~0.15 vol% CO) within the first 2 hours and practically remained unchanged over the next 2 hours. The catalyst was then heated gradually and retested (Fig. 5-11).

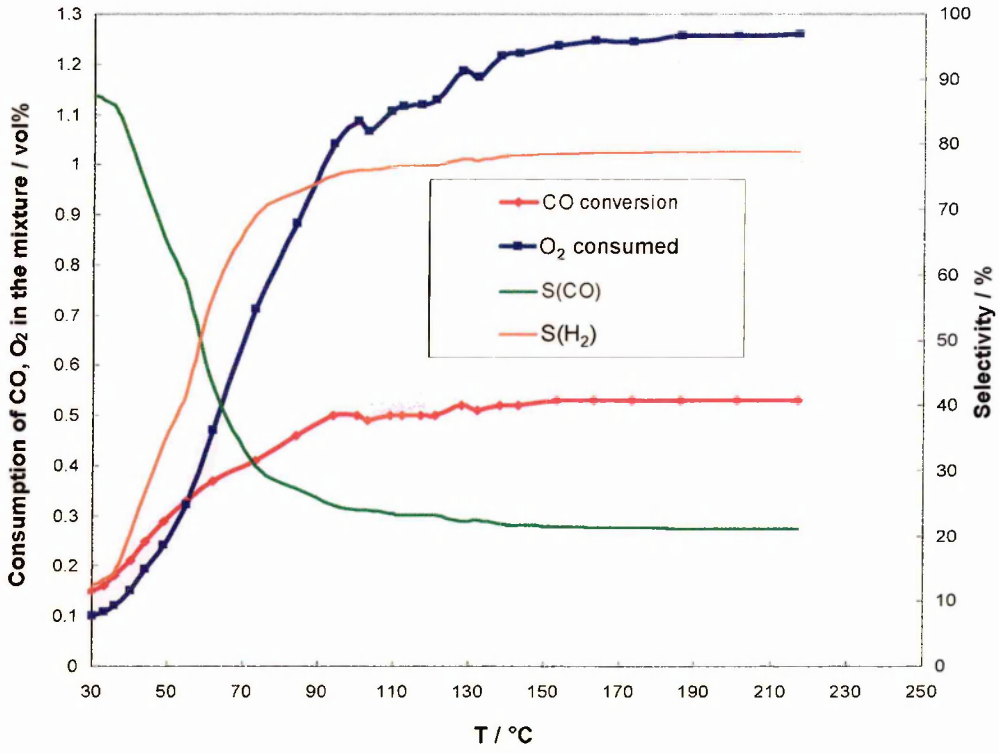

FIGURE 5-11: The consumption profiles of CO and O_2 for CO oxidation on (1:2)CoPt(low) catalyst, after being allowed to stand under a λ_5 gas mixture for about 4 hours.

The profile of the aged sample again showed lower activity compared to the fresh sample at the same temperature. For example, at 50 °C just under 60 % CO conversion (<0.30 vol% CO) was observed (Fig. 5-11) while the fresh catalyst converted ~80 % CO (~0.40 vol% CO) to CO_2 (Fig. 5-7). Complete oxidation of CO was achieved at 125 °C compared to 80 °C for the fresh sample.

During the deactivation period, a smaller consumption of oxygen than CO was observed which is reflected in higher values of CO selectivity, 85–90% for the (1:2)CoPt(low) catalyst, and 80–85% for the (1:1)CoPt(low) catalyst during this period. Table 5-4 compares the data obtained for the aged and unaged CoPt catalysts.

Table 5-4: THE ACTIVITY-SELECTIVITY DATA FOR THE AGED AND UNAGED CoPt CATALYSTS

Catalyst	*T*(50) / °C	*S*(CO)/%	*T*(100) / °C
(1:2)CoPt/Al_2O_3(low)	40*	47*	108
(1:1)CoPt/Al_2O_3(low)	64*	28*	78
(1:2)CoPt/Al_2O_3(low)-aged	44	71	125
(1:1)CoPt/Al_2O_3(low)-aged	40	66	118

* Values reported are for 75% CO conversion

From the results obtained in the time-dependent experiments, it is quite clear that Co-promoted Pt catalysts are very active towards CO oxidation with very good CO selectivity. Even after being left under the gas mixture for several hours, the CoPt catalysts continue to convert CO to CO_2. This suggests that the highly active nature of these catalysts could be due to the fact that CoO_x may supply active oxygen for the oxidation to occur at lower temperatures.

Fig. 5-12 shows the CO oxidation profile for (1:2)CoPt(high) catalyst. Starting at ~20% CO conversion (0.10 vol% CO), the catalyst seemed to be slightly sluggish as

compared to the low–dispersed analogue. With the rise in temperature, the CO oxidation also increased with almost complete conversion of CO to CO_2 by 160 °C. When (1:1)CoPt(high) catalyst was tested under similar conditions, it gave very similar results (Fig. 5-13). Complete CO oxidation occurs at ~130°C.

The high–dispersed catalysts were found to be less active compared to their low–dispersed analogues. However, the CO selectivity in both the low- and high–dispersed systems, was found to be comparable. The increased amount of Co in both the (1:1)CoPt (low and high) catalysts appears to be responsible for bringing the temperature of complete CO conversion down considerably.

Table 5-5 summarises *T*(100), *T*(50) and the corresponding values of the selectivity towards CO for the fresh Co-promoted Pt catalysts studied in this work.

Table 5-5: THE ACTIVITY-SELECTIVITY FOR THE CoPt CATALYSTS

Catalyst	CO/M	*T*(50) / °C	*S*(CO)/%	*T*(100) / °C
5% Pt(low)	0.29	172	45	205
(1:2)CoPt/Al_2O_3(low)	0.19	40*	47*	108
(1:1)CoPt/Al_2O_3(low)	0.16	64*	28*	78
5% Pt(high)	0.51	166	41	197
(1:2)CoPt/Al_2O_3(high)	0.26	98	77	154
(1:1)CoPt/Al_2O_3(high)	0.23	63	79	104

* Values reported for ~75% CO conversion

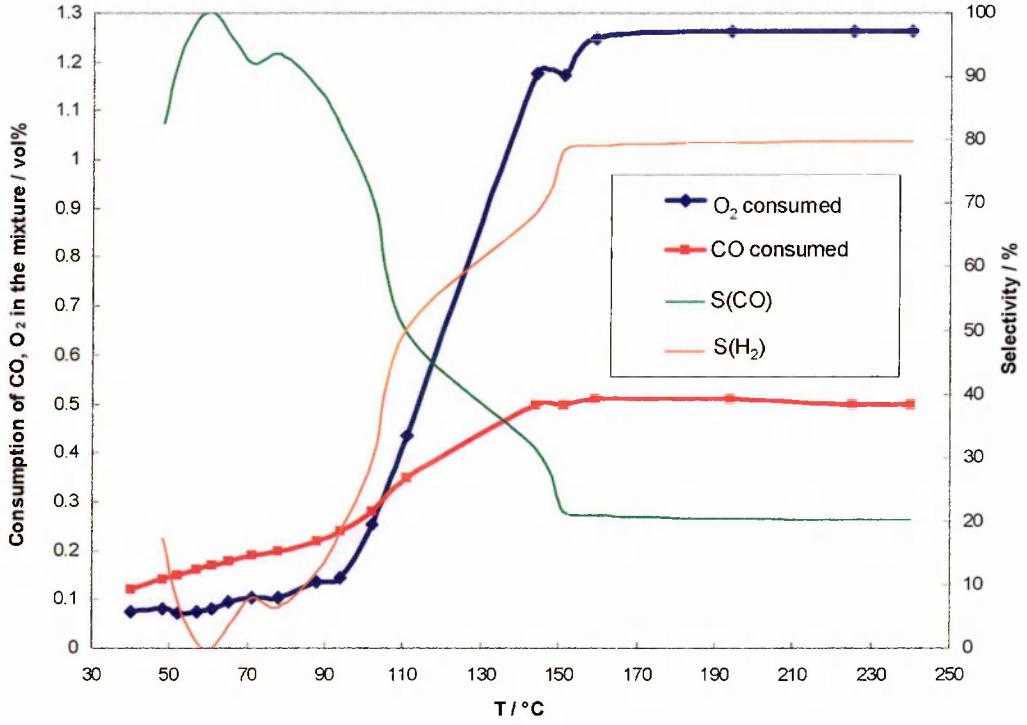

FIGURE 5-12: The consumption profiles of CO and O_2 on (1:2)CoPt/Al_2O_3(high) catalyst in λ_5 gas mixture

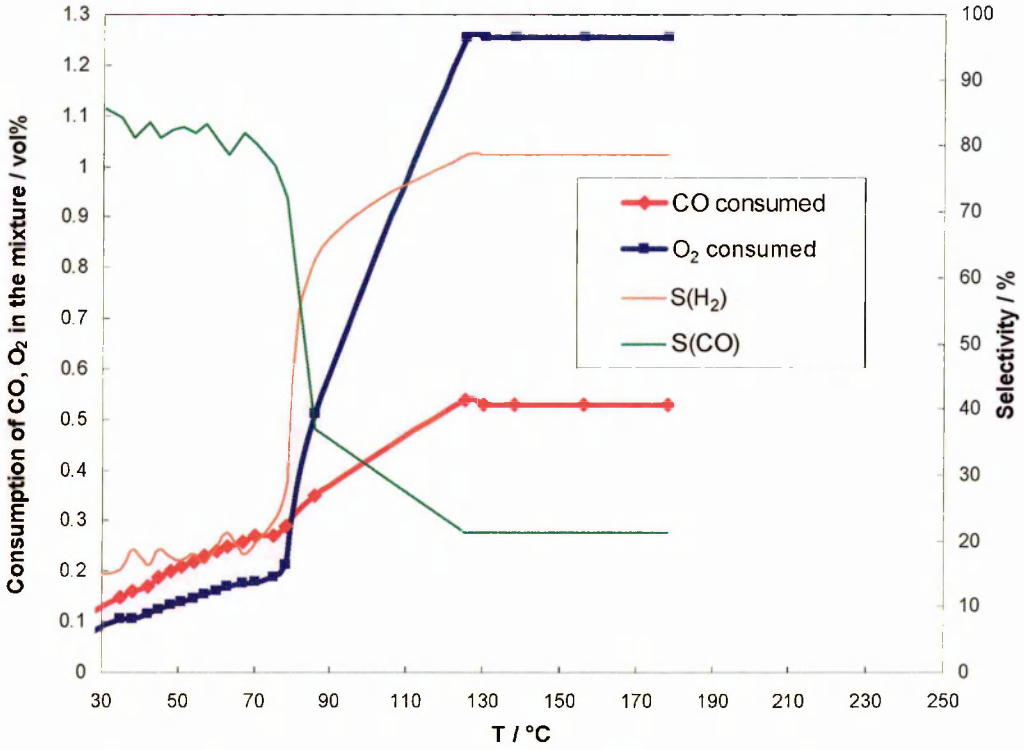

FIGURE 5-13: The consumption profiles of CO and O_2 on (1:1)CoPt/Al_2O_3(high) catalyst in λ_5 gas mixture

From the results given in Table 5-5, all the Co-promoted catalysts also seem to have increased activity towards CO oxidation. In particular, the performance of the low–dispersed catalysts is found to be of immense interest from the point of view of their activity towards CO oxidation in the preferred temperature range in respect of use in commercial applications such as zero-emission vehicles.

PROPOSED MECHANISM

Under dry conditions, cobalt oxide has been shown to be active for CO oxidation below 220 K [22]. The catalytic activity of cobalt oxide combined with noble metals has also been extensively studied [23]. Most of these studies were made by traditional CO oxidation activity measurements [24].

On the basis of the literature, the CO oxidation by Co-Pt catalysts can be visualised as follows:

CO is adsorbed on platinum (S_{Pt}) through its C atom, and O_2 is adsorbed on the cobalt sites (S_{CoO_x}) by a dissociative mechanism. The reaction between the adsorbed CO and the adsorbed O takes place either at the interface between Pt and CoO_x or by the oxygen-spillover to the Pt sites. The sequences of elementary steps in the proposed mechanism are same as that shown for Sn in equations 4, 5 and 6 except that M = Co.

It has been proposed that dissociated oxygen formed at O-vacancies on cobalt oxide is involved in the oxidation of carbon monoxide [25]. Pre-reduction is believed to be important for the low temperature CO oxidation activity. After pre-reduction treatment, the whole of the catalyst surface is reduced and when the λ_5 gas mixture (containing excess oxygen compared to CO) is let in, oxygen is taken up by the reduced cobalt species. This can be explained in terms of the creation of O-vacancies in the CoO_x. Even at room temperature, these O-vacancies appear to be suitable locations for the activation of oxygen i.e. for the dissociation of O_2. The CO

does not block the surface for O_2 adsorption on cobalt oxide as it does on platinum. Since O_2 activation takes place closer to the CO adsorption site i.e. Pt on the surface, higher CO oxidation rates are obvious as observed in our studies.

5.1.4 Fe-PROMOTED Pt CATALYSTS

From the transmission electron micrographs (Fig. 3-3), it was found that the presence of FeO_x in the promoted catalyst has no effect on the size of the Pt particles. There is also no evidence for the presence of a separate phase of FeO_x in the transmission electron micrographs. This indicates that FeO_x is highly dispersed in the catalyst. The EDX analysis performed on the area occupied by the Pt particles shows the presence of Fe, whereas the examination of areas where no Pt particles are located also shows no Fe. This observation suggests that FeO_x is associated only with Pt particles as expected from the preparation conditions. Also, the shift in the reduction temperature for Pt particles in TPR spectrum for the Fe-promoted Pt catalyst reflects strong Fe-Pt interactions. These Fe-Pt interactions once again support the proximity of FeO_x and Pt particles in Fe-Pt/Al_2O_3 catalyst.

When the λ_5 gas mixture (excess oxygen) was introduced over the (1:2)FePt(low) catalyst after pre-reduction at 40 °C (Fig. 5-14), the catalyst was found to be very active. At the start of the test, 50% CO conversion (0.25 vol% CO) was observed at 40 °C. The entire CO was found to be oxidized by 100 °C with total consumption of oxygen in the mixture by the same temperature. The (1:1)FePt(low) catalyst shows a very similar CO oxidation profile (Fig. 5-15). At the start of the test, almost 60% CO (0.30 vol% CO) was converted to CO_2. Complete CO consumption was observed by 92 °C.

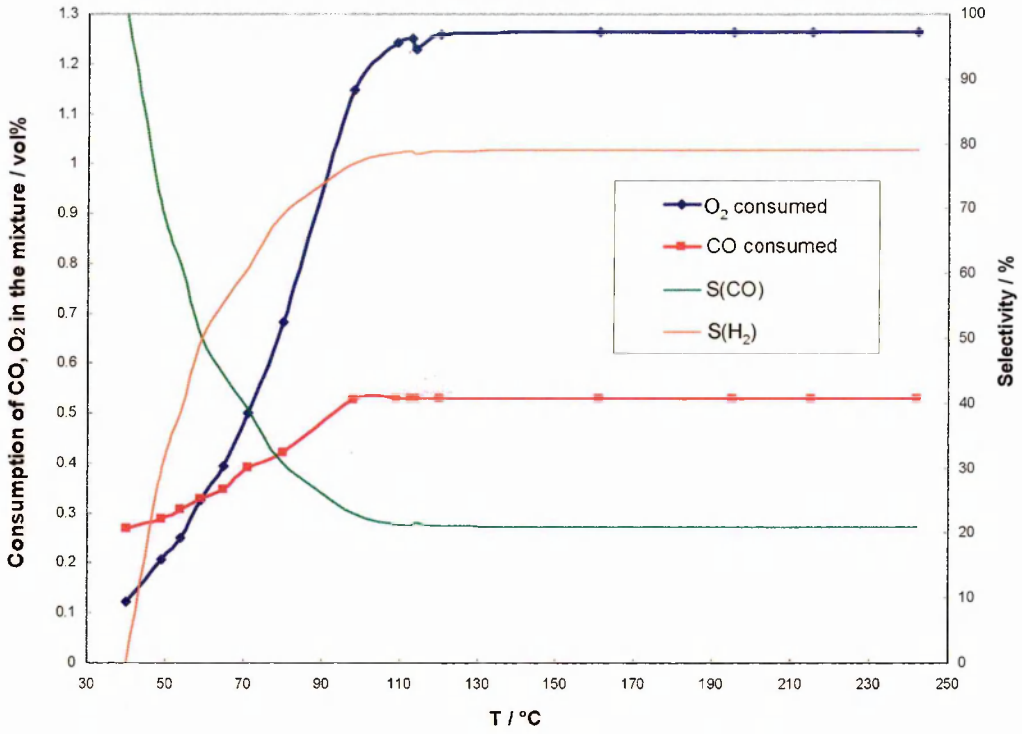

FIGURE 5-14: The consumption profiles of CO and O_2 on (1:2)FePt/Al_2O_3(low) catalyst in λ_5 gas mixture

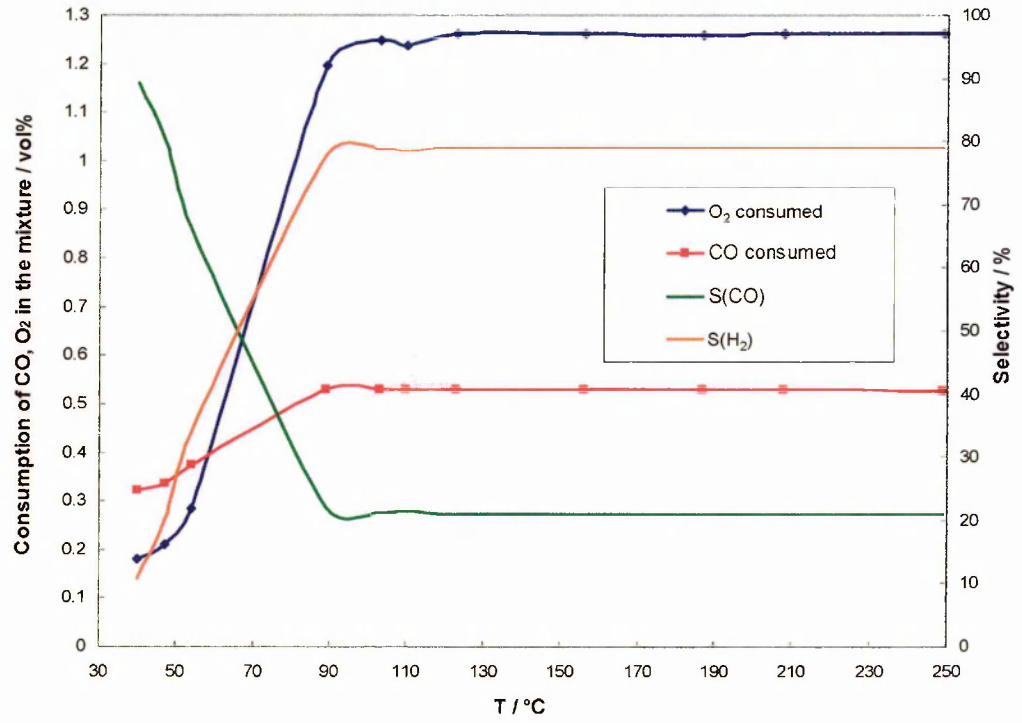

FIGURE 5-15: The consumption profiles of CO and O_2 on (1:1)FePt/Al_2O_3(low) catalyst in λ_5 gas mixture

The high CO conversion at the beginning of the test observed for the (1:2) and (1:1)FePt(low) catalysts occurs at exceptionally high values of CO selectivity. The selectivity decreases sharply as the remaining CO in the mixture is converted to CO_2 and attains a stoichiometric value of 20% after the complete CO oxidation is achieved.

Once again in order to probe the high initial activity of the Fe-promoted catalysts, time-dependent studies were performed on the FePt(low) catalysts. Similar results to those of the Co-promoted catalysts were obtained. Both (1:2) and (1:1)FePt(low) catalysts examined in the present study showed slight deactivation during the first hour from the time the catalysts were put on-stream. Further deactivation was slow, staying unchanged for a further period of 3 hours. A similar observation has been reported for Pt supported on various supports used as a CO oxidation catalyst in the absence of hydrogen, under similar reaction conditions [26,27,28,29]. After the decrease in CO conversion became very slow, the CO oxidation profile of the catalyst was recorded by raising the temperature gradually.

Even after leaving the reduced catalysts under the λ_5 gas mixture for about 4 hours, they maintained CO conversion levels of <20% (0.10 vol% CO) and ~30% (~0.15 vol% CO) over (1:2) and (1:1)FePt(low) catalysts respectively, while consuming slightly less oxygen. As a result of lower oxygen consumption, the selectivity towards CO for (1:2) and (1:1)FePt(low) catalysts were found to be high. These results are in good agreement with the results on the unaged samples (Fig. 5-14 and 5-15).

Table 5-6: THE ACTIVITY-SELECTIVITY DATA FOR THE AGED AND UNAGED FePt CATALYSTS

Catalyst	*T*(50) / °C	*S*(CO)/%	*T*(100) / °C
(1:2)FePt/Al_2O_3(low)	40	100	100
(1:1)FePt/Al_2O_3(low)	40*	89*	92
(1:2)FePt/Al_2O_3(low)-aged	44	81	122
(1:1)FePt/Al_2O_3(low)-aged	56	68	85

* Values reported are for 60% CO conversion

The (1:2)FePt(high) catalyst showed low activity at the beginning of the test and its CO oxidation profile (Fig. 5-16) is similar to that of the monometallic Pt/Al_2O_3 catalyst. However, with a rise in temperature, the activity of the catalyst is found to have improved. 50% CO conversion (0.25 vol% CO) has been achieved by 97 °C. Complete CO conversion was observed by 143 °C. The CO oxidation profile for the (1:1)FePt(high) catalyst, shown in Fig. 5-17, is very similar to that of the (1:2)FePt(high) catalyst. Gradual CO oxidation was observed with simultaneous oxygen consumption. The 50% CO conversion (0.25 vol% CO) was observed at 90 °C. From the oxygen consumption profile, it was confirmed that the entire CO (0.50 vol% CO) was oxidized by 188 °C. With high CO coverage, practically no hydrogen oxidation takes place over FePt(high) catalysts. As a result, selectivity values were as high as ~80% for (1:2) and ~60% for (1:1)FePt(high) catalyst. Again, the FePt(high) catalysts showed lower activity, as they converted lesser amounts of CO in the mixture to CO_2 at the temperatures below 90 °C when compared to the low–dispersed analogues.

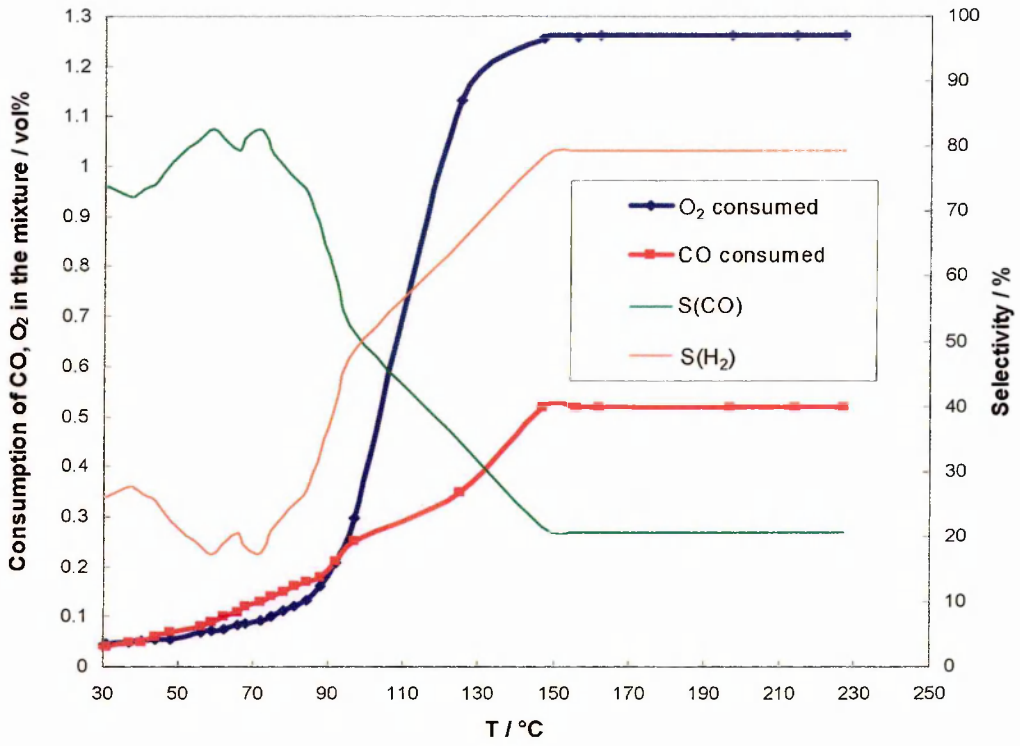

FIGURE 5-16: The consumption profiles of CO and O_2 on (1:2)FePt/Al_2O_3(high) catalyst in λ_5 gas mixture

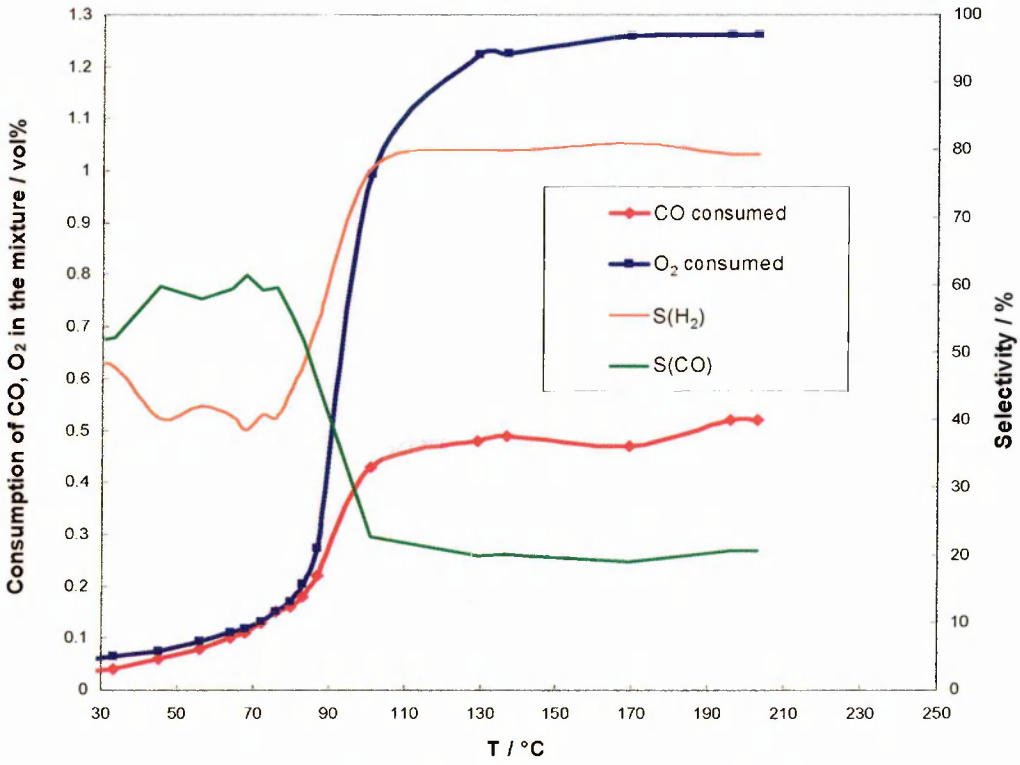

FIGURE 5-17: The consumption profiles of CO and O_2 on (1:1)FePt/Al_2O_3(high) catalyst in λ_5 gas mixture

The $T(100)$, $T(50)$ and the selectivity towards CO values for all Fe-promoted Pt catalysts are given in Table 5-7.

Table 5-7: THE ACTIVITY-SELECTIVITY OF THE FePt CATALYSTS

Catalyst	CO/M	$T(50)$ / °C	$S(CO)$/%	$T(100)$ / °C
5% Pt(low)	0.29	172	45	205
(1:2)FePt/Al_2O_3(low)	0.16	40	100	100
(1:1)FePt/Al_2O_3(low)	0.14	40*	89*	92
5% Pt(high)	0.51	166	41	197
(1:2)FePt/Al_2O_3(high)	0.24	97	47	133
(1:1)FePt/Al_2O_3(high)	0.22	90	37	188

* Values reported are for 60% CO conversion

From the results described in Table 5-7, it is evident that all the Fe-promoted catalysts have significantly increased CO oxidation activity. This increased activity of the Fe–Pt catalysts suggests the presence of a different mechanism where the FeO_x provides active oxygen to the neighbouring CO for the oxidation to occur (equations 4, 5 and 6 where M = Fe).

Iron is expected to be present in the Fe–Pt catalyst as Fe^{n+} (n = 2, 3) but not as Fe^0. Similar observations were reported by Liu and co-workers during their study on Fe promotion of Pt/Al_2O_3 catalysts [6]. CO is not expected to be adsorbed or may be very weakly adsorbed on iron as compared to Pt. Oxygen in the gas stream oxidises Fe to FeO_x. It is this FeO_x that is thought to provide the active oxygen for CO oxidation at temperatures as low as 40 °C. The suggestion by Mergler *et. al.* [25] about the creation of O-vacancies on the Co-promoted catalysts could also be extended to Fe-promoted

catalysts, according to which FeO_x would act as a site for the activation of the O_2. The oxygen in the gas mixture replenishes the active oxygen on FeO_x sites once it gets reduced after each cycle, thereby making Fe-promoted Pt/Al_2O_3 catalysts highly active towards CO oxidation. In contrast, under similar conditions, no formation of CO_2 is observed over the unpromoted Pt catalyst. FeO_x taking up oxygen from the gas phase and the CO desorption from the Pt surface together contributes towards the CO oxidation. From these results it is postulated that FeO_x acts as an active oxygen provider. It creates a non-competitive site for oxygen such that it no longer must compete with CO for the Pt sites. As a result, a more active catalyst is generated due to the presence of Fe on Pt as compared to the Pt-only catalyst.

The performance of the low–dispersed catalysts is very interesting from the fact that the temperature of complete CO conversion has been brought down to the temperature range which is highly preferred for the commercial applications, while maintaining the high value of CO selectivity.

5.2 STUDIES ON HEAT-TREATED CATALYSTS

The inherent high activity of the bimetallic catalysts has been reported by various workers [30]. Some of the bimetallic catalysts, specially Fe- and Co-promoted catalysts, prepared in the present study using the SOMC route were so active that the temperature of the catalyst bed increased by ~50–60 °C at the beginning of the experiment. To understand how such an abrupt temperature-rise could affect the behaviour of the catalysts, we planned to perform heat-treated experiments on some of these catalysts.

From the studies made in this work, it was observed that the low–dispersed catalysts performed better than the high–dispersed ones in almost all the cases. In view of these considerations, we decided to perform heat-treatment on the low–dispersed catalysts only. In these experiments, the catalyst being studied was reduced for 40 minutes in a CO/H_2 mixture at 40 °C, and then heated to 200 °C under the λ_5 gas mixture. The catalyst was then allowed to cool down to room temperature or until the CO conversion dropped to almost zero. Thereafter, the oxidation of CO was studied by monitoring CO conversion as a function of the temperature. This treatment was carried out so that all the catalysts were treated thermally in exactly the same manner and gave a common basis to discuss the oxidation results. It is felt that these studies should be able to give better comparison of the selectivity of the catalysts towards CO.

Fig. 5-18 shows a typical heat-treatment experiment, plotting CO oxidation and O_2 consumption together with the selectivity profiles for the (1:1)SnPt(low) catalyst. For convenience, the results from heat-treatment experiments will be shown as the consumption of CO and O_2 as a function of temperature; this is after the catalysts had been heated to 200 °C and allowed to cool down to room temperature under the reaction gas mixture for about 1 hour, or until CO conversion fell to zero.

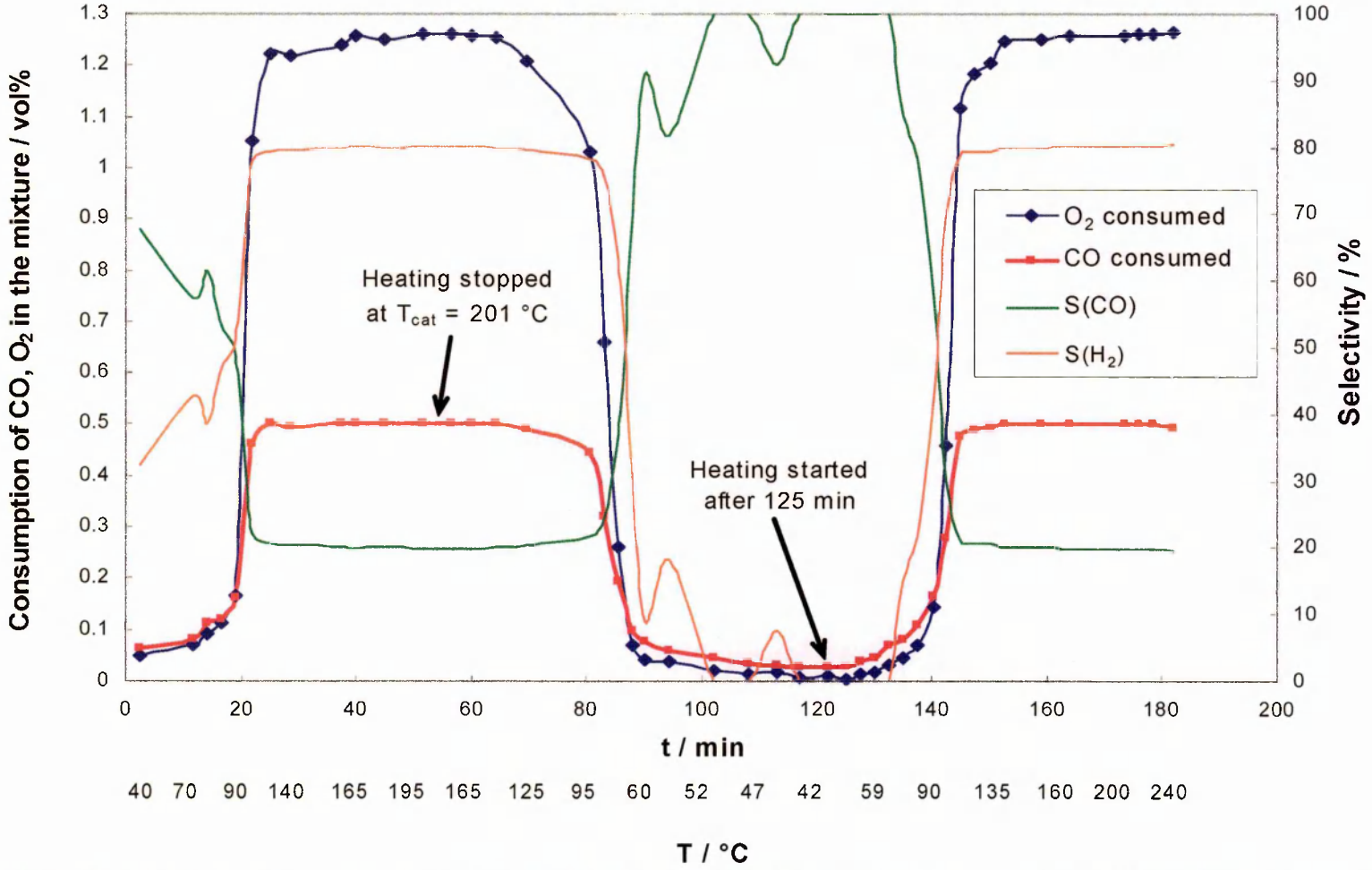

FIGURE 5-18: The CO oxidation studies on the heat-treated (1:1)SnPt/Al_2O_3(low) catalyst in λ_5 gas mixture. During heat treatment, the catalyst was preheated to 200 °C and then cooled to room temperature before studying the CO oxidation.

5.2.1 HEAT-TREATMENT STUDIES OF THE Pt CATALYST

The activity of the unpromoted Pt/Al_2O_3(low) catalyst remained unaffected even after heating the catalyst to 200 °C, allowing the conversion to fall to nearly zero and performing the test. The activity profile for CO oxidation on the heat-treated catalyst looked like that of a fresh catalyst at lower temperature up to ~100 °C (Fig. 5-19). With a slow rise in temperature, a gradual increase in the CO conversion was observed up to 110–120 °C reaching 50% (0.25 vol% CO) at ~170 °C, and almost 100% (0.50 vol% CO) at 205 °C. The performance of the heat-treated catalyst remained unaffected compared to the untreated catalyst (Fig. 5-1).

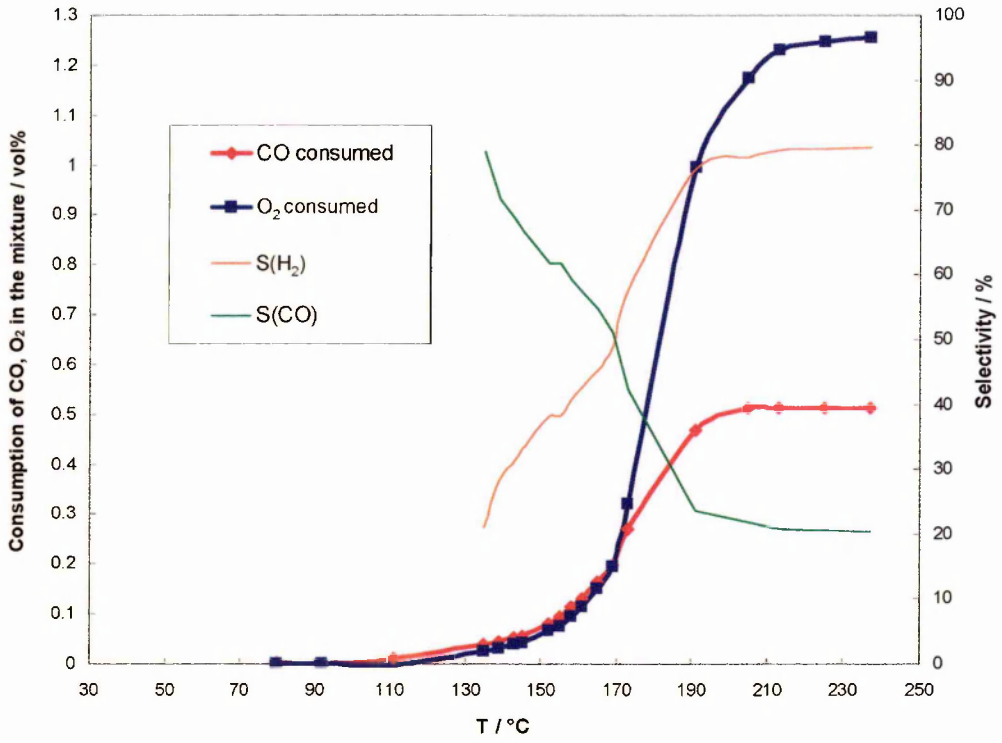

FIGURE 5-19: The CO oxidation studies on the heat–treated 5%Pt/Al_2O_3(low) in λ_5 gas mixture

The selectivity values of the untreated and heat-treated Pt catalysts are given in Table 5-8.

Table 5-8: THE ACTIVITY-SELECTIVITY DATA FOR THE ALUMINA SUPPORTED Pt(LOW) CATALYSTS

Catalyst	T(25) / °C	T(50) / °C	S(CO)%	T_{max} / °C
5%Pt	160	172	45	203
5%Pt(heat treated)	161	160	45	205

5.2.2 HEAT-TREATMENT STUDIES OF FePt CATALYSTS

The CO oxidation profile for the heat-treated (1:2) and (1:1)FePt(low) catalysts are shown in Figs. 5-20 and 5-21 respectively. These can be compared with the untreated samples (Figs. 5-14 and 5-15). During the cooling down period, from 200 °C to room temperature, the CO conversion over the (1:2)FePt(low) decreased by 25% (0.13 vol% CO) within two hours. Thereafter, it decreased very slowly over the next 2 hours. After leaving the catalyst to cool down to room temperature, it retained its high activity (~60% (~0.30 vol% CO) CO conversion) even at temperatures below 30 °C. When tested in the normal way, the heat-treated catalyst quickly converted the whole of the CO in the mixture to CO_2 at just over 100 °C. The higher CO conversion and smaller oxygen consumption are reflected in the higher (about 80%) value for the CO selectivity for the heat-treated (1:2)FePt(low) catalyst (Fig. 5-20). Quick CO conversion led to a sharp decrease in the CO selectivity values with the rise in temperature. Heating the (1:1)FePt(low) catalyst and then allowing it to cool down for nearly three hours did not seem to affect its activity significantly: at 30 °C, the CO conversion stood at about 40% (~0.20%). For the heat-treated (1:1)FePt(low) catalyst the CO selectivity values were slightly lower than for the (1:2)FePt(low) catalyst (Fig. 5-21): starting at 50% at

the beginning of the test it decreased quickly to the stoichiometric value of 20% as soon as the whole of CO was oxidised.

Table 5-9 summarises the results for the treated and untreated Fe-promoted Pt catalysts.

Table 5-9: THE ACTIVITY-SELECTIVITY AND RELATED PARAMETERS FOR THE UNTREATED AND HEAT-TREATED FePt(LOW) CATALYSTS

Catalyst	T(50) / °C	S(CO)/%	T_{max} / °C
(1:2)FePt/Al_2O_3(low)	40	100	100
(1:1)FePt/Al_2O_3(low)	40*	89*	92
(1:2)FePt/Al_2O_3(low)#	30	81	111
(1:1)FePt/Al_2O_3(low)#	47	47	125

* Values reported are for 60% CO conversion

Heat-treated sample

The small shift towards slightly higher values of T_{max} in the heat-treated FePt(low) catalysts compared to untreated catalysts could be attributed to a change in the number or nature of active sites as a result of heat-treatment at 200 °C. In addition a large decrease in CO selectivity was observed for the (1:1)FePt(low) catalyst after heat treatment.

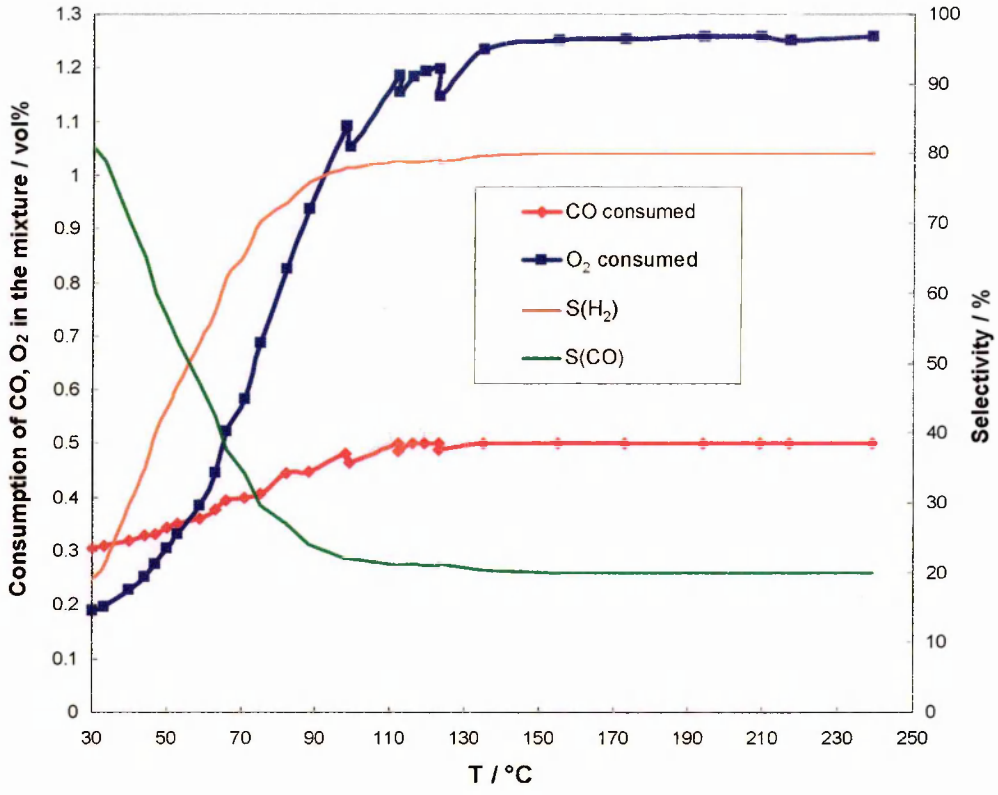

FIGURE 5-20: The CO oxidation studies on the heat-treated (1:2)FePt/Al_2O_3(low) in λ_5 gas mixture

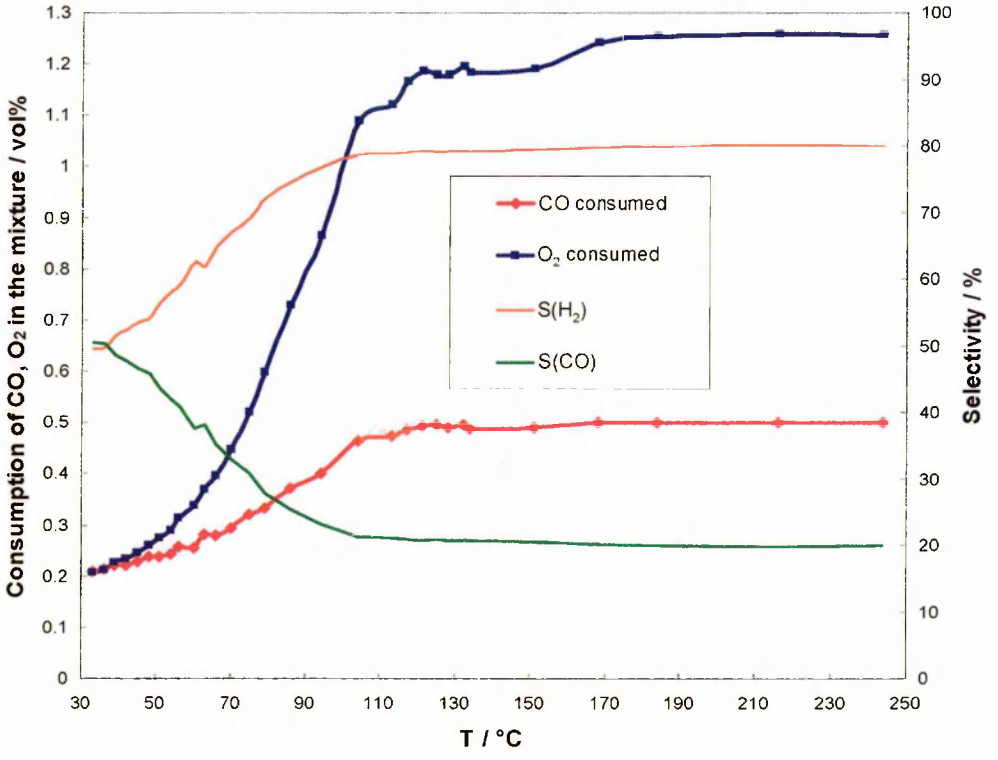

FIGURE 5-21: The CO oxidation studies on the heat-treated (1:1)FePt/Al_2O_3(low) in λ_5 gas mixture

5.2.3 HEAT-TREATMENT STUDIES OF CoPt CATALYSTS

The CO oxidation profiles for the heat-treated (1:2) and (1:1)CoPt(low) catalysts are shown in Figs. 5-22 and 5-23, respectively. The CO oxidation profiles are qualitatively similar to that obtained for the catalysts that were not given any heat-treatment prior to the test (Figs. 5-7 and 5-8). The heat-treated (1:2)CoPt(low) catalyst was found to be quite active even at 25 °C, converting over 60% (>0.30 vol% CO) of CO in the mixture to CO_2. From Fig. 5-22, it is evident that the oxygen consumption was slightly less as compared to the CO conversion, and as a result, the maximum observed value of the CO selectivity of ~80% was observed at 40 °C for the heat-treated (1:2)CoPt(low) catalyst. With gradual rise in temperature the catalyst oxidised the remaining CO in the mixture to CO_2 achieving complete conversion by ~130 °C. The heat-treated (1:1)CoPt(low) catalyst was found to be similarly active (Fig. 5-23), showing about 60% CO conversion (0.30 vol% CO) at 40 °C. An increase in temperature led to an increase in CO conversion, and complete CO oxidation was achieved by 130 °C. The (1:1)CoPt catalyst is found to be a poor performer (Fig. 5-23) in terms of selectivity. For the (1:1)CoPt(low) catalyst the selectivity values for CO oxidation are found to be quite low (less than 40%) at the beginning of the test and decreased further to the stoichiometric values of 20% at complete oxidisation by ~130 °C.

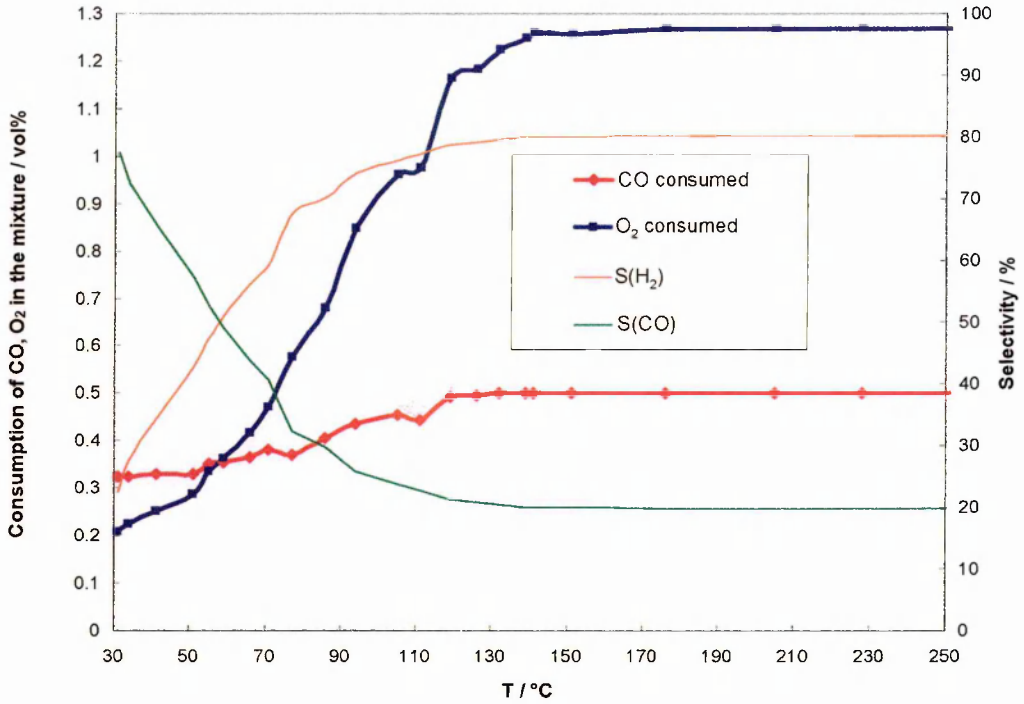

FIGURE 5-22: The CO oxidation studies on the heat-treated (1:2)CoPt/Al_2O_3(low) in λ_5 gas mixture

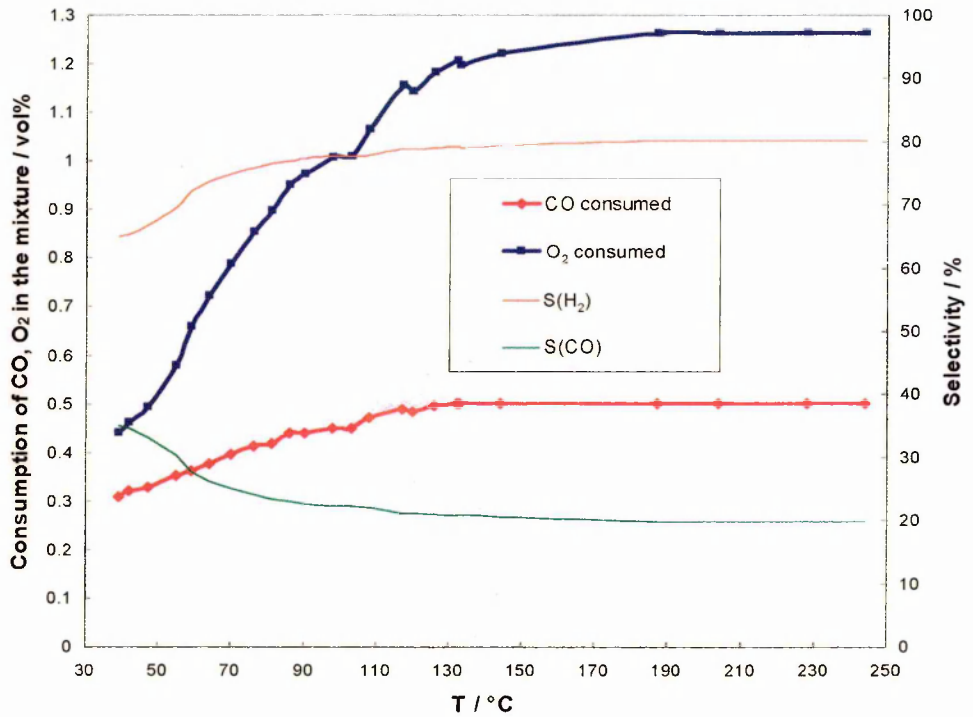

FIGURE 5-23: The CO oxidation studies on the heat-treated (1:1)CoPt/Al_2O_3(low) in λ_5 gas mixture

Table 5-10 summarises the results for the treated and untreated Co-promoted Pt catalysts.

Table 5-10: THE ACTIVITY-SELECTIVITY AND RELATED PARAMETERS FOR THE UNTREATED AND HEAT-TREATED CoPt(LOW) CATALYSTS

Catalyst	T(50) / °C	S(CO)/%	T_{max} / °C
(1:2)CoPt/Al_2O_3(low)	40*	47	108
(1:1)CoPt/Al_2O_3(low)	64*	28	78
(1:2)CoPt/Al_2O_3(low)#	63*	45	130
(1:1)CoPt/Al_2O_3(low)#	59	28	132

* Values reported for ~75% CO conversion

Heat treated samples

The slight increase in temperature for maximum conversion for the heat-treated samples could again be attributed to a change in number or nature of active sites as a result of heat-treatment at 200 °C.

The results obtained from the heat-treatment studies performed on all the low–dispersed catalysts are summarised in Table 5-11.

Table 5-11: THE ACTIVITY-SELECTIVITY DATA FROM THE HEAT-TREATED LOW–DISPERSED CATALYSTS

Catalyst	*T*(50) / °C	*S*(CO)/%	T_{max} / °C
5% Pt	172	45	205
(1:2)FePt	*T*(61) = 30	81	111
(1:1)FePt	47	47	125
(1:2)CoPt	*T*(65) = 31	22	130
(1:1)CoPt	*T*(62) = 32	35	132

From the results summarised in Table 5-11, it is clear that all these bimetallic catalysts prepared by the SOMC route are significantly more active than the Pt-only catalyst even after heat-treatment. The heat-treated bimetallic catalysts compared to the corresponding untreated catalysts, showed slightly lower activity which was highlighted by a small increase in the temperature of 100% CO conversion. However, apart from the (1:1)FePt(low) catalyst, the selectivity values were not significantly affected. It is thought that this change in performance of the catalyst could be due to the reduction in the number or nature of the active sites for the CO adsorption and that this is likely be due to sintering or poisoning/fouling of the catalyst surface. Out of all the above studied catalysts, the (1:2)FePt(low) catalyst seemed to be the most efficient.

5.3 DRY CO TESTS IN 0.50% OXYGEN (λ_2)

In order to test the selectivity of catalysts under more realistic conditions, a gas mixture with a slight excess of O_2, just above the stoichiometric amount required for oxidizing CO, was used. For the present study, a dry gas composition of 0.50% O_2, 0.50% CO, ~ 25% H_2 and balance N_2 was used. All the conditions were exactly the same as described in the previous section.

5.3.1 Pt CATALYST

The results of CO oxidation on 5%Pt/Al_2O_3(low) and 5%Pt/Al_2O_3(high) catalysts are shown in Figs. 5-24 and 5-25, respectively. Very low activity in the lower temperature region again reflected the effect of CO poisoning on both the low and high–dispersed Pt catalyst. At 40 °C, there was no activity observed for these Pt catalysts. Increasing the temperature of the catalyst slowly from 40 °C to about 140 °C, produced less than 10% conversion of CO (< 0.05 vol% CO) into CO_2. The

CO conversion reached about 10% by ~160 °C and 50% (0.25 vol% CO) by 200 °C. It is interesting to note that with equal amounts of CO and O_2 in the λ_2 mixture, the maximum CO conversion achieved by the Pt(low) catalyst was ~90% (0.45 vol% CO) at 250 °C, whereas for the high–dispersed Pt catalysts almost all the CO was converted to CO_2 by 235 °C. In contrast both the Pt low and high–dispersed catalysts converted the entire CO to CO_2 by ~200 °C and were generally more active throughout when tested under the λ_5 gas mixture.

During the experiments, it was observed that a small amount of oxygen was consumed from the beginning, while no CO was oxidized. This was not observed for tests performed with the λ_5 gas mixture. It is logical to assume therefore that this oxygen was used for the oxidation of hydrogen. This translates into a higher selectivity towards hydrogen to begin with. The CO oxidation increases with the rise in temperature and as a result the selectivity towards CO also increases gradually. Once the entire CO was converted to CO_2, the CO and H_2 selectivities attained the stoichiometric values of 50%.

Table 5-12: TABLE FOR THE ACTIVITY-SELECTIVITY OF THE ALUMINA SUPPORTED Pt CATALYSTS UNDER λ_2 GAS MIXTURE

Catalyst	CO/M	$T(50)$ / °C	$S(CO)$/%	T_{max} / °C
5% Pt(low)	0.29	$T(52)$=207	53.5	$T(92)$=239
5% Pt(high)	0.51	197	49	235

From the results presented in Table 5-12, the two Pt catalysts seemed to perform in a very similar way.

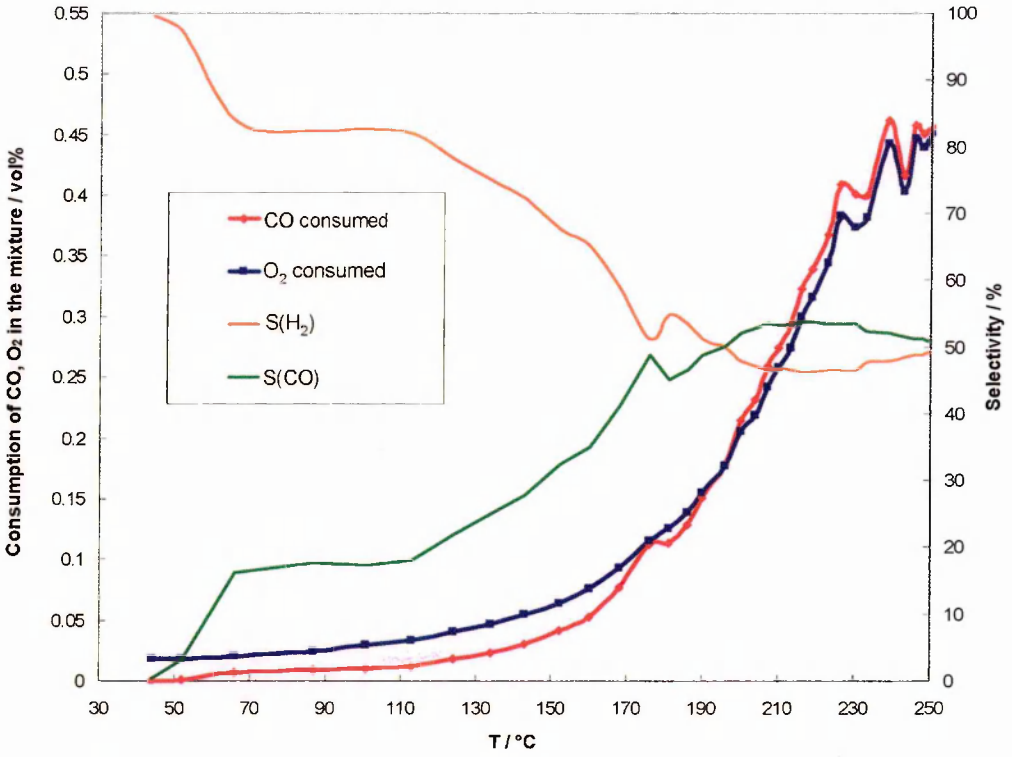

FIGURE 5-24: The consumption profiles of CO and O_2 on 5%Pt/Al_2O_3(low) catalyst in λ_2 gas mixture

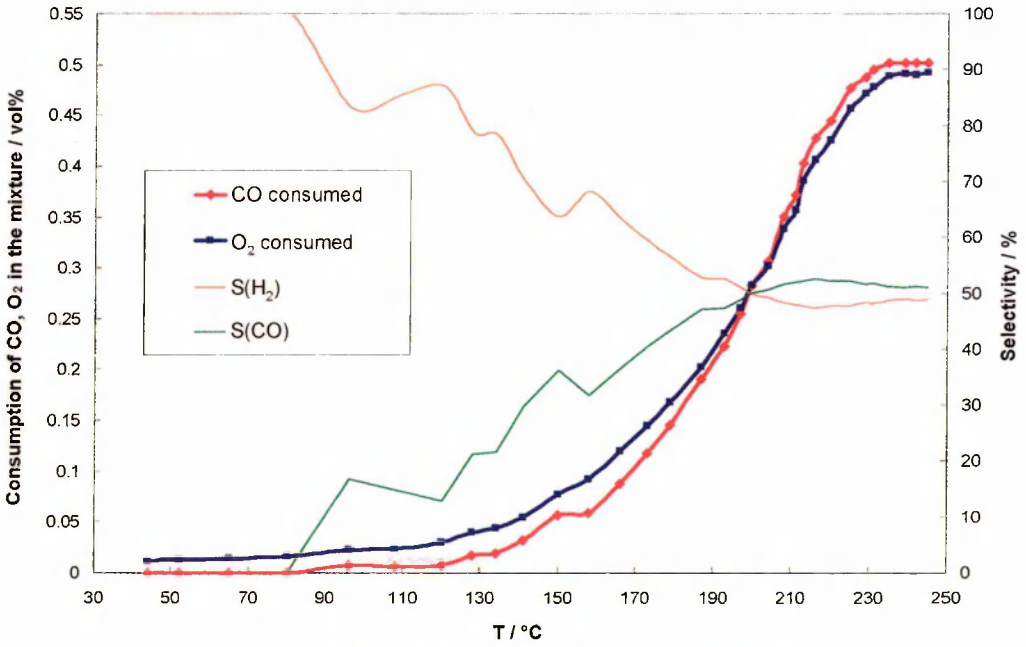

FIGURE 5-25: The consumption profiles of CO and O_2 on 5%Pt/Al_2O_3(high) catalyst in λ_2 gas mixture

5.3.2 Sn-PROMOTED Pt CATALYSTS

For the Sn-promoted catalysts the tests showed lower activity for the λ_2 tests than the λ_5 tests with equivalent CO conversion at higher temperatures. For the (1:2)SnPt(low) catalyst (Fig. 5-26), the initial CO conversion at 40 °C was found to be less than 10% (0.05 vol% CO) with a selectivity of 50% to CO, increasing gradually with increasing temperature to reach a maximum conversion of approximately 80% (0.40 vol% CO) at 180 °C with a selectivity of ~50%. As the temperature was increased further the CO conversion decreased to about 70% (0.35 vol% CO) while the O_2 consumption remained high at about 90%, reflected in a decrease in CO selectivity to ~ 40%. The results for the (1:1)SnPt(low) catalyst (Fig. 5-27) were similar with slightly higher activities at the same temperature of 50% CO conversion (0.25 vol% CO) and ~58% selectivity to CO at 107 °C compared to 134 °C for (1:2)SnPt(low) catalyst. A more marked decrease in CO conversion and selectivity was observed, however, for the (1:1)SnPt(low) catalyst with increasing temperature. Increasing the catalyst temperature further to 240 °C resulted in a decrease in the CO conversion to 70% and CO selectivity value fell slightly below 40% by the end of the test at 250 °C.

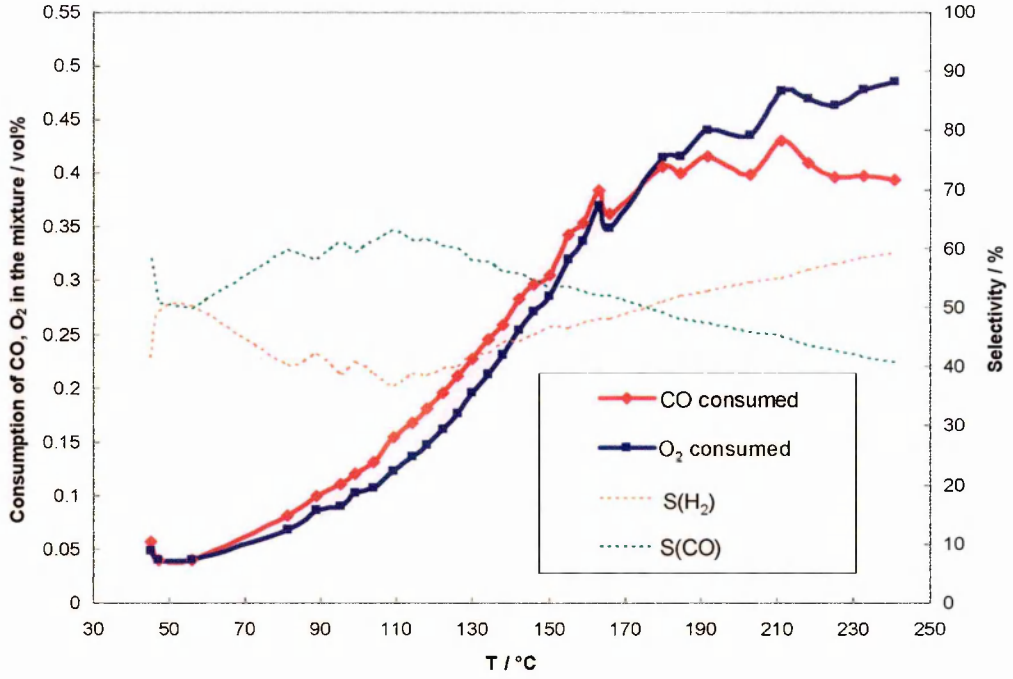

FIGURE 5-26: The consumption profiles of CO and O_2 on (1:2)SnPt/Al_2O_3(low) catalyst in λ_2 gas mixture

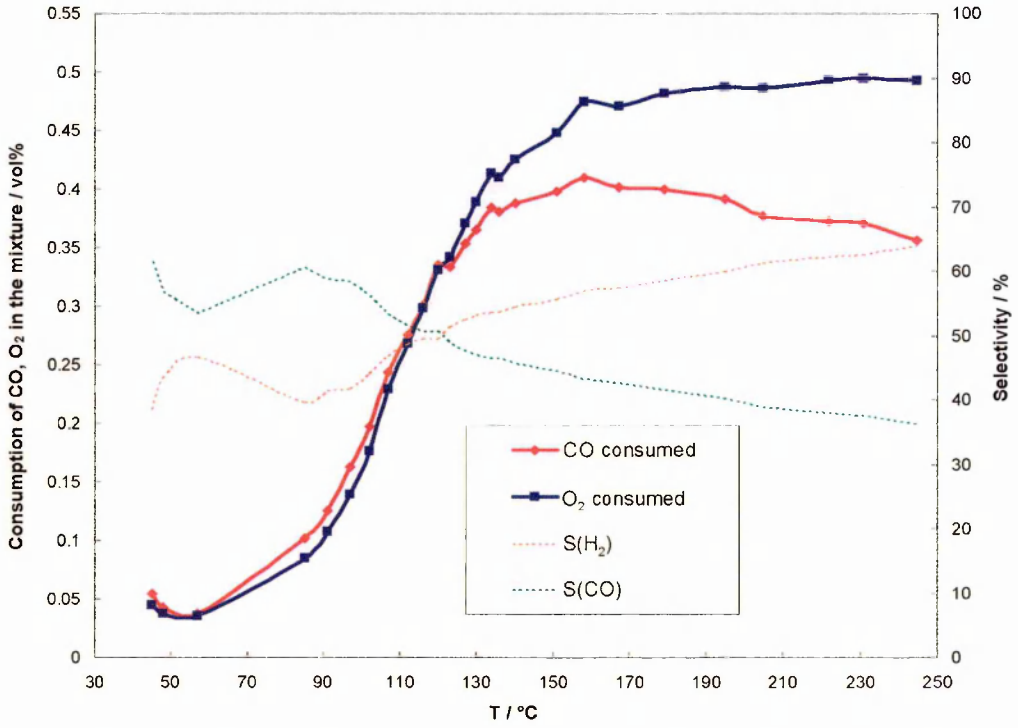

FIGURE 5-27: The consumption profiles of CO and O_2 on (1:1)SnPt/Al_2O_3(low) catalyst in λ_2 gas mixture

Similar results were observed for the high–dispersed catalysts, although activities are generally lower. About 5% CO conversion (0.025 vol% CO) was observed over the (1:2)SnPt(high) catalyst at 45 °C (Fig. 5-28) with ~45% selectivity whereas (1:1)SnPt(high) catalyst converted less than 10% (<0.05 vol% CO) by 60 °C (Fig. 5-29) with CO selectivity of 70%. With the rise in temperature, CO was oxidized with simultaneous consumption of oxygen in the reaction. Increasing the temperature to 100 °C increased the CO conversion from 10% to just less than 30% (<0.15 vol% CO) over the (1:2)SnPt(high) catalyst, with CO selectivity in the range 40–50%. At 210 °C, a maximum CO conversion of just over 70% (>0.35 vol% CO) was observed, which stayed at 70% until the catalyst reached 240 °C and started to drop thereafter, however, a gradual decrease from ~50% to ca 35% was observed in the CO selectivity towards the end of the test at 250 °C.

However, the maximum CO conversion observed over the (1:1)SnPt(high) catalyst was ~75% (0.38 vol% CO) at a temperature just below 140 °C. Thereafter the CO conversion decreased to almost 50% by the end of the test at 250 °C, while very little oxygen was left in the mixture by the end of the test. A gradual decrease in the selectivity from 70% to below 30% was observed by the end of the test at 250 °C. The decrease in selectivity was expected as CO was being desorbed from the surface and oxygen was still being consumed by the catalyst for oxidation of hydrogen.

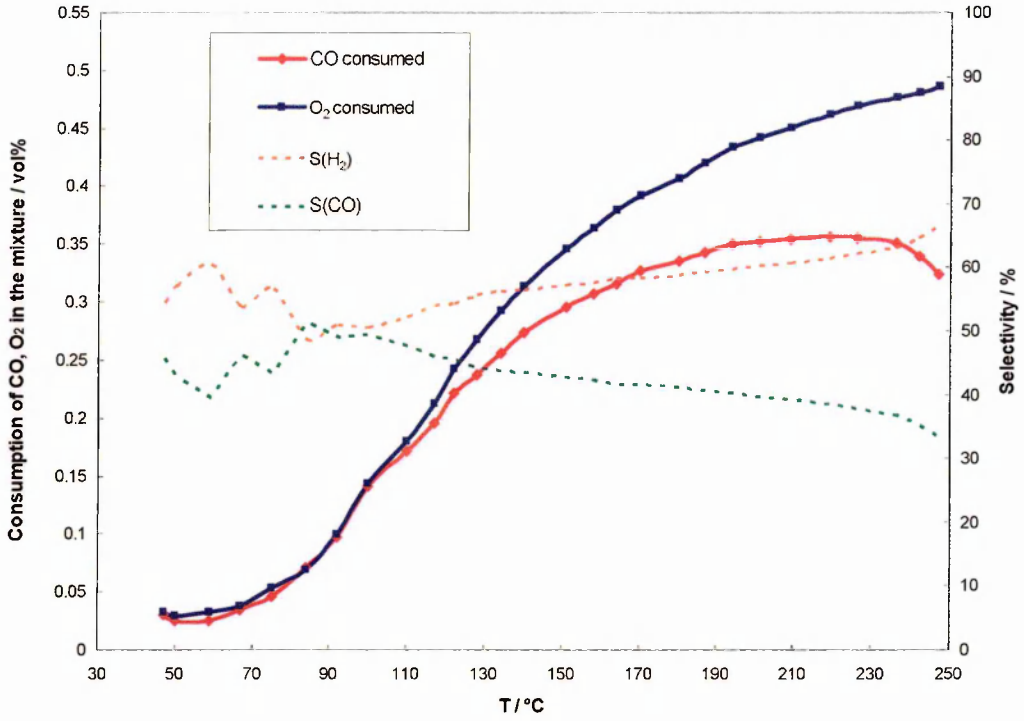

FIGURE 5-28: The consumption profiles of CO and O_2 on (1:2)SnPt/Al_2O_3(high) catalyst in λ_2 gas mixture

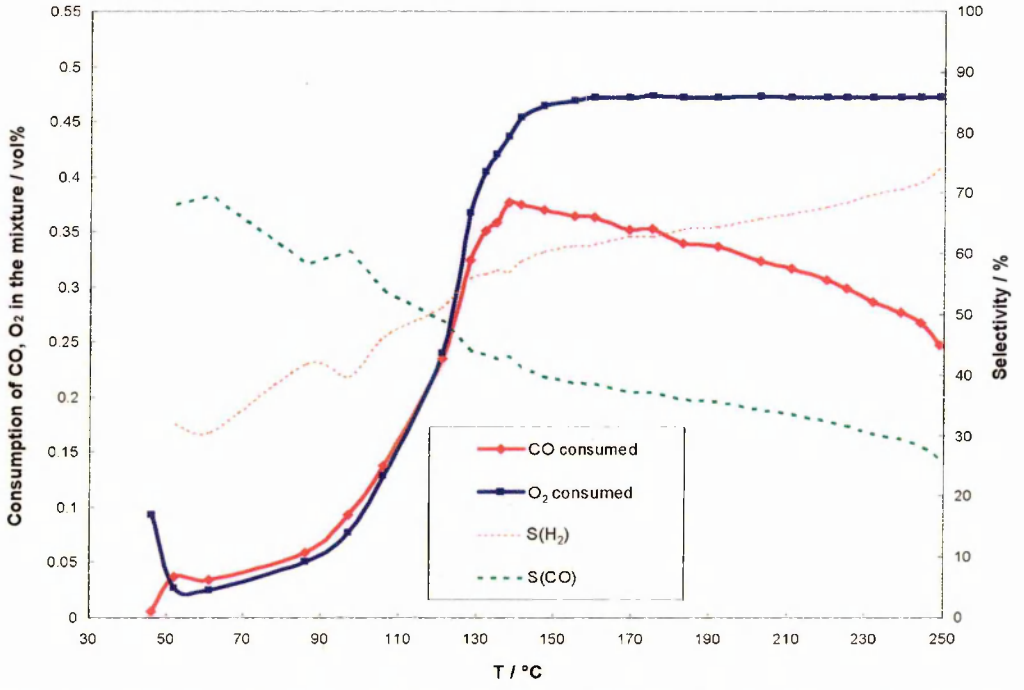

FIGURE 5-29: The consumption profiles of CO and O_2 on (1:1)SnPt/Al_2O_3(high) catalyst in λ_2 gas mixture

Table 5-13 summarises T_{max}, $T(50)$ and selectivity data for all Sn-promoted Pt catalysts when tested under λ_2 gas mixture.

Table 5-13: THE ACTIVITY-SELECTIVITY DATA FOR THE SnPt CATALYSTS UNDER λ_2 GAS MIXTURE

Catalyst	CO/M	$T(50)$ / °C	$S(CO)$/%	T_{max} / °C
5% Pt(low)	0.29	$T(52)$=207	~54	$T(92)$=239
(1:2)SnPt/Al_2O_3(low)	0.13	134	58	$T(86)$=211
(1:1)SnPt/Al_2O_3(low)	0.08	107	53	$T(82)$=158
5% Pt(high)	0.51	197	49	235
(1:2)SnPt/Al_2O_3(high)	0.20	130	44	$T(71)$=219
(1:1)SnPt/Al_2O_3(high)	0.20	122	49	$T(75)$=138

* T_{max} is the temperature at which maximum CO oxidation is observed

From the results presented in Table 5-13, it is clear that low-dispersed catalysts have performed better than the high-dispersed catalysts in terms of their activity and selectivity towards the CO oxidation. Sn-promoted catalysts showed very similar CO selectivity to the respective unpromoted Pt catalyst. However, the maximum CO conversions observed for SnPt catalysts were lower than for the Pt only catalyst.

The λ_2 results obtained over the Sn-promoted Pt catalysts did not show 100% conversion of CO present in the gas mixture, in contrast to the results obtained under the λ_5 mixture over the same catalysts where 100% CO conversion was achieved in all cases. In addition the CO conversion showed a definite leveling off or even decrease at higher temperatures, most apparent for the (1:1)SnPt(high) catalyst. This was not observed for the λ_5 tests or the Pt catalyst under the λ_2 test (but may reflect the generally higher temperatures required for comparable activities for the Pt catalyst). It would appear that the promotional effect of the tin becomes less apparent and indeed

the presence of SnO_x is inhibitive for the (1:1)SnPt(high) catalyst at higher temperatures (cf: 100% CO conversion (0.50 vol% CO) with 50% CO selectivity at 230 °C for Pt(high) and 60% CO conversion (0.30 vol% CO) with 26% selectivity to CO for (1:1)SnPt(high) catalyst). This would suggest that H_2 is being preferentially oxidized at these temperatures over the promoted catalysts. An alternative suggestion is that there is insufficient O_2 present in the λ_2 mixture to fully replenish the active oxygen required for the promotional effect or indeed that O_2 is being consumed by the catalyst (probably tin-containing component of the catalyst) itself and hence is less available to oxidize CO (or H_2). As we were unable to monitor the H_2, it is difficult to comment on H_2 oxidation (hence selectivities are shown as dotted lines) which makes it difficult to determine which explanation is most likely.

5.3.3 Fe-PROMOTED Pt CATALYSTS

As with the λ_5 tests, the formation of CO_2 was observed as soon as the λ_2 gas mixture was introduced over the (1:2)FePt(low) catalyst. Nearly 55% of CO (0.28 vol% CO) was found to be oxidised to CO_2 by 50 °C (Fig. 5-30) and the formation of CO_2 continued until ~100 °C. An unusual levelling off in the CO conversion profile of this catalyst was observed between 100–150 °C. As the temperature of the catalyst increased beyond 150 °C, the catalyst increased again in activity and converted the entire CO to CO_2 by 180 °C. The (1:1)FePt(low) catalyst behaved in a comparable way to (1:2)FePt(low) with a similar performance initially, only now instead of just levelling off in the activity, a distinct dip in the CO conversion profile is noticeable over the (1:1)FePt(low) catalyst (Fig. 5-31). The catalyst seems to slow the conversion of CO to CO_2 at just above 100 °C, where the CO conversion drops from ~70% (~0.35 vol% CO) to ~50% CO conversion (0.25 vol% CO). As the catalyst temperature

reached ~165 °C, it seems to regain its activity and by 210 °C approximately 95% of CO (0.48 vol% CO) was converted. A slight decrease in CO conversion was observed as the temperature was further increased to 220 °C, similar to the Sn-promoted catalysts. The O_2 consumption however carries on increasing throughout the run, initially at the same rate before slowing to its maximum, and no dip is observed between 100 °C and 165 °C.

A dip in the CO conversion is again observed for both the FePt(high) catalysts. Soon after the λ_2 gas mixture was introduced over the FePt(high) catalysts, the temperature of the catalyst started to rise and the formation of CO_2 was observed. Just over 20% (>0.10 vol% CO) of CO was converted into CO_2 over the (1:2)FePt(high) catalyst by 50 °C (Fig. 5-32) while the (1:1)FePt(high) catalyst showed the similar conversion at 40 °C (Fig. 5-33). The formation of CO_2 continued up to ~110 °C, when the CO conversion stayed almost constant at ~40% (0.20 vol% CO) for sometime over both the FePt(high) catalysts before decreasing slightly to ~35% (~0.18 vol% CO) over (1:2)FePt(high) and 30% (0.15 vol% CO) over (1:1)FePt(high) catalyst above ~115 °C until about 170 °C. The O_2 consumption however increases at a steady rate throughout the profile until it reaches 90% conversion. The catalysts regained their activity to oxidize CO to CO_2, as the temperature was gradually increased from 170 °C resembling the profile for Pt/Al_2O_3(high) (although at higher activity). Towards the end of the test, the (1:2)FePt(high) catalyst converted just under 90% of CO (<0.45 vol% CO) to CO_2 while the (1:1)FePt(high) catalyst dropped marginally to ~80% (0.40 vol% CO).

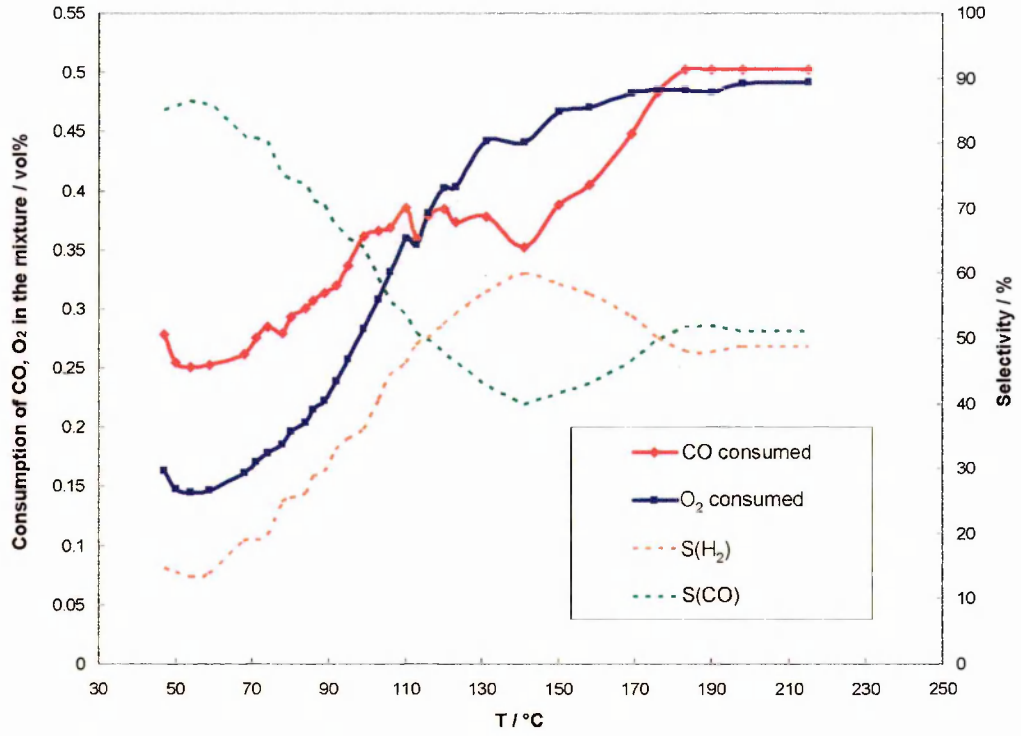

FIGURE 5-30: The consumption profiles of CO and O_2 on (1:2)FePt/Al_2O_3(low) catalyst in λ_2 gas mixture

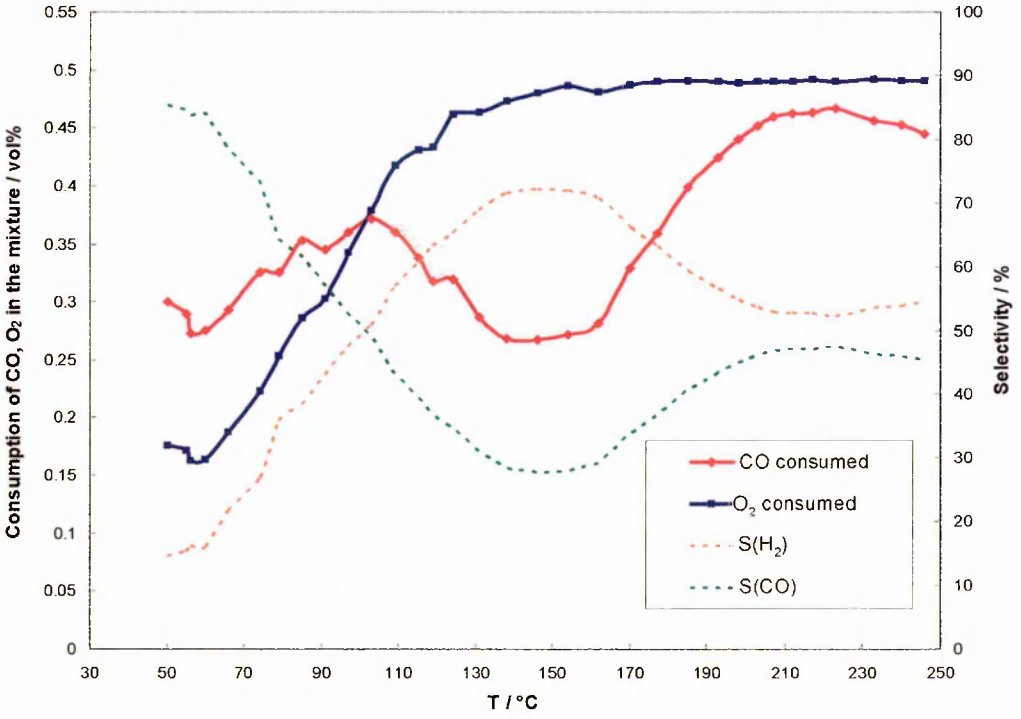

FIGURE 5-31: The consumption profiles of CO and O_2 on (1:1)FePt/Al_2O_3(low) catalyst in λ_2 gas mixture

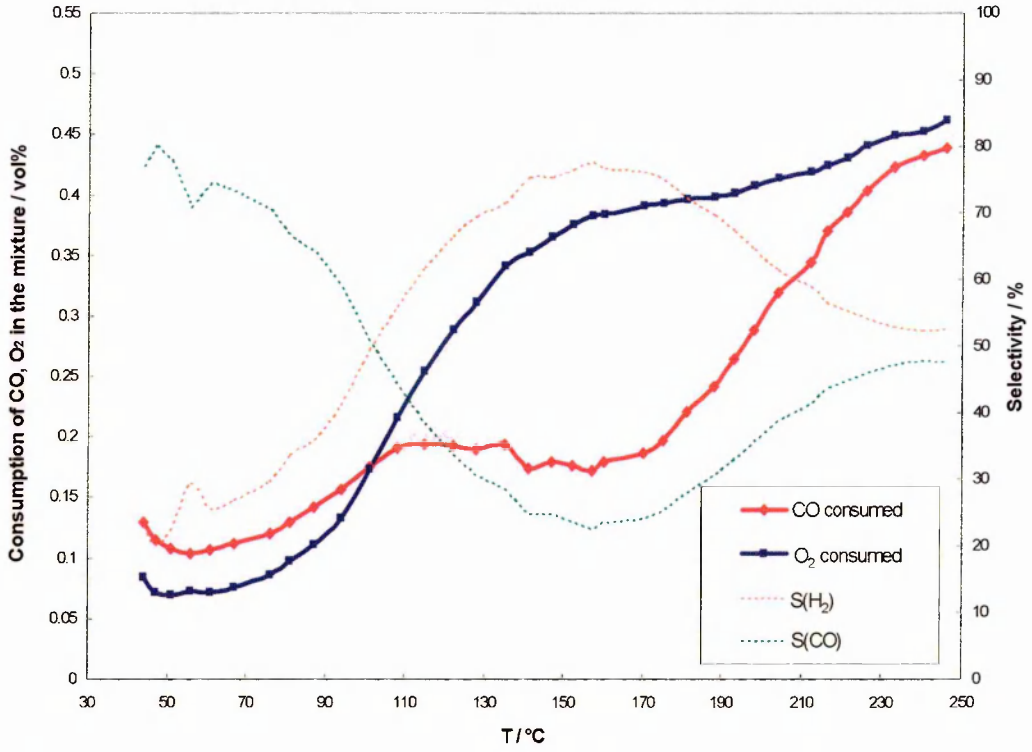

FIGURE 5-32: The consumption profiles of CO and O_2 on (1:2)FePt/Al_2O_3(high) catalyst in λ_2 gas mixture

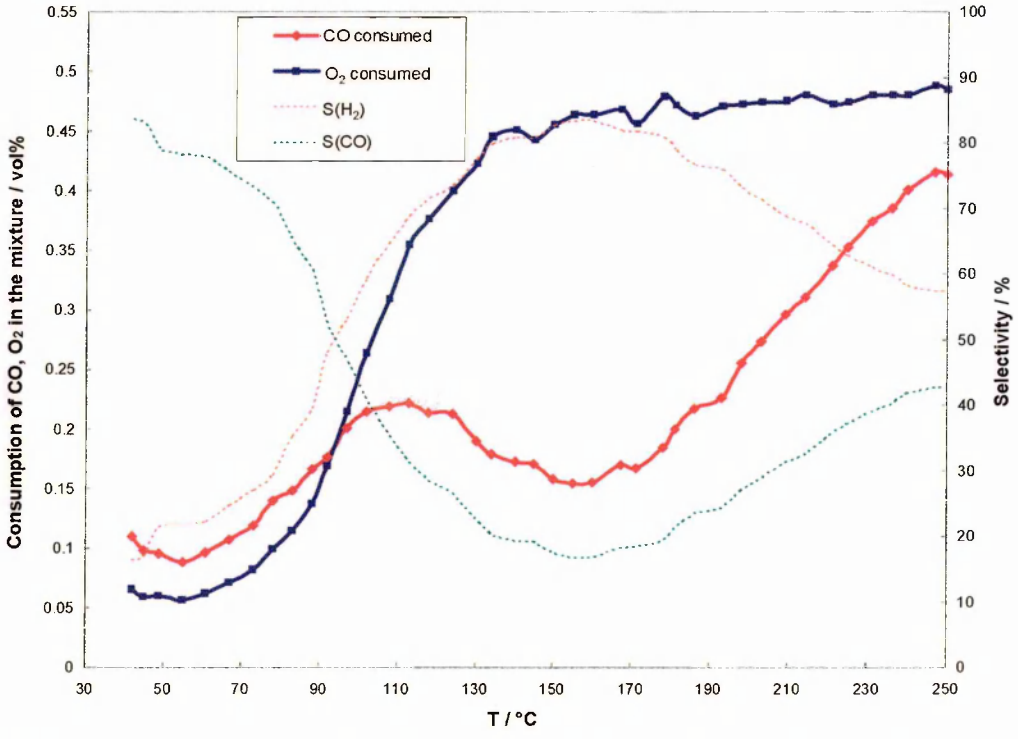

FIGURE 5-33: The consumption profiles of CO and O_2 on (1:1)FePt/Al_2O_3(high) catalyst in λ_2 gas mixture

Table 5–14 summarises $T(50)$, T_{max} and the selectivity data for all the Fe-promoted Pt catalysts when tested under the λ_2 gas mixture.

Table 5-14: THE T_{max} , $T(50)$, AND SELECTIVITY OF THE FePt CATALYSTS UNDER λ_2 GAS MIXTURE

Catalyst	CO/M	$T(50)$ / °C	$S(CO)$/%	T_{max} / °C
5% Pt(low)	0.29	$T(52)$=207	53.5	$T(92)$=239
(1:2)FePt/Al_2O_3(low)	0.16	50	86	183
(1:1)FePt/Al_2O_3(low)	0.14	$T(55)$=56	84	$T(\sim 94)$=223
5% Pt(high)	0.51	197	49	235
(1:2)FePt/Al_2O_3(high)	0.24	~190	31	$T(88)$=246
(1:1)FePt/Al_2O_3(high)	0.22	198	27	$T(83)$=247

From the results presented in Table 5–14, it is seen that the low–dispersed Fe-promoted catalysts have performed significantly better than the high–dispersed. This could be due to the fact that the low–dispersed catalysts have larger proportion of the optimum sized particles required for the CO oxidation to take place.

From the results it appears that the dispersion of the metallic component of a catalyst plays a very significant role in causing the Fe–Pt interactions. The results from TEM and EDX show that the addition of Fe has little effect on the particle size of the Pt particles and further analysis also showed that FeO_x is in physical contact with Pt particles. An indication of strong Fe–Pt interactions is also evident from the TPR profiles. The effect of these interactions is reflected in the superior activity of the promoted catalysts even under limited oxygen conditions.

From the CO oxidation profiles shown in Figs. 5-30 to 5-33, the initial high CO conversion at temperatures below 60 °C over the promoted catalysts could be explained as the promoting effect of FeO_x towards the CO oxidation by providing active oxygen. However, it seems that FeO_x responsible for the initial high CO conversion became depleted of its active oxygen as the temperature of the catalyst reached about 110 °C. There appears to be insufficient O_2 remaining in the λ_2 mixture at this point, as the consumption of O_2 is already quite high, to reoxidise the Fe and replenish the active oxygen. No halt/dip was observed in the tests performed on the same catalysts under the λ_5 gas mixture suggesting that the excess oxygen (1.25%) in the λ_5 mixture was able to oxidise CO to CO_2. At temperatures above 170 °C, the oxidation profile was similar to the Pt/Al_2O_3 catalyst although the slight promotion effect by FeO_x could not be ruled out. Unfortunately as we were not able to monitor H_2 directly it is not possible to determine definitively whether the dip in CO performance is related to a corresponding increase in the H_2 oxidation as we expect. We are not able to rule out the possible alternative explanation that O_2 is taken up by the catalyst itself, oxidising iron to a different, less active, form of oxide. This does seem unlikely however as similar results would be expected to be seen with the λ_5 tests when more O_2 was present.

5.3.4 Co-PROMOTED Pt CATALYSTS

As the λ_2 gas mixture was passed over the reduced (1:2)CoPt(low) catalyst, the CO conversion and the temperature of the catalyst were found to rise sharply (Fig. 5-34). At the start of the test, it was observed that over 50% CO (0.25 vol% CO) was already oxidized, while a slightly smaller amount of oxygen had been consumed. This gives support to the proposed mechanism for Co-promoted catalysts, in which the reduced cobalt takes up oxygen from the gas mixture and provides active oxygen for

the oxidation of CO even at low temperature. The CO oxidation increases with the rise in temperature and the complete CO conversion was observed at ~170 °C. For (1:1)CoPt(low) catalyst a very similar trend was observed (Fig. 5-35). About 65% of CO (0.33 vol% CO) was oxidized at the beginning of the test at 40 °C. A rise in temperature resulted in an increased CO conversion. The complete oxidation of CO was observed at ~140 °C. No dip was observed between 100-170 °C in the CO conversion profile as seen for the Fe-promoted analogues suggesting that the CoO_x was more easily reoxidised and able to replenish its active oxygen. The Co-promoted catalysts were therefore superior to the Fe-promoted catalysts. A decrease in CO conversion was observed, however, at temperatures above ~200 °C similar to the other promoted catalysts which was more pronounced for the (1:1)CoPt(low) catalyst.

The CO oxidation profile for (1:2)CoPt(high) catalyst is shown in Fig. 5-36. Starting at ~20% (~0.10 vol% CO) CO conversion, the catalyst seems to be slightly sluggish as compared to its low–dispersed analogue. With the rise in temperature, the CO oxidation also increased with almost complete conversion of CO to CO_2 by 197 °C. When the (1:1)CoPt(high) catalyst was tested under similar conditions, it gave a very similar result (Fig. 5-37). The complete CO oxidation occurred at ~140 °C. The increased amount of Co appears to be responsible for bringing the temperature of complete CO conversion down to ~140 °C. It was interesting to note that all the Co-promoted Pt catalysts did convert CO to CO_2 fully, but the extent of conversion fell slightly as the temperature reached just over 200 °C. As with the other catalysts the CO conversions under the λ_2 mixture were lower than the comparative test under the λ_5 mixture at the same temperature, however, the selectivities were higher. A drop in the CO consumption was observed while O_2 consumption remained steady at temperatures above ~ 190 ° C for the tests in λ_2 mixture which was not observed for the λ_5 tests.

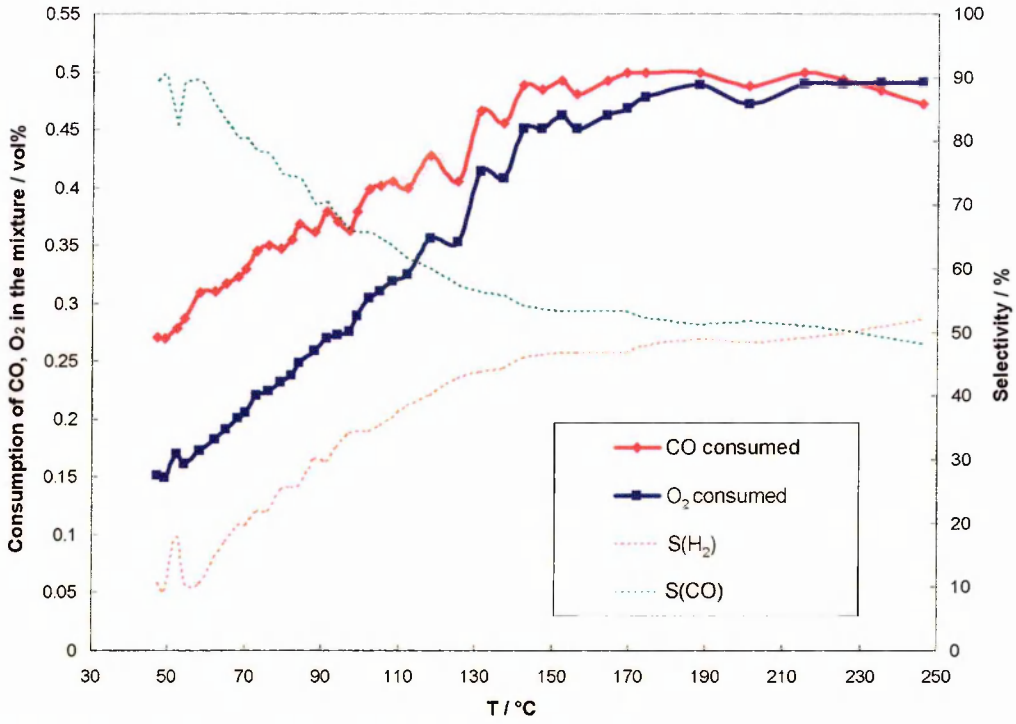

FIGURE 5-34: The consumption profiles of CO and O_2 on (1:2)CoPt/Al_2O_3(low) catalyst in λ_2 gas mixture

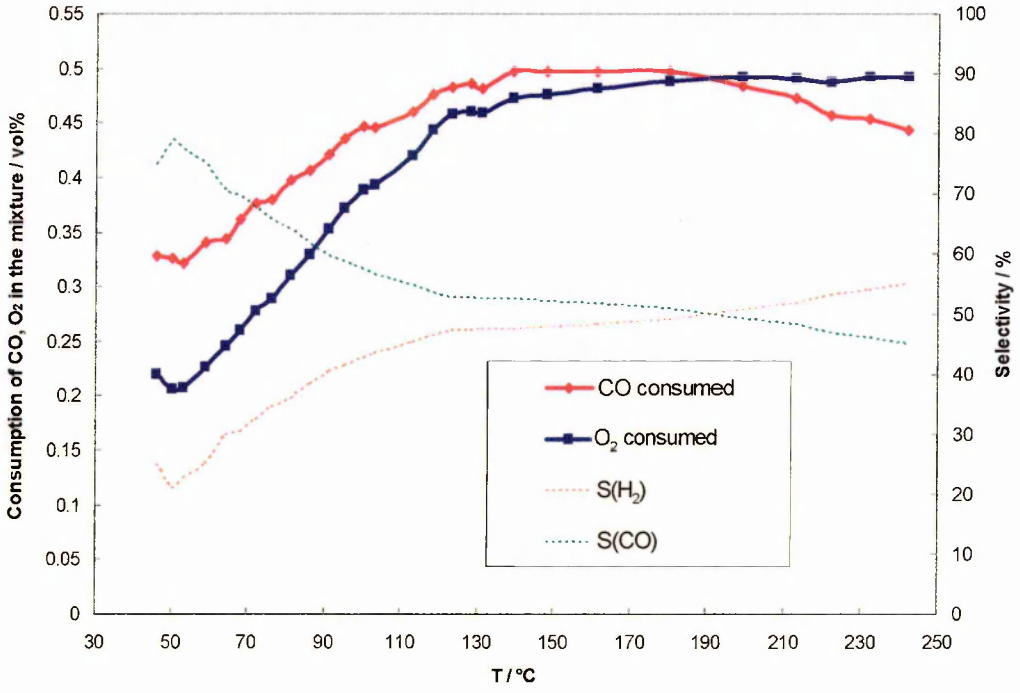

FIGURE 5-35: The consumption profiles of CO and O_2 on (1:1)CoPt/Al_2O_3(low) catalyst in λ_2 gas mixture

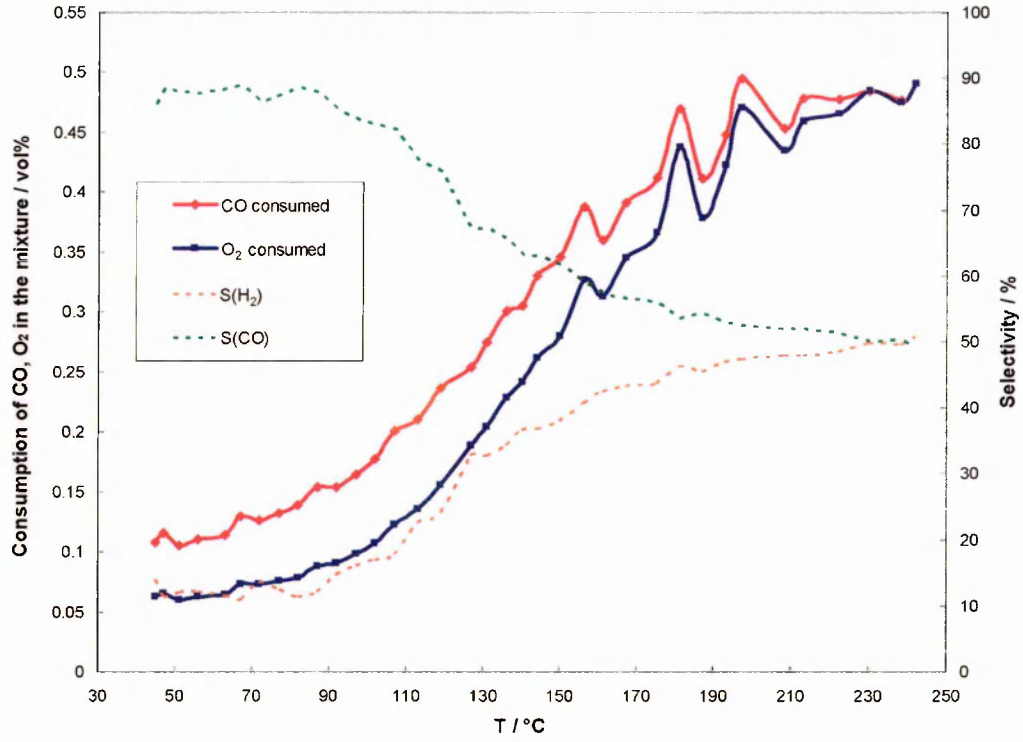

FIGURE 5-36: The consumption profiles of CO and O_2 on (1:2)CoPt/Al_2O_3(high) catalyst in λ_2 gas mixture

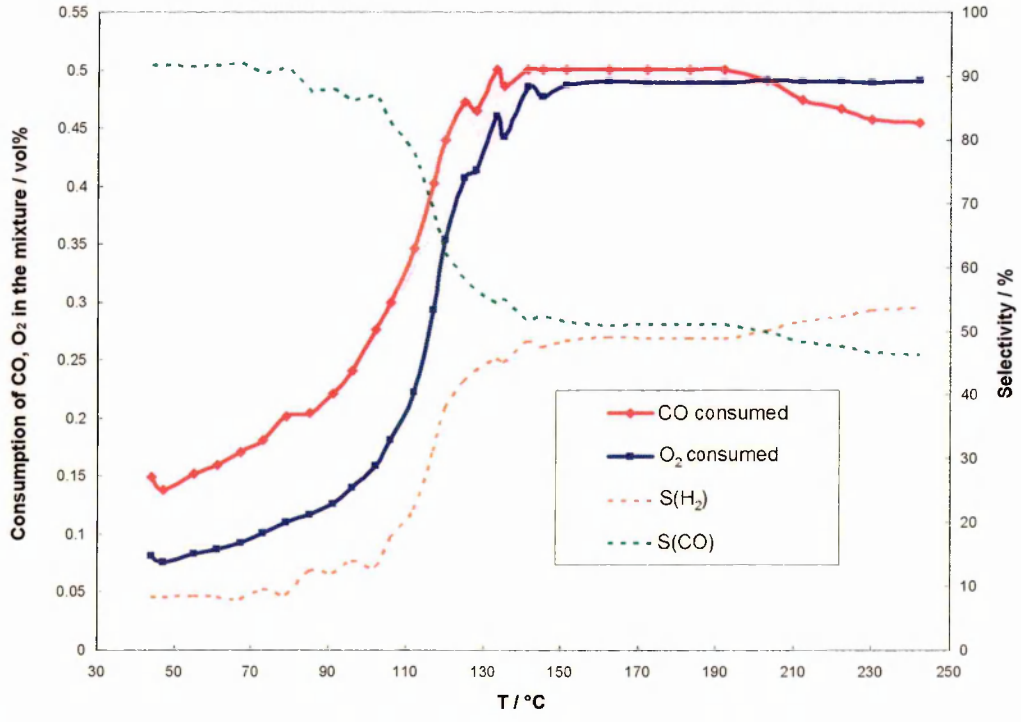

FIGURE 5-37: The consumption profiles of CO and O_2 on (1:1)CoPt/Al_2O_3(high) catalyst in λ_2 gas mixture

Table 5-15 summarises $T(50)$, T_{max} and the selectivity data for all Co-promoted Pt catalysts when tested under λ_2 gas mixture.

Table 5-15: THE ACTIVITY-SELECTIVITY DATA FOR THE CoPt CATALYSTS UNDER λ_2 GAS MIXTURE

Catalyst	CO/M	$T(50)$ / °C	$S(CO)$/%	T_{max} / °C
5% Pt(low)	0.29	$T(52)$=207	53.5	$T(92)$=239
(1:2)CoPt/Al_2O_3(low)	0.19	$T(54)$=49	91	169
(1:1)CoPt/Al_2O_3(low)	0.16	$T(64)$=53	77	139
5% Pt(high)	0.51	197	49	235
(1:2)CoPt/Al_2O_3(high)	0.26	127	67	$T(99)$=197
(1:1)CoPt/Al_2O_3(high)	0.23	~100	86.5	141

From the results presented in Table 5-15, the performance of the Co-promoted Pt low–dispersed catalysts was found to be better than that of the high–dispersed catalysts. Similarly (1:1) catalysts exhibited higher activity with similar selectivities than the (1:2) catalysts. A dip in the CO activity was seen for the catalysts at higher temperatures with some of the catalysts never reaching 100% CO conversion as discussed previously.

For each system the low–dispersed catalysts were found to exhibit better performance than the high–dispersed catalysts, For the Co catalysts the (1:1) catalysts were generally more active than (1:2) catalysts with (1:1)CoPt/Al_2O_3(low) showing the best performance out of all the catalysts studied.

Achieving high selectivity and the ability to completely oxidize CO in the limited supply of oxygen at reasonable temperatures makes these catalysts a good

candidate for the practical applications such as in cleaning of the feedstock gas for fuel cells.

5.4 WET RESULTS

All the catalysts prepared by the SOMC route, were screened under a simulated reformate gas mixture at the Johnson Matthey Technology Centre, Sonning Common, UK. The sample preparation, pre-treatment and experimental details have been given in Chapters 2 and 4.

The results for all the (1:2)M-Pt/Al_2O_3(low) catalysts [where M = Cr, Mn, Fe, Co, Ni, Cu and Sn] have been given in Chapter 4. The results for the (1:2)MPt(high) [where M = Sn and Co] and (1:1)MPt, [where M = Sn, Fe and Co] both low and high–dispersed catalysts are shown in Fig. 5-38. The results of these studies are shown in terms of the amount of CO left un-oxidised by the catalyst (in ppm) as a function of space velocity (in $cm^3 h^{-1} g_{cat}^{-1}$) (Fig. 5-38). The catalysts were compared to a good promoted catalyst prepared at Johnson Matthey Technology Centre, UK.

From Fig. 5-38, it is again observed that the low–dispersed catalysts performed better than the corresponding high–dispersed catalysts over the entire range of space velocity. Sn-promoted catalysts show a very flat trend showing similar CO conversion at low and high space velocities. Of all the bimetallic catalysts tested, the performance of the low–dispersed Fe- and Co-promoted Pt catalysts were the best and were very comparable to the Johnson Matthey promoted catalyst.

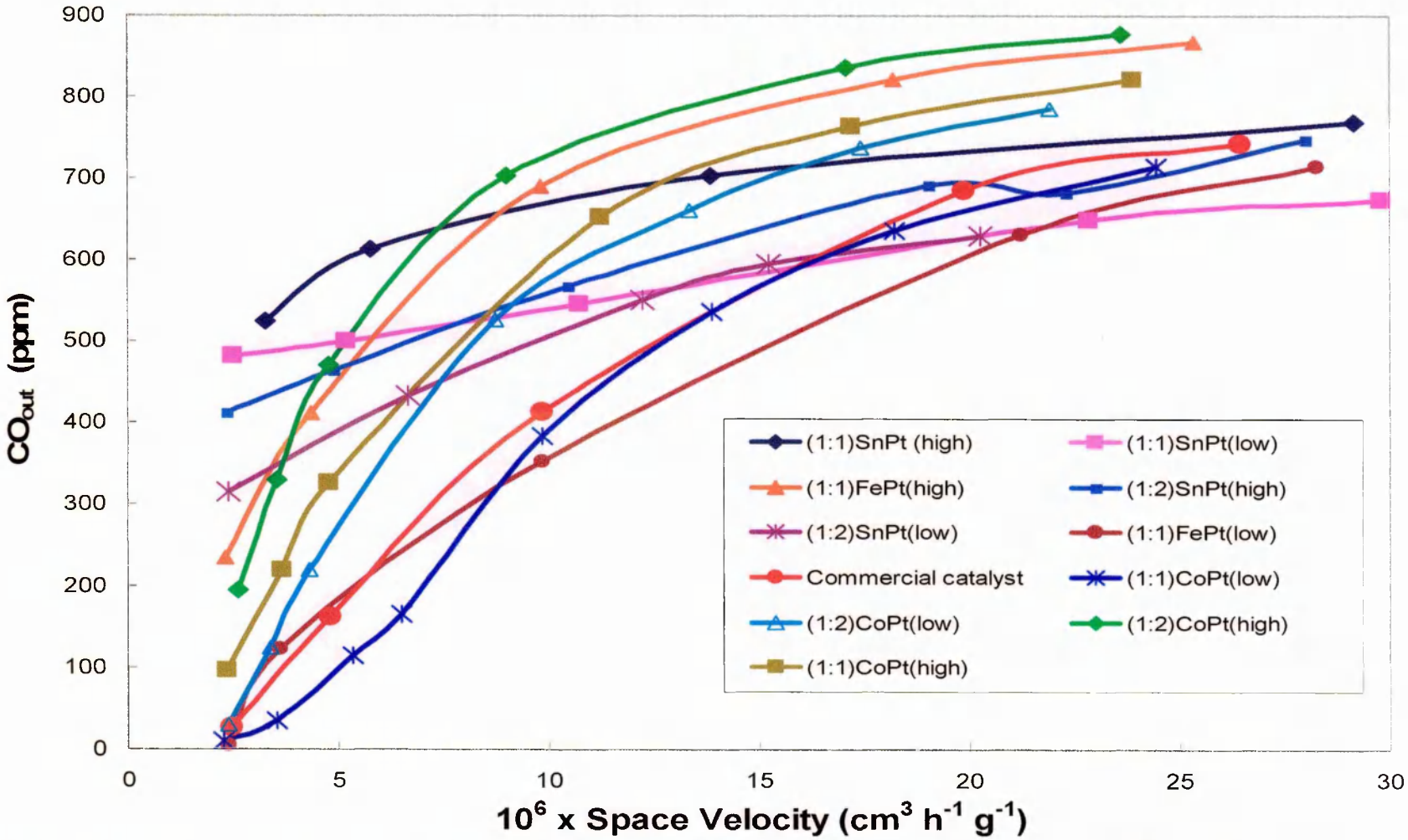

FIGURE 5-38: The plot of CO_{out} *vs.* Space Velocity at 150 °C, under a flowing gas mixture containing 60% H_2, 0.1% CO, 20% CO_2, 0.15% O_2

5.5 CONCLUSIONS

From the studies performed on the bimetallic catalysts under the λ_5 gas mixture, Fe- and Co- promoted catalysts performed significantly better than Sn-promoted catalysts. Interestingly, the Fe- and Co-promoted catalysts continued to convert CO to CO_2 even when left to cool under the λ_5 gas mixture for few hours. Mild heat-treatment did not seem to affect the performance of these catalysts significantly.

The performance of the low–dispersed catalysts, especially Fe- and Co-promoted ones, is very interesting considering the fact that the temperature of complete CO conversion has been brought down to the temperature range which is highly preferred for the commercial applications, while maintaining a high value of CO selectivity.

Under the λ_2 gas mixture, the Fe- and Co-promoted catalysts again performed significantly better than other catalysts tested. The ability of low–dispersed Fe- and Co-promoted bimetallic catalysts to oxidise CO in the λ_2 mixture to CO_2 with high CO selectivity makes them good candidates for the practical applications. The Fe-promoted catalysts experienced a significant drop in activity during the tests. However, both the Co-promoted bimetallic catalysts, low– and high–dispersed, converted the entire CO to CO_2 under the λ_2 gas mixture with good CO selectivity and hence making them one the best candidates for the commercial applications.

This observation was nicely supported by the performance of the Fe- and Co-promoted bimetallic catalysts under the simulated reformate gas mixture at JMTC. Fe- and Co-promoted catalysts performing similar, if not better than the Johnson Matthey promoted catalyst.

5.6 REFERENCES

1 M. Herskowitz and C. N. Kennedy, *Can. J. Chem. Eng.*, **61**, 194, (1983)

2 S. Völkening, K. Bedürftig, K. Jacobi, J. Wintterlin and G. Ertl, *Phys. Rev. Lett.*, **83**, 2672, (1999)

3 T. Engel and G. Ertl, *Advances in Catalysis*, (Eds. W. G. Frankenburg, V. I. Komarewsky and E. K. Rideal), Academic Press, NY, **28**, 1, (1979)

4 S. H. Oh, G. B. Fisher, J. E. Carpenter and D. W. Goodman, *J. Catal.*, **100**, 360, (1986)

5 Y. Nishiyama and H. Wise, *J. Catal.*, **32**, 50, (1974)

6 X. Liu, O. Korotkikh and R. Farrauto, *Appl. Catal. A: Gen.*, **226**, 293, (2002)

7 S. H. Oh and R. M. Sinkevitch, *J. Catal.*, **142**, 254, (1993)

8 G. Ertl, *Adv. Catal.*, **37**, 231, (1990)

9 T. A. Nijhuis, M. Makkee, A. D. van Langeveld and J. A. Moulijn, *Appl. Catal. A*, **164**, 237, (1997)

10 M. Rinnemo, D. Kulginov, S. Johansson, K. L. Wong, V. P. Zhdanov and B. Kasemo, *Surf. Sci.*, **376**, 297, (1997)

11 V. P. Zhdanov and B. Kasemo, *Appl. Surf. Sci.*, **74**, 147, (1994)

12 M. J. Kahlich, H. A. Gasteiger and R. J. Behm, *J. Catal.*, **171**, 93, (1997)

13 D. H. Kim and M. S. Lim, *Appl. Catal. A: Gen.*, **224**, 27, (2002)

14 A. N. Akın, G. Kılaz, A. İ. İsli and Z. İ. Önsan, *Chem. Eng. Sci.*, **56**, 881, (2001)

15 K. Grass and H. G. Lintz, *J. Catal.*, **172**, 446, (1997)

16 A. Boulahouache, G. Kons, H. G. Lintz and P. Schulz, *Appl. Catal. A*, **91**, 115, (1992)

17 J. Völter and U. Kürschner, *Appl. Catal.*, **8**, 167, (1983)

18 R. Burch and A. J. Mitchell, *Appl. Catal.*, **6**, 121, (1983)

19 V. M. Deshpande, W. R. Patterson and C. S. Narasimhan, *J. Catal.*, **121**, 165, (1991)

20 K. C. Taylor, *Stud. Surf. Sci. Catal.*, **30**, 97, (1987)

21 F. Maire, M. Capelle, G. Meunier, J. F. Beziau, D. Bazin, H. Dexpert, F. Garin, J. L. Schmitt and G. Maire, *Stud. Surf. Sci. Catal.*, **96**, 749, (1995)

22 D. A. H. Cunningham, T. Kobayashi, N. Kamijo, and M. Haruta, C*atal. Lett.*, **25**, 257, (1994)

23 N. P. Siswana and D. L. Trimm, *Catal. Lett.*, **46**, 27, (1997)

24 M. Skoglundh, H. Johansson, L. Löwendahl, K. Jansson, L. Dahl, and B. Hirschauer, *Appl. Catal. B,* **7**, 299, (1996)

25 Y. J. Mergler, A. van Aalst, J. van Delft and B. E. Nieuwenhuys, *Appl. Catal. B*, **10**, 245, (1996)

26 N. W. Cant, *J. Catal.* **62**, 173, (1980)

27 J. Sarkany and R. D. Gonzalez, *Appl. Catal.*, **5**, 85, (1983)

28 N. W. Cant, P. C. Hicks and B. S. Lennon, *J. Catal.*, **54**, 732, (1978)

29 N. W. Cant, *J. Catal.* **74**, 411, (1982)

30 J. H. Sinfelt, *Bimetallic Catalysts: Discoveries, Concepts and Applications*, Wiley, New York (1983)

6

Conclusions

The main aim of the work presented in this thesis was to promote the catalytic performance of Pt/Al_2O_3 for the selective removal of CO from hydrogen-rich streams for fuel cells using the selective addition of a second metal/metal oxide. Two samples of Pt/Al_2O_3 catalyst with different dispersions of platinum (29% (low-) and 51% (high-dispersed)) were modified using a Surface Organometallic Chemistry (SOMC) route with a range of promoter metals, including Sn, and some of the transition metals such as, Fe, Co, Cr, Mn, Ni and Cu. This method of preparation was chosen as it is important that the platinum and second metal are in intimate contact and the technique is believed to result in the deposition of the second metal onto the Pt surface via a selective reaction between an organometallic precursor of the second metal and hydrogen adsorbed on the Pt surface. In the present study, organometallic precursors such as, tetra-butyl tin ($Sn(n\text{-}C_4H_9)_4$), ferrocene ($Fe(C_5H_5)_2$), cobaltocene ($Co(C_5H_5)_2$), manganese-acetylacetonate ($Mn(acac)_2$) were employed. The prepared catalysts were characterised and tested for selective removal of carbon monoxide in the presence of hydrogen.

After initial screening of all the catalysts under a gas mixture containing 1.25% O_2, 0.50% CO, ~25% H_2, and balance N_2 (dry tests) and under a simulated reformate

mixture containing 60% H_2, 0.1% CO, 20% CO_2, 0.15% O_2 and balance nitrogen (wet tests), the Sn, Fe and Co catalytic systems performed significantly better than the unpromoted catalyst and consequently, were selected for detailed study*.

Under the conditions employed during the preparation of catalysts by the SOMC route, the reaction of the second metal precursor with the reduced Pt surface is believed to result in the selective deposition of the second metal on the Pt surface of the reduced Pt/Al_2O_3 catalyst and thus direct contact between the two metals/metal oxides. Characterisation of the catalysts using a number of different techniques provided evidence that this had indeed occurred for the catalysts studied:

- TEM/EDX of Sn-, Fe- and Co-promoted catalysts indicated the presence of the second metal only in areas where Pt was also present;
- ICP/AES confirmed the presence of the two metals in the catalysts, although the loading was somewhat less for the higher loaded catalysts than the nominal values; *e.g.* for (1:2) and (1:1) Co-promoted high-dispersed catalysts, only 0.33% and 0.67% Co was found in the system, in comparison to the expected value of 0.44% and 0.80%, respectively, suggesting that there may be a limit to the deposition under the conditions used;
- CO chemisorption indicated a decrease in CO uptake as a result of lowering of the exposed Pt surface sites relative to the unpromoted Pt catalyst and TEM indicated no significant change in the particle size upon the addition of second metal;

The reduction peaks in the TPR profile for Fe- and Co-promoted bimetallic catalysts shifted in comparison to the unpromoted catalyst suggesting an interaction of the two metal species in the catalyst as a result of their physical proximity. However, no significant uptake of hydrogen was observed for Sn-promoted catalysts. The

presence of this highly reduced state of the platinum may provide an explanation for this low uptake of hydrogen by the tin-promoted catalysts.

We believe from previous studies with other systems that all the second metals are likely to exist as the metal oxide in the presence of air, although no direct evidence of this for the catalysts studied in this thesis was obtained.

A range of Sn-, Fe- and Co-promoted catalysts were further tested using dry gas mixtures with different O_2:CO ratios (O_2:CO = 2.5 and O_2:CO = 1 referred to as the λ_5 and the λ_2 mixtures respectively, where λ_1 corresponds to stoichiometric amounts for the reaction $CO(g) + 0.5O_2(g) \rightarrow CO_2(g)$ and the simulated reformate gas mixture (wet tests). A significant improvement in the performance of the catalysts was observed for all three systems but in particular for the Fe- and Co-promoted catalysts under both gas mixtures compared to the unpromoted Pt/Al_2O_3. The Fe-promoted catalysts experienced a significant drop in activity *e.g.* 70% (>0.35 vol% CO) to ~50% CO conversion (0.25 vol% CO) over (1:1)FePt(low) catalyst between 100 – 130 °C, during the λ_2 tests which could be due to insufficient O_2 remaining (in the λ_2 mixture) to reoxidise the Fe and replenish the active oxygen. However, both the FePt and CoPt systems brought the temperature for the complete CO oxidation down to the temperature range (80 – 120 °C) which is highly preferred for commercial applications, while maintaining the high value of CO selectivity. The performance of the low–dispersed catalysts was found to be significantly better than the high–dispersed catalysts. This could be due to the fact that the low–dispersed catalysts have larger proportion of the optimum-sized particles required for the CO oxidation to take place.

The enhanced activity of the promoted Pt catalysts is believed to be due to the presence of a metal oxide, MO_x (M = Fe and Co) which provides a site for O_2

adsorption and dissociation allowing oxidation of CO on a neighbouring Pt site to occur and therefore reducing the normal inhibition observed in the oxidation of CO on Pt catalysts. This enhancement appears to be particularly significant for the Fe and Co systems. The lack of such an enhancement for the other metals studied (Cr, Mn, Ni and Cu) would suggest that either such a mechanism is not so important for the other metals or that the preparation was not so successful. Little characterisation was performed for these metals and indeed ICP-AES suggested lower loadings than expected for the Cr and Ni systems.

* Temperature for maximum CO conversion was brought down to
  - 140 – 160 °C over Sn-promoted;
  - 80 – 120 °C over Co-promoted and;
  - ~100 °C over Fe-promoted catalysts compared to 200 °C for Pt-only catalyst.